MICROCOPY RESOLUTION TEST CHART

NATIONAL BUREAU OF STANDARDS – 1963 – A

Shock Dynamics Laboratory

Department of Physics

WASHINGTON STATE UNIVERSITY
1890
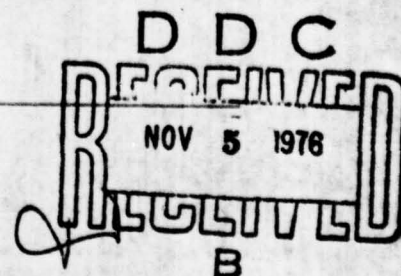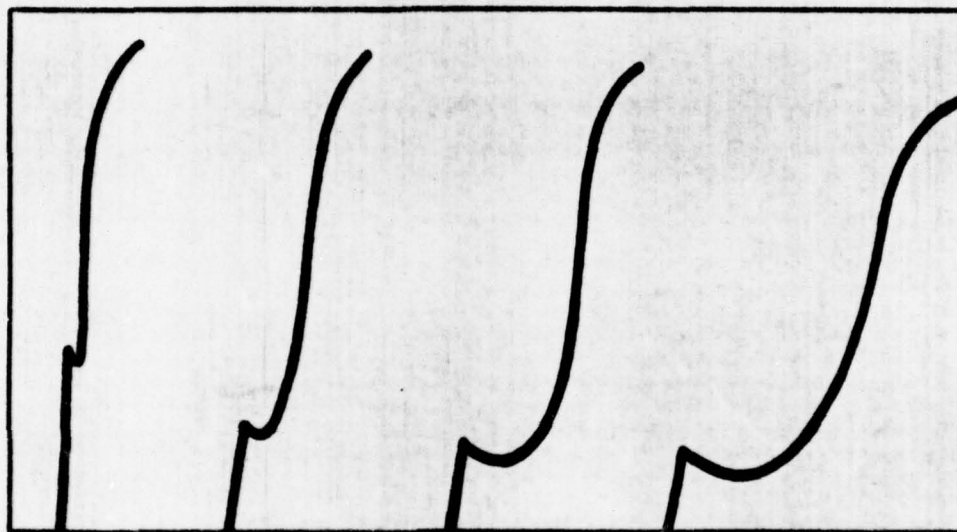
Washington State University

Pullman, Washington 99163

The front cover shows stress time
profiles for LiF. Specimen thicknesses
are, from left to right, .478mm, 1.978mm,
4.065mm, 5.892mm. Vertical scale, 4 kbar/cm;
horizontal scale, 0.1μsec/cm.

AD

AMMRC CTR 76-18

KINETICS OF SHOCK-INDUCED PHASE TRANSITIONS

JUNE 1976

J. W. SWEGLE, G. E. DUVALL, AND J. J. DICK

DEPARTMENT OF PHYSICS
WASHINGTON STATE UNIVERSITY
PULLMAN, WASHINGTON 99163

The major part of this work was presented by J. W. Swegle as a Dissertation
in partial fulfillment of the requirements for a Ph.D. in Physics,
Washington State University.

FINAL REPORT - CONTRACT DAAG46-75-C-0035

Prepared for

ARMY MATERIALS AND MECHANICS RESEARCH CENTER
Watertown, Massachusetts 02172

The findings in this report are not to be construed as an official Department of the Army position, unless so designated by other authorized documents.

Mention of any trade names or manufacturers in this report shall not be construed as advertising nor as an official indorsement or approval of such products or companies by the United States Government.

DISPOSITION INSTRUCTIONS

Destroy this report when it is no longer needed.
Do not return it to the originator.

REPORT DOCUMENTATION PAGE

READ INSTRUCTIONS
BEFORE COMPLETING FORM

1. REPORT NUMBER	2. GOVT ACCESSION NO.	3. RECIPIENT'S CATALOG NUMBER
AMMRC CTR-76-18		

4. TITLE (and Subtitle)	5. TYPE OF REPORT & PERIOD COVERED
KINETICS OF SHOCK-INDUCED PHASE TRANSITIONS.	Final Report
	6. PERFORMING ORG. REPORT NUMBER
	WSU-SDL-75-02

7. AUTHOR(s)	8. CONTRACT OR GRANT NUMBER(s)
J. W. Swegle, G. E. Duvall, and J. J. Dick	DAAG46-75-C-0035 NEW

9. PERFORMING ORGANIZATION NAME AND ADDRESS	10. PROGRAM ELEMENT, PROJECT, TASK AREA & WORK UNIT NUMBERS
Department of Physics Washington State University Pullman, Washington 99163	D/A Project: 1W062105A661 AMCMS Code: 612105.11.07000 Agency Accession:

11. CONTROLLING OFFICE NAME AND ADDRESS	12. REPORT DATE
Army Materials and Mechanics Research Center Watertown, Massachusetts 02172	June 1976
	13. NUMBER OF PAGES
	223

14. MONITORING AGENCY NAME & ADDRESS(if different from Controlling Office)	15. SECURITY CLASS. (of this report)
	Unclassified
	15a. DECLASSIFICATION/DOWNGRADING SCHEDULE

16. DISTRIBUTION STATEMENT (of this Report)

Approved for public release; distribution unlimited.

17. DISTRIBUTION STATEMENT (of the abstract entered in Block 20, if different from Report)

18. SUPPLEMENTARY NOTES

19. KEY WORDS (Continue on reverse side if necessary and identify by block number)

Finite difference code   Measuring instruments
Phase transitions
Shock waves
Stress relaxation
Two-dimensional flow

20. ABSTRACT (Continue on reverse side if necessary and identify by block number)

A method is developed for performing and interpreting shock wave experiments in two-dimensional strain using a light gas gun. The experimental configuration consists of the impact of a projectile on a wedge whose impact face makes an angle α with the projectile impact face. The instrumentation consists of resistance wires stretched parallel to and offset from the wedge rear surface in order to detect free surface motion. The system has the capability of making measurements over a continuous range of shock propagation distances in a single experiment. The repeatability of the technique is good to within three to four percent.

DD FORM 1473   EDITION OF 1 NOV 65 IS OBSOLETE
1 JAN 73

ALPHA   403 690

The analytical technique consists of a Lagrangian finite-difference code written specifically to handle wedge impact problems. It includes material strength, stress relaxation, and phase transitions. Experiments were done on aluminum wedges and on iron and KCl wedges shocked past their transition points. Comparisons with computer calculations of the problems show excellent agreement.

ACKNOWLEDGMENT

TABLE OF CONTENTS

LIST OF FIGURES

Figure

LIST OF TABLES

1. INTRODUCTION

1.1 Motivation

The aim of this work is to develop a method for performing and interpreting shock wave experiments in two-dimensional strain using a light gas gun.[1] The primary application of this is in the study of the kinetics of shock-induced phase transitions in solids. The motivation for this study has been detailed elsewhere.[2,3] The geometry of two-dimensional strain is intended to provide a quick survey technique for estimating the transition points and kinetics of phase transitions in various materials.

An overall perspective of the events leading to the present stage of development of the study of phase transitions and their kinetics has been given in other works.[4] Phase transitions are detected in shock wave experiments by the two-wave structure that is generated.[5] The kinetics of the phase transition are studied by measuring the rate at which this two-wave structure develops.[4] This is normally done under conditions of uniaxial strain produced by normal impact of the plane face of a projectile on the plane front surface of a sample. The shock proceeds through the sample and some shock parameter is measured in a plane parallel to the impact plane, usually at the rear surface of the sample. This type of experiment has some advantages. The one-dimensional strain case is relatively easy to interpret, and many analytical techniques exist for this purpose.[6,7] Also, there are many highly refined measurement techniques which may be employed in the one-dimensional experiment.[8]

1

The two-dimensional strain experiment, on the other hand, is more difficult to analyze. The added dimension naturally brings a greater degree of complexity to the problem. Much work has been done in multidimensional geometries,[9] of course, but the majority of work has considered the uniaxial strain case. The situation is much the same regarding measurement techniques. Although measurements have been made in other than one-dimensional geometries, particularly in experiments involving the use of explosives, the most sophisticated advances are in instrumentation that is not readily adaptable to multidimensional geometries. The VISAR[10] and quartz guage[11] are examples of instruments capable of making continuous measurements of shock wave parameters with good precision and accuracy in plane wave experiments. This kind of resolution is not available for two-dimensional experiments.

There is, however, one major disadvantage involved with using one-dimensional geometry to study the kinetics of phase transitions. In this type of study it is required to determine the evolution of the wave as it propagates through the material. A one-dimensional experiment makes a measurement at only one propagation distance through the sample, namely, the sample thickness. In-situ gauges such as the electromagnetic gauge[12] do not have this limitation, but still require one gauge per measurement position. Thus, several experiments are required in order to observe the evolution of the wave structure, and information still is obtained only at discrete propagation intervals. Beyond this there is great difficulty involved in preparing very thin samples so that very short propagation distances can be studied. The one-dimensional geometry proves to be expensive and time consuming when applied to the study of the kinetics of phase transitions.

Two-dimensional geometry, despite its added complications, offers the possibility of sampling over a continuous range of propagation distances in a single experiment.[13] This attribute may justify the complexity of the problem. The two-dimensional geometry has been successfully used to obtain Hugoniot data for some materials,[14,15] and it has been used in the study of the kinetics of phase transitions.[16,17]

The development of an easy-to-use measurement technique along with a means for analyzing the experiments would overcome the major objections to the two-dimensional geometry. It would then provide a very useful method for quickly locating phase transitions and estimating their reaction rates. The development of a measurement technique and analytical method is the subject of this work.

1.2 General Description of the Problem

1.2.1 Impact Configuration

The specific two-dimensional flow geometry chosen is that of a plane projectile face impacting a wedge whose impact surface is tilted at an angle α to the projectile face, and whose rear surface is parallel to the plane of the projectile face as shown in Fig. 1.1. This misalignment of projectile and target impact surfaces is actually present in all so-called "plane impact" experiments, due to the experimental difficulties involved in aligning the two surfaces so that they are parallel. In the two-dimensional geometry the degree of misalignment is two orders of magnitude larger and is controlled.

The impact of the projectile on the target produces a condition of two-dimensional steady flow in the region where rarefactions from the ends of the wedge have not affected the problem. As can be seen in Fig. 1.1,

3
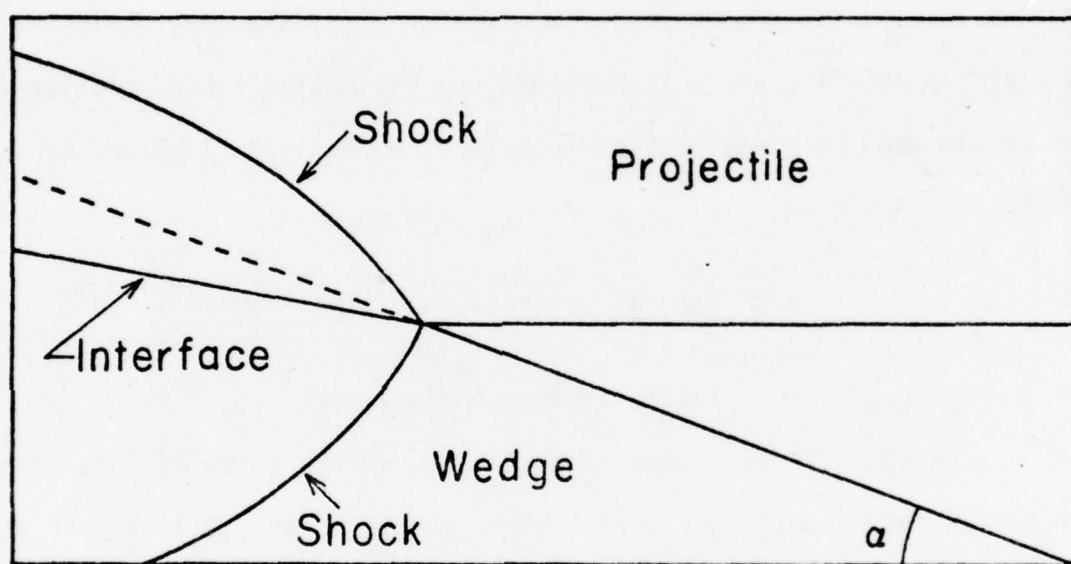
Fig. 1.1. Two-dimensional flow configuration

shocks connected to the contact point between projectile and wedge extend into the material. The flow is steady in the sense that regardless of the position of the contact point, shock parameters are the same at equal distances along the shock from the contact point. In fact, if the reference frame used is one in which the contact point is at rest, and interactions with the boundaries of the material are not considered, then parameters are unchanging with time at every point in the material. Any rate-dependent effects which occur are manifested by the variation of parameters from point to point in the material. For example, stress-relaxation would result in a decay of the shock strength with distance along the shock from the contact point. This picture of steady flow is not valid if, for instance, the velocity of the contact point is subsonic with respect to either material. This condition would result in material jetting ahead of the contact point.[18] This and other instabilities are not dealt with in this work.

In the reference frame in which the contact point is at rest, the back surface of the wedge approaches the contact point with the projectile velocity. As it gets closer to the contact point, it intersects points on the shock which are closer to the contact point, and which may have different parameters if rate-dependent effects are present. Thus in a reference frame in which the wedge is at rest, as the contact point moves to the tip of the wedge the distance that the shock that interacts with the wedge free surface has propagated changes continuously from its maximum value down to zero. A single experiment allows the shock parameters to be monitored over a continuous range from those for zero propagation distance to those for some maximum distance determined by the geometry of the wedge. This is essentially equivalent to an infinite number of one-dimensional experiments.

1.2.2 Measurement Technique

In order to monitor the shock parameters for a continuous range of propagation distances in the two-dimensional experiment, a measurement technique is required which allows some parameter to be continuously monitored along the length of the wedge from the thick end to the tip. The instrumentation that was chosen is a variation of the slanted resistor technique[19] which has been used to monitor the free surface motion of samples in uniaxial strain experiments. In the one-dimensional case a resistance wire is mounted at an angle to the back surface of a specimen as shown in Fig. 1.2. As the back surface of the specimen moves out as a whole, it contacts the wire and shorts out that length of the wire between the specimen and the contact point. Monitoring the resistance of the wire provides a continuous history of free surface position.

The modification for the two-dimensional experiment is to place the resistance wire parallel to and offset from the back surface of the wedge, as shown in Fig. 1.3. As the shock sweeps along the wedge free surface, it causes the free surface to move off and contact the wire, shorting it out. Monitoring the resistance of the wire provides the time of arrival of the wedge free surface at a given distance from its initial position at every point down the length of the wedge. Using two wires with different offsets in the same experiment provides the time of the arrival of the wedge free surface at two distances for every position along the length of the wedge.

If all points on the wedge free surface moved off with a velocity normal to the original free surface, and if the velocity of points on the free surface stayed constant at all distances from their initial position, then the data from the two resistance wires would provide a continuous record of the free surface velocity as a function of position down the

6
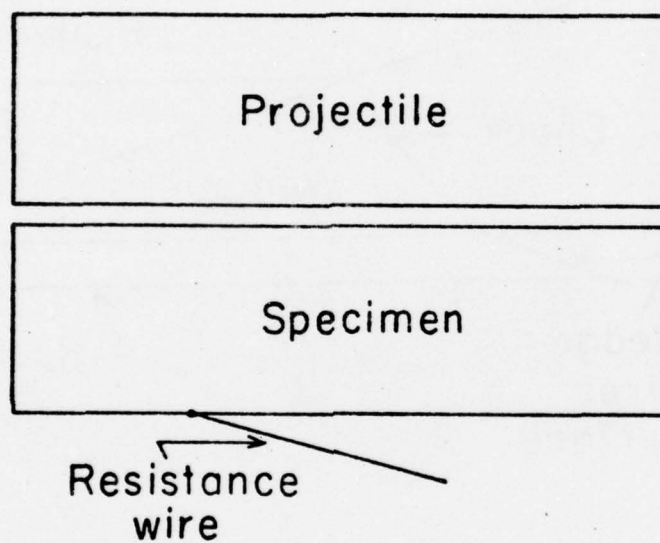
Fig. 1.2. Slanted resistance wire technique
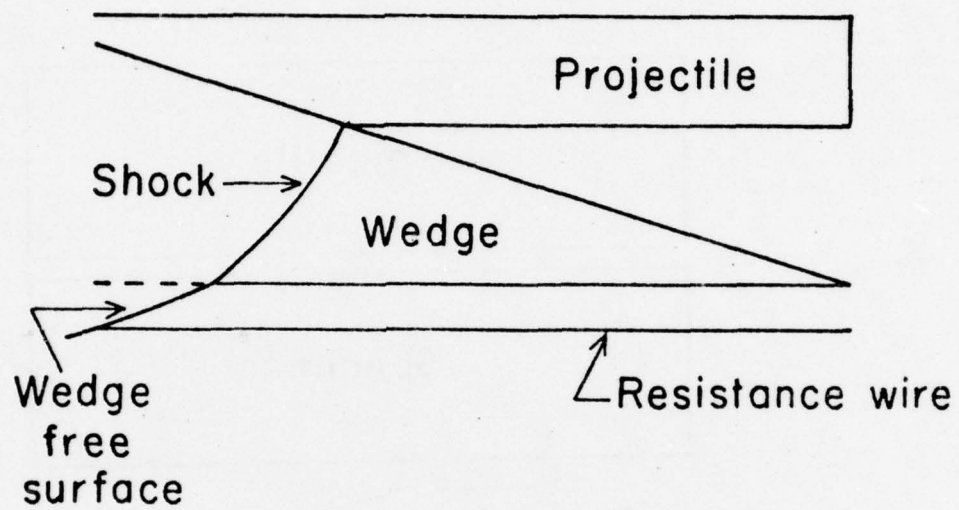
Fig. 1.3. Resistance wire measurement technique for two-dimensional flow

wedge. However, points on the free surface may move off with a velocity that is not normal to the free surface,[20] especially if the material is elastic.[21] Also, multi-wave structure may cause the free surface velocity to change with distance from its initial position. Thus, in general what is measured is related to the time average between the two offsets of the wires of the particle velocity at the free surface.

When rate effects and two-wave structures are involved, the shock strength will change with propagation distance, and thus the particle velocity will vary as a function of position along the wedge. The data from the wedge impact experiment using two resistance wires will provide the particle velocity as a function of position along the wedge, and thus can be used in the study of phase transitions and their rate effects.

1.2.3 Method of Analysis

Given a general experimental technique a means of analyzing the problem is required in order to properly design the experiments. Design considerations include projectile velocity, flyer material, wedge size and angle, target design, and placement of the resistance wires. Once the experiment has been performed, a means of interpreting the data is required in order to relate it to material properties.

Considering the overall complexity of the two-dimensional geometry and the different types of rate-dependent material properties involved, it was felt that the problem was much too complicated to rely on purely analytical solutions. Closed-form solutions, if they could be found, would require tremendous effort and be restricted by the simplifying assumptions required. The best overall means of analyzing the problem would seem to be by means of numerical techniques utilizing a digital computer.[22]

The numerical technique chosen must be capable of handling the entire general problem including multi-wave structures and their interactions with all boundaries and interfaces, material strength and its rate-dependent effects, and phase transitions. It must also be able to handle multiple materials and many different types of equations of state. In order to do this the technique must solve the system of partial differential equations describing the problem, subject to the proper boundary conditions. Many general techniques exist for the numerical solution of partial differential equations.[23,24] Among those that have been employed in codes written to solve shock propagation problems are the finite element method,[25] the method of characteristics,[26,27] and finite-difference methods.[28] The finite-difference methods are best adapted to the present problem because of the relative ease with which they handle different materials and the formation of multiple shocks.[29]

Finite-difference methods approximate the partial differential equations by finite-difference equations and apply these equations to a grid in time and space. Given the initial values of all variables at all points in the spatial mesh, the solution proceeds by a time-stepping technique to provide the values of all variables at all mesh points at later times.

Eulerian finite-difference methods apply the equations to a grid fixed in space through which the material moves, while Lagrangian finite-difference methods apply the equations to a grid which is fixed in the material and moves with it.[30] Eulerian methods have the disadvantage that material history is difficult to follow, while Lagrangian methods have the disadvantage that the grid becomes distorted as the material moves, and the calculation becomes inaccurate as the mesh distortion becomes large. Lagrangian codes are generally most useful for small impact velocities, and

10

Eulerian codes are most useful for large impact velocities where mesh distortion is very large.[31] There are also many techniques which combine both Eulerian and Lagrangian features in order to try to overcome the disadvantages of each.[32,33,34]

The primary intent of the present work requires keeping close track of material histories, and material distortion is not expected to be large, so a Lagrangian finite-difference method was chosen as the means for analyzing and interpreting the experiments.

Codes exist which utilize the above mentioned numerical techniques.[35,36,37,38,39,40] However, most are designed to be quite general and handle many different types of problems; they are thus quite bulky and inefficient in a specific application. Also, they do not contain the specific types of material properties and rate-dependent effects desired for this work. Therefore, a Lagrangian finite-difference code was written explicitly to solve the problem of a projectile impacting a wedge. It contains material strength, elastic plastic and strain-rate dependent behavior, and treats phase transitions. This may be used to interpret and analyze the two-dimensional experiments.

1.3 Summary

The intent of this work is to provide a measurement technique for use in two-dimensional strain experiments, and a method for interpreting and analyzing the experiments. The two-dimensional geometry is that of a projectile impacting a wedge, and the measurement technique is to record the free surface velocity as a continuous function of position along the wedge by use of resistance wires to detect free surface motion. A two-dimensional Lagrangian finite-difference code developed to handle wedge

11

impact problems is the basis for designing the experiments and interpreting the results. The primary application is in the study of the kinetics of phase transitions. However, the capability for performing and interpreting gas gun experiments in two dimensions may become useful in a wide variety of other problems.

2. SHOCK POLAR THEORY APPLIED TO INTERSECTING FLOWS

In order to gain a better understanding of the wedge impact experiment, it will be helpful to consider the problem from an analytical standpoint before proceeding to a computer solution. If all material strength effects, phase transitions, and rate-dependent effects are ignored, the problem can be treated as the intersection of two fluid flows.[41] Obviously this treatment neglects the main problems of interest, but it gives an approximate view of the general behavior of the wedge-projectile system.

By treating the material as a fluid, so that no stress deviators are allowed, shear waves cannot be produced. Therefore the main assumption is that the jump conditions[42,43] apply to the components of flow normal to the shock, and the tangential components are conserved across the shock. Under this assumption the components of flow behind the shock can be found. No interactions of the shocks with any of the material boundaries other than the impacting surfaces are considered.

The problem can be most easily analyzed from a reference frame in which the point of contact between the target and projectile is at rest, shown in Fig. 2.1. In the laboratory frame, or unprimed frame, this point moves down the face of the target with speed $V_p/\sin \alpha$. In the primed frame, the contact point is at rest. Thus the velocity components of the contact point in the unprimed frame are

$$V_x = -V_p/\tan \alpha \qquad (2.1)$$

$$V_y = -V_p \qquad (2.2)$$

This gives the velocity of the primed frame with respect to the unprimed

13

Projectile $\dot{x} = 0$
$\dot{y} = -V_p$
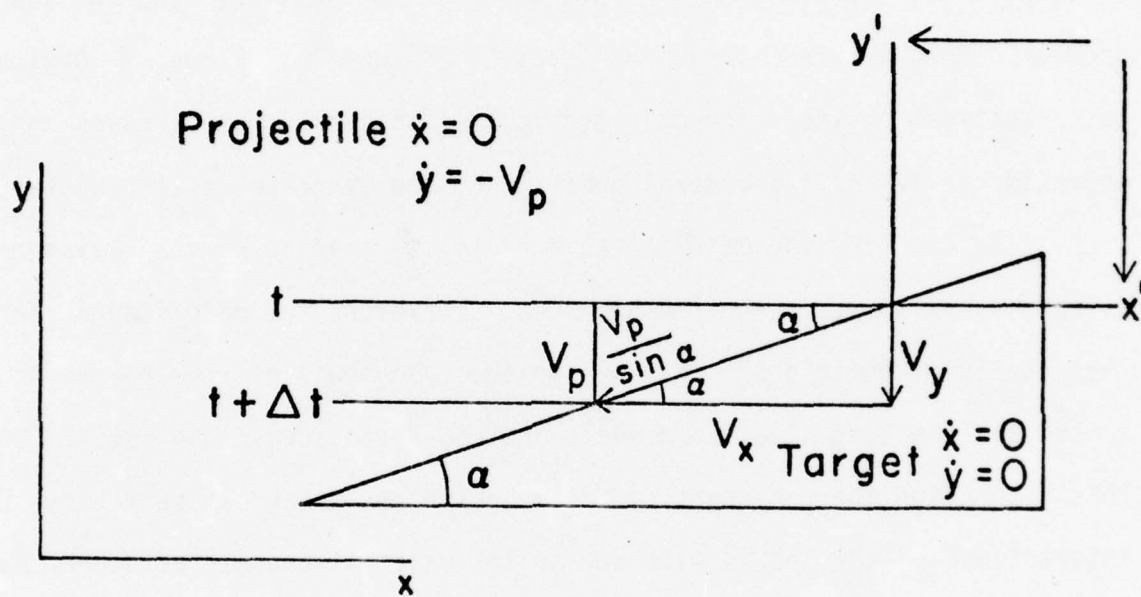
Fig. 2.1. Velocity components in two-dimensional flow configuration

frame. In general, if the primed coordinate system has velocity V_x and V_y in the unprimed system, the velocity transformation equations are

$$\dot{x}' = \dot{x} - V_x \tag{2.3}$$

$$\dot{y}' = \dot{y} - V_y \tag{2.4}$$

Since the target is at rest in the unprimed system and the projectile has velocity V_p in the -y direction, their velocities in the primed system become

$$\text{projectile:} \quad \dot{x}' = 0 - (-V_p/\tan \alpha) = V_p/\tan \alpha \tag{2.5}$$

$$\dot{y}' = (-V_p) - (-V_p) = 0 \tag{2.6}$$

$$\text{target:} \quad \dot{x}' = 0 - (-V_p/\tan \alpha) = V_p/\tan \alpha \tag{2.7}$$

$$\dot{y}' = 0 - (-V_p) = V_p \tag{2.8}$$

The angle ϕ made by the target velocity with the x' axis is

$$\phi = \tan^{-1}[V_p/(V_p/\tan \alpha)] = \alpha \tag{2.9}$$

The magnitude of the target velocity V_t in the primed frame is

$$|V_t| = \sqrt{(V_p/\tan \alpha)^2 + V_p^2} = V_p/\sin \alpha \tag{2.10}$$

In the system at rest with respect to the point of contact the configuration becomes that shown in Fig. 2.2.

To analyze this, consider a coordinate system in which a shock is at rest and the incoming flow is inclined at some angle θ, as in Fig. 2.3. The regular jump conditions apply to the normal components of the flow, and the tangential components of the flow are unchanged.

15
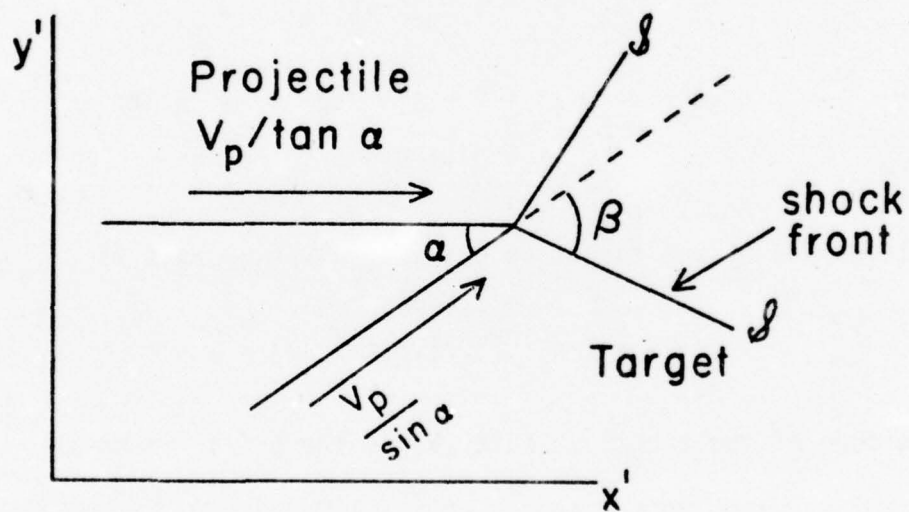
Fig. 2.2. Two-dimensional flow configuration in a coordinate system in which the contact point is at rest
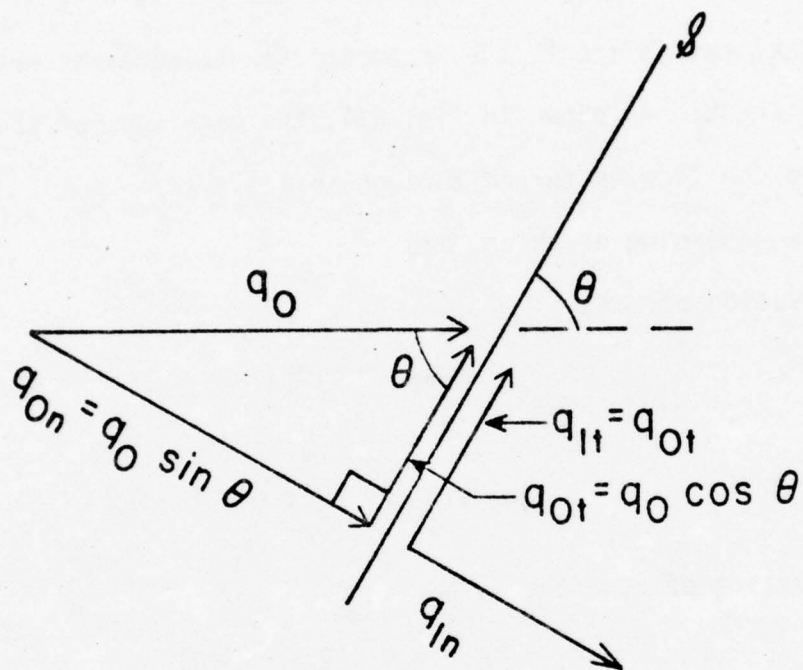
Fig. 2.3. Flow velocities for a stationary
oblique shock

The mass and momentum jump conditions for the normal components are:

$$\text{Conservation of mass: } \rho_o q_{on} = \rho_1 q_{1n} \qquad (2.11)$$

$$\text{Conservation of momentum: } P_1 - P_0 = \rho_o q_{on}(q_{on} - q_{1n}) \qquad (2.12)$$

It can be seen from Eq. (2.12) that since the pressure P_1 behind the shock is greater than that in front, the incoming flow velocity is greater than that behind the shock. As shown in Fig. 2.4, the magnitude of the flow is decreased and the flow is turned through an angle δ.

The governing equations are

1) Conservation of mass

$$\rho_o q_{on} = \rho_1 q_{1n} \qquad (2.13)$$

or

$$\rho_o q_o \sin \theta = \rho_1 q_1 \sin (\theta - \delta) \qquad (2.14)$$

2) Conservation of momentum

$$P_1 - P_0 = \rho_o q_{on}(q_{on} - q_{1n})$$

$$= \rho_o q_o \sin \theta [q_o \sin \theta - q_1 \sin(\theta - \delta)] \qquad (2.15)$$

3) Compatibility in tangential direction

$$q_{ot} = q_{1t} \qquad (2.16)$$

or

$$q_o \cos \theta = q_1 \cos(\theta - \delta) \qquad (2.17)$$

If the Hugoriot, or R-H curve,[44] of the material is added in the form of a U_s-U_p relation,

$$U_s = A + B U_p, \qquad (2.18)$$

where U_s is shock speed relative to the material ahead, and U_p is the change

18
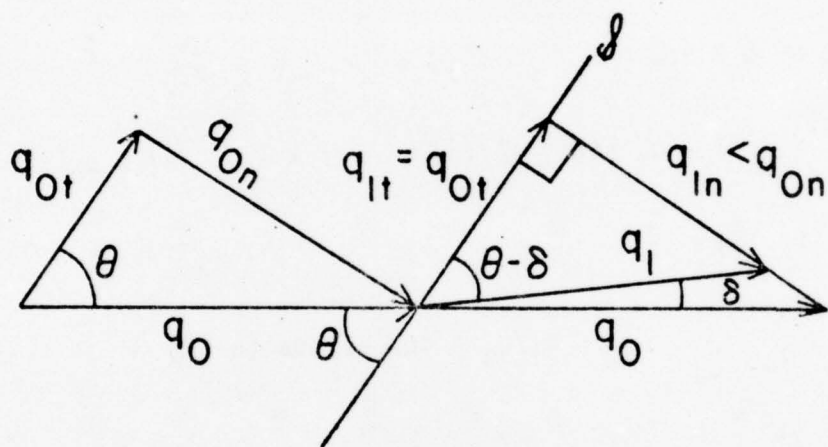
Fig. 2.4. Turning of the flow by an oblique shock

in particle velocity across the shock, the problem can be solved. In this case the shock moves parallel to itself with velocity $q_0 \sin\theta$ relative to the material ahead, and the change in particle velocity is

$$q_{on} - q_{1n} = q_0 \sin\theta - q_1 \sin(\theta-\delta) \qquad (2.19)$$

The Hugoniot equation is

$$q_0 \sin\theta = A + B[q_0 \sin\theta - q_1 \sin(\theta-\delta)] \qquad (2.20)$$

Dividing by $q_0 B \sin\theta$

$$1 - q_1 \sin(\theta-\delta)/(q_0 \sin\theta) = 1/B - A/(B q_0 \sin\theta) \qquad (2.21)$$

From Eq. (2.17)

$$q_1/q_0 = \cos\theta/[\cos(\theta-\delta)] \qquad (2.22)$$

So

$$[1 - A/(q_0 \sin\theta)]/B = 1 - [\tan(\theta-\delta)/\tan\theta] \qquad (2.23)$$

Given q_0 and θ, this can be solved for δ, and then

$$q_1 = q_0 \cos\theta/[\cos(\theta-\delta)] \qquad (2.24)$$

Given θ and q_0 the flow behind the shock can be found. Holding q_0 constant and letting θ vary yields the locus of endpoints of q_1 for different θ, which is called a shock polar,[45] Fig. 2.5. If θ equals 90 degrees, there is a one-dimensional shock and no turning, so δ equals 0. As θ decreases, q_1 increases while δ increases to a maximum value and then decreases again to zero for the value θ_{min} for which the shock speed $q_0 \sin\theta$ is equal to the sound velocity and there is no shock, so that q_1 is equal to q_0 and again δ equals 0.

20
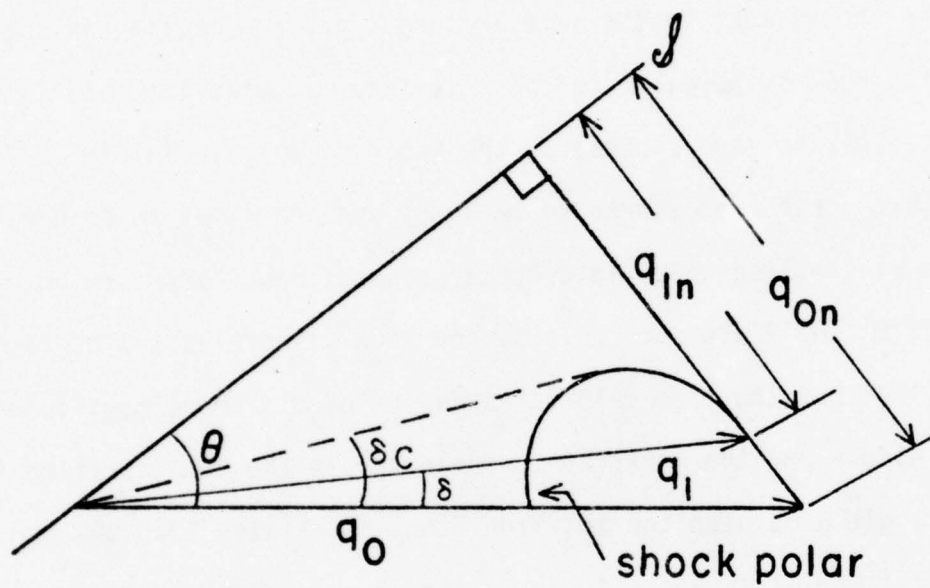
Fig. 2.5. Shock polar

The curved line in Fig. 2.5 shows the locus of all flows that can be reached by a shock for an incoming flow velocity q_0. δ_c is the maximum angle through which a flow of q_0 can be turned. Applying this to the shot configuration of Fig. 2.2, shock polars can be drawn for each of the incoming flows, Fig. 2.6. The target-projectile interface will be turned at some angle depending on the direction of the flow behind the shocks. The pressure behind the shocks must be the same in target and projectile and the flow in each region must be parallel to the interface, so that the materials do not separate. Looking more closely at the shock polars, as in Fig. 2.7, it may be seen that for the pressures to be equal and the flows to be parallel there must be a single line which intercepts point of equal pressure on each shock polar. If P' and P are such points, the flow velocities are of magnitude q_1 and q_1'. Thus the flow velocities may be of different magnitude so that there is slip along the interface. Obviously if the configuration is such that the angle α between the incoming flows is greater than the sum of the two critical angles δ_c and δ_c', as in Fig. 2.8, a shock cannot turn the flows so that they are parallel to the interface, and stable flow cannot exist. So for a given projectile velocity, there is a maximum wedge angle α for which stable flow can occur.

This analysis points out two restrictions on the wedge angle and projectile velocity in order to assure stable flow. The incoming flow velocities must be greater than the shock velocity, and the sums of the critical angles for the two flows must be greater than the wedge angle.

Variables behind the shock can be found graphically by use of the method of shock polars, or the problem can be solved explicitly. Equations (2.15) and (2.17) can be written for both the unprimed and primed flows.
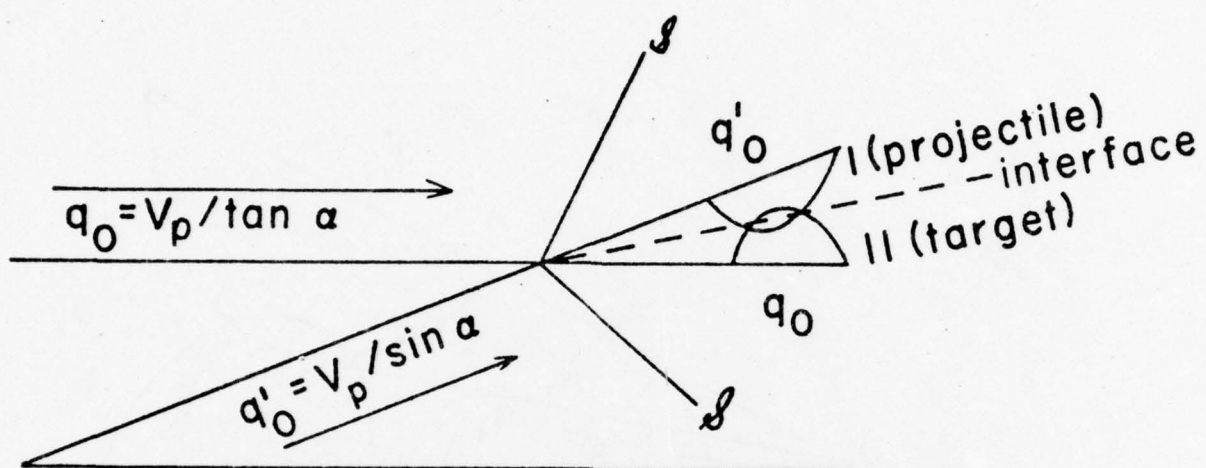
Fig. 2.6. Shock polars for the two-dimensional flow configuration
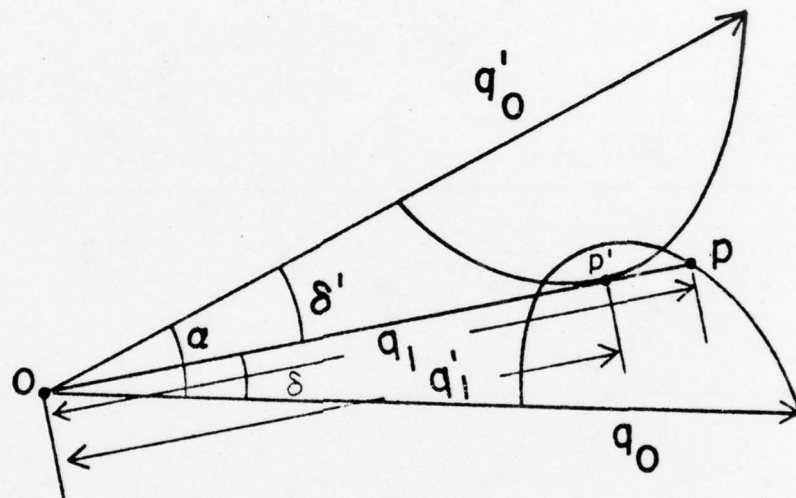
Fig. 2.7. Solution of the two-dimensional flow
configuration by the method of shock
polars
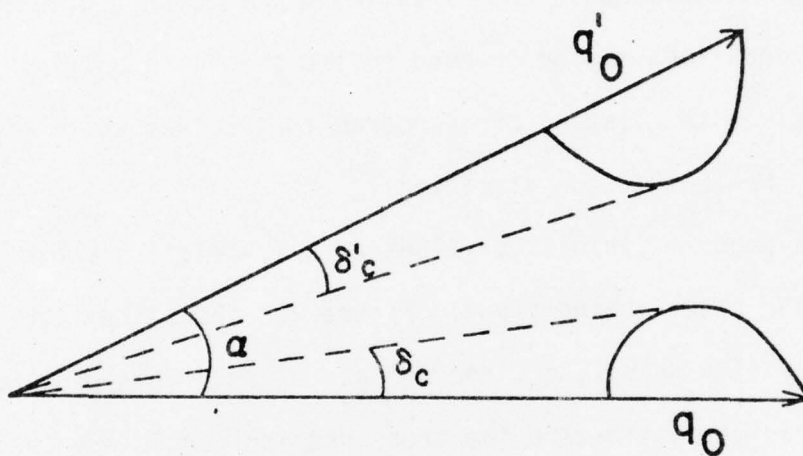
Fig. 2.8. Condition of unstable flow

There also exists a U_s-U_p relation for each material plus the two equations

$$\delta + \delta' = \alpha \tag{2.25}$$

and

$$P_1 = P_1' \tag{2.26}$$

yielding eight equations in the variables q_1, θ, δ, P_1, q_1', θ', δ', and P_1'. These equations may be reduced to two involving only θ and θ'. Appendix A gives the listing of a program that solves these simultaneous equations by Newton-Raphson iteration.[46]

This program yields the values of all variables behind the two shocks created by the intersecting flows. Figure 2.9 shows the flow variables which the program yields when α, q_o, and q_o' are given. This provides a simple method for rapidly estimating the pressures and particle velocities produced for a given wedge angle and projectile velocity.
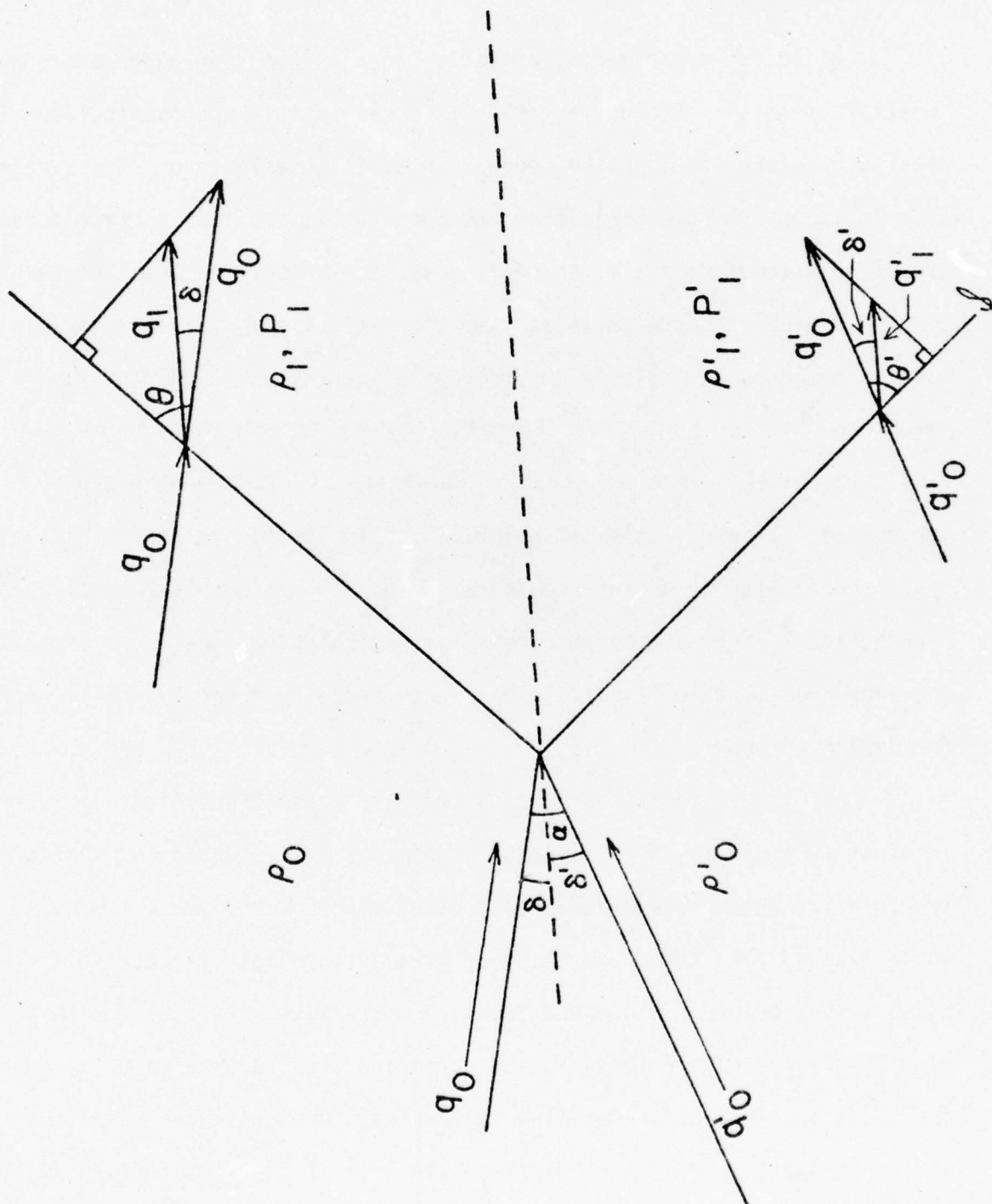
Fig. 2.9. Intersection of two flows

27

3. EXPERIMENTAL METHOD

Designing experiments basically requires choosing wedge angle and impactor velocity. Choices are made to assure stable supersonic flow with desired pressure level in the wedge. In addition effects of stress relaxation in transforming materials on the shock waves and free surface motion should be estimated; estimates of free surface velocities are also helpful.

Choice of wedge angle and impactor velocity for given materials was made using computer analysis (hydrodynamic) described in Chapter 2. One obtains curves like those shown in Fig. 3.1 for aluminum on potassium chloride (low pressure phase). Curvature at low pressure end of the curves indicates onset of instability. In addition free surface velocity was estimated by adding a calculation of flow through a Prandtl-Meyer rarefaction.[20] For polymorphic materials calculations were done separately for each phase; phase II calculations were hence in error but still useful for design purposes.

For stress relaxation associated with phase transitions it is of interest to estimate the separation of phase I and II waves and characteristic length along which stress relaxation takes place on the phase I wave; one would like to make the measurement of free surface velocity due to the phase I wave before disturbance from the phase II wave arrives at that position as well as have an idea at what position free surface velocity changes due to stress relaxation will be manifested. Computational results for stress relaxation in KCl are displayed in Figs. 3.2 and 3.3; computations are based on analysis given in a previous report.[2]

28
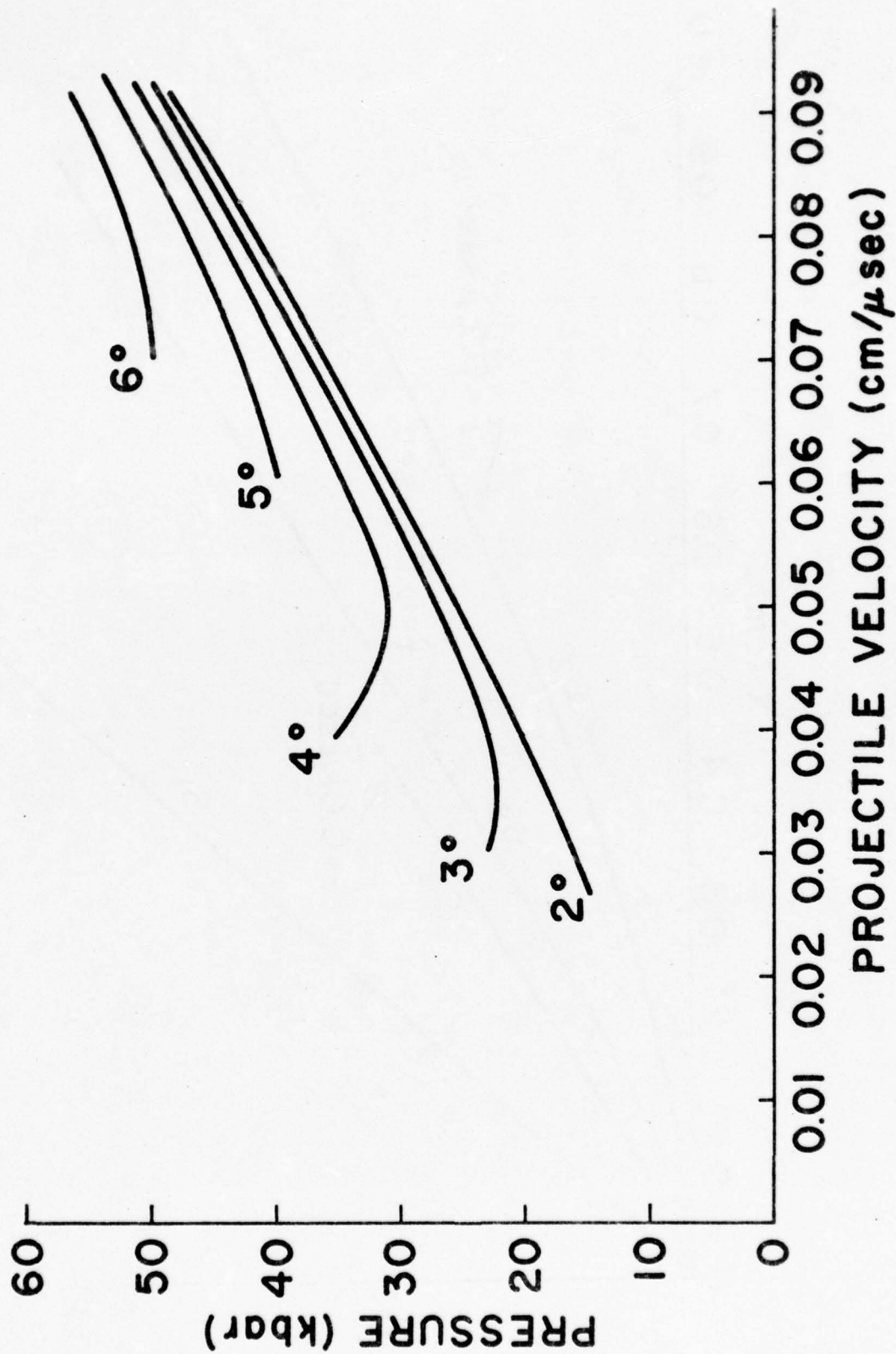
Fig. 3.1. Pressure-particle velocity curves for several collision angles for aluminum impacting potassium chloride
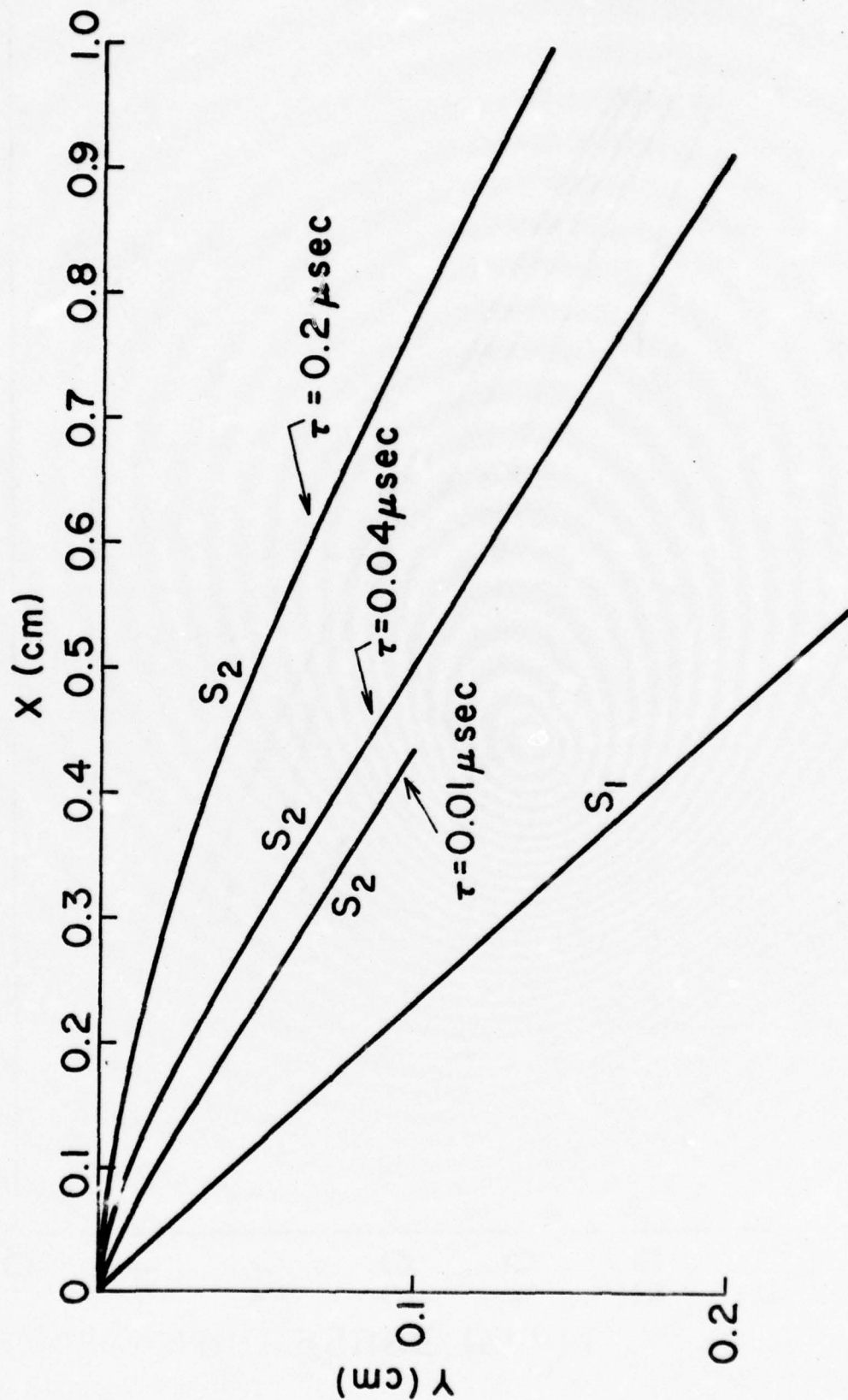
Fig. 3.2. Calculated wave profiles in potassium chloride wedge showing variation of phase II wave S_2 with relaxation time
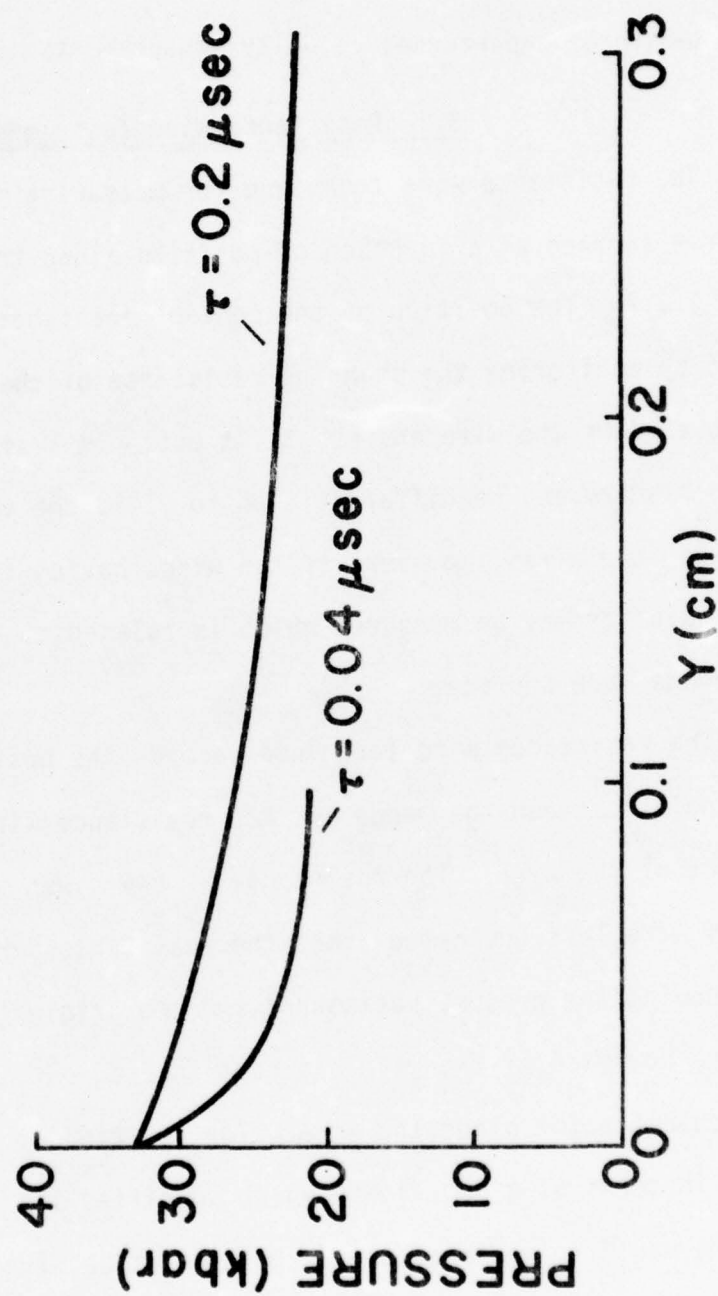
Fig. 3.3. Calculated pressure relaxation on phase I wave in potassium chloride wedge for two values of relaxation time

At the wedge tip one also needs to consider what happens as impact disturbance reaches the tip and reflects as a rarefaction. For some distance back from the tip the rarefaction will disturb free surface motion before ribbon shorting is completed at that position, placing a limit on the domain of unperturbed velocity measurements.

3.1 Resistance Wire Technique

The resistance wire technique for measuring particle velocity at the wedge free surface as a function of position along the wedge is described in Section 1.2.2. The position of the contact point between wedge and wire is followed by monitoring the changing resistance of the wire as the contact point moves down the wire and shorts it out. If a single wire is used, this position history may be differentiated to yield the velocity of the contact point along the wire. However, if two wires having different offsets are used, a quantity may be measured which is related to the particle velocity at the wedge free surface.

The resistance wire technique records the position history of the contact point between the wedge and the resistance wire by monitoring the resistance of the wire. The resistance at any given time is equal to the length of wire left unshorted times the resistance per unit length of the wire. Knowing the present resistance and the original length of the wire determines how much of the wire has been shorted out and thus the position of the contact point along the wire. The position of the contact point must be given in terms of a coordinate which specifies its location. One such coordinate would be distance along the wire. Thus the position of the contact point would be specified by the length of wire shorted out. However, what is of interest is the position of the contact point in relation to the wedge. Since the wire extends past either end of the wedge, the length of

32

wire shorted out does not specify the position of the contact point in relation to the wedge.

The coordinate which will be used to specify the position of the contact point will be the distance x along the original wedge free surface. Thus x will be zero at one end of the wedge and be equal to the wedge length at the other end. The length of wire shorted out may be related to x by knowing the distances that the wire extends past either end of the wedge. All points on a line normal to the original wedge free surface and passing through wedge position x will also have coordinate x. Thus when the contact point is said to be at wedge coordinate x, it is meant that a line through the contact point normal to the original wedge free surface will intersect the original position of the wedge free surface at coordinate x. x is essentially a Lagrangian coordinate in that it gives positions relative to the original location of the wedge free surface and not to its present position. The measured free surface velocity at wedge coordinate x is the distance between two wires divided by the difference in time between the contact point on wire 1 being at wedge coordinate x and the contact point on wire 2 being at wedge coordinate x.

The measured free surface velocity is not equal to the actual free surface velocity if points on the wedge free surface do not have velocities normal to the original wedge free surface. In Fig. 3.4 point P_1 on the wedge free surface has contacted the wire with offset D_1 at wedge coordinate x_1. If the velocity of point P_1 were normal to the original wedge free surface, point P_1 would also contact the wire with offset D_2 at wedge coordinate x_1. However, if the velocity of P_1 is not normal to the original wedge free surface, a different point, say P_2, will contact the wire with offset D_2 at wedge coordinate x_1. This will occur at time $t + \delta t$. At this

33
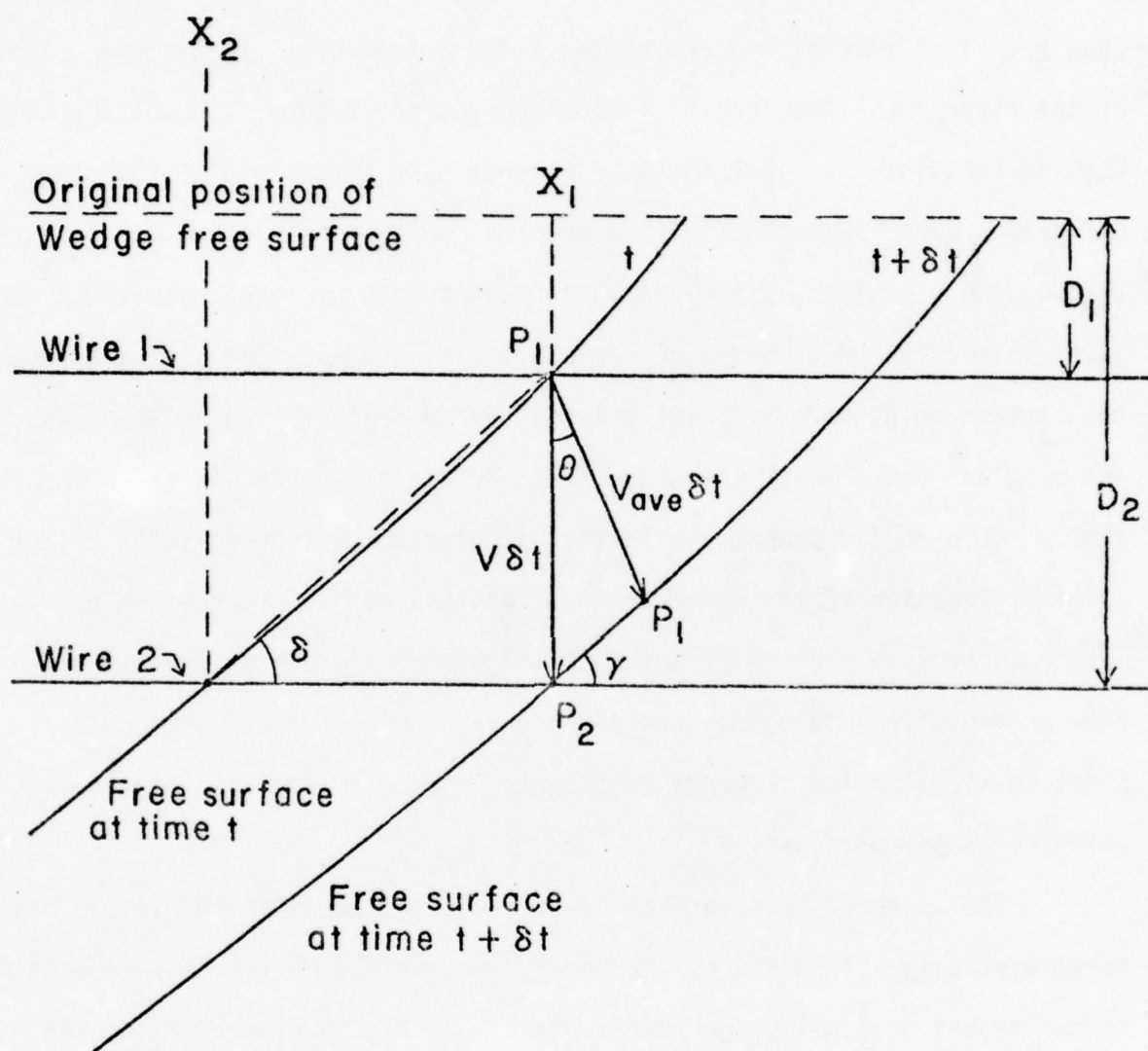
Fig. 3.4. Resistance wire monitor for free surface velocity

time point P_1 on the free surface will not be a contact point with wire 2. In the time δt the distance moved by point P_1 will be $|\vec{V}_{ave}|\delta t$ where $\vec{V}_{ave}$ is the time average of the velocity of point P_1 during the time δt, which is just the vector from point P_1 at t to point P_1 at $t + \delta t$. $\vec{V}_{ave}$ makes an angle θ with the normal to the original free surface. The angle made by the line joining points P_2 and P_1 on the free surface at time $t + \delta t$ and wire 2 is γ.

To produce a free surface velocity from the resistance wire data, the data is reduced as though points on the wedge free surface do have velocities normal to the original free surface. Thus the measured velocity of the free surface at wedge coordinate X is $\vec{V}$ which is normal to the original free surface and has magnitude

$$V = \frac{D_2 - D_1}{\delta t} \tag{3.1}$$

This can be related to the actual time averaged velocity of point P_1 by use of the law of sines.

$$V = \frac{V_{ave} \cos(\theta - \delta)}{\cos \gamma} \tag{3.2}$$

If the points on the free surface do not have velocities normal to the original wedge free surface, the same point on the wedge free surface does not contact both wires at the same wedge coordinate, and the measured velocity is not equal to the actual time averaged velocity of either of the two points which do contact the wires at that wedge coordinate. Although it would be desirable to follow the history of a single point on the free surface, the measured quantity is unimportant so long as it is understood exactly what is being measured. A computer code can simulate the same resistance wire records that are produced in the experiment.

35

Even though the measured velocity is not that of a single point on the free surface, the discrepancy is not large. In Fig. 3.4 the deflection angle of the free surface is greatly exaggerated. This angle would normally be less than 10 degrees. The ratio of V to V_{ave} has its maximum when θ is equal to γ, at which point the ratio is equal to sec γ. As θ increases to 2γ the ratio decreases back to 1. If γ is equal to 10 degrees, V is 1.5% greater than V_{ave} at the maximum. In most cases of interest the measured value of velocity is within a few percent of the true time-averaged value, even though the value of θ is not found by this method.

It is also possible to measure the average angle of free surface deflection by use of the two-wire technique. The deflected free surface may not be a straight line if rate-dependent effects are involved, but at any time t the wedge coordinates x_1 and x_2 of the two contact points are known. The tangent of the average angle of deflection δ of the free surface between the two wires is then

$$\tan \delta = (D_2 - D_1)/(x_2 - x_1) \tag{3.3}$$

Changes in any of the measured quantities will reflect unsteady behavior, and a computer simulation of the resistance-wire data can be used to identify the rate-dependent effects involved.

3.2 Circuitry and Electronics

In order to monitor the position of the contact points between the wedge and the wires, the wires are made part of the voltage divider network shown in Fig. 3.5. The relation of the wires to the target is shown in Fig. 3.6. The wire is stretched between two terminals. The terminal nearest the high end of the wedge is at ground, as is the wedge. The other terminal is at voltage V_M. The variable resistance shown in Fig. 3.5 consists of the

36
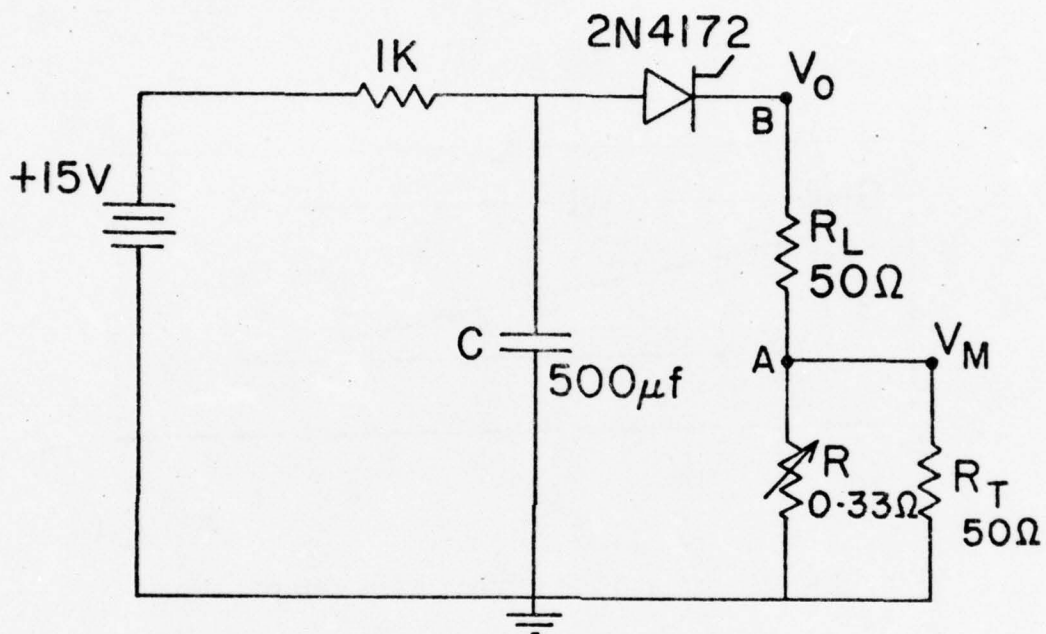
Fig. 3.5.   Single wire voltage divider network
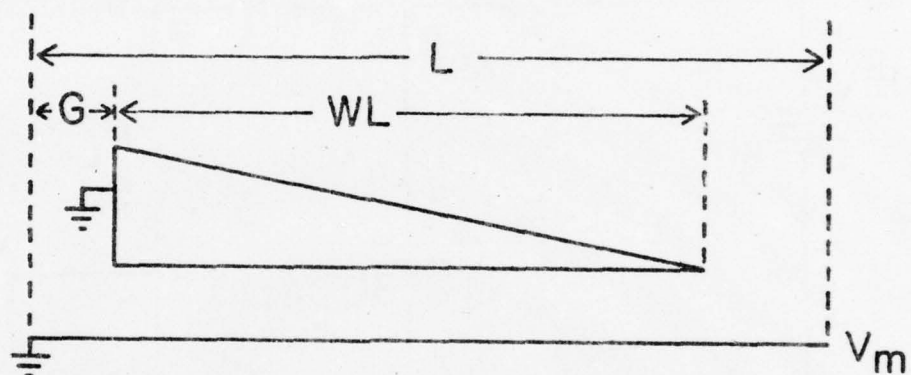
Fig. 3.6. Wedge and resistance wire setup

wire and wedge system. As the contact point between wedge and wire moves down the wire, that portion of the wire between the grounded terminal and the contact point comes to ground potential, and the variable resistance R consists of the resistance in that portion of the wire between the contact point and the ungrounded terminal. The values of the capacitor C and load resistor R_L are chosen so that the voltage V_o across the network stays effectively constant over the time interval of the experiment. As R decreases the voltage V_M varies. This voltage is measured with an oscilloscope which has termination resistance R_T. Thus, V_o, V_M, R_L, and R_T are known at all times during the experiment, and the resistance R is given by

$$R(t) = \frac{R_L}{\frac{V_o}{V_M(t)} - \frac{R_L}{R_T} - 1} \qquad (3.4)$$

If the resistance per unit length, K, of the wire is uniform, and the distances in Fig. 3.6 are known, the position of the contact point can be found. Taking the wedge coordinate X as being zero at the tip and increasing toward the thick end of the wedge, the coordinate of the contact point at time t is

$$x(t) = WL + G + \frac{R(t)}{K} - L \qquad (3.5)$$

where WL, G, and L are defined in Fig. 3.6.

The average free surface deflection angle is

$$\tan \delta = \frac{D_2 - D_1}{x_2(t) - x_1(t)} \qquad (3.6)$$

and the measured free surface velocity at X is

39

$$V(x) = \frac{D_2 - D_1}{\delta t(x)} \tag{3.7}$$

where $\delta t(x)$ is the time interval between the contact point on the first wire being at x and the contact point on the second wire being at x.

The above procedure may be followed for each of the two wires used. A typical photographic record of the oscilloscope trace of the voltage V_M measured across the parallel combination of the variable wire resistance R and the oscilloscope termination resistance R_T is shown in Fig. 3.7. The 2N4172 SCR is triggered just prior to impact so that the voltage of the capacitor appears across the resistance network. The oscilloscope is triggered externally at impact by use of a pin placed in the target. The voltage stays constant until shocks have propagated through the wedge and the free surface has moved out to contact the wire. The jump is produced by the sudden shorting of a finite length of the wire at first contact. As the contact point proceeds down the wire toward the wedge tip, the variable resistance R decreases and the voltage V_M decreases. As can be seen from Eq. (3.4), there is a non-linear relation between the resistance R and the voltage V_M so that a constant rate of wire shorting does not produce a voltage-time profile with a constant slope. The data points are read from the photographic record by means of a travelling microscope giving horizontal and vertical coordinates of the trace.

When the voltage profile $V_M(t)$ is obtained, Eq. (3.4) can be used to obtain the resistance history. This requires that the quantities R_L, R_T, and V_0 be measured. All components in the circuit in Fig. 3.2 except the resistance wire and the 50 ohm cable termination at the oscilloscope are in an external power supply container. Point A in Fig. 3.5 at which the

40
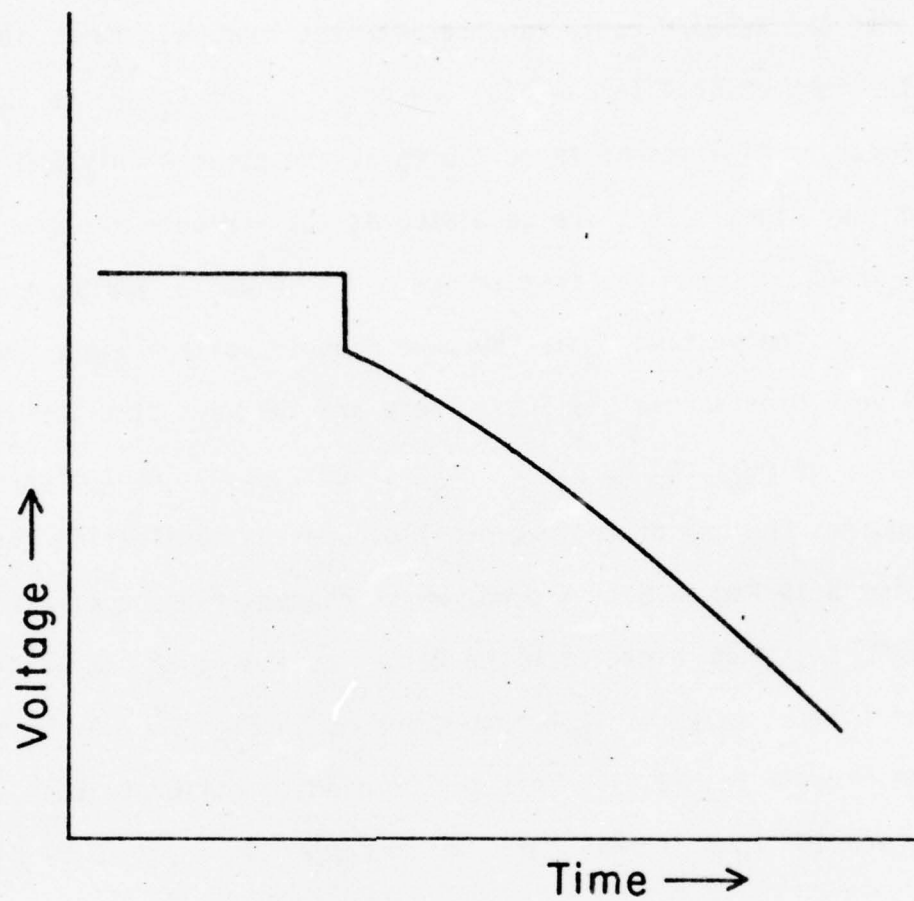
Fig. 3.7.   Voltage record from resistance wire experiment

resistance is measured is on the target at the non-grounded wire terminal. Fifty ohm RG58A/U cable runs between the load resistance and point A, and also from point A to the oscilloscope. R_L and R_T are 50 ohms to provide proper termination of these cables at the power supply and the oscilloscope for any signals that are generated at the variable resistance. Resistances R_L and R_T include the resistances of these cables and connections.

The voltage V_O is the power supply voltage minus the approximately .8 volt drop across the SCR. There are two ways of determining this voltage. It may be measured by use of an oscilloscope during the experiment. This requires the use of another oscilloscope and termination resistance from point B in Fig. 3.5 to ground, which changes the actual circuit. However, if V_O is known, along with the values of the other components in the circuit, the initial value of V_M before the jump in Fig. 3.7 may be determined from the circuit Eq. (3.4). This may be used to calibrate the oscilloscope used to measure V_M. In this case, V_O is replaced in Eq. (3.4) by

$$V_O = V_{Mo} \left(\frac{R_L}{R_O} + \frac{R_L}{R_T} + 1 \right) \tag{3.8}$$

where V_{Mo} is the value of V_M before the wedge contacts the wire, and R_O is the initial resistance of the wire installed in the target. Equation (3.4) then becomes

$$R(t) = \frac{R_L}{\frac{V_{Mo}}{V_M(t)} \left(\frac{R_L}{R_O} + \frac{R_L}{R_T} + 1 \right) - \frac{R_L}{R_T} - 1} \tag{3.9}$$

which depends only on the ratio of V_{Mo} to $V_M(t)$. If the voltage deflection is uniform up and down the oscilloscope face, then

42

$$\frac{V_{Mo}}{V_M(t)} = \frac{h_o f_D}{h(t) f_D} = \frac{h_o}{h(t)} \qquad (3.10)$$

where f_D is the voltage deflection factor of the oscilloscope, h_o is the distance on the scope face from the zero voltage line or baseline to the initial voltage level, and $h(t)$ is the distance from the baseline to the voltage level at time t. Thus the voltage deflection of the scope need not be known.

Alternatively, the scope used to measure V_M may be carefully calibrated, and the value of V_{Mo} may be used to calculate V_o by use of Eq. (3.8). Either method requires the calibration of one oscilloscope and the use of it to measure a voltage.

Once $R(t)$ is determined, Eq. (3.5) yields $X(t)$ once WL, G, K, and L are measured. Determination of X for both wires requires measurement of R_L, R_T, R_o, V_o, V_{Mo}, $V_M(t)$, WL, G, K, and L for both wires. $x_1(t)$ and $x_2(t)$ are given as tabulated data pairs of X and t. The data points are not generally read at matching values of time or x coordinate, so that interpolation must be used in order to find values of x_1 and x_2 at the same time value, or the time values for which the contact points are at the same wedge coordinate. A maximum number of data points must be read in order to assure adequate interpolation.

After interpolating to find $x_2(t)$, $x_1(t)$, and $\delta t(x)$, Eqs. (3.6) and (3.7) yield the average free surface deflection angle δ and the measured free surface velocity $V(x)$, once D_2-D_1 is known. However, it was discovered that because of measurement errors, the above procedure is inadequate for determining $V(x)$. Data from different shots built to be as identical as possible were not repeatable. For some of the many quantities that had to

43

be measured, a change in value of only one or two percent produced a ten or twenty percent change in $V(x)$.

The amount of error produced depends on the distance D_2-D_1 between the two resistance wires. Because of the possibility of quantities changing in time due to rate-dependent effects, it is desirable to make D_2-D_1 as small as possible so that changes are not obscured by the time averaging that occurs between the two wires. The smaller this distance, however, the smaller the time interval $\delta t(x)$ that the free surface requires to cross it. Plotting the contact point position versus time as in Fig. 3.8, $\delta t(x)$ is the horizontal distance between the two curves at constant wedge coordinate. If at some point errors in values of the measured quantities have caused either curve to be only one percent away from the true value, the total error in time at that point may be a very sizeable fraction of $\delta t(x)$. Very small errors in the calculated values of $x(t)$ could produce unacceptable error in $\delta t(x)$ and thus $V(x)$.

Because of these difficulties an alternate data reduction technique was devised in which values of $\delta t(x)$ are read directly from the photographic record of the oscilloscope trace so that none of the above measurements or calculations are involved. The procedure is to build the circuits for the two wires so that all components match as closely as possible. The single-wire circuit in Fig. 3.5 is modified to become the two-wire circuit of Fig. 3.9. With this arrangement the same voltage V_o is across both resistance networks. Again, the values of the resistances and capacitances are such that V_o is essentially constant during the time of the experiment regardless of changes in R_1 and R_2. Resistances R_1 and R_2 were matched by use of an impedance bridge to better than .002 ohms. Special terminations were built whose resistances also matched to the same accuracy. Leads and cables were

44
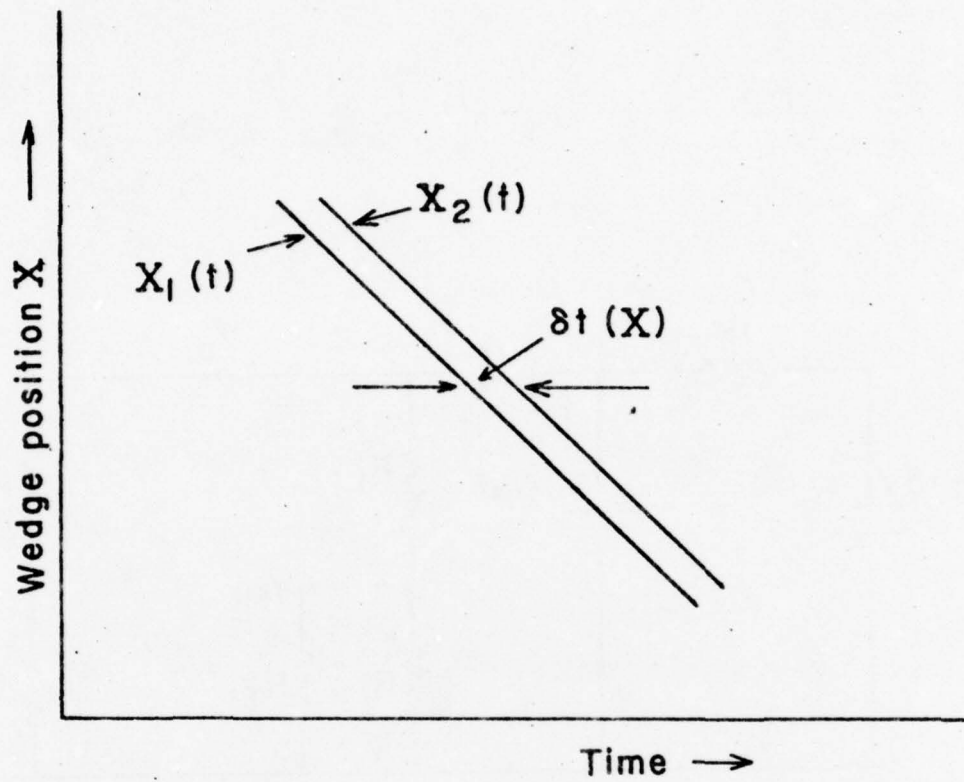
Fig. 3.8. Contact point histories

45
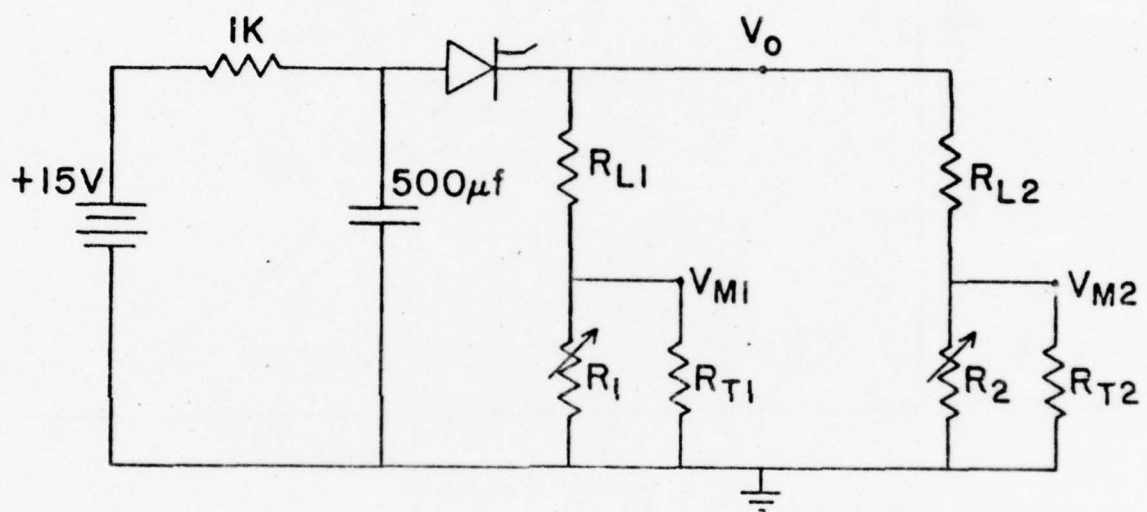
Fig. 3.9   Two wire voltage divider network

all matched to the same length. The targets were built so that both wires had the same length when mounted so that R_{o1} and R_{o2} matched to within .01 ohms. By carefully building the circuits to be identical, the initial voltages V_{M1o} and V_{M2o} can be made to match to better than .01%. If the values of R_L, R_T, and V_o in Eq. (3.4) are the same for both circuits, along with the values of WL, G, K, and L in Eq. (3.5), then identical values of $V_{M1}(t)$ and $V_{M2}(t)$ will yield the same values of $x_1(t)$ and $x_2(t)$.

Voltages $V_{M1}(t)$ and $V_{M2}(t)$ are measured on a Tektronix 7844 dual-beam oscilloscope on which both beams can be swept by the same time base. Signals from the two wires go through different vertical amplifiers whose gains and baselines can be set so that the traces are superimposed on the screen when identical signals are introduced at each input. With this system each point on the screen corresponds to the same time and same voltage for both traces. Since equal voltages correspond to equal wedge coordinates, all that is required to measure δt is to calibrate the time base by use of timing marks and read the horizontal distance between the two traces at equal vertical displacements. The time calibration is used to determine δt from this distance.

With this procedure none of the actual values of any of the quantities R_L, R_T, R_o, V_o, WL, G, K, or L for either of the two wire systems need be used in the calculation of δt so long as care is taken to see that corresponding values match as closely as possible between the two systems. To insure that they do, the initial values of voltages V_{M1} and V_{M2} can be compared with a differential amplifier. Since the wire length L and resistance per unit length K combine to produce R_o, and R_{o1} matches R_{o2} if the initial voltages match, the only other quantities of concern are the wedge length WL, and distance G from the wedge end to the ground terminal on the wire. WL is

47

naturally the same for both wires and the target can be easily built so that the values of G match.

This procedure also has the advantage that voltage calibrations of the oscilloscope have no role in the determination of δt. So long as a given vertical displacement corresponds to the same voltage for each beam, the value of the voltage is unimportant. In fact, the deflection factor need not be constant up and down the scope face so long as it is the same everywhere for both beams.

Thus, with the use of matching systems and a dual-beam oscilloscope, the values of δt may be read directly from a single photographic record, and the measured velocity V may be determined immediately at each desired vertical position on the record. Since no interpolation needs to be done, it is not necessary to read a large number of data points. In order to pair each value of measured velocity with the wedge position at which it occurred, Eqs. (3.4) and (3.5) may be used to determine $x(t)$ for one of the two traces. Then $V(x)$ will be given as pairs of values of V and x. It is necessary to know the values of R_L, R_T, V_o, WL, G, K, and L to determine $x(t)$, but since $x(t)$ is to be used as given and not differenced with another position history, there is no problem produced by the small errors that may be present in $x(t)$.

Figure 3.10 shows a record obtained in a two-wire experiment utilizing matching systems and a dual-beam oscilloscope. Nominal values for the components in the circuit of Fig. 3.6 are 50 ohms for the load and termination resistances, 500 micro-farads for the capacitor, and 33 ohms for the resistance wires. The initial value of V_M is about four volts, given that the power supply voltage is 15V and there is approximately .8 volt drop across the SCR. The wire is a ribbon .003 inches wide by .0005 inches thick with

48
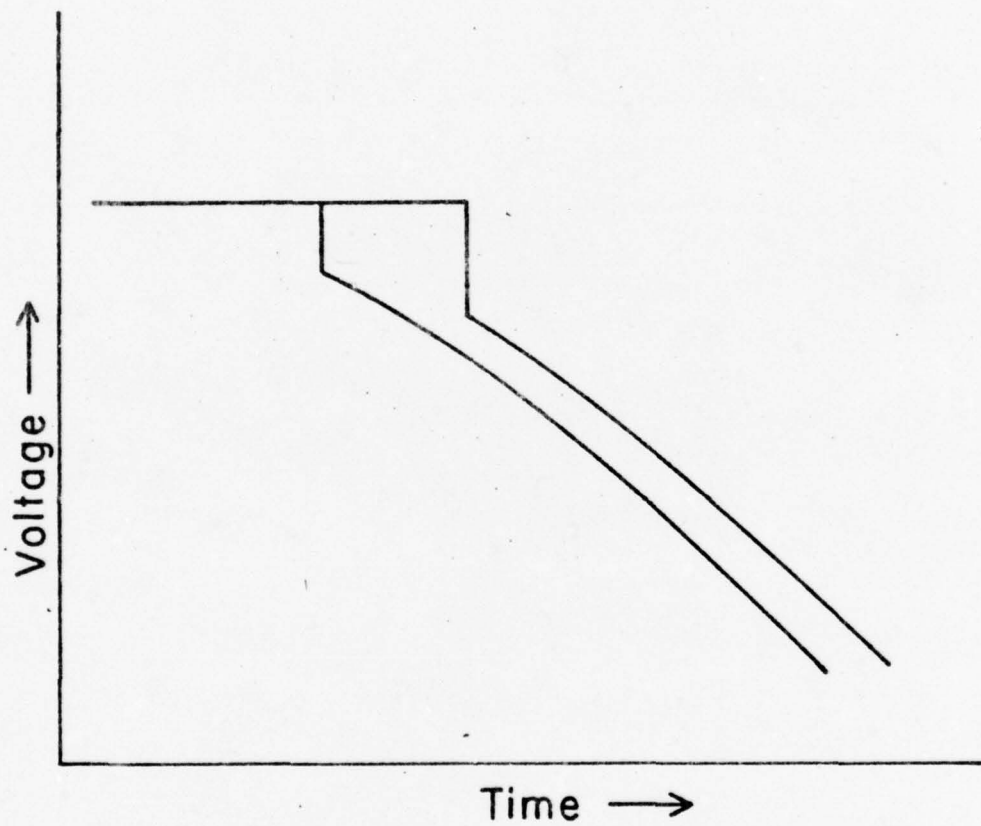
Fig. 3.10   Resistance wire record using dual beam
oscilloscope

a composition of 92% platinum and 8% tungsten and a resistance per unit length of 6.48 ohms per centimeter.

A schematic of the electronic set-up used in the shots with the dual-beam oscilloscope is shown in Fig. 3.11. The SCR is triggered by the output of the first velocity pin which is about four centimeters from the high point of the wedge. Depending on the projectile velocity the voltage V_o will appear across the resistance network 40 to 80 microseconds before impact. The power dissipated in the wires is about one-half watt so there is no problem with wire heating. The oscilloscope is triggered externally from a trigger pin set flush with the high end of the wedge. The total duration of the experiment depends on the wedge angle and projectile velocity, but is usually about five microseconds.

3.3 Wedge and Target Preparation

The largest wedge which may be used with the four inch diameter WSU gas gun is approximately 2.8 inches square. All wedges used to date have been 1.75 inches square. The wedge angles which have been used are four and five degrees. In order to prepare the wedges a jig is first manufactured whose top face makes the proper angles with its bottom surface. Blocks of the wedge material are screwed to the face of the jig and the block is then milled parallel to the bottom surface of the jig. Milling continues until the wedge tip is near the desired thickness. While still fixed to the jig, the top surface of the wedge is then lapped preferentially until the wedge surface is parallel to the jig back surface to an acceptable degree. This is checked by using a 400 power microscope with a depth of field less than one micron and a dial indicator attached to the lens to measure the difference in distance from the bottom of the jig to the top of

50
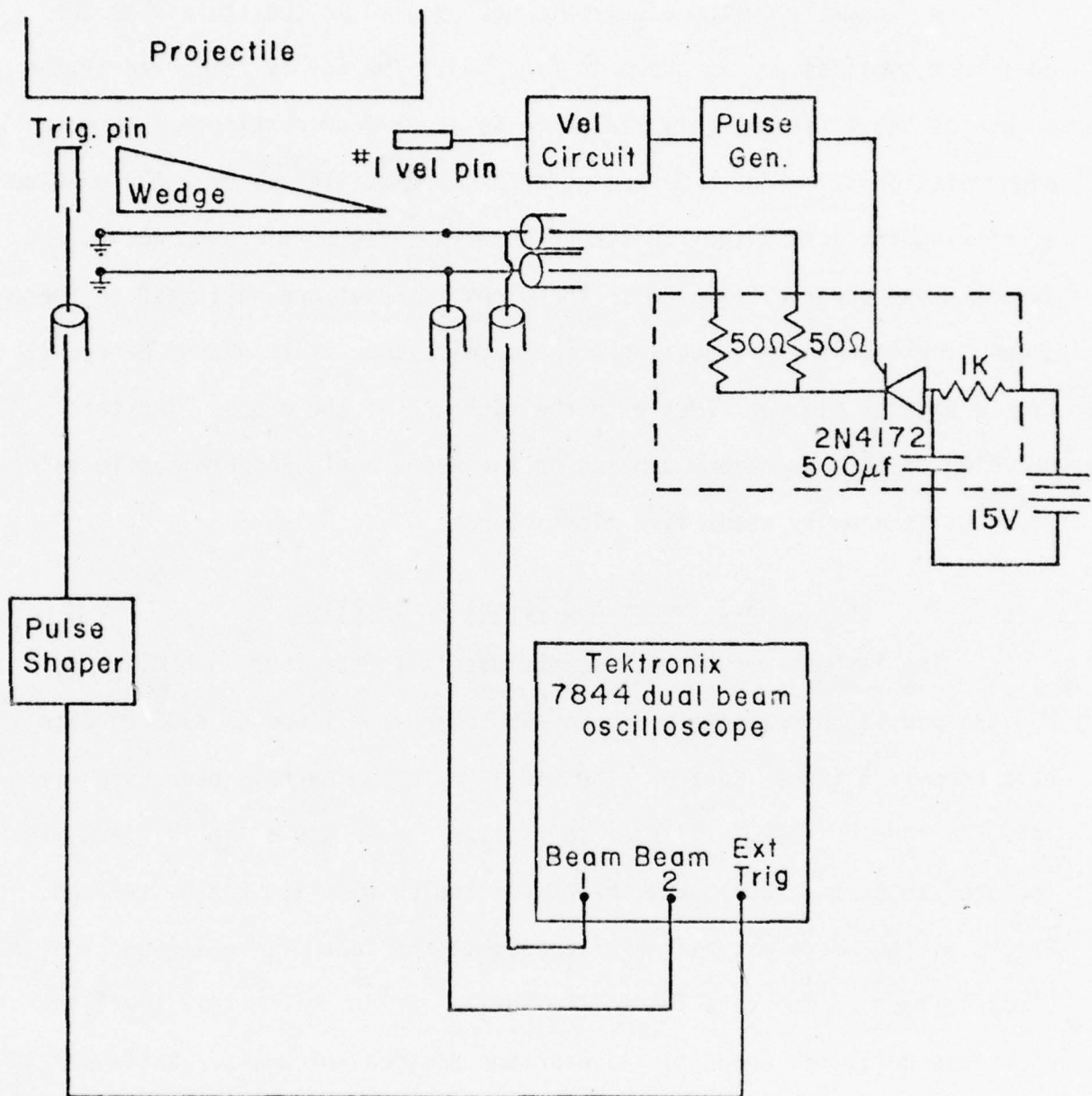
Fig. 3.11. Electronic setup for resistance wire shot using dual beam oscilloscope

the wedge surface over the area of the wedge. This difference is held to a maximum of two microns. If the wedge material is an electrical conductor, it is then ready to be mounted in the target. If it is a non-conductor, a conducting film must be deposited on the back surface of the wedge in order to short the resistance wires. The KCl wedges used had a gold film approximately 1.3 microns thick vacuum evaporated on the back surface.

The target assembly is a one piece structure machined from a block of 6061-T6 aluminum. As can be seen in Fig.3.12, the target is six inches in diameter. The rim of the impact side is the target mounting surface. This fits flush against the target holder fixed to the end of the gun barrel. The target holder is mechanically aligned to lie in a plane perpendicular to the axis of the gun barrel. The flange around the outside of the target is used to clip the target to the target holder. The wedge mounting surface is recessed below the target mounting surface slightly more than the wedge thickness. The wedge is secured to the wedge mounting surface by use of the same screw holes used to hold the wedge in the jig. There is an opening directly underneath the wedge so that it is supported only along the outside edges. The distances from the points of support to the wires are such that no signals from these points can interfere with the wire shorting. At either end of the opening steps are cut into the wedge mounting surface to depths equal to the offsets desired for the two wires. At the end at which the wire is to be grounded the steps are cut directly into the aluminum target. At the other end a block of insulating material is inserted into the wedge mounting surface and the steps are cut into this. The target mounting surface, wedge mounting surface, and wire mounting steps are all machined without moving the target in its holding device on the mill so that all should be in parallel planes. Figure 3.13 shows the target dimensions and

52
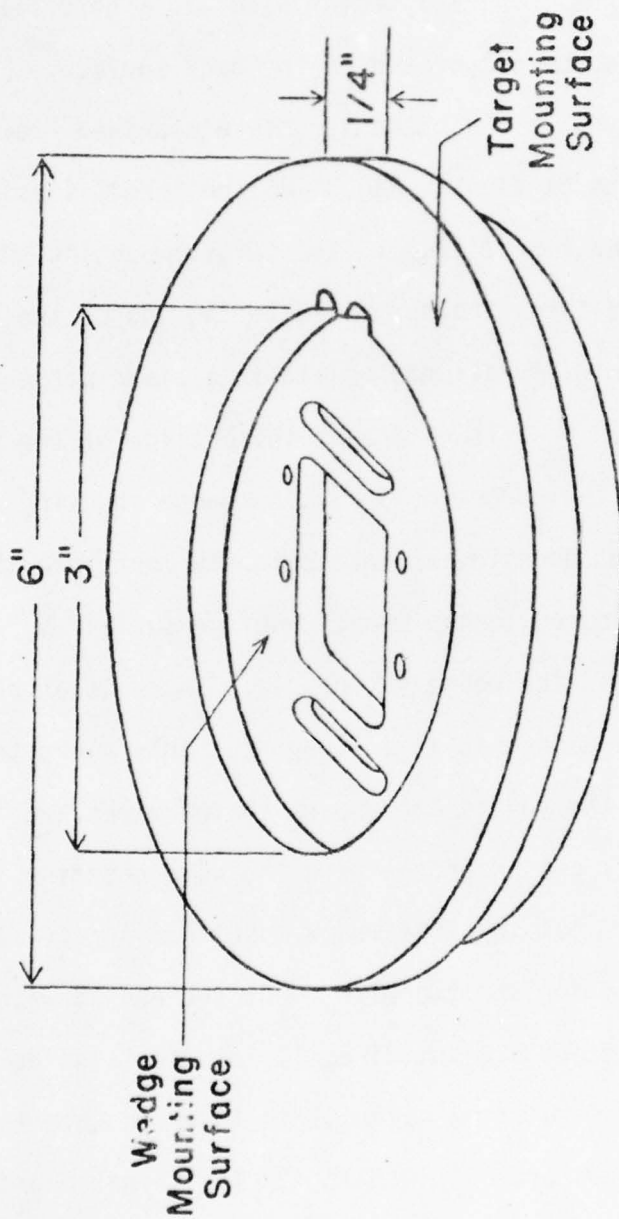
Fig. 3.12. Target assembly

Fig. 3.13. Target dimensions, all dimensions are in inches.

54

Fig. 3.14 shows front and rear views of a target block before the wedge and wires are attached.

Figure 3.15 shows how the wires are mounted in the target. There is enough distance between the wires so that the contact of the wedge with the first will not affect the second. The wires are attached by inserting them through tapered holes and securely fitting tapered pins into the holes. At the grounded end the wire goes through an opening in the target just beyond the step and is inserted into holes which taper toward the impact side of the target. Between the step and the hole is the wire tightening device illustrated in Fig. 3.16. At the other end the wire must not come into contact with the grounded wedge so the wire is secured with the assembly shown in Fig. 3.17. On the non-impact side of the target a block of insulating material is mounted over the opening beyond the non-grounded step. In this block are copper rods into which the tapered holes are placed. In this case the taper is toward the non-impact side, and the point at which the wire enters the rod is below the insulated step. The leads which run to the power supply and to the oscilloscopes are soldered to these rods on the non-impact side of the wedge.

In order to insure that the wires make a good electrical contact with the grounded steps, the steps and wires are coated with conducting silver paint. Care is taken to see that the paint extends precisely to the edge of the step and does not run over onto the wires beyond the step. This not only insures a good contact of the wire to the wedge but establishes an exact ground point at which the resistance of the wire begins. This is important in establishing the initial wire length L and gap distance G.

Before the wires are mounted they are washed in an acetone and then alcohol bath in order to remove grease. The wire is then loosely stretched

55
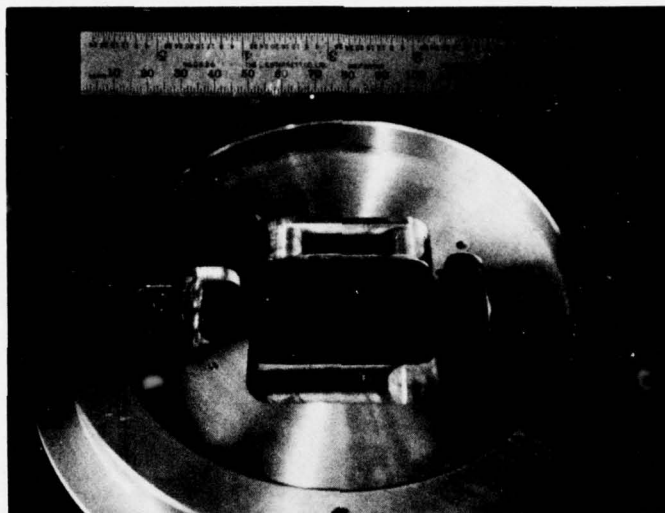
(a)
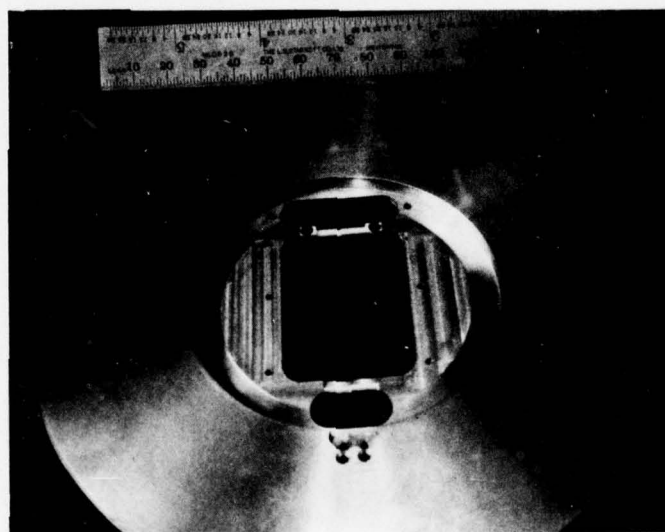
(b)

Fig. 3.14. Uncompleted target assembly.
(a) Rear view (b) Front view
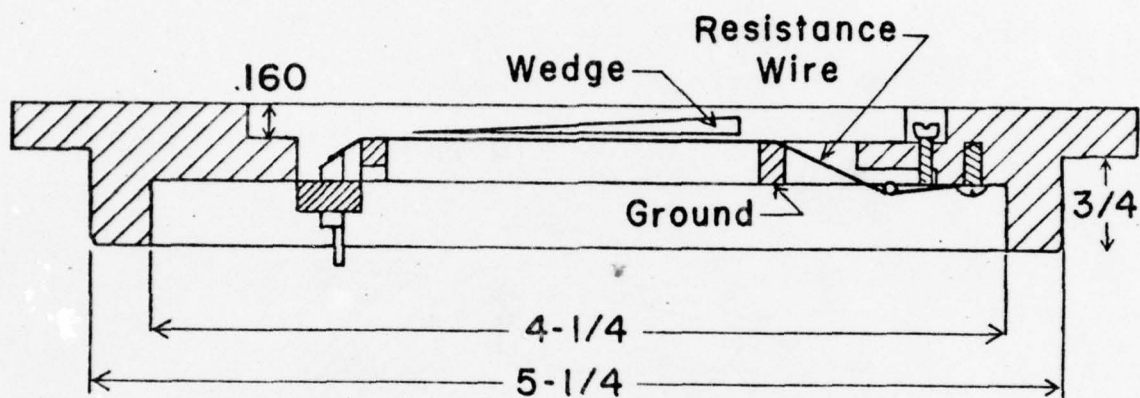
Fig. 3.15. Cross-section of target assembly, all dimensions are in inches.

57
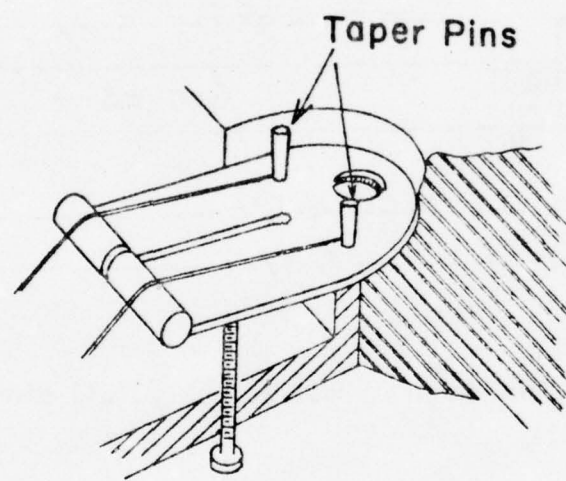
Fig. 3.16.   Wire tightening assembly

across the steps and secured at either end with the tapered pins. Before tightening, the wires are checked on a microscope with a travelling stage to insure that they run parallel to the length of the wedge. Using the 400 power microscope with focal length of less than one micron and attached dial indicator they are tightened until the wire is snug against the steps. They are then checked over their length for sag between the steps and side to side tilt. The sag and tilt are typically kept to within two microns. The wedge is then cleaned and mounted and the same microscope is used to measure the distance from the wires to the wedge rear surface in order to insure that the wires run parallel to the wedge rear surface. The change in this distance over the length of the wire is typically held to within two microns. If the wires are properly in place, they are painted with conducting paint at the grounded steps.

In the early shots a difficulty was encountered with noisy signals. They would be smooth and clean for approximately the first half of the record and then break into noise and irregular oscillations. There are several openings from the impact side of the target to the opposite side on which the wires are exposed, and it was felt that a possible explanation for the noisy signals was that metal particles generated by jetting occurring during the impact of the trigger pin were creating a conducting plasma in the region between the wires and the wedge. Whatever the actual cause of the noise, it stopped when all openings through the target were sealed off. Thus, the final step in target preparation is to seal off any paths through the target. This is accomplished by placing thin cover plates over the openings at the tip and high end of the wedge and sealing them to the wedge and the target with epoxy. Figure 3.18 shows front and rear views of a completed target.
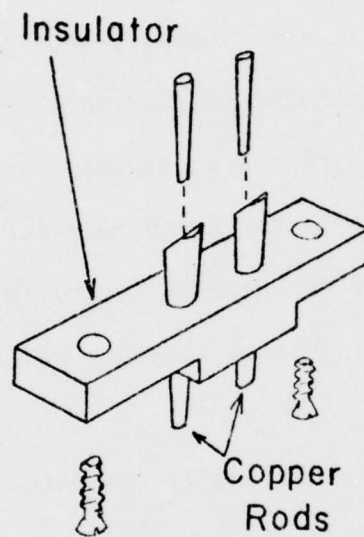
Fig. 3.17. Wire mount-
ing assembly
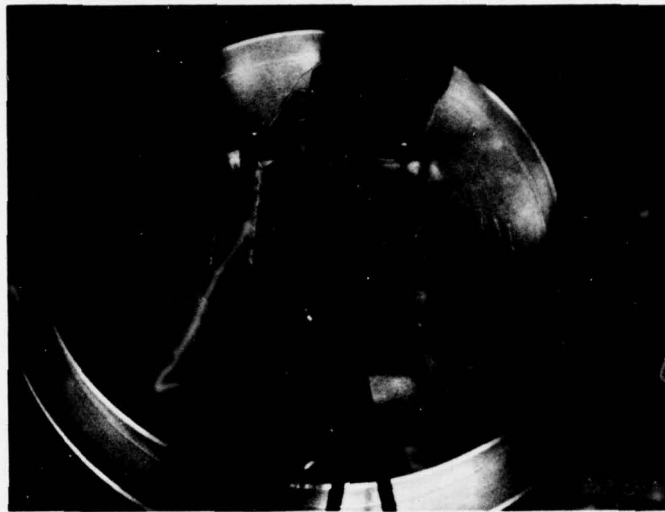
(a)

(b)

Fig. 3.18.   Completed target assembly.
(a) Rear view (b) Front view

61

Since the wedge mounting surface is recessed below the target mounting surface, the projectile must have the outer rim of its impact face recessed from the center of the impact face by an equal amount so that the projectile will not strike the target mounting surface before the entire surface of the wedge has been impacted. The projectile grounding pin and oscilloscope trigger pin must be placed close enough to the wedge so that they are impacted by the protrudent center of the projectile. However, they must be far enough from the wedge so that signals in the projectile from the pin impacts will not interfere with the wedge impact. Thus the pins must be located behind the high side of the wedge.

3.4 Error Analysis

Given a description of the resistance wire technique for measuring free surface velocity, the next step is to consider the sources of error in the experiment and the effect they will have on the outcome. Papers on the slanted resistor technique[47],[48] for determining free surface motion in one dimension consider the possible errors involved in that technique and many also apply to the present technique.

The major restriction is that the velocity of the contact point along the wire must be greater than wave speed in the wire. This insures that no signals will propagate ahead of the contact point into the wire, changing its resistance or altering its position. Other sources of error fall into five categories which are considered in the following sections.

3.4.1 Errors in Circuit Analysis

The first and most obvious source of error is the assumption that the circuits for the two wires are identical. Even though the components are made to match as closely as possible, there are differences. It is necessary

62

to know how differences in the components will affect the problem so a decision can be made as to how large a difference is allowable. The circuit can be tested before the shot by triggering the SCR and comparing the voltages across the two wires with a differential amplifier. It must be known how large a voltage difference can be allowed if a given error limit is to be observed.

From Eqs. (3.4) and (3.5), the position of the contact point is

$$x(t) = WL + G - L + \frac{\frac{R_L}{K}}{\frac{V_o}{V_M(t)} - \frac{R_L}{R_T} - 1} \qquad (3.11)$$

Therefore if the positions of the two contact points are equal,

$$WL + G_1 - L_1 + \frac{\frac{R_{L1}}{K_1}}{\frac{V_o}{V_{M1}} - \frac{R_{L1}}{R_{T1}} - 1} = WL + G_2 - L_2 + \frac{\frac{R_{L2}}{K_2}}{\frac{V_o}{V_{M2}} - \frac{R_{L2}}{R_{T2}} - 1} \qquad (3.12)$$

The assumption is that when x_2 is equal to x_1, V_{M2} is equal to V_{M1}. However, from Eq. (3.12)

$$V_{M2} = V_o \left[\frac{R_{L2}/K_2}{G_1 - G_2 + L_2 - L_1 + \frac{R_{L1}/K_1}{\frac{V_o}{V_{M1}} - \frac{R_{L1}}{R_{T1}} - 1}} + \frac{R_{L2}}{R_{T2}} + 1 \right]^{-1} \qquad (3.13)$$

This expression gives the exact values of V_{M2} and V_{M1} for which x_2 is equal to x_1. Naturally, when all components match identically, Eq. (3.13) reduces to

$$V_{M2} \equiv V_{M1} \qquad (3.14)$$

63

for x_2 equal to x_1. However, if the components do not match identically, the voltages will be unequal when $x_2 = x_1$. In that case, referring to Fig. 3.19, δt should not be taken as the time between points of equal voltage on the two traces, but as the time between V_{M2} and V_{M1} for which x_2 is equal to x_1. The true time difference would be δt_T between V_{M2} and V_{M1} rather than the measured difference δt_M between points of equal voltage. The error δt_e depends on the slope of the trace. If the trace is vertical δt_e will be zero for all δV, while the flatter the trace, the larger δt_e for a given δV. If M is the slope of the straight line joining V_{M2} and V_{M1} on trace 2, then

$$\delta t_e = \delta V/M \tag{3.15}$$

If only δt is assumed to be in error on the right hand side of Eq. (3.1), then the percentage error in the measured velocity V is the same as that in δt.[49]

In order to estimate the effects of errors, Eq. (3.13) is used to find the value of V_{M2} which should be paired with V_{M1} for time-differencing purposes. Equation (3.15) then gives the error in the measured time difference.

The above procedure may be used to calculate the error produced by the differences between R_{L1} and R_{L2} and between R_{T1} and R_{T2}. If all other quantities match, Eq. (3.13) becomes

$$V_{M2} = V_o \left[\frac{R_{L2}}{R_{L1}} \left(\frac{V_o}{V_{M1}} - \frac{R_{L1}}{R_{T1}} - 1 \right) + \frac{R_{L2}}{R_{T2}} + 1 \right]^{-1} \tag{3.16}$$
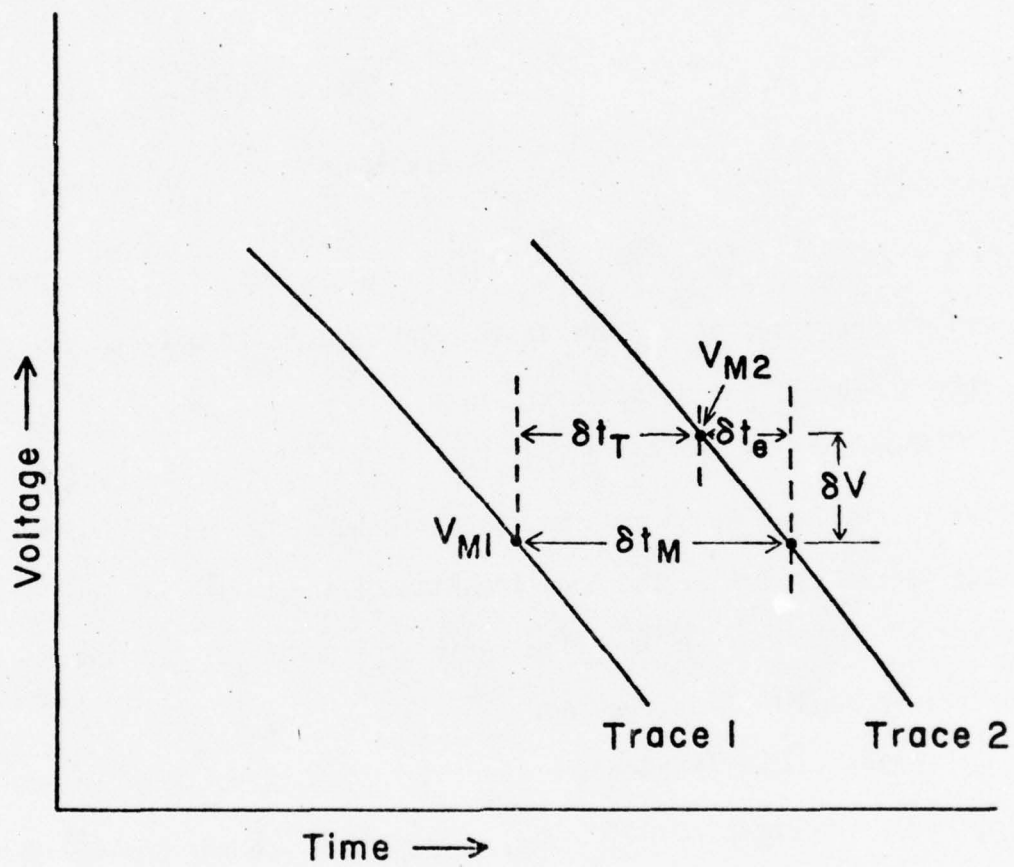
Fig. 3.19. Time error in dual beam oscilloscope record

Assuming

$$R_{L2} = R_{L1} + \delta L$$

$$R_{T2} = R_{T1} + \delta T$$

$$R_{L1} = 50\Omega = R_{T1}$$ \hfill (3.17)

$$V_o = 14.2 \text{ volts},$$

Table 3.1 gives the value of δV for different values of δL, δT, and V_{M1}. In general δV decreases as V_{M1} decreases, and is a maximum for a given value of V_{M1} when δL and δT are of different sign.

Given δV, δt_e is found from Eq. (3.15). The slope M of the trace will vary from problem to problem, but in general the slope increases as the voltage decreases due to the non-linearity of the circuit. Thus for positions near the tip of the wedge the time error δt_e is smaller for two reasons: δV is decreasing and M is increasing.

For a typical problem the slope is about .5 volts/microsecond at the beginning of the shorting history, increasing to 1.5 volts/microsecond. For the stated error limit of .002 ohms difference between R_{L1} and R_{L2} and between R_{T1} and R_{T2}, the maximum δt_e would be about .3 nanoseconds in this case. This would be a one percent error if the total time taken for the free surface to cross the distance between the wires were only 30 nanoseconds. Typically this time has been closer to 250 to 500 nanoseconds, so that δt_e is truly negligible. In fact, even if δL and δT were .01 ohms, δt_e would be only about 1.6 nanoseconds. Thus the error created by the given mismatch in the load and termination resistance is negligible.

66

TABLE 3.1. Error produced by mismatch in
load and termination resistance

δL(ohms)	δT(ohms)	V_{M1}(volts)	V_{M2}(volts)	δV(volts)
.002	.002	4	3.999930142	-.000069857
-.002	.002	4	4.000160002	.000160002
-.002	-.002	4	4.00006986	.000069860
.002	-.002	4	3.999840002	-.000159997
-.002	.002	3	3.000120002	.00012002
-.002	.002	2	2.000080002	.000030002
-.002	.002	1	1.000040001	.000040001
-.002	.002	.5	.500020000	.000020000
-.01	.01	4	4.00030069	.000300067

The load and termination resistances are permanent, so care can be taken to find pairs of precision resistors that match very closely. The wire resistances, however, are determined by the length of resistance wire stretched across the steps in the target and the resistance per unit length of the wire. The targets must be carefully built in order to insure that the lengths of the two wires are as close as possible. The grounded steps must be carefully painted with conducting paint to establish the ground points for the wires so that the two wire lengths L_1 and L_2 and the two gap distances G_1 and G_2 match as closely as possible.

The wires come from the same spool and thus the resistances per unit length differ only by non-uniformities in dimension and composition of the wire produced during its manufacture. The resistance per unit length of the two wires is therefore probably the most closely matching quantity of the two circuits. In fact the error in this quantity is probably less than errors which would be produced in measurements of the length and resistance of pieces of wire in order to measure the resistance per unit length.

There is also the question of the change in the resistance per unit length of the wires as they are stretched across the steps and the tension in them increases. The wires are not tightened to the point where plastic yielding occurs, and both wires should have roughly the same amount of tension in them, so this effect should not cause difficulty. In addition, the resistance of a wire was monitored as the tension was changed, and no consistent change was noticed. Therefore the resistances per unit length of the two wires will be taken as equal.

Equation (3.13) may be used to determine the effect of differences in the gap distances G_1 and G_2 and in the wire lengths L_1 qnd L_2. The length of the wire may be replaced by its resistance divided by its resistance per unit

68

length. Thus the analysis will give the allowable error in both the gap distances and the initial resistances of the two wires. Defining

$$\Delta L \equiv G_1 - G_2 + L_2 - L_1 \tag{3.18}$$

and taking all other quantities to match exactly, Eq. (3.13) becomes

$$V_{M2} = V_0 \left[\frac{R_L/K}{\Delta L + \dfrac{R_L/K}{\dfrac{V_0}{V_{M1}} - \dfrac{R_L}{R_T} - 1}} + \frac{R_L}{R_T} + 1 \right]^{-1} \tag{3.19}$$

If L_2-L_1 is equal to zero, ΔL is equal to G_1-G_2, and Eq. (3.19) gives the error resulting from differences in the gap distances only. Also, if G_1-G_2 is equal to zero, ΔL is equal to L_2-L_1, and Eq. (3.19) gives the error resulting from differences in wire lengths only. Thus the single parameter ΔL can be used to determine the effect of errors in gap distances only, the errors in wire lengths only, or combinations of the two. Differences in wire lengths will result in differences of the initial wire resistances, so this analysis gives the effects of mismatches in the initial resistances of the wires. Table 3.2 gives values of δV for given values of ΔL. Also given is the difference in resistance ΔR which ΔL would correspond to if ΔL were due purely to differences in resistances of the wires. Thus, if G_1 is taken equal to G_2,

$$\Delta L = \Delta R/K \tag{3.20}$$

where the resistance per unit length K of the wire is taken as 6.48 ohms per centimeter. The other quantities in Eq. (3.19) are given as follows:

69

TABLE 3.2. Error produced by mismatch in
gap distance or initial resistance

ΔL(centimeters)	ΔR(ohms)	V_{M1}(volts)	V_{M2}(volts)	δV(volts)
.01	.0648	4	4.003434	.003434
.001	.00648	4	4.0003438	.0003438
.0001	.C00648	4	4.00003438	.00003438
.005	.03240	4	4.001718	.001718
.005	.03240	3	3.0030047	.0030047
.005	.03240	2	2.004648	.004648
.005	.03240	1	1.006649	.006649
.005	.03240	.5	.5077825	.0077825
.005	.03240	.1	.108753827	.003753827
.005	.03240	10^{-3}	.01003027	.009003027
.005	.03240	10^{-6}	.01003027	.00900556
.005	.03240	10^{-20}	.009005562	.009005562
.0005	.003240	10^{-20}	.000901585	.000901585
.001	.00648	10^{-20}	.001802942	.001802942
.01	.0648	10^{-20}	.017988	.017988
.00416	02696	10^{-20}	.007493987	.007493987
.00416	.02696	4	4.001429479	.001429479

$$R_L = 50 \text{ ohms}$$

$$R_T = 50 \text{ ohms} \tag{3.21}$$

$$V_o = 14.2 \text{ volts}$$

There are several general features which may be noted from Table 3.2. For a given ΔL, δV increases as V_{M1} decreases. The maximum value of V_{M1} is about four volts for the case considered. The minimum value of V_{M1} is greater than zero and is determined by the length of wire which extends past the tip of the wedge, for the resistance in that portion of the wire is never shorted. However, for the cases considered in Table 3.2, δV increases by a factor of approximately five as V_{M1} decreases from four volts essentially to zero volts. However, the slope of the trace increases as V_{M1} decreases. In the experiments to date it has increased from about .5 volts/microsecond to about 1.5 volts/microsecond. Therefore, from Eq. (3.15), the time error δt_e would increase by a factor of about 1.7 as V_{M1} dropped from four volts to zero volts.

The last two rows in Table 3.2 give an example for a specific case. If the time taken for the free surface to cross the wires were of the order of .500 microseconds, a value of .005 microseconds for δt_e would represent a one percent error. Since the error is largest when V_{M1} approaches zero, and the slope of the trace is about 1.5 volts/microsecond at this point, a value of .0075 volts for δV would correspond to a one percent error. The next to last row in Table 3.2 shows that this would be produced by a difference of .00416 cm between G_1 and G_2, or a difference of .027 ohms between the initial resistances of the two wires. The last row shows that when V_{M1} is equal to four volts, δV is about 1.4 millivolts for those

71

errors in G or L. Therefore, with the aid of this analysis, it is possible to assemble the target, trigger the SCR in the current supply circuit, measure the difference between the voltages across the two wires with a differential amplifier, and determine whether the error which will be caused by a mismatch in the components is within the desired error bounds. In the above case, if the differential amplifier shows a difference of less than 1.4 millivolts, the error will be less than one percent.

A second source of error in the circuit analysis is the assumption that the voltage V_o across the resistance network is constant. The voltage V_o is produced by the discharge of the capacitor across the resistance network, and thus is continuously changing. Since V_{M1} is measured at time t and V_{M2} is measured at time $t + \delta t$, V_o does not have the same value at the time of each measurement. If in Eq. (3.12) the voltages are written as *functions of time*, and it is assumed that all other components match exactly, the equation reduces to

$$\frac{V_o(t)}{V_{M1}(t)} = \frac{V_o(t + \delta t)}{V_{M2}(t + \delta t)} \tag{3.22}$$

where t is the time at which the measurement of V_{M1} occurs, and $t + \delta t$ is the time at which the measurement of V_{M2} occurs. Thus the voltage V_{M2} which should be compared to V_{M1} for purposes of time differencing is

$$V_{M2} = \frac{V_o(t + \delta t)}{V_o(t)} V_{M1} \tag{3.23}$$

The circuit of Fig. 3.9 may be solved to yield $V_o(t)$ if $R_1(t)$ and $R_2(t)$ are known. However, an estimate of the error can be obtained as follows. The differential equation describing capacitor discharge is[50]

72

$$\frac{dV}{dt} = \frac{-V}{RC} \tag{3.24}$$

which has the solution for constant R

$$V = V_0 \exp\left(-\frac{t - t_0}{RC}\right) \tag{3.25}$$

where V_0 is the voltage at time t_0 and C is the capacitance. Until the first shorting occurs R has the constant value R_{max} which is the total resistance of the network in Fig. 3.6 when R_1 and R_2 have their maximum values. If the load and termination resistances are 50 ohms, and the initial resistance of each wire is 33 ohms, then R_{max} is equal to 34.94 ohms. Taking the time t_0 at which discharge starts as time zero, the voltage across the network is given by

$$V(t) = V_0 \exp\left(\frac{-t}{R_{max}C}\right) \qquad t < t_1, \tag{3.26}$$

up to the time t_1 at which shorting first occurs. At this time the resistances of the wires will begin to decrease and the voltage across the network will begin to drop more rapidly. However, the minimum voltage obtainable would occur if the resistance of both wires dropped suddenly to zero at time t_1 and stayed there. In this case the voltage across the network would be given by

$$V(t) = V_0 \exp\left(\frac{-t_1}{R_{max}C}\right) \exp\left(\frac{-(t - t_1)}{R_{min}C}\right) \qquad t > t_1 \tag{3.27}$$

where R_{min} is the total resistance of the network when both R_1 and R_2 are equal to zero. If the load and termination resistances are 50 ohms, then R_{min} is equal to 25 ohms.

73

The maximum value the voltage could have is for that case in which the wires do not short but maintain their maximum resistance. This case is described by Eq. (3.26). Therefore the true value of the voltage across the resistance network at any time t greater than t_1 is bracketed between

$$V_{max}(t) = V_0 \exp(\frac{-t}{R_{max}C}) \qquad (3.28)$$

and

$$V_{min}(t) = V_0 \exp(\frac{-t_1}{R_{max}C}) \exp(\frac{-(t - t_1)}{R_{min}C}) \qquad (3.29)$$

From Eq. (3.23)

$$\delta V = V_{M1} - V_{M2} = V_{M1}[1 - \frac{V_0(t + \delta t)}{V_0(t)}] \qquad (3.30)$$

An estimate of δV which is always greater than δV is

$$\delta V' = V_{M1}[1 - \frac{V_{min}(t + \delta t)}{V_{max}(t)}] \qquad (3.31)$$

The voltage error is always less than

$$\delta V' = V_{M1}[1 - \exp(\frac{(t - t_1)(R_{min} - R_{max}) - R_{max}\delta t}{R_{min}R_{max}C})] \qquad (3.32)$$

The term in brackets in Eq. (3.32) increases as $t-t_1$ increases. However, experiments usually last only about three microseconds after the first shorting occurs. If $t-t_1$ is taken as five microseconds, then for δt equal to .5 microseconds, the term in brackets is equal to .00015. By the end of the experiment V_{M1} is very small, but even if it were equal to its maximum value

74

of 4 volts, $\delta V'$ would have a value of .0006. Even at a minimum trace slope of .5 volts/microseconds, this corresponds to an error of less than .3 percent in the value of δt. Therefore the error introduced by decay of voltage across the resistance network is negligible.

3.4.2 Oscilloscope Irregularities

Once the target is built so that the components match and the initial voltages across the two wires have been checked with a differential amplifier and found to match within the desired limits, the errors produced by the electronic circuitry consisting of the wires and current supply are bounded. However, the signal must pass through the oscilloscope before data traces are recorded, and this may produce errors also. It is possible that the oscilloscope may be the largest source of error, and the source whose errors are the most difficult to analyze and estimate.

In order to reduce the data it is assumed that the time bases and vertical gains can be calibrated so that any given point on the screen corresponds to the same time and the same voltage for both traces. Because of non-linearities and irregularities in the oscilloscope this is certainly not the case, although the amount of error will of course vary from oscilloscope to oscilloscope. All that can be done is to use very careful calibration procedures to insure that equal vertical deflections correspond to equal voltages for both traces and that the measured time between points on the two traces is actually equal to the real time difference between the two events.

The time bases can be calibrated by use of a timing mark generator, and these calibration points can be used to reduce the data. Voltage calibration lines may also be used. In fact the data traces themselves may be used as partial voltage calibrations. Once the initial voltages across the two wires have been found to match within a satisfactory error, the gains of

75

the two vertical amplifiers may be set so that when the baselines of the two traces are superimposed, the initial levels will also be superimposed. However, gains and baselines may drift after they have been set, and the baselines and initial levels may not be superimposed on the data record. If this is the case the data can be adjusted accordingly.

If it is known from differential amplifier measurements that the initial voltages across the two wires are essentially equal, but neither the baselines nor the initial levels are superimposed on the data trace, the data can be adjusted by assuming that the baseline positions and vertical amplifier gains were not set correctly. Figure 3.20 gives an example of a record in which neither the baselines nor the initial trace levels are superimposed. It is obvious that the baseline positions are incorrect, and if the distances H1 and H2 from each baseline to the corresponding initial trace level are not equal, then the gains of the amplifiers are also incorrect. In order to determine H1 and H2, it is necessary to have a means of determining which baseline belongs to which data trace.

In reducing the data the position of each point on the data trace is assigned an X and Y coordinate by means of a microscope with a travelling stage. The stage and photograph are moved until the microscope cross-hairs are centered on a point on the trace, and the X and Y coordinates of that point are read from the calibrated micrometers which drive the stage. Thus the origin of the X-Y coordinate system is arbitrary. These coordinates are utilized in Fig. 3.20. The Y coordinate is in the direction of voltage displacement, and the X coordinate is in the direction of time displacement. The baselines B1 and B2 have Y coordinates YB1 and YB2, and the initial trace levels have Y coordinates YI1 and YI2. The data traces are given by X-Y coordinate pairs represented as Y1(X) and Y2(X). If the baselines and

76
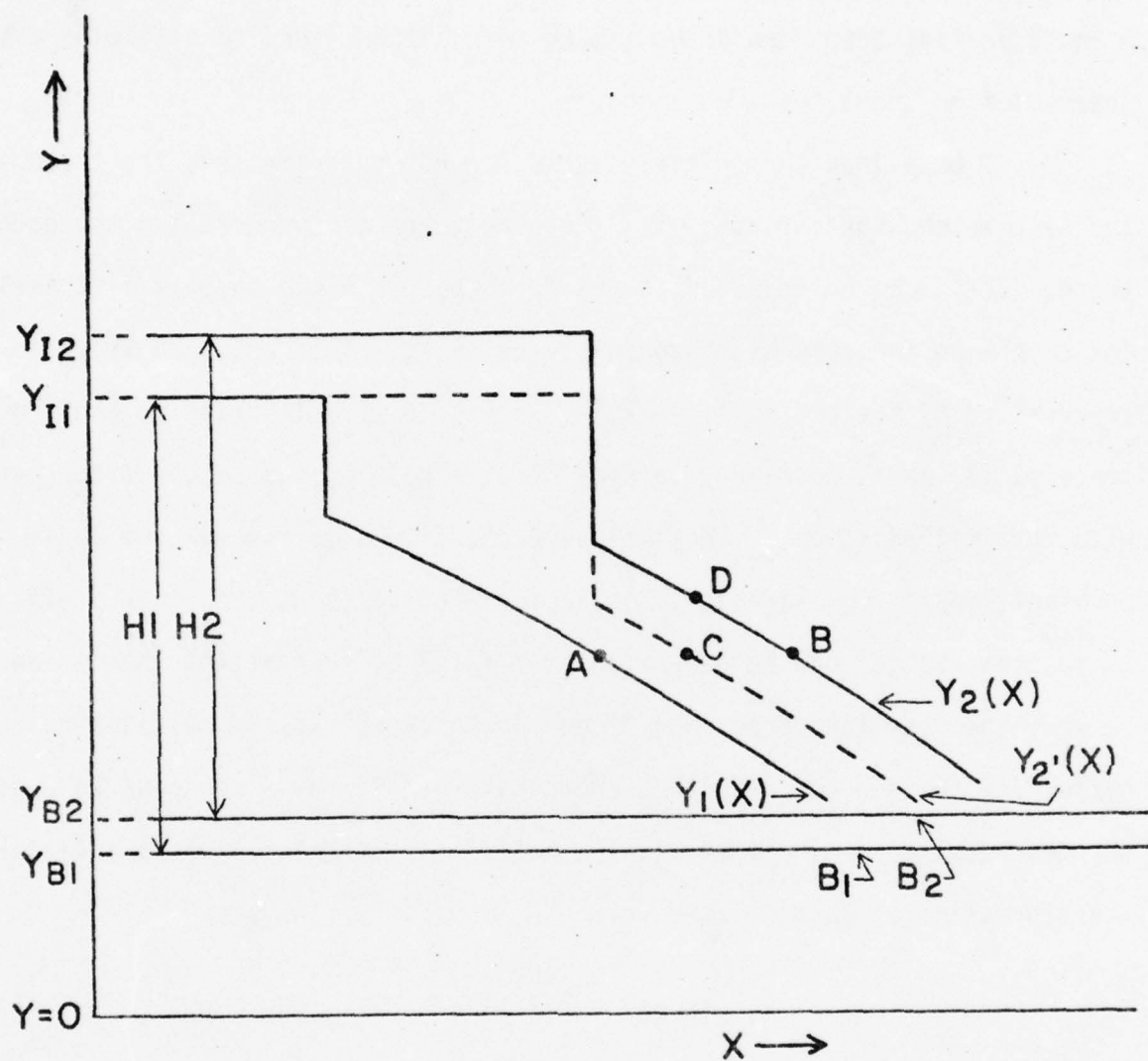
Fig. 3.20. Data correction for errors in gain and baseline settings

initial levels were superimposed, data reduction would consist of determining the X coordinates of data pairs with equal Y coordinates, such as points A and B in Fig. 3.20. and using timing mark calibrations to determine a time interval from these two X coordinates.

If baselines and initial levels are not superimposed, the trace for the wire which shorts first, $Y1(X)$, can be taken as correct, and the second trace, $Y2(X)$, can be adjusted to the form that it would have if its baseline and gain were the same as those for trace $Y1(X)$. This adjusted trace is represented by the dotted line $Y2'(X)$ in Fig. 3.20. In order to construct trace $Y2'(X)$ it is necessary to know how the gain of the second trace varies with vertical position. The simplest procedure is to assume that it is constant, so that voltage is a linear function of the Y coordinate. If this is so, then $Y2'(X)$ can be generated from $Y2(X)$ by subtracting the distance between the baselines from each Y coordinate of $Y2(X)$, and multiplying the difference between the resulting coordinate and YB1 by a constant so that H2 becomes equal to H1. Alternatively, $Y2'(X)$ can be thought of as a linear transformation of $Y2(X)$ of the form

$$Y2'(X) = aY2(X) + b \qquad (3.33)$$

where a and b are determined from the requirements that $Y2'(X)$ equals YI1 when $Y2(X)$ equals YI2, and $Y2'(X)$ equals YB1 when $Y2(X)$ equals YB2. The resulting transformation is

$$Y2'(X) = \frac{YI1 - YB1}{YI2 - YB2} (Y2(X) - YB2) + YB1 \qquad (3.34)$$

The procedure to be used when the baselines and initial levels are not superimposed is to use points of equal Y coordinates on traces $Y1(X)$ and $Y2'(X)$, represented by points A and C in Fig. 3.20. However, it is not

necessary to construct curve Y2'(X). Equation (3.34) can be inverted to give Y2(X) as a function of Y2'(X). This yields the point D in Fig. 3.20 on curve Y2(X) which corresponds to point C on curve Y2'(X). Thus if point A in Fig. 3.20 has coordinate Y1, the time interval is not determined by the X coordinates of points A and B, but by the X coordinates of points A and D, where point D on curve Y2(X) has the Y coordinate Y2, where

$$Y2 = \frac{YI2 - YB2}{YI1 - YB1} (Y1 - YB1) + YB2 \qquad (3.35)$$

The above analysis may also be used to determine the magnitude of error produced by differences in baseline levels and initial voltage levels that are too small to be detected. For instance, when attempting to set the baselines so that they are superimposed, the two traces merge into a single one with a greater thickness, and it is difficult to estimate the setting at which they are truly superimposed. One estimate is that it would be possible to superimpose the two only to within 10 percent of a trace width. This value could then be used for the distance between the two baselines and for the difference between the distances H1 and H2 in Fig. 3.20. Equation (3.35) could then be used to determine how far the point D would be from point B, and the error in the time interval δt could then be determined, given the slope of the trace.

The error in δt will depend on the trace thickness and the slope of the trace. Values for these and other quantities may be taken from a representative shot in order to estimate the magnitude of the error involved. The trace thickness for shot number 75-080 was .22 millimeters and the distance between baselines and initial levels was about 30 millimeters. Assuming a difference of .022 millimeters between the baseline levels and between the distances H1 and H2, the maximum difference between Y2 and Y1 from Eq. (3.35)

79

is .037 millimeters when Y1 is at two-thirds of its maximum value. The trace drops 16 millimeters in three microseconds so the average slope is 5.3 millimeters per microsecond. Thus, the error in the time interval δt is 6.9 nanoseconds. The time taken for the free surface to cross the distance between the wires is .59 microseconds, so the maximum error that could be produced by differences too small to detect between baselines and initial levels is about 1.2 percent.

3.4.3 Wire Irregularities

The next source of error to be considered involves the way in which the wires are installed in the target. Errors involving the resistance per unit length of the wire and the establishment of the ground point on the wires were dealt with in Section 3.4.1. Errors will also be produced if the wires are not strung parallel to the rear surface of the wedge, or if they do not run parallel to the sides of the wedge.

Figure 3.21 considers the case in which the wires do not run parallel to the sides of the wedge. The figure shows the wedge seen from directly above and the two resistance wires underneath. Instead of being parallel to the sides of the wedge and normal to its ends, the wires make angles θ_1 and θ_2 respectively with the sides. Thus when the contact point on the first wire reaches wedge coordinate X which is a distance D from the high end of the wedge, the length of wire shorted out is not D but D', where

$$D' = D/\cos \theta_1 \tag{3.36}$$

The apparent wedge coordinate of the contact point is X_A, which is X plus the extra length of wire which has been shorted out, or

$$X_A = X + D(\sec \theta_1 - 1) \tag{3.37}$$

80
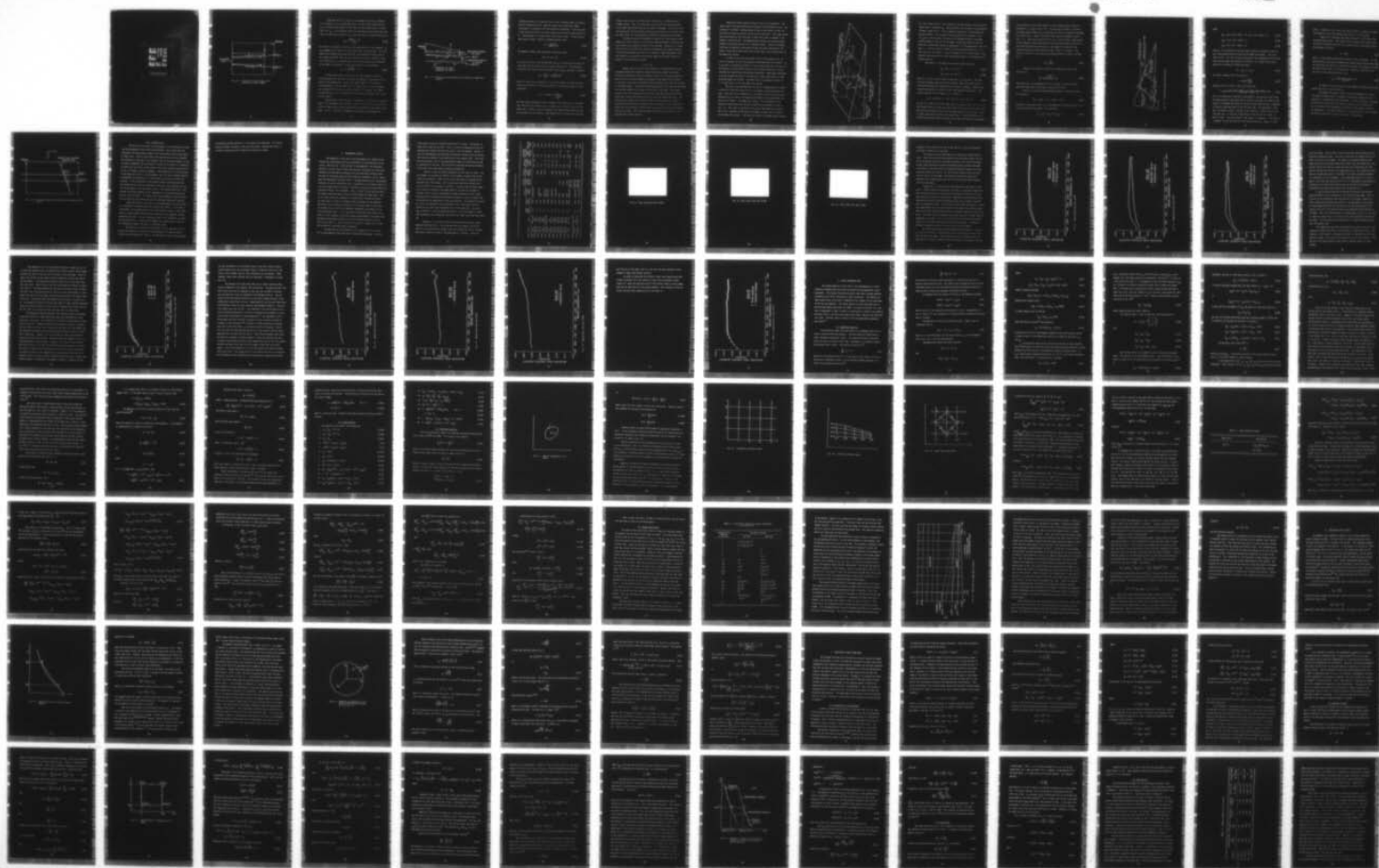
MICROCOPY RESOLUTION TEST CHART

NATIONAL BUREAU OF STANDARDS-1963-A
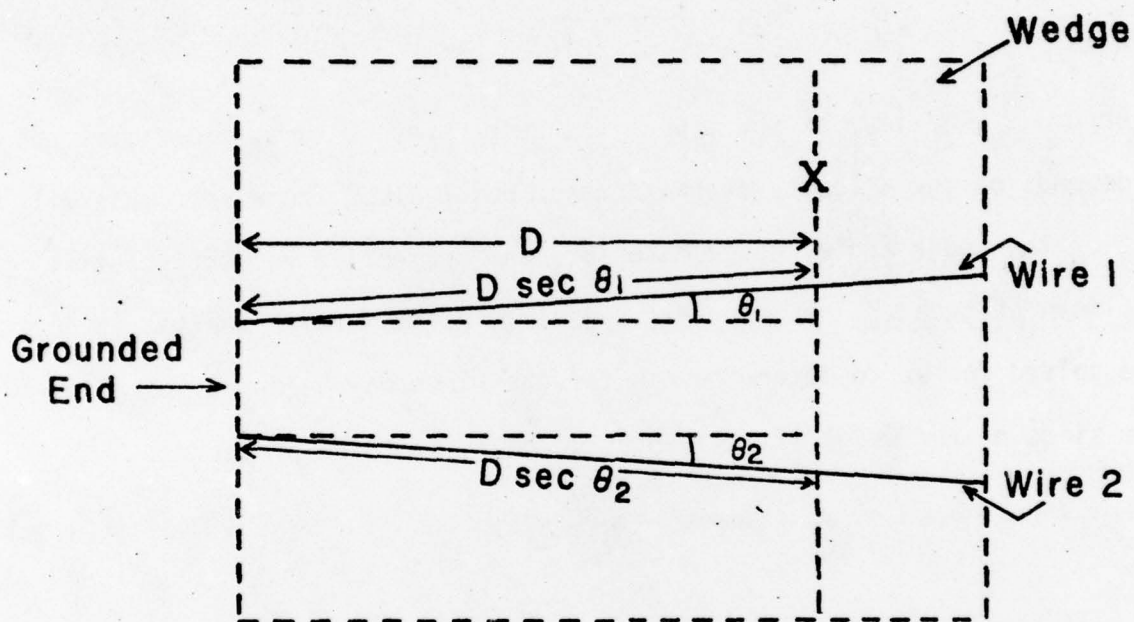
Fig. 3.21. Error due to wires being out of
parallel to sides of wedge

81

Since the contact on the first wire appears to be at x_A although
it is actually at x, the indicated time of arrival of the contact point at
x_A is in error by the amount of time taken for the contact point to travel
from x to x_A. If the average velocity of the contact point during the time
taken to travel this interval is V_{C1}, then the error in arrival time at x_A is

$$e_{t1} = \frac{D(\sec \theta_1 - 1)}{V_{C1}} \qquad (3.38)$$

This error is a maximum at the tip of the wedge where D is at a maximum. It
also depends on the velocity of the contact point along the wire. This will
depend on the wedge angle, wedge material, and projectile velocity, but it
must always be greater than the wave velocity in the wire. Equation (3.38)
can be solved for θ_1 to determine how far the wires may be out of parallel
to the sides of the wedge if a given error bound is to be preserved.

$$\theta_1 = \arccos[\frac{V_{C1}e_{t1}}{D} + 1]^{-1} \qquad (3.39)$$

If the time interval required for the free surface to cross the
distance between the two wires is one-half microsecond, a one percent error
would be five nanoseconds. Assuming the wedge length is 1.75 inches or
4.445 centimeters, and the velocity of the contact point is one centimeter
per microsecond, the angle θ_1 is .047 radians or 2.7 degrees. The amount
by which the wire is out of parallel to the sides of the wedge is not a very
critical factor.

The wire may also be strung out of parallel to the wedge free surface.
Figure 3.22 illustrates this situation. There is an error produced which is
similar to that caused by the wires being out of parallel to the sides of the
wedge. In Fig. 3.22 wire 1 is assumed to be parallel to the wedge free

82
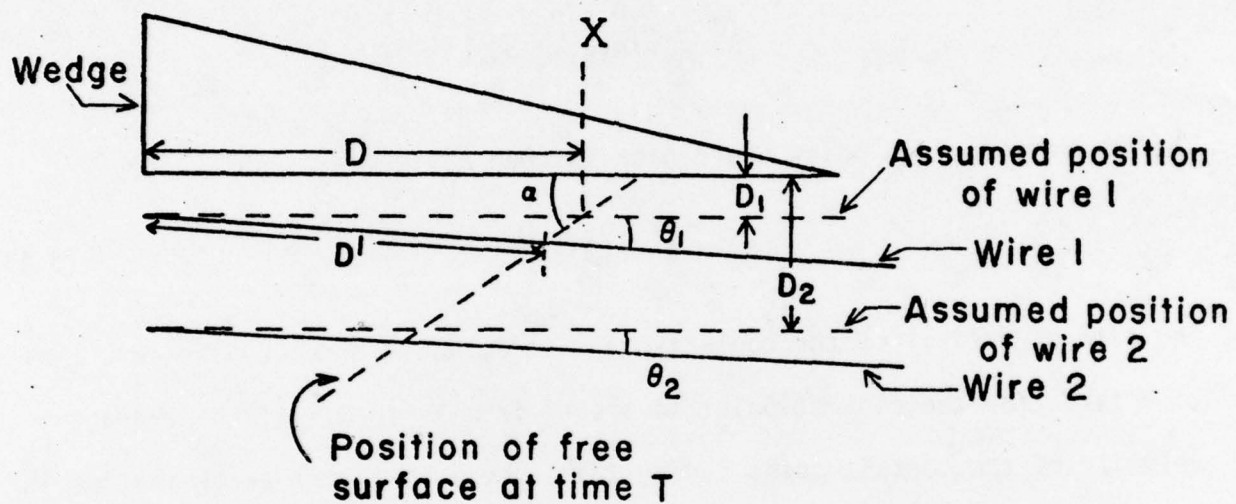
Fig. 3.22. Error due to wires being out of parallel to wedge free surface

surface and offset a distance D_1 from it, but it actually makes an angle θ_1 with its assumed position. When the contact point would be at wedge coordinate X, a distance D from the high end of the wedge, if the wire were in the correct position, the actual length of wire that has been shorted is D'. The distance D' is found by use of the law of sines. If the free surface makes an angle α with its original position, then

$$D' = \frac{D \sin \alpha}{\sin(\theta_1 + \alpha)} \qquad (3.40)$$

The apparent contact point coordinate is then X_A, where

$$X_A = X - (D - D') \qquad (3.41)$$

The time of arrival of the contact point at X_A is in error by the amount of time taken for the contact point to travel from X_A to X. If the average velocity of the contact point during this time is V_{C1}, the error in time is

$$e_{t1} = \frac{D}{V_{C1}} \left[1 - \frac{\sin \alpha}{\sin(\theta_1 + \alpha)} \right] \qquad (3.42)$$

Equation (3.42) may be solved for θ_1 to find the amount by which the wires may be out of parallel to the free surface if a given error bound is to be maintained.

$$\theta_1 = \alpha + \arcsin\left[\frac{\sin \alpha}{1 - \frac{e_{t1} V_{C1}}{D}} \right] \qquad (3.43)$$

The free surface deflection angle α depends on the wedge angle, wedge material, and projectile velocity, but it appears to be roughly the same as the wedge angle. Taking α to be five degrees, the contact point velocity to be one centimeter per microsecond, a one percent error in time to be five nano-

84

seconds, and D to be its maximum value, the angle θ_1 is .0056 degrees or .000098 radians. Thus it is much more critical that the wire be parallel to the wedge free surface than to the sides of the wedge. In fact, for the case considered, the wire should only be out of parallel by 4.4 microns over the wedge length of 4.4 centimeters to maintain a one percent error bound.

If the wires are out of parallel or sag or tilt with respect to the wedge free surface, there is also an error produced because of the fact that the distance D_2-D_1 between the wires is not constant. Equation (3.1) shows that this will also affect the value of the measured free surface velocity. If the distance between the wires is .02 inches or .0508 centimeters, then the distance D_2-D_1 should not vary by more than five microns in order to maintain a one percent error bound.

3.4.4 Tilt

Another source of error to be considered is the possibility of misalignment between the projectile impact face and the wedge free surface. Given ideal conditions, these two surfaces should lie in parallel planes so that the line of contact between the projectile and wedge impact surfaces is parallel to the end of the wedge and thus intersects the sides of the wedge at 90 degree angles. The line of contact between the shock front and the wedge free surface should also be normal to the side of the wedge. The contact points on two wires placed side by side and having the same offset from the wedge free surface should then always be at the same wedge coordinate. Any relative tilt between the projectile impact face and wedge rear surface would mean that the lines of contact would not be normal to the side of the wedge, and the coordinates of the contact points on wires with equal offsets would not be equal. This situation would obviously have an effect on the measured free surface velocity.

85

There are several possible causes of tilt in the experiment. The impact face of the projectile may not be normal to the projectile axis. The projectile is allowed a limited amount of play in the barrel, so that its axis may not always be parallel to the axis of the barrel. The target holder may be misaligned so that the plane in which the target is mounted is not normal to the gun barrel. The wedge mounting surface and target mounting surface in the target may not lie in parallel planes. Finally, the wedge itself may be improperly constructed so that the plane determined by the normal to the impact face and the side of the wedge is not perpendicular to the wedge free surface.

In order to calculate the effect of tilt in the general case, it would be necessary to solve the complete three-dimensional flow problem. It is possible to estimate the effect of tilt by considering only the case of a hydrodynamic, no-rate-effects material with no phase transitions, and·by ignoring wave interactions with material boundaries. Under these conditions it can be assumed that there is no curvature to the shock front or to the deflected wedge free surface. The shock front in the wedge will then lie in a single plane, as will the wedge free surface.

The case to be considered will be that of a wedge-projectile impact in which the projectile impact face is not parallel to the wedge free sur-face. There will be no irregularity in the wedge itself, so that the plane determined by the side of the wedge and the normal to the wedge impact sur-face will be normal to the wedge free surface. The orientation of the coordinate system which will be used to describe the problem is shown in Fig. 3.23. The Y axis is parallel to the side of the wedge free surface, the X axis is parallel to the end of the wedge, and the Z axis is normal to the wedge free surface. Thus the unit normal to the wedge impact surface,

86

Fig. 3.23. Wedge impact configuration for the case of relative tilt between projectile and wedge

$\hat{n}_w$, lies in the YZ plane. The negative of the unit normal to the projectile impact face is designated $\hat{n}_p$. Thus $\hat{n}_p$ points into the body of the projectile instead of away from it. This is done for simplicity in illustrating the two unit vectors. For the zero tilt case $\hat{n}_p$ would lie along the Z axis. If $\hat{n}_p$ lay in the YZ plane, the contact line between projectile and wedge would be normal to the side of the wedge, and the only effect of the tilt would be to effectively change the wedge angle α by the magnitude of the tilt angle δ. The tilt angle is probably less than the uncertainty in α, so this case is of no interest. $\hat{n}_p$ will be taken to lie in the XZ plane. This should be the case which will have the greatest effect on the measured free surface velocity.

The normals to the wedge and projectile impact faces are

$$\hat{n}_w = \sin \alpha \; \hat{j} + \cos \alpha \; \hat{k} \tag{3.44}$$

$$\hat{n}_p = \sin \delta \; \hat{i} + \cos \delta \; \hat{k} \tag{3.45}$$

where $\hat{i}$, $\hat{j}$, and $\hat{k}$ are unit normals along the X, Y, and Z axes. The line of contact between wedge and projectile impact faces will be the line of intersection between the planes with unit normals $\hat{n}_p$ and $\hat{n}_w$. Therefore the line of intersection is parallel to the cross product of $\hat{n}_w$ and $\hat{n}_p$. The vector along the line of contact, $\hat{n}_c$, is given by

$$\hat{n}_c = -\sin \alpha \cos \delta \; \hat{i} - \sin \delta \cos \alpha \; \hat{j} + \sin \alpha \sin \delta \; \hat{k} \tag{3.46}$$

$\hat{n}_c$ will lie in the plane of the shock front, as shown in Fig. 3.23. $\hat{n}_i$ is a unit vector which lies along the intersection of the plane of the shock front and the plane formed by the side of the wedge, which is the YZ plane. Thus $\hat{n}_c$ and $\hat{n}_i$ determine the plane of the shock front. If the orientation of $\hat{n}_i$ in the YZ plane were known, the plane of the shock front would be determined.

88

Let the angle in the YZ plane between $\hat{n}_i$ and the wedge impact surface be designated θ, as shown in Fig. 3.23. Let the point at which $\hat{n}_i$ intersects the wedge impact surface be A, and the point at which it intersects the wedge free surface be B. Figure 3.24 shows a side view of the wedge at times t and $t + \delta t$. Since the projectile tilt is all in the XZ plane, intersections of the projectile impact plane and the YZ plane are parallel to the Y axis. Since the projectile has velocity V_p in the negative Z direction, the distance between the intersections at times t and $t + \delta t$ is $V_p \delta t$. The velocity of point A is the distance D_A moved by point A in time δt divided by δt

$$V_A = \frac{V_p}{\sin \alpha} \tag{3.47}$$

Likewise, the velocity of point B is distance D_B in Fig. 3.24 divided by δt

$$V_B = \frac{V_p \sin \theta}{\sin \alpha \sin(\theta - \alpha)} \tag{3.48}$$

These velocities are independent of the tilt angle δ, and are the same velocities these points would have in the zero tilt case.

Since $\hat{n}_i$ is in the YZ plane and makes angle $\theta - \alpha$ with the Y axis, it is given by

$$\hat{n}_i = -\cos(\theta - \alpha)\, \hat{j} - \sin(\theta - \alpha)\, \hat{k} \tag{3.49}$$

The normal to the shock front, $\hat{n}_s$, is perpendicular to both $\hat{n}_c$ and $\hat{n}_i$, so it lies along their cross-product. It is given by

$$\hat{n}_s = n_{sx}\, \hat{i} + n_{sy}\, \hat{j} + n_{sz}\, \hat{k} \tag{3.50}$$

89
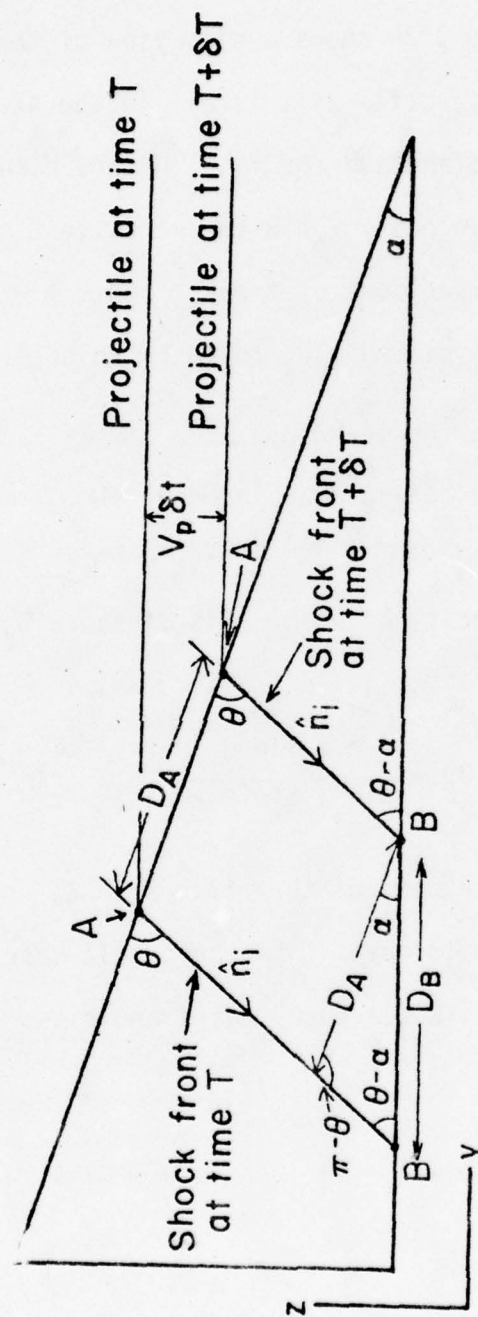
Fig. 3.24. Side view of wedge and shock front

90

where

$$n_{sx} = \sin \delta \cos \alpha \sin(\theta - \alpha) + \sin \alpha \sin \delta \cos(\theta - \alpha) \qquad (3.51)$$

$$n_{sy} = -\sin \alpha \cos \delta \sin(\theta - \alpha) \qquad (3.52)$$

$$n_{sz} = \sin \alpha \cos \delta \cos(\theta - \alpha) \qquad (3.53)$$

Given $\hat{n}_s$ it is possible to find the vector $\hat{n}_f$ which is parallel to the contact line between the shock front and the wedge free surface. This line, shown in Fig. 3.24 lies in the XY plane and is the intersection of the shock plane and the wedge free surface, or XY plane. $\hat{n}_f$ is given by the cross-product of the normals to these two planes

$$\hat{n}_f = -n_{sy} \hat{i} + n_{sx} \hat{j} \qquad (3.54)$$

The angle γ between the X axis and $\hat{n}_f$ is

$$\gamma = \arctan(\frac{-n_{sx}}{n_{sy}}) \qquad (3.55)$$

Equations (3.51), (3.52), (3.54), and (3.55) give

$$\gamma = \arctan \left[\frac{\sin \delta \cos \alpha \sin(\theta - \alpha) + \sin \alpha \sin \delta \cos(\theta - \alpha)}{\sin \alpha \cos \delta \sin(\theta - \alpha)} \right] \qquad (3.56)$$

This is the quantity of interest in the problem. Since points A and B have the same velocities they would have in the zero tilt case, all points on the contact line between the shock and the free surface have the same Y component of velocity they would have if the tilt were zero. The difference is that this line makes an angle γ with the Y axis, whereas γ would be zero if the tilt were zero. In fact Eq. (3.56) gives a value of zero for γ when δ is equal to zero. The only unknown in the problem is the angle θ. The analysis in Chapter 2 gives the value of θ for the zero-tilt case. Since δ is very

small, θ should be very close to the no-tilt value. In order to estimate the effect of tilt on the problem, this value of θ will be used.

Figure 3.25 illustrates the effect the angle γ will have on the resistance wire records. The contact point on one wire will always trail its zero tilt position relative to the contact point on the other wire by the distance H, given by

$$H = L \tan \gamma \tag{3.57}$$

where L is the distance between the two wires in the X direction. For the no-rate-effects case being considered, the contact points should sweep along the wires with the velocity V_B with which the contact line between the shock and free surface moves in the Y direction. From Eqs. (3.48) and (3.57) the error in time produced by this lag is

$$e_t = \frac{L \tan \gamma \sin \alpha \sin(\theta - \alpha)}{V_p \sin \theta} \tag{3.58}$$

The effect of this time error can be reduced by reducing the distance between the wires in the Y direction.

The methods of Chapter 2 yield a value of 36 degrees for θ when a five degree aluminum wedge is impacted by an aluminum projectile with a velocity of .09 centimeters per microsecond. If the tilt angle δ is assumed to be one milliradian, Eq.(3.56) yields a value of 13 milliradians for γ. If L is taken as .3173 centimeters, the error in time from Eq. (3.58) is 3.5 nanoseconds. This would constitute a .7 percent error if the time taken for the free surface to cross the wires was .5 microseconds.

92
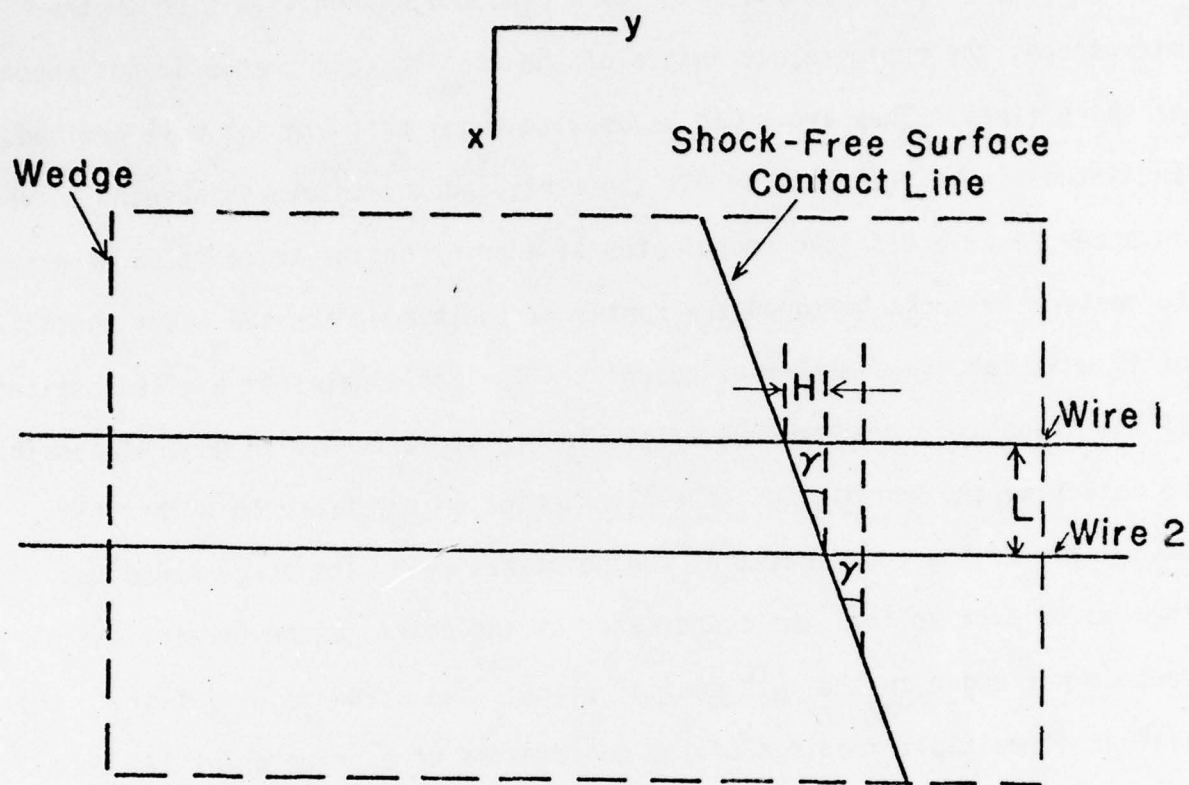
Fig. 3.25. Top view of wedge and resistance wires showing effect of tilt

93

3.4.5 Reading Errors

The last source of error to be considered is that involved with reading the photographic records with the microscope. When viewed under the microscope, the photographic images of the oscilloscope traces do not appear as sharp lines. They are broad bands with edges that are not well defined. The intensity of the trace is not constant, and the thickness appears to vary. In order to determine the coordinates of a point on the trace it is necessary to center the cross hairs on the center of the trace, and the exact position of this is largely a matter of judgment. The coordinates of a given setting of the stage are given to .001 millimeters, but it is not in general possible to determine the coordinates of a given point on the trace to within this accuracy. If the coordinates of the point are read, the stage moved and then moved back so that the coordinates of the point can be reread, the numbers do not agree in the last decimal place. The standard deviation in the scatter of multiple readings of the coordinates of a given point may be as much as .005 millimeters. Of course, this figure depends on several factors such as the given point being read and the individual taking the readings.

Given that there is some error in the coordinates of any given point, it is desirable to know how this error affects the results. It may have a large effect in the determination of the free surface velocity, since differences are taken between points that are relatively close together, thereby magnifying the error. In fact, although a plot of the coordinates of points on two traces which are fairly close together may appear smooth, a plot of the differences between the points is relatively rough.

The best way to determine the magnitude of errors generated in the process of reading the records with the microscope is to read the entire record twice and compare the results. This was done for one of the dual-beam

94

oscilloscope records obtained in a resistance wire experiment. The results, which are shown in Chapter 4 with other data taken, indicate that there is at most a one percent error produced by reading the records.

4. EXPERIMENTAL RESULTS

The objective of this work is the development of a method for performing and interpreting shock wave experiments in two-dimensional strain using a light gas gun. Since the work is developmental, the techniques themselves are the results rather than the data produced by the techniques. Therefore the experiments performed using the measurement technique were not done to investigate some particular physical phenomenon, but to investigate the measurement technique itself. The demonstration that a measurement technique is useful requires not only a presentation of the theory behind it, but also evidence that the theory is workable in practice and that physically meaningful results can be produced. Thus, as ideas for the technique were developed, shots were done to test the effectiveness of these ideas. Not all of these shots were successful in producing the information desired, but they were all useful in furthering the development of the technique. Refinement of the technique continued in this fashion until an end result was reached that was felt to be workable, repeatable, and capable of producing meaningful data. This is not meant to imply that the present technique is to be accepted as the final stage of development in two-dimensional measurement techniques and that no further refinement needs to be done. This is just the first step, and much work remains to improve the accuracy and resolution of two-dimensional techniques.

The data that will be presented in this chapter will not include all the developmental shots that lead to the present technique. Only the

final results using the finished technique will be shown, The purpose of these final shots was two-fold. First, it had to be demonstrated that the technique was workable and that the results could be repeated. Second, it had to be demonstrated that physically meaningful results could be obtained that could be compared to the predictions of the computer code. This would not only provide a test of the experimental method, but would also provide an evaluation of the code. The criteria for choosing the design parameters of the final shots were based on these two objectives.

Table 4.1 gives the design parameters for the final six shots. The shot numbers do not have any relation to the number of shots fired in this series of experiments. Shots 79, 80, and 81 were done to demonstrate the repeatability of the method. This required building three targets which were as similar to one another as possible. In order that the three wedges be as similar as possible, the wedge material was chosen to be 6061-T6 aluminum, which is easily machinable and whose properties are well known. The projectiles are machined from 6061-T6 aluminum, so this also meant that the projectile and wedge would be the same material. The projectile velocity was to be .09 centimeters per microsecond for all three shots, but this turned out to be the least repeatable part of the experiment. As can be seen in Table 4.1, shots 79 and 81 were within .5% of one another at about .088 centimeters per microsecond, but shot 80 was about 4.5% lower than these two.

Figures 4.1, 4.2, and 4.3 show the dual-beam oscilloscope records obtained from these shots. As can be seen from the figures, the initial levels of the traces did not always match, even though the initial voltages were known to match to within a few hundredths of a percent. Since the

97

TABLE 4.1 Summary of experimental results

Shot #	Impactor	Wedge	Wedge angle (degrees)	Projectile speed (cm/μsec)	Measured free surface speed (cm/μsec)	Predicted free surface speed from code (cm/μsec)	Predicted free surface speed (analytic) (cm/μsec)	Measured free surface disturbance speed (cm/μsec)	Predicted free surface disturbance speed (analytic) (cm/μsec)	Wedge tip thickness (cm)
75-001	Copper	Armco Iron	5.0	0.075	0.079-0.050	-	-	0.97 ± .03	0.97	0.015
75-008	6061-T6 Aluminum	1060 Aluminum	5.0	0.085	-	-	0.085	1.12	1.10	0.013
75-021	6061-T6 Aluminum	1060 Aluminum	5.0	0.087	0.084-0.090-0.079	-	0.087	1.14	1.13	0.011
75-042	1060 Aluminum	1060 Aluminum	5.0	0.089	0.070-0.110	-	0.088	1.26 ± .02	1.14	0.017
75-057	6061-T6 Aluminum	Single Crystal KCl	4.0	0.055?	0.054-0.072 (in 2 cm)	-	-	0.71 ± .01	0.92	0.030
75-064	1060 Aluminum	1060 Aluminum	5.0	0.088	0.090-0.074	-	0.088	0.99 ± .01	1.14	0.021
75-067	6061-T6 Aluminum	1060 Aluminum	4.0	0.074	0.092-0.102	-	0.075	1.20 ± .01	1.19	0.019
75-079	6061-T6 Aluminum	6061-T6 Aluminum	5.0	0.088	0.091	0.094	0.088	1.14	1.16 ± .02	0.012
75-080	6061-T6 Aluminum	6061-T6 Aluminum	5.0	0.084	0.086	0.090	0.084	1.08	1.08	0.010
75-081	6061-T6 Aluminum	6061-T6 Aluminum	5.0	0.088	0.092	0.094	0.088	1.14	1.16 ± .02	0.010
75-082	Copper	Armco Iron	5.1	0.068	0.060-0.076	0.061-0.070 (in 1 cm)	-	0.84 ± .01	0.86	0.005
75-083	6061-T6 Aluminum	Polycrystalline KCl	4.0	0.056	0.066-0.078	0.052-0.070 (in 2.7 cm)	-	0.95 ± .02	0.94	0.092
75-084	6061-T6 Aluminum	Single Crystal KCl	3.9	0.056	0.051-0.066	0.052-0.070 (in 2.7 cm)	-	0.95 ± .02	0.94	0.067
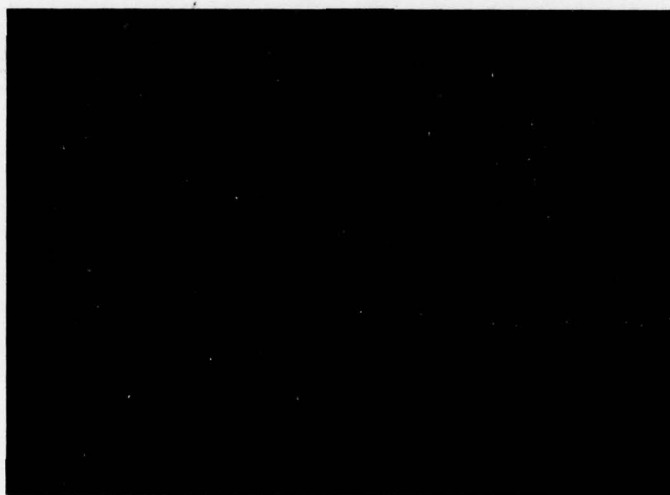
Fig. 4.1 Data record from shot 75-079
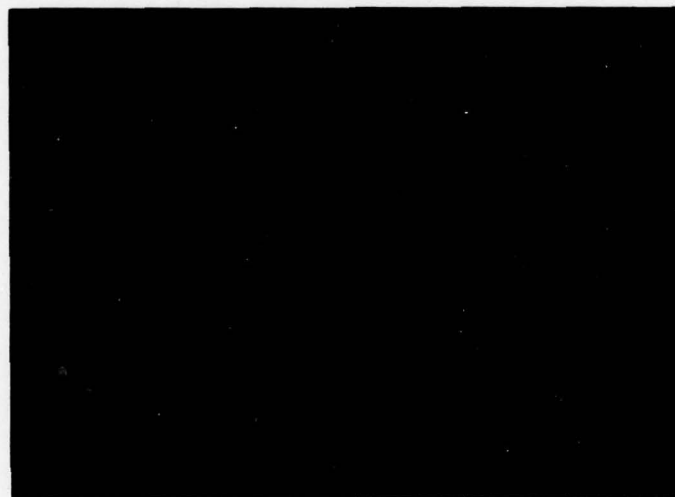
Fig. 4.2 Data record from shot 75-080

Fig. 4.3. Data record from shot 75-081

mismatch in the initial levels was larger than this, the data adjustment described in Section 3.4.2 was made.

The traces are very smooth and even, without any visible signs of noise. They continue decreasing smoothly up to the point at which the contact line between projectile and wedge has moved to the tip of the wedge. At this time the projectile impacts the wedge mounting surface described in Section 3.3 and waves begin to propagate through the target, which may cause the signals to break up. By this time the contact point has moved close to the tip of the wedge. The voltage at which the signal quits represents the voltage across that part of the wire which extends beyond the tip of the wedge.

Figures 4.4, 4.5, and 4.6 show the reduced data from shots 79, 80, and 81. These records of free surface velocity as a function of wedge position include both the curve for which the adjustment of Section 3.4.2 was made and that for which it was not made. Depending on the positions of the baselines and initial levels the adjusted values may be larger or smaller than the unadjusted values. In all three of these shots the baseline levels were superimposed, but the initial level of the second trace, which corresponds to the wire with the larger offset, was greater than that of the first trace. This means that the adjusted free surface velocity is larger than the unadjusted, so in Figs. 4.4, 4.5, and 4.6 the top line gives the corrected values of free surface velocity as a function of position. The wedge coordinate is defined so that it is zero at the tip of the wedge.

All three records show the same general type of behavior. There is an increase in velocity at the beginning, which corresponds to points near the high end of the wedge. Later comparisons with the computer code will show that this initial increase is due to rarefactions generated at the high

102
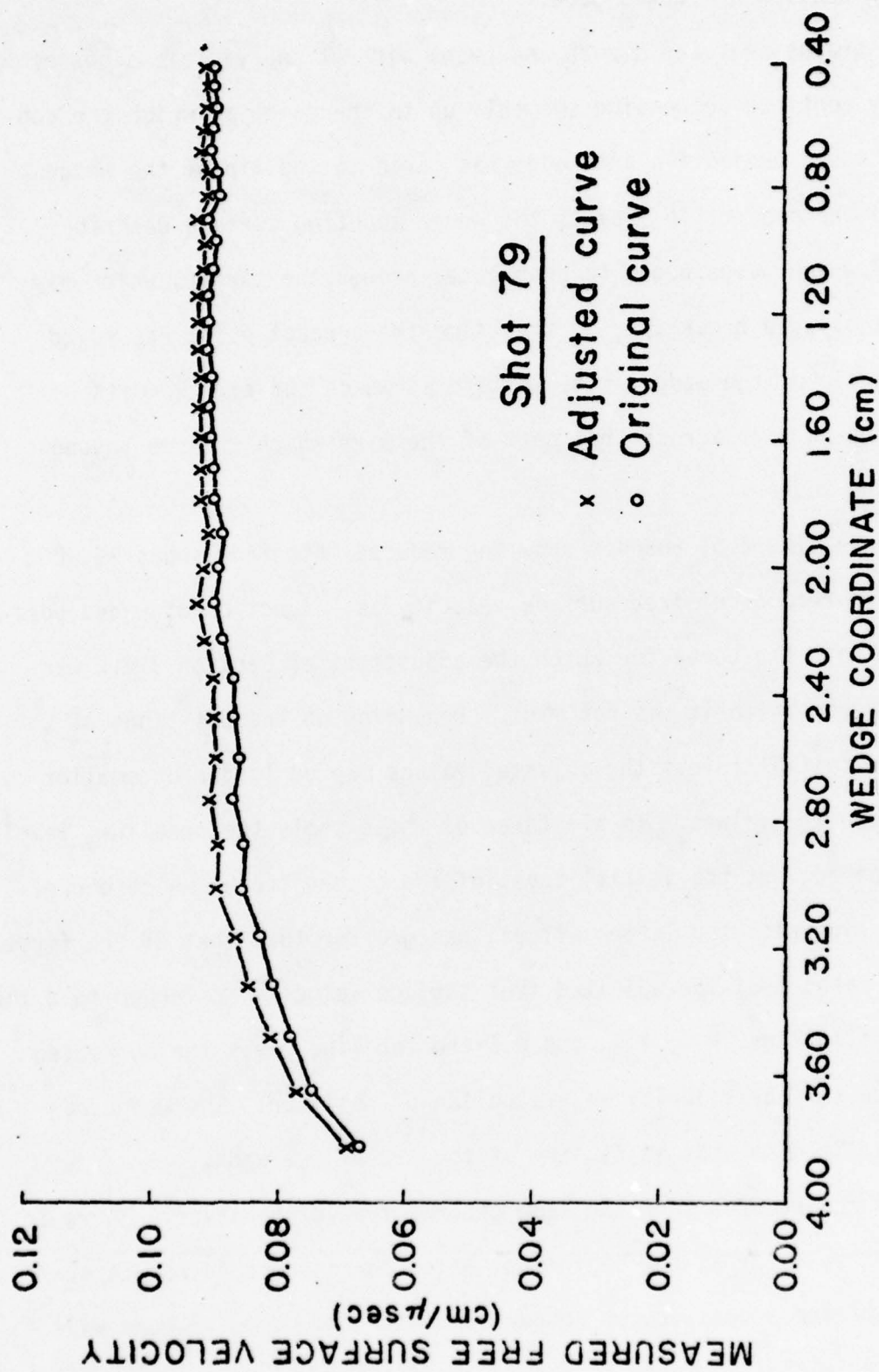
Fig. 4.4. Reduced data from shot 75-079

Shot 79

x Adjusted curve
○ Original curve

WEDGE COORDINATE (cm)

MEASURED FREE SURFACE VELOCITY (cm/μsec)

103
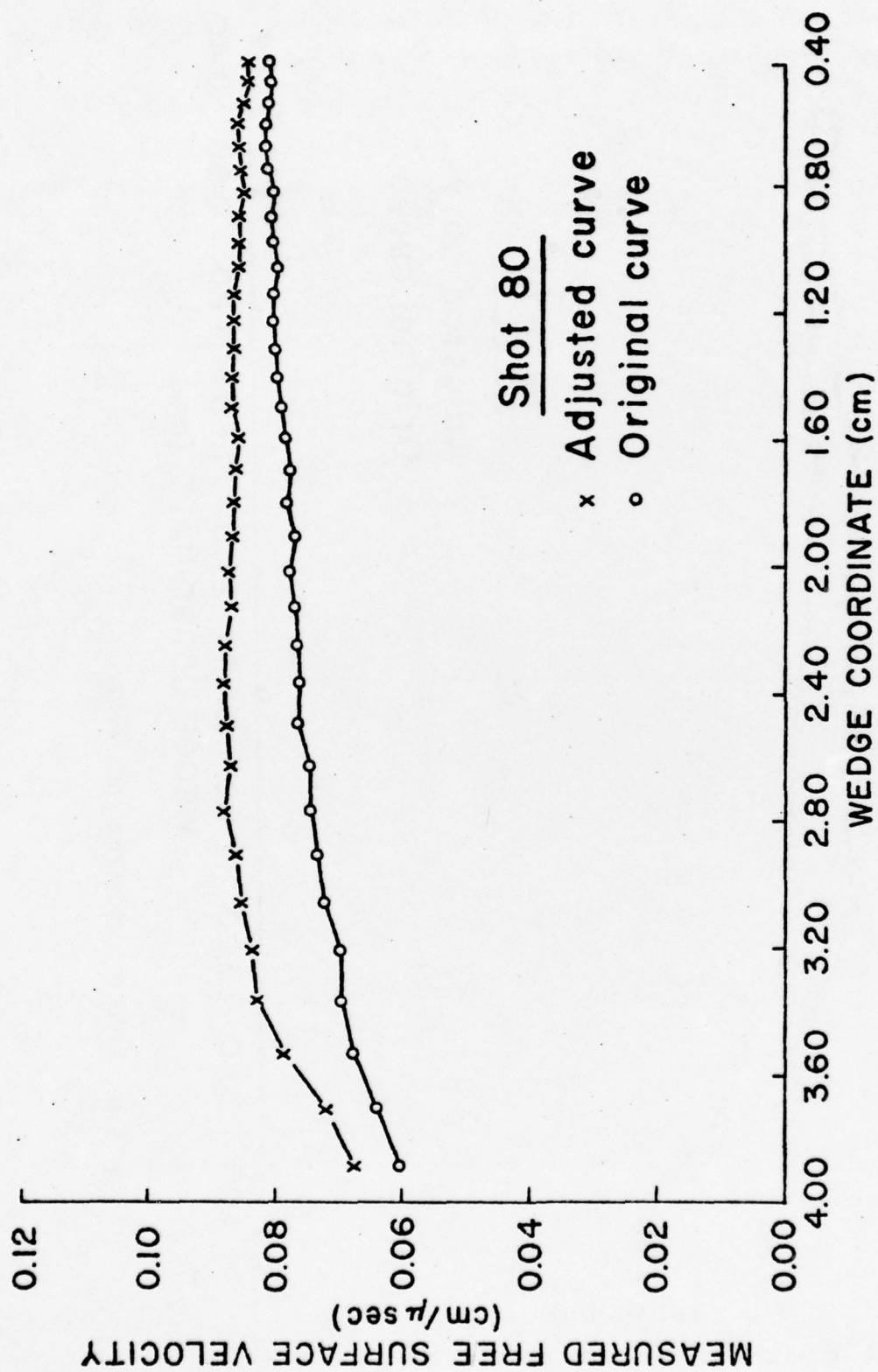
Fig. 4.5. Reduced data from shot 75-080
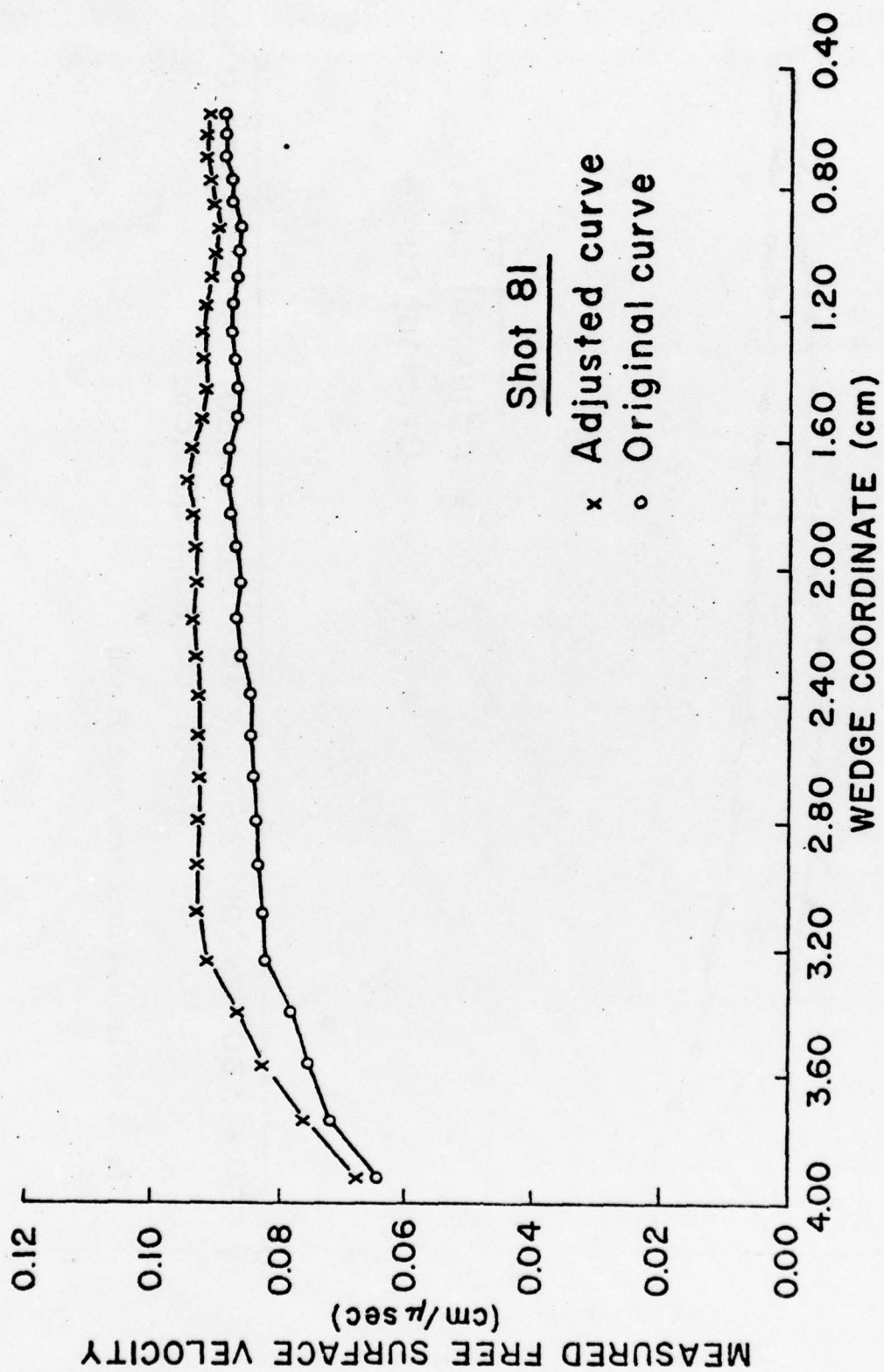
Fig. 4.6. Reduced data from shot 75-081

105

end of the wedge. This surface is free to move away from the wedge, and the resulting rarefactions decay the shock so that the free surface velocity is lower at this end of the wedge. The contact line between projectile and wedge along with the attached shocks moves faster than the rarefactions from the end, and by the time this region has outrun the rarefactions the free surface velocity has attained its steady-state value. The reduced data show that this steady-state value is attained in the region of wedge coordinate 3.2 centimeters to 3.4 centimeters. Since the wedge length is 4.45 centimeters, this shows that only the first 1 to 1.2 centimeters of the wedge are affected by the rarefactions from the end, and the rest of the wedge is described by the steady flow picture given in Section 1.2.1.

It may be noticed that the record does not extend to the maximum wedge coordinate, which corresponds to the high end of the wedge. This is also due to the rarefactions from the high end of the wedge. Because of these rarefactions the wedge free surface is concave upward in the region of large wedge coordinate, and the point on the free surface which first contacts the wire is not the point which was originally at the high end of the wedge. Thus, the discontinuities in voltage seen in Figs. 4.1, 4.2, and 4.3 would be present even if the wire did not extend beyond the high end of the wedge. For this reason the records begin at a wedge coordinate smaller than the maximum value.

The reduced data show that the measured free surface velocity is not completely constant even after it has attained its steady state value. The roughness in the record is attributed to scatter in the data and not to any physical changes in the sign of the acceleration of the free surface. A comparison of the three reduced records shows no apparent pattern to these changes.

106

The repeatability of the measurement technique is shown by Fig. 4.7 in which the adjusted curves of measured free surface velocity versus wedge position for shots 79, 80, and 81 are plotted on the same graph. Table 4.1 shows that shot 80 had the lowest measured projectile velocity and that 81 had the highest. The measured free surface velocities for the shots show this same order. Shots 79 and 81 had the same projectile velocity to within less than 1%. The adjusted measured free surface velocity curves for these two shots show a maximum deviation of about 5% in the region about 3.2 centimeters from the tip of the wedge, and the curves overlap in the region close to the tip. The average deviation between the two curves is at most 2% to 3%. The projectile velocity of shot 80 was about 5% lower than the projectile velocity of shots 79 and 81, and the curve of measured free surface velocity for this shot is also about 5% lower than the curve for those shots.

The comparisons between measured free surface velocity and measured projectile velocity for these three shots show that repeatability of the technique is very good. This comparison is not meant to imply that the free surface velocity is linearly related to the projectile velocity in general. The shots were as similar in all respects as possible, and it was hoped that the projectile velocities would be the same on all three in order to facilitate a comparison. However, it is not possible to control the projectile velocity with that much accuracy. Because of this the comparison is not as straightforward as could be hoped. However, if all else is held constant, the free surface velocity does increase with increasing projectile velocity. The results of these three shots show that even with the small disparities in projectile velocity, the repeatability is good enough that there are no anomalous results in which a smaller projectile velocity yields a larger free surface velocity. Furthermore, the methods of Chapter 2 indicate that for

107
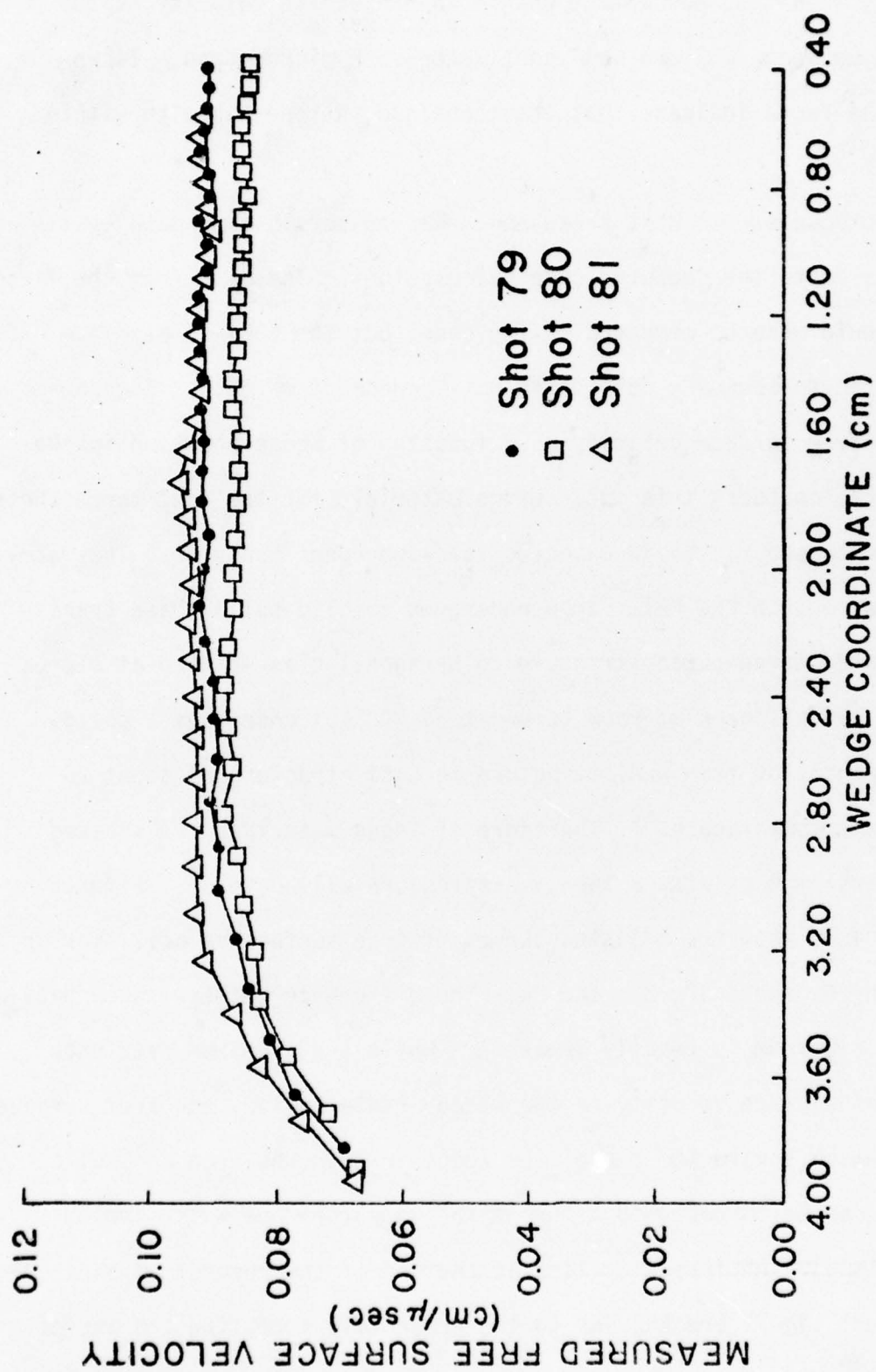
Fig. 4.7. Comparison of shots 75-079, 75-080, and 75-081

108

the case considered, the percentage change in the free surface velocity
should roughly equal the percentage change in projectile velocity as the
latter varies between .088 and .034 centimeters per microsecond. Taken
together, these facts indicate that the technique is repeatable to within
3% to 4%.

The purpose of the next three shots was to obtain some data that
could be compared to the computer code calculations. The data from the first
three shots could also be compared to the code, but the 6061-T6 aluminum
was not expected to show any detectable rate-dependent effects. The con-
stancy of the free surface velocity as a function of wedge position in the
steady-state region bears this out. Wedge materials for the next three shots
were therefore chosen for their expected rate-dependent behavior. The mate-
rials chosen were iron and KCl. Iron undergoes a solid-solid phase transi-
tion from body-centered-cubic structure to hexagonal-close-packed at a pres-
sure of about 130 kilobars at room temperature.[51] KCl undergoes a solid-
solid phase transition from NaCl structure to CsCl structure at about 20
kilobars at room temperature.[52] Therefore if these materials are shocked
past their transition points, a two-wave structure will develop. Figures
4.8, 4.9, and 4.10 show the adjusted curves of free surface velocity versus
wedge position for shots 82, 83, and 84. The difference between these data
and those for aluminum is readily apparent. While the aluminum data show
a constant free surface velocity in the steady-state region, the free surface
velocity increases toward the tip of the wedge in both the iron and KCl
wedges. This can be compared to a run of the computer code which includes
phase transitions. The irregularities at the end of the records of shots 82
and 83 represent signal breakup due to the projectile impacting the target
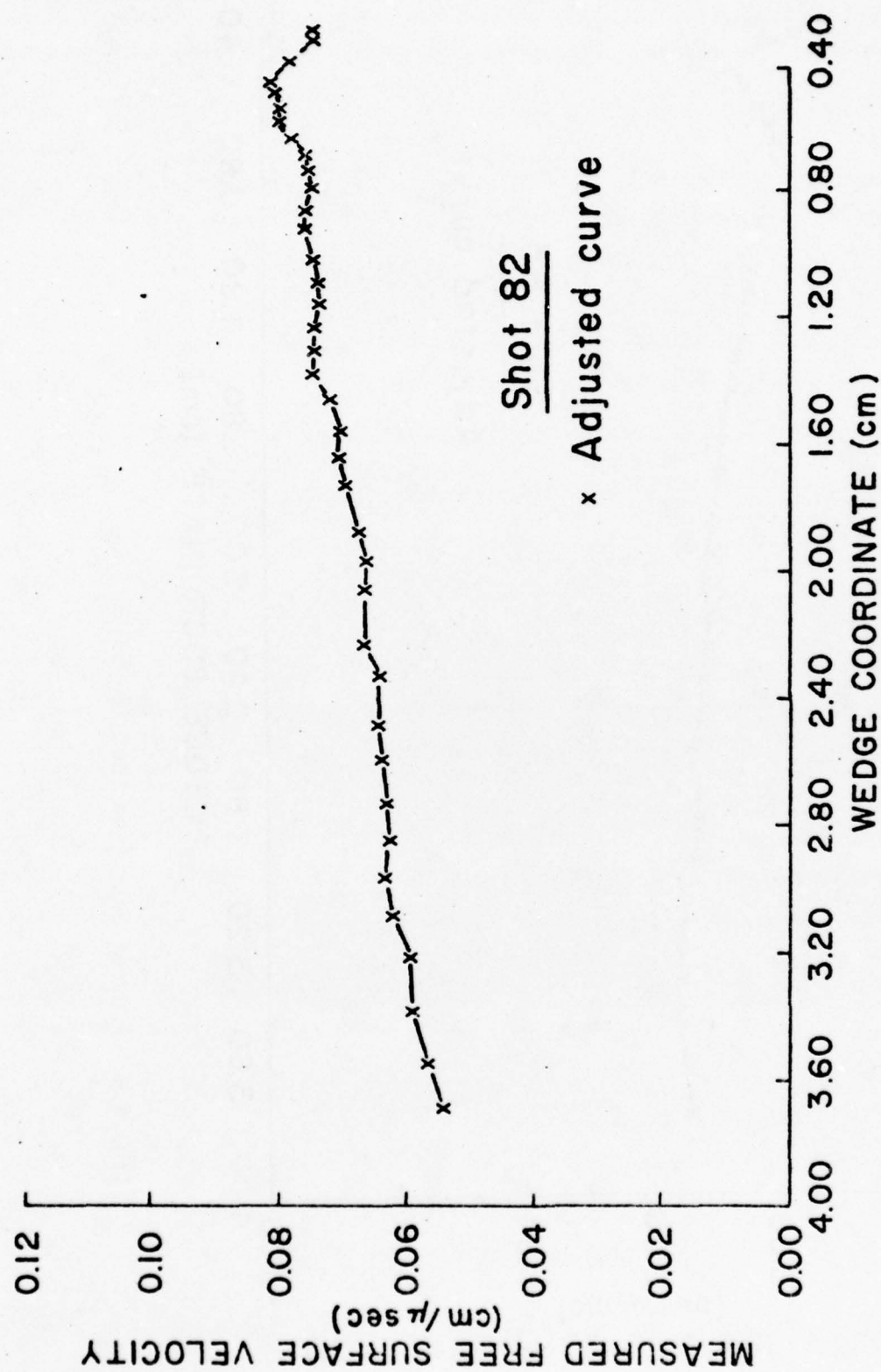
Fig. 4.8. Reduced data from shot 75-082
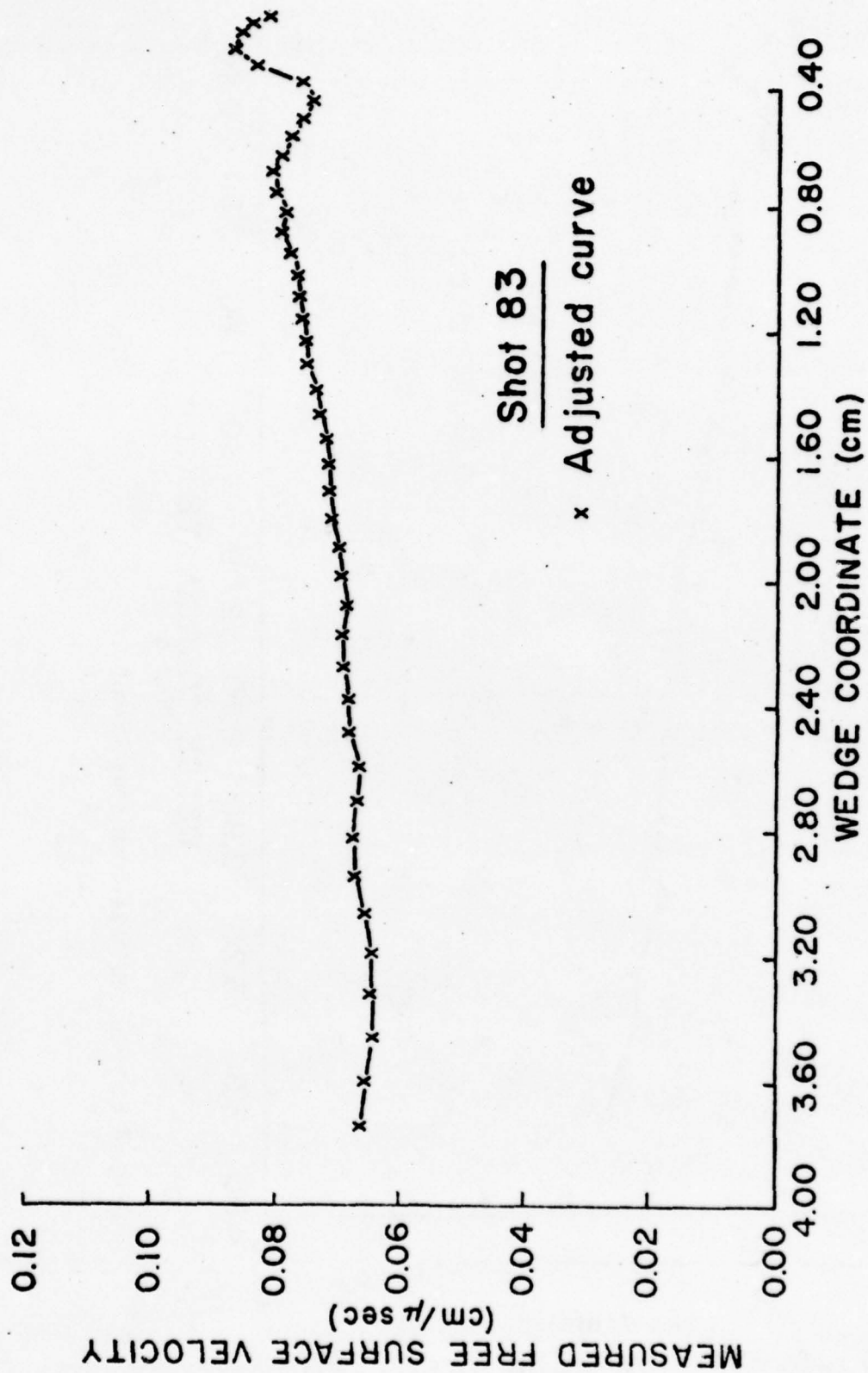
Fig. 4.9. Reduced data from shot 75-083

111
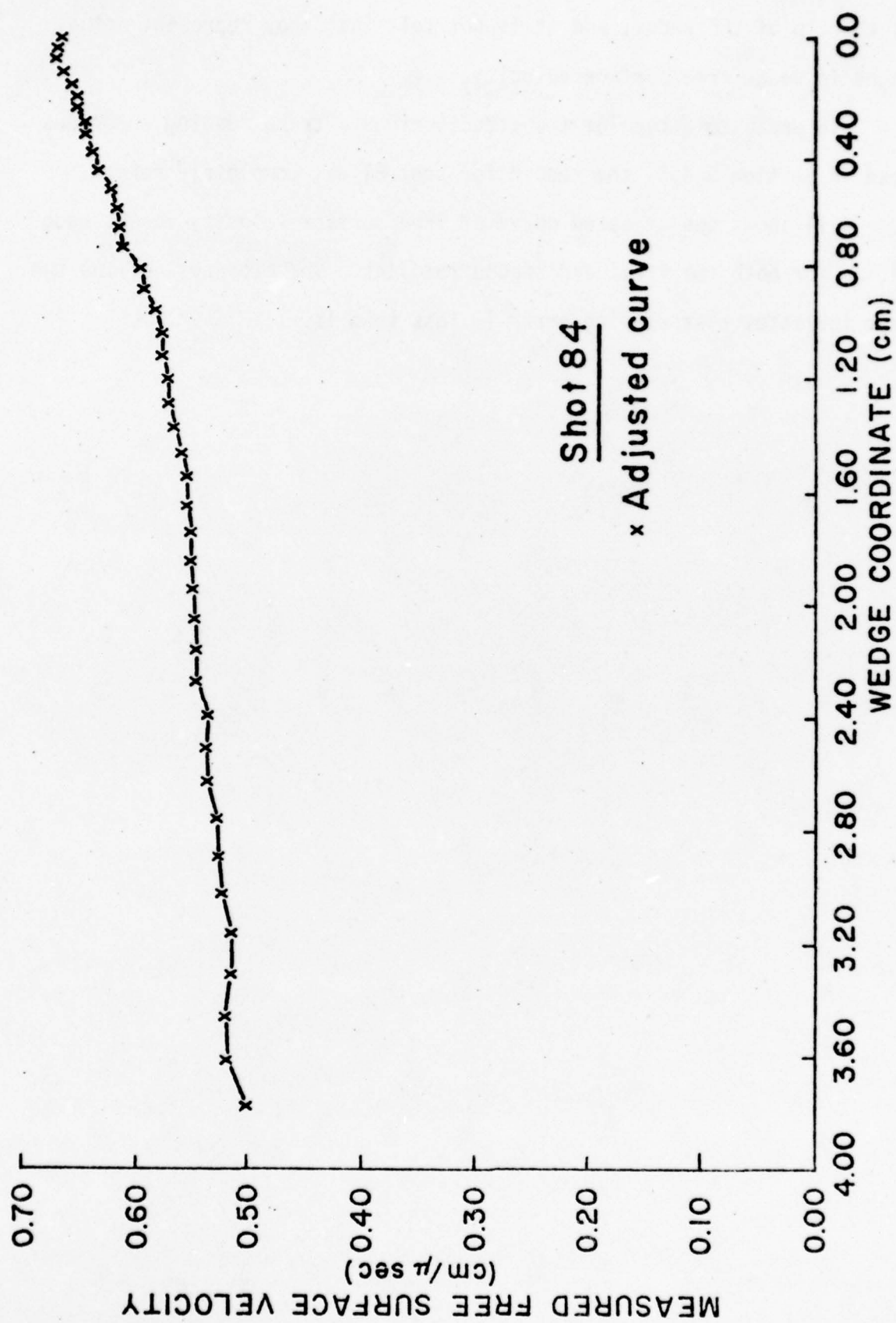
Fig. 4.10. Reduced data from shot 75-084

past the tip of the wedge, and it is not felt that they represent actual changes in wedge free surface velocity.

In order to determine the effects of data trace reading error described in Section 3.4.5, the record for shot 81 was completely reread. Figure 4.11 shows the adjusted curve of free surface velocity versus wedge position for both the first and second readings. The closeness of the two curves indicates that reading error is less than 1%.
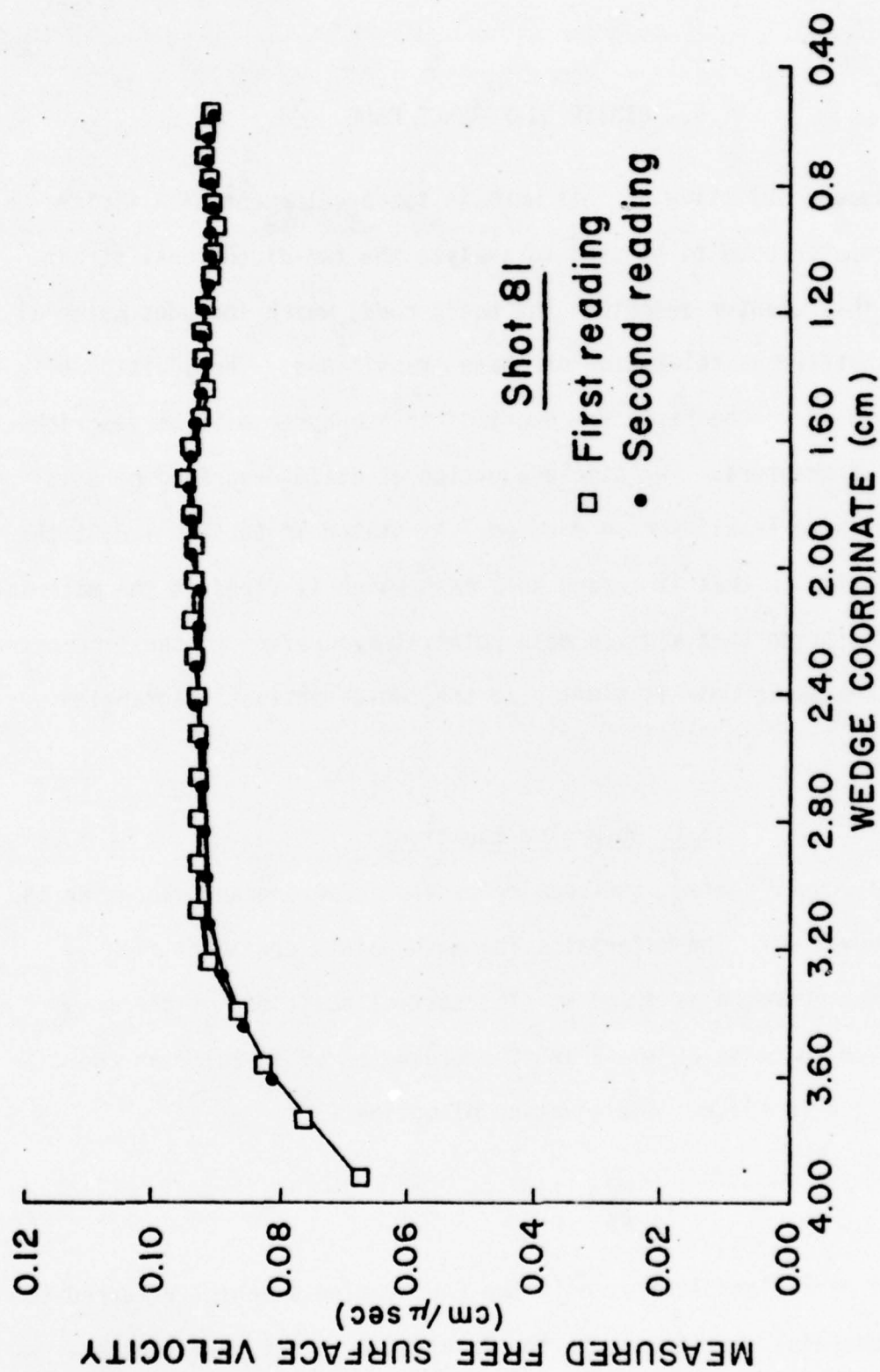
Fig. 4.11. Effect of reading errors on shot 75-081

5. FINITE DIFFERENCE CODE

The second objective of this work is the development of a finite-difference computer code to be used to analyze the two-dimensional strain experiment. This chapter describes the basic code, which includes material strength but not stress relaxation or phase transitions. The addition of these capabilities to the basic framework of this chapter will be described in the next two chapters. The simple equation of state described here is modified when phase transitions are added. As stated in Section 1.2.3, the code is Lagrangian in that it refers to a mesh which is fixed in the material and moves with it, so that a given mesh point always refers to the same material point. The basic code is similar to the two-dimensional Lagrangian code Toody.[37]

5.1 Governing Equations

As previously stated, the code refers to a Lagrangian mesh which is fixed in and moves with the material. The mesh points are identified by their Lagrangian coordinates j and k. The spatial positions of the mesh points are given in terms of the X and Y coordinates of an Eulerian coordinate system fixed in space. The equation of motion is[53]

$$\frac{d\vec{V}}{dt} = \frac{1}{\rho} \nabla \cdot \overset{\leftrightarrow}{\sigma}$$ (5.1)

where $\vec{V}$ is the particle velocity, $\vec{\sigma}$ is the Cauchy stress tensor referred to the Eulerian coordinate system, ∇ is the Eulerian gradient operator, and d/dt is the convective derivative.[54]

$$\frac{df}{dt} = (\frac{\partial}{\partial t} + \vec{v} \cdot \nabla)f \tag{5.2}$$

The convective derivative gives the change in a quantity as seen by an observer moving with the flow. This need not be evaluated by the use of the right-hand side of Eq. (5.2) but merely by taking the time derivative of a quantity while holding the Lagrangian coordinates constant.

In component form the equation of motion in two dimensions becomes

$$\rho d\dot{x}/dt = \partial \sigma_{xx}/\partial x + \partial \sigma_{xy}/\partial y \tag{5.3}$$

$$\rho d\dot{y}/dt = \partial \sigma_{xy}/\partial x + \partial \sigma_{yy}/\partial y \tag{5.4}$$

where $\dot{x}$ and $\dot{y}$ are the convective derivatives of x and y. Conservation of mass is implicit in the Lagrangian form because the mass contained within each mesh is constant.

The equation of state will be elastic-plastic. Hooke's law in incremental form is

$$d\sigma_{ij} = \lambda \, d\Delta \; \delta_{ij} + 2\mu \, d\varepsilon_{ij} \tag{5.5}$$

where $d\Delta$ is the dilatation, $\overleftrightarrow{\varepsilon}$ is the strain tensor, δ_{ij} is the Kronecker delta, and λ and μ are the Lamè constants.

Introducing the stress and strain deviators

$$S_{ij} = \sigma_{ij} - \sigma_m \, \delta_{ij} \tag{5.6}$$

and

$$de_{ij} = d\varepsilon_{ij} - d\varepsilon_m \, \delta_{ij} \tag{5.7}$$

116

where

$$\sigma_m = (\sigma_{xx} + \sigma_{yy} + \sigma_{zz})/3 \equiv -P \qquad (5.8)$$

$$d\epsilon_m = (d\epsilon_{xx} + d\epsilon_{yy} + d\epsilon_{zz})/3 = d\Delta/3 = dV/3V \qquad (5.9)$$

Hooke's law may be written

$$dS_{ij} + d\sigma_m \delta_{ij} = \lambda \, d\Delta \, \delta_{ij} + 2\mu(de_{ij} + d\epsilon_m \delta_{ij}) \qquad (5.10)$$

Equating the deviator parts,

$$dS_{ij} = 2\mu \, de_{ij} = 2\mu(d\epsilon_{ij} - \delta_{ij} \, dV/3V) \qquad (5.11)$$

If these changes occur in time dt,

$$\dot{S}_{ij} = 2\mu(\dot{\epsilon}_{ij} - \delta_{ij} \, \dot{V}/3V) \qquad (5.12)$$

where the velocity strains[55] are defined as

$$\dot{\epsilon}_{ij} = (1/2)(\partial \dot{x}_i/\partial x_j + \partial \dot{x}_j/\partial x_i) \qquad (5.13)$$

By definition the sum of the diagonal elements of the strain deviator tensor is equal to zero; in two-dimensional strain $\dot{V}/V$ is equal to the sum of $\dot{\epsilon}_{xx}$ and $\dot{\epsilon}_{yy}$.

A constitutive equation must satisfy the criterion of frame-indifference,[56] which means it should be correct for coordinate transformations in which distance and time intervals are unchanged, including rigid body motion. If $\dot{S}_{ij}$ is the ordinary Lagrangian derivative, Eq. (5.12) is not frame-indifferent under rigid body motion. Considering the x component,

$$\dot{S}_{xx} = 2\mu(\dot{\epsilon}_{xx} - \dot{V}/3V) \qquad (5.14)$$

117

For a rigid body rotation both $\dot{\varepsilon}_{xx}$ and $\dot{V}/V$ are zero, implying $\dot{\overset{\leftrightarrow}{S}}_{xx}$ is zero. However, for rigid body rotations the magnitude of the force $\overset{\leftrightarrow}{S} \cdot \vec{n}$ acting on a face with unit normal $\vec{n}$ is unchanged, but the individual components $S_{xx}n_x$ etc. related to an Eulerian coordinate system fixed in space are changed. Thus, if the body under consideration rotates rigidly through some angle α about the z-axis, the total change in S_{xx} is not zero, even though the right-hand side of the above equation is zero. Tensors transform under rotation according to the rule[57]

$$S'_{ij} = a_{im}a_{jn}S_{mn} \tag{5.15}$$

where repeated subscripts imply summation.

For rotation about a z-axis through the infinitesimal angle α,

$$A = ||a_{ij}|| = \begin{pmatrix} 1 & \alpha & 0 \\ -\alpha & 1 & 0 \\ 0 & 0 & 1 \end{pmatrix} \tag{5.16}$$

Thus

$$S'_{xx} = S_{xx} + 2S_{xy}\alpha \tag{5.17}$$

$$S'_{yy} = S_{yy} - 2S_{xy}\alpha \tag{5.18}$$

$$S'_{xy} = S_{xy} + (S_{yy} - S_{xx})\alpha \tag{5.19}$$

Just as the strain is the symmetric part of the velocity gradient tensor, the rotation is the anti-symmetric part. Thus the velocity strain tensor is given in Eq. (5.13) and the rate of rotation or vorticity tensor[55] is

$$V_{ij} = (1/2)(\partial \dot{x}_i/\partial x_j - \partial \dot{x}_j/\partial x_i) \tag{5.20}$$

118

Therefore, the rate of rigid body rotation in the x-y plane is

$$V_{xy} = (1/2)(\partial \dot{x}/\partial y - \partial \dot{y}/\partial x) \tag{5.21}$$

In time δt the angle through which the body rotates is $\alpha = V_{xy}\delta t$. So

$$S_{xx}(t + \delta t) = S_{xx}(t) + 2S_{xy} V_{xy} \delta t \tag{5.22}$$

or

$$[S_{xx}(t + \delta t) - S_{xx}(t)]/\delta t = 2S_{xy} V_{xy} \tag{5.23}$$

In the limit the contribution to $\dot{S}_{xx}$ due purely to rigid body rotation is

$$\dot{S}_{xx} = 2S_{xy} V_{xy} \tag{5.24}$$

The full set of frame-indifferent equations including changes in $\overset{\leftrightarrow}{S}$ due both to distortion of the mesh and rotation of the mesh is

$$\dot{S}_{xx} = S_{xy}(\partial \dot{x}/\partial y - \partial \dot{y}/\partial x) + 2\mu(\dot{\epsilon}_{xx} - \dot{V}/3V) \tag{5.25}$$

$$\dot{S}_{yy} = -S_{xy}(\partial \dot{x}/\partial y - \partial \dot{y}/\partial x) + 2\mu(\dot{\epsilon}_{yy} - \dot{V}/3V) \tag{5.26}$$

$$\dot{S}_{xy} = (1/2)(S_{yy} - S_{xx})(\partial \dot{x}/\partial y - \partial \dot{y}/\partial x) + 2\mu\dot{\epsilon}_{xy} \tag{5.27}$$

The Von Mises yield condition[58] is

$$J_2 \leq Y_0^2/3 \tag{5.28}$$

where $J_2 = (1/2)S_{ij}S_{ij}$ is the second invariant of the stress deviator tensor, and Y_0 is the yield strength in simple tension.

In two-dimensional strain ϵ_{xx}, ϵ_{yy}, and ϵ_{xy} are the only non-zero strain components. Then, from Eq. (5.11), S_{xx}, S_{yy}, S_{xy}, and S_{zz} are the only non-zero

stress deviators, and

$$J_2 = (1/2)(S_{xx}^2 + S_{yy}^2 + S_{zz}^2 + 2S_{xy}^2) \qquad (5.29)$$

By definition $S_{ii}=0$, so

$$S_{zz} = -(S_{yy} + S_{xx}) \qquad (5.30)$$

and

$$J_2 = S_{xx}^2 + S_{yy}^2 + S_{xy}^2 + S_{xx}S_{yy} \qquad (5.31)$$

In Eq. (5.12) the deviator stress should be related only to the elastic part of the deviator strain. If the material is completely elastic the elastic strain is the total strain. However, in plasticity theory, the deviator strain is normally decomposed into elastic and plastic parts. Elastic-plastic theory is implemented here by performing the calculation in Eq. (5.25), (5.26), and (5.27) as though the material were completely elastic by using the total strain in the equations. The Von Mises yield criterion is then applied to determine whether the material behavior is elastic or plastic. If the inequaility in Eq. (5.28) is satisfied, the material is elastic; if not, it is plastic. Plotted in principal stress deviator space, the equality in Eq. (5.28) defines a sphere centered on the origin. The fact that the sum of the principal stress deviators must vanish requires all obtainable points in this space to lie on a plane through the origin. The intersection of this plane with the sphere described by the yield criterion is a circle. If the material state is such that the point defined By S_1, S_2, and S_3 lies within this circle, the material is elastic; if the point is outside the circle, it is plastic. Plastic flow is described by assuming that the stress deviators are maintained at the elastic limit. Thus if at any time Eqs. (5.25), (5.26),

120

and (5.27) give a point which lies outside the yield circle, the material is assumed to flow plastically and the stress state is moved normally back to the yield surface. This limits the stress component associated with the plastic strain.[59]

The stress state is moved normally back to the yield surface by multiplying each of the principal stress deviators by the same constant, so that the equality in Eq. (5.28) is satisfied. However, it is not necessary to compute the principal stress deviators in order to do this. The principal stress deviators are obtained from the components of the stress deviator tensor in a representation with respect to any other set of axes by a transformation of the type described by Eq. (5.15). The principal stress deviators are a linear combination of any other set of non-principal stress deviators. Thus, multiplying all non-principal stress deviators by a given constant is equivalent to multiplying the principal stress deviators by that constant. Therefore elastic-plastic behavior is implemented by calculating the stress deviators from Eq. (5.25), (5.26), and (5.27) using the total strain. If Eq. (5.28) is violated, each stress deviator is multiplied by the same constant so that the equality holds in Eq. (5.28).

The increase in internal energy produced by adding an amount of heat dQ to unit mass and doing work dW on it is

$$dE = dQ + dW \tag{5.32}$$

In the present case

$$dE = dQ + V\sigma_{ij} d\varepsilon_{ij} \tag{5.33}$$

In terms of stress deviators and P,

$$dE = dQ + VS_{ij} d\varepsilon_{ij} - VP(dV/V) \tag{5.34}$$

121

It is assumed that there is no transfer of heat to or from the mass element, $dQ=0$. If the above amount of work is done in time dt, then

$$\dot{E} = VS_{ij}\dot{\epsilon}_{ij} - VP(\dot{V}/V)$$

$$= V(S_{xx}\dot{\epsilon}_{xx} + S_{yy}\dot{\epsilon}_{yy} + 2S_{xy}\dot{\epsilon}_{xy} - P\dot{V}/V) \qquad (5.35)$$

The equation of state for the mean pressure will start from the general equation[60]

$$P = P_H + \rho\Gamma(E - E_H) \qquad (5.36)$$

where the subscript H refers to quantities on the Hugoniot. If the Hugoniot is represented by an equation of the form

$$U_s = C_0 + su_p \qquad (5.37)$$

then

$$P_H = \rho_0 C_0^2 \eta / (1 - s\eta)^2 \qquad (5.38)$$

and

$$E_H = P_H\eta/2\rho_0 \qquad (5.39)$$

where

$$\eta = 1 - \rho_0/\rho \qquad (5.40)$$

If it is assumed that $\rho\Gamma = \rho_0\Gamma_0 = $ constant, then

$$P = \rho_0 C_0^2 \eta / (1 - s\eta)^2 + \rho_0\Gamma_0 [E - C_0^2\eta^2/2(1 - s\eta)^2]$$

$$= \rho_0 C_0^2 \eta (1 - \Gamma_0\eta/2)/(1 - s\eta)^2 + \rho_0\Gamma_0 E \qquad (5.41)$$

122

The bulk sound speed is given by

$$C_b = (\partial P/\partial \rho)_S^{\frac{1}{2}} \qquad (5.42)$$

where s denotes entropy. Differentiating the expression for P,

$$c_b^2 = (\rho_0 C_0/\rho)^2 (1 - \Gamma_0 \eta + s\eta)/(1 - s\eta)^3 + \rho_0 \Gamma_0 P/\rho^2 \qquad (5.43)$$

The elastic sound speed is

$$c_L^2 = (K + 4\mu/3)/\rho \qquad (5.44)$$

while the bulk sound speed is

$$c_b^2 = K/\rho \qquad (5.45)$$

K and μ are related by

$$\mu = 3(1 - 2\nu)K/2(1 + \nu) \qquad (5.46)$$

where ν is Poisson's ratio. Then

$$\mu = 3(1 - 2\nu)\rho c_b^2/2(1 + \nu) \qquad (5.47)$$

Putting in μ and K, the expression for c_L^2 becomes

$$c_L^2 = 3(1 - \nu)c_b^2/(1 + \nu) \qquad (5.48)$$

c_b^2 is thus known as a function of P and ρ, and μ and c_L^2 are found from the above equations, assuring that Poisson's ratio is constant.

Shocks are handled in the program by use of the Von Neumann and Richtmeyer method of artificial viscosity.[61] This involves replacing P by P+q where q is the artificial viscosity. The inclusion of this term spreads the shock over a few meshes, so that shocks become regions where quantities are

123

changing rapidly, rather than discontinuities, allowing the difference equations to describe the situation. The artificial viscosity will be the same as that used in TOODY

$$q = \rho A B_1^2 (\dot{V}/V)^2 - \rho A^{\frac{1}{2}} B_2 C_L (\dot{V}/V), \qquad \dot{V}/V < 0 \qquad (5.49a)$$

$$= 0, \; \dot{V}/V > 0 \qquad (5.49b)$$

where A is the mesh area, included so that the constants B_1 and B_2 are dimensionless.

5.2 Recapitulation

The equations to be used in the program are:

1. $\sigma_{xx} = S_{xx} - (P + q)$ (5.50a)

2. $\sigma_{yy} = S_{yy} - (P + q)$ (5.50b)

3. $\sigma_{xy} = S_{xy}$ (5.50c)

4. $\rho \, d\dot{x}/dt = \partial\sigma_{xx}/\partial x + \partial\sigma_{xy}/\partial y$ (5.3)

5. $\rho \, d\dot{y}/dt = \partial\sigma_{xy}/\partial x + \partial\sigma_{yy}/\partial y$ (5.4)

6. $\dot{\varepsilon}_{xx} = \partial\dot{x}/\partial x$ (5.51a)

7. $\dot{\varepsilon}_{yy} = \partial\dot{y}/\partial y$ (5.51b)

8. $\dot{\varepsilon}_{xy} = (1/2)(\partial\dot{y}/\partial x + \partial\dot{x}/\partial y)$ (5.51c)

9. $\dot{V}/V = \partial\dot{x}/\partial x + \partial\dot{y}/\partial y$ (5.52)

10. $C_b^2 = (\rho_0 C_0/\rho)^2 (1 - \Gamma_0 n + sn)/(1 - sn)^3 + \rho_0 \Gamma_0 P/\rho^2$ (5.43)

11. $\mu = 3(1 - 2\nu)\rho C_b/2(1 + \nu)$ (5.47)

12. $\dot{S}_{xx} = S_{xy}(\partial\dot{x}/\partial y - \partial\dot{y}/\partial x) + 2\mu(\dot{\varepsilon}_{xx} - \dot{V}/3V)$ (5.25)

13. $\dot{S}_{yy} = -S_{xy}(\partial\dot{x}/\partial y - \partial\dot{y}/\partial x) + 2\mu(\dot{\varepsilon}_{yy} - \dot{V}/3V)$ (5.26)

14. $\dot{S}_{xy} = (1/2)(S_{yy} - S_{xx})(\partial\dot{x}/\partial y - \partial\dot{y}/\partial x) + 2\mu\dot{\epsilon}_{xy}$ (5.27)

15. $J_2 = S_{xx}^2 + S_{xy}^2 + S_{yy}^2 + S_{xx}S_{yy}$ (5.31)

16. If $J_2 > Y_0^2/3$, $S_{ij} = S_{ij}\sqrt{Y_0^2/3J_2}$ (5.53)

17. $C_L^2 = 3(1 - \nu)C_b^2/(1 + \nu)$ (5.48)

18. $q = \rho A B_1^2 (\dot{V}/V)^2 - \rho A^{\frac{1}{2}}B_2 C_L(\dot{V}/V)$, $\dot{V}/V < 0$ (5.49a)

    $= 0$, $\dot{V}/V > 0$ (5.49b)

19. $\dot{E} = V[S_{xx}\dot{\epsilon}_{xx} + S_{yy}\dot{\epsilon}_{yy} + 2S_{xy}\dot{\epsilon}_{xy} - (P + q)\dot{V}/V]$ (5.54)

20. $P = \rho_0 C_0^2 \eta (1 - \Gamma_0 \eta/2)/(1 - s\eta)^2 + \rho_0\Gamma_0 E$ (5.41)

5.3 Difference Equations

The finite difference scheme to be used was developed by Mark Wilkins and is used in HEMP[38] and TOODY. It is based on the identity

$$\int_A d\vec{A} \times \nabla\psi = \oint_C \psi d\vec{l}$$ (5.55)

where ψ is a scalar function defined over an area A enclosed by the curve C. Taking a small area in the x-y plane, as shown in Fig. 5.1,

$$d\vec{A} = \hat{k}dA$$ (5.56)

where $\hat{k}$ is the unit vector in the z direction and dA is the area enclosed by curve C. If the area is small enough, the left-hand integrand may be taken as constant and equal to its value at the point x,y. Thus

$$\int_A d\vec{A} \times \nabla\psi = dA(\hat{k} \times \nabla\psi)$$
$$= dA(-\hat{i}\partial\psi/\partial y + \hat{j}\partial\psi/\partial x)$$ (5.57)

125
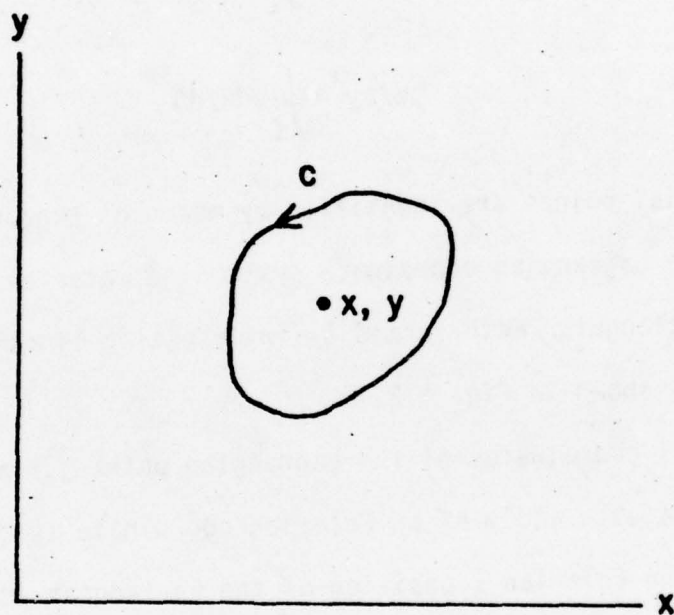
Fig. 5.1.   Path of integration in X-Y
plane

So

$$dA(-\hat{i}\partial\psi/\partial y + \hat{j}\partial\psi/\partial x) = \hat{i}\oint_C \psi dx + \hat{j}\oint_C \psi dy \qquad (5.58)$$

where $\hat{i}$ and $\hat{j}$ are unit vectors in the x and y directions. Therefore approximate formulas for the partial derivatives are

$$\partial\psi/\partial x \simeq \oint_C \psi dy/dA \qquad (5.59a)$$

$$\partial\psi/\partial y \simeq -\oint_C \psi dx/dA \qquad (5.59b)$$

Material points are identified by means of Lagrangian coordinates j and k. In the Lagrangian coordinate system the material is represented by an unchanging rectangular mesh formed by intersecting lines of constant j and constant k, as shown in Fig. 5.2.

Spatial coordinates of the Lagrangian point j,k are given in terms of the coordinates x and y of an Eulerian coordinate system fixed in space. Thus $x_{j,k}$ is the Eulerian x position of the Lagrangian point j,k, and $y_{j,k}$ is its y position. Plotting positions of each of the Lagrangian points j,k in the Eulerian x,y system as in Fig. 5.3 produces a mesh that defines the shape of the material.

Equations (5.59a) and (5.59b) approximating the partial derivatives may be applied to the quadrilaterals formed in the Eulerian system by the intersections of lines of constant j and k. If ψ is some function defined in the j,k plane, as in Fig. 5.4, $\psi_{j,k}$ will denote the value of ψ at the position of the Lagrangian mesh point j,k. For convenience of notation, when referring to Fig. 5.4 the position of j,k will be denoted by point 1, j,k-1 by point 2, j-1,k-1 by point 3, and j-1,k by point 4. If ψ were constant

127
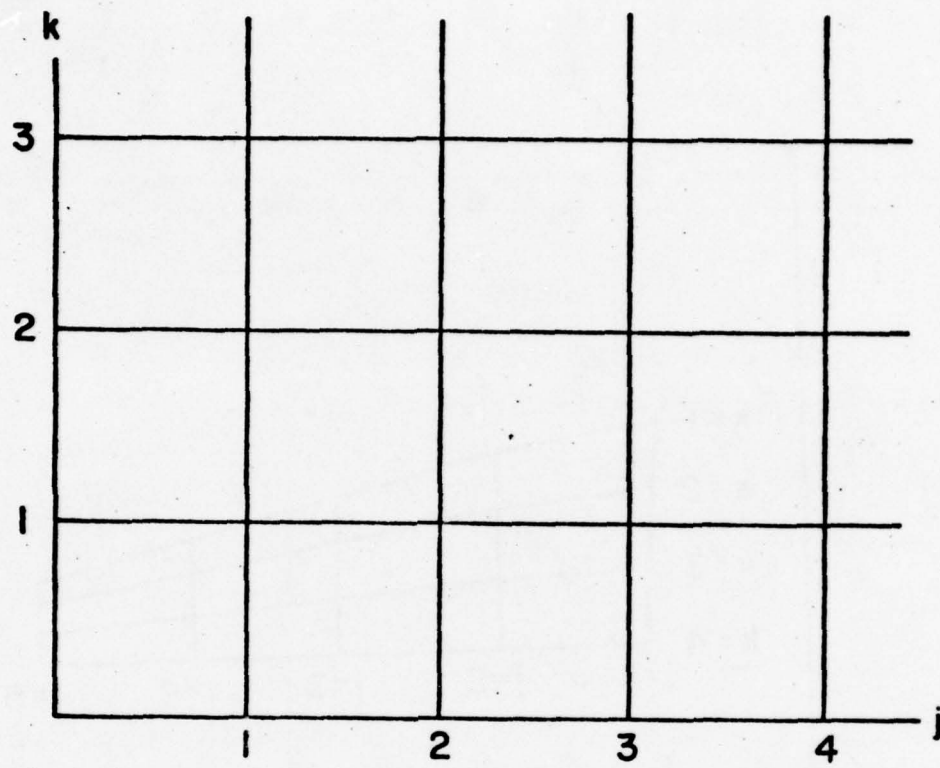
Fig. 5.2.   Lagrangian coordinate system
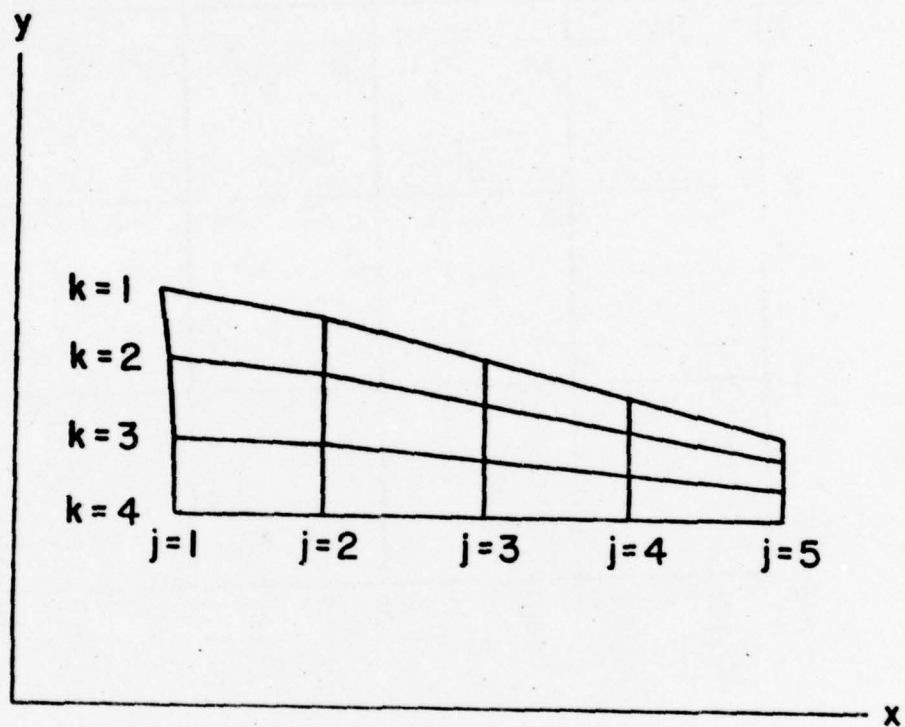
Fig. 5.3. Eulerian coordinate system
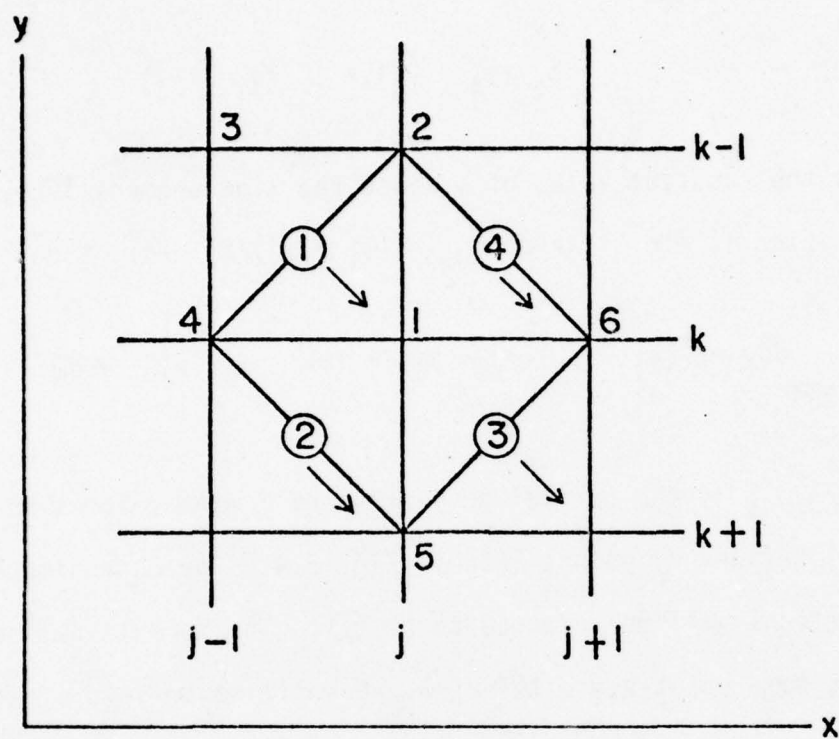
Fig. 5.4.   Space index organization

along each of the line segments $\overline{12}$, $\overline{23}$, $\overline{34}$, $\overline{41}$, then

$$\oint_{\overline{1234}} \psi dy = \psi_{\overline{12}}(y_2 - y_1) + \psi_{\overline{23}}(y_3 - y_2)$$

$$+ \psi_{\overline{34}}(y_4 - y_3) + \psi_{\overline{41}}(y_1 - y_4) \qquad (5.60)$$

where $\psi_{\overline{12}}$ is the constant value of ψ along the line segment $\overline{12}$, y_1 is the y position of point 1, etc. Taking $\psi_{\overline{12}} = (\psi_1 + \psi_2)/2$, etc., then

$$\oint_{\overline{1234}} \psi dy = [(\psi_1 - \psi_3)(y_2 - y_4) + (\psi_2 - \psi_4)(y_3 - y_1)]/2 \qquad (5.61)$$

Now $\oint_{\overline{1234}} \psi dy / A_{1234}$ is the partial derivative of ψ with respect to x within the quadrilateral defined by points 1234 in Fig. 5.4. For convenience of notation this quadrilateral will be referred to as ①. The formula defines the partial derivative at some point x,y within ①. Quantities defined within a mesh quadrilateral are assumed constant throughout it. Therefore the formula for the partial derivative of ψ with respect to x in quadrilateral ① is

$$\partial \psi / \partial x \big|_{①} = [(\psi_1 - \psi_3)(y_2 - y_4) + (\psi_2 - \psi_4)(y_3 - y_1)]/2A_{①} \qquad (5.62)$$

Similarly

$$\partial \psi / \partial y \big|_{①} = -[(\psi_1 - \psi_3)(x_2 - x_4) + (\psi_2 - \psi_4)(x_3 - x_1)]/2A_{①} \qquad (5.63)$$

where $A_{①}$ is the area of quadrilateral ①. This defines derivative values within the mesh quadrilateral in terms of quantities known at the mesh points. However, the derivatives of some quantities are required at the mesh points instead of the mesh centers. For these cases Eq. (5.60) will be used. For example, if the derivative of some quantity ψ is required at point 1 in Fig.

131

5.4, Eq. (5.60) is applied to the quadrilateral defined by the points 2, 4, 5, and 6. Since the line segments $\overline{62}$, $\overline{24}$, etc. pass through the mesh centers, respective mean values of ψ along these line segments are $\psi_{\textcircled{4}}$, $\psi_{\textcircled{1}}$ etc. A straightforward application of Eq. (5.60) yields

$$\partial\psi/\partial x \Big|_1 = [\psi_{\textcircled{4}} \ (y_2 - y_6) + \psi_{\textcircled{1}}(y_4 - y_2) + \psi_{\textcircled{2}}(y_5 - y_4)$$

$$+ \ \psi_{\textcircled{3}}(y_6 - y_5)]/A_{2456} \tag{5.64}$$

Similarly

$$\partial\psi/\partial y \Big|_1 = -[\psi_{\textcircled{4}}(x_2 - x_6) + \psi_{\textcircled{1}}(x_4 - x_2) + \psi_{\textcircled{2}}(x_5 - x_4)$$

$$+ \ \psi_{\textcircled{3}}(x_6 - x_5)]/A_{2456} \tag{5.65}$$

where A_{2456} is the area of the quadrilateral defined by points 2, 4, 5, and 6 in Fig. 5.4.

To implement Eqs. (5.62) and (5.65) in the code, the shorthand notation of Fig. 5.4 must be replaced by notation using the general j,k indices. Mesh points have integral j,k indices, and mesh centers have half-integral indices. For example, quadrilateral ③ has the indices $j+\frac{1}{2},k+\frac{1}{2}$. To avoid half-integers, quantities defined at mesh centers will be given the index of the mesh point with the next highest j,k value, as indicated by the arrows in Fig. 5.4. Thus mesh ① has index j,k, ② has j,k+1, ③ j+1,k+1, and ④ j+1,k. Even though quantities known at mesh centers will have integral space indices, they will be understood to be defined at the mesh centers. Table 5.1 lists quantities known at mesh centers along with those known at mesh points. With this convention Eqs. (5.62) and (5.63) become

TABLE 5.1. Space centering scheme

Mesh points	Mesh centers
$\dot{x}, \dot{y}, x, y$	$V, \dot{\varepsilon}_{ij}, A, \dot{V}/V, S_{ij}, E,$ q, P, μ, W_{xy}

$$\left.\partial\psi/\partial x\right|_{j,k} = [(\psi_{j,k} - \psi_{j-1,k-1})(y_{j,k-1} - y_{j-1,k})$$

$$+ (\psi_{j,k-1} - \psi_{j-1,k})(y_{j-1,k-1} - y_{j,k})]/2A_{j,k} \qquad (5.66)$$

$$\left.\partial\psi/\partial y\right|_{j,k} = -[(\psi_{j,k} - \psi_{j-1,k-1})(x_{j,k-1} - x_{j-1,k})$$

$$+ (\psi_{j,k-1} - \psi_{j-1,k})(x_{j-1,k-1} - x_{j,k})]/2A_{j,k} \qquad (5.67)$$

Equation (5.66) may be used to derive a formula for the area of the mesh center with index j,k. Setting $\psi = x$ in Eq. (5.66)

$$A_{j,k} = [(x_{j,k} - x_{j-1,k-1})(y_{j,k-1} - y_{j-1,k})$$

$$+ (x_{j,k-1} - x_{j-1,k})(y_{j-1,k-1} - y_{j,k})]/2 \qquad (5.68)$$

Density is required in many of the equations, which means that a mesh volume must be defined. The mesh may be thought of as three-dimensional, with no motion allowed in the z-direction. Choosing unit length for mesh parallelepipeds in the z-direction makes mesh volume numerically equal to mesh area in the x-y plane, and mesh volume and mesh area become interchangeable.

Using j,k indexing, Eqs. (5.64) and (5.65) become

$$\left.\partial\psi/\partial x\right|_{j,k} = [\psi_{j+1,k}(y_{j,k-1} - y_{j+1,k}) + \psi_{j,k}(y_{j-1,k} - y_{j,k-1})$$

$$+ \psi_{j,k+1}(y_{j,k+1} - y_{j-1,k}) + \psi_{j+1,k+1}(y_{j+1,k} - y_{j,k+1})]/A'_{j,k} \qquad (5.69)$$

$$\left.\partial\psi/\partial y\right|_{j,k} = -[\psi_{j+1,k}(x_{j,k-1} - x_{j+1,k}) + \psi_{j,k}(x_{j-1,k} - x_{j,k-1})$$

$$+ \psi_{j,k+1}(x_{j,k+1} - x_{j-1,k}) + \psi_{j+1,k+1}(x_{j+1,k} - x_{j,k+1})]/A'_{j,k} \qquad (5.70)$$

where $A'_{j,k}$ is the area of the quadrilateral defined by points 2, 4, 5, and 6

134

in Fig. 5.4. Figure 5.4 shows that $A'_{j,k}$ contains one-half the area of each of the 4 mesh centers surrounding point j,k. Thus

$$A'_{j,k} = [A_{j,k} + A_{j,k+1} + A_{j+1,k+1} + A_{j+1,k}]/2 \qquad (5.71)$$

Time indices will be denoted by superscripts. Thus t^n is time at the nth time step, and $\psi^n_{j,k}$ is the value of ψ at the nth time step and the position of the mesh point j,k. Linear interpolation is used to find values of quantities at half-integral times:

$$\psi^{n+\frac{1}{2}}_{j,k} = (\psi^{n+1}_{j,k} + \psi^n_{j,k})/2 \qquad (5.72)$$

Time derivatives are centered at integral time values

$$\partial\psi/\partial t|^n_{j,k} = (\psi^{n+\frac{1}{2}}_{j,k} - \psi^{n-\frac{1}{2}}_{j,k})/(t^{n+\frac{1}{2}} - t^{n-\frac{1}{2}}) \qquad (5.73)$$

However

$$t^{n+\frac{1}{2}} - t^{n-\frac{1}{2}} = (t^{n+1} + t^n - t^n - t^{n-1})/2$$

$$= (t^{n+1} - t^{n-1})/2 \qquad (5.74)$$

Substituting Eqs. (5.69), (5.70), and (5.73) into Eqs. (5.3) and (5.4) yields

$$\dot{x}^{n+\frac{1}{2}}_{j,k} = \dot{x}^{n-\frac{1}{2}}_{j,k} + (t^{n+1} - t^{n-1}) [\sigma_{xx_{j+1,k}} (y_{j,k-1} - y_{j+1,k})$$

$$+ \sigma_{xx_{j,k}} (y_{j-1,k} - y_{j,k-1}) + \sigma_{xx_{j,k+1}} (y_{j,k+1} - y_{j-1,k})$$

$$+ \sigma_{xx_{j+1,k+1}} (y_{j+1,k} - y_{j,k+1}) - \sigma_{xy_{j+1,k}} (x_{j,k-1} - x_{j+1,k})$$

135

$$-\sigma_{xy_{j,k}} (x_{j-1,k} - x_{j,k-1}) - \sigma_{xy_{j,k+1}} (x_{j,k+1} - x_{j-1,k})$$

$$-\sigma_{xy_{j+1,k+1}} (x_{j+1,k} - x_{j,k+1})]^n / 2(\rho A')^n_{j,k} \qquad (5.75)$$

$$\dot{y}^{n+\frac{1}{2}}_{j,k} = \dot{y}^{n-\frac{1}{2}}_{j,k} + (t^{n+1} - t^{n-1}) [\sigma_{xy_{j+1,k}} (y_{j,k-1} - y_{j+1,k})$$

$$+\sigma_{xy_{j,k}} (y_{j-1,k} - y_{j,k-1}) + \sigma_{xy_{j,k+1}} (y_{j,k+1} - y_{j-1,k})$$

$$+ \sigma_{xy_{j+1,k+1}} (y_{j+1,k} - y_{j,k+1}) - \sigma_{yy_{j+1,k}} (x_{j,k-1} - x_{j+1,k})$$

$$- \sigma_{yy_{j,k}} (x_{j-1,k} - x_{j,k-1}) - \sigma_{yy_{j,k+1}} (x_{j,k+1} - x_{j-1,k})$$

$$- \sigma_{yy_{j+1,k+1}} (x_{j+1,k} - x_{j,k+1})]^n / 2(\rho A')^n_{j,k} \qquad (5.76)$$

where, from Eq. (5.71)

$$(\rho A')^n_{j,k} = (\rho V')^n_{j,k} = (M')^n_{j,k} = [M_{j,k} + M_{j,k+1} + M_{j+1,k+1} + M_{j+1,k}]/2 \quad (5.77)$$

where $M_{j,k}$ is the constant mass of the mesh center with index j,k, equal to its initial volume times initial density, and $\sigma^n_{nm_{j,k}} = S^n_{nm_{j,k}} - (P+q)^n_{j,k} \delta_{nm}$.

Setting $\psi = x$ in Eq. (5.73)

$$\dot{x}^n_{j,k} = \partial x / \partial t \ ^n_{j,k} = (x^{n+\frac{1}{2}}_{j,k} - x^{n-\frac{1}{2}}_{j,k})/(t^{n+\frac{1}{2}} - t^{n-\frac{1}{2}}) \qquad (5.78)$$

Adding 1/2 to each time index,

$$x^{n+1}_{j,k} = x^n_{j,k} + (t^{n+1} - t^n) \dot{x}^{n+\frac{1}{2}}_{j,k} \qquad (5.79)$$

Similarly,

$$y^{n+1}_{j,k} = y^n_{j,k} + (t^{n+1} - t^n) \dot{y}^{n+\frac{1}{2}}_{j,k} \qquad (5.80)$$

136

Expressions for $\partial\dot{x}/\partial x$, $\partial\dot{x}/\partial y$, $\partial\dot{y}/\partial x$, and $\partial\dot{y}/\partial y$ follow directly from Eqs. (5.66) and (5.67) with appropriate substitutions for ψ. Since no time derivatives are involved in these equations, all terms have the same time index.

So from Eqs. (5.51a), (5.51b), (5.51c), and (5.52),

$$\dot{\varepsilon}_{xx}{}_{j,k}^{n+\frac{1}{2}} = \partial\dot{x}/\partial x\big|_{j,k}^{n+\frac{1}{2}} \tag{5.81}$$

$$\dot{\varepsilon}_{yy}{}_{j,k}^{n+\frac{1}{2}} = \partial\dot{y}/\partial y\big|_{j,k}^{n+\frac{1}{2}} \tag{5.82}$$

$$\dot{\varepsilon}_{xy}{}_{j,k}^{n+\frac{1}{2}} = (\partial\dot{x}/\partial y + \partial\dot{y}/\partial x)_{j,k}^{n+\frac{1}{2}}/2 \tag{5.83}$$

$$(\dot{V}/V)_{j,k}^{n+\frac{1}{2}} = (\dot{\varepsilon}_{xx} + \dot{\varepsilon}_{yy})_{j,k}^{n+\frac{1}{2}} \tag{5.84}$$

Density is given by

$$\rho_{j,k}^{n+1} = M_{j,k}/V_{j,k}^{n+1} \tag{5.85}$$

Due to the dependence of μ on C_b^2 and thus on P, E, and S_{ij}, the rest of the differenced equations cannot be easily solved explicitly while keeping precise centering. μ needs to be known at time $t^{n+\frac{1}{2}}$ but since C_b^2 is not yet known at time t^{n+1}, the old value of C_b^2 must be used in the equation for μ. Thus

$$\mu_{j,k}^{n+\frac{1}{2}} = [3(1 - 2\nu)\rho C_b^2/2(1 + \nu)]_{j,k}^{n} \tag{5.86}$$

Differencing the stress deviator equation,

$$\dot{S}_{xx}{}_{j,k}^{n} = (S_{xx}^{n+\frac{1}{2}} - S_{xx}^{n-\frac{1}{2}})_{j,k}/(t^{n+\frac{1}{2}} - t^{n-\frac{1}{2}}) \tag{5.87}$$

137

Stresses are needed at integral times in the equation of motion, so, adding 1/2 to time indices,

$$\dot{S}_{xx_{j,k}}^{n+\frac{1}{2}} = (S_{xx_{j,k}}^{n+1} - S_{xx_{j,k}}^{n})/(t^{n+1} - t^{n})$$

$$= (S_{xy}W_{xy})_{j,k}^{n+\frac{1}{2}} + [2\mu(\dot{\varepsilon}_{xx} - \dot{V}/3V)]_{j,k}^{n+\frac{1}{2}} \qquad (5.88)$$

where

$$W_{xy} = 2V_{xy} \qquad (5.89)$$

and V_{xy} is defined in Eq. (5.21). Thus

$$S_{xx_{j,k}}^{n+1} = S_{xx_{j,k}}^{n} + (t^{n+1} - t^{n})[S_{xy}W_{xy} + 2\mu(\dot{\varepsilon}_{xx} - \dot{V}/3V)]_{j,k}^{n+\frac{1}{2}} \qquad (5.90)$$

Likewise

$$S_{yy_{j,k}}^{n+1} = S_{yy_{j,k}}^{n} + (t^{n+1} - t^{n})[-S_{xy}W_{xy} + 2\mu(\dot{\varepsilon}_{yy} - \dot{V}/3V)]_{j,k}^{n+\frac{1}{2}} \qquad (5.91)$$

$$S_{xy_{j,k}}^{n+1} = S_{xy_{j,k}}^{n} + (t^{n+1} - t^{n})[(1/2)(S_{yy} - S_{xx})W_{xy} + 2\mu\dot{\varepsilon}_{xy}]_{j,k}^{n+\frac{1}{2}} \qquad (5.92)$$

This set of equations is not usable, since $S_{ij}^{n+\frac{1}{2}}$ is not known. However, using

$$S_{ij}^{n+\frac{1}{2}} = (S_{ij}^{n+1} + S_{ij}^{n})/2 \qquad (5.93)$$

in all equations, and substituting Eqs. (5.90) and (5.91) in Eq. (5.92) there results an equation that can be solved explicitly for S_{xy}^{n+1}. The result is

$$S_{xy}^{n+1} = \{S_{xy}^{n}(1 - a_1^2) + 2\Delta t\mu\dot{\varepsilon}_{xy} + a_1[S_{yy}^{n} - S_{xx}^{n} + \Delta t\mu(\dot{\varepsilon}_{yy} - \dot{\varepsilon}_{xx})]\}/(1 + a_1^2) \qquad (5.94)$$

where $a_1 = \Delta t W_{xy}/2$ and a_1, μ, $\dot{\varepsilon}_{xy}$, $\dot{\varepsilon}_{yy}$, and $\dot{\varepsilon}_{xx}$ are evaluated at $t^{n+\frac{1}{2}}$. All quantities are evaluated at the space point j,k, and $\Delta t \equiv t^{n+1} - t^{n}$.

138

With S_{xy}^{n+1} known the other two equations are

$$S_{xx_{j,k}}^{n+1} = S_{xx_{j,k}}^n + \Delta t\{(1/2)(S_{xy_{j,k}}^{n+1} + S_{xy_{j,k}}^n) \, W_{xy_{j,k}}^{n+\frac{1}{2}} + [2\mu(\dot{\epsilon}_{xx} - \dot{V}/3V)]_{j,k}^{n+\frac{1}{2}}\} \quad (5.95)$$

$$S_{yy_{j,k}}^{n+1} = S_{yy_{j,k}}^n + \Delta t\{-(1/2)(S_{xy_{j,k}}^{n+1} + S_{xy_{j,k}}^n) \, W_{xy_{j,k}}^{n+\frac{1}{2}} + [2\mu(\dot{\epsilon}_{yy} - \dot{V}/3V)]_{j,k}^{n+\frac{1}{2}}\} \quad (5.96)$$

Then

$$J_{2_{j,k}}^{n+1} = [S_{xx}^2 + S_{xy}^2 + S_{yy}^2 + S_{xx}S_{yy}]_{j,k}^{n+1} \quad (5.97)$$

If $J_{2_{j,k}}^{n+1} > Y_0^2/3$, then

$$S_{rq_{j,k}}^{n+1} = S_{rq_{j,k}}^{n+1} \, (Y_0^2/3J_{2_{j,k}}^{n+1})^{\frac{1}{2}} \quad (5.98)$$

while if $J_2 < Y_0^2/3$ there is no change.

The artificial viscosity is

$$q_{j,k}^{n+1} = -\rho_{j,k}^{n+1} \sqrt{V_{j,k}^{n+1}} \, (\dot{V}/V)_{j,k}^{n+\frac{1}{2}} [B_1^2 \sqrt{V_{j,k}^{n+1}} \, |\dot{V}/V|_{j,k}^{n+\frac{1}{2}} + B_2 C_{L_{j,k}}^n] \text{ if } \dot{V}/V < 0$$

$$= 0 \text{ if } \dot{V}/V > 0 \quad (5.99)$$

This equation is not exactly centered, since it uses the values of C_L and $\dot{V}/V$ at times t^n and $t^{n+\frac{1}{2}}$, respectively. In Eq. (5.99)

$$C_{l_{j,k}}^n = C_{b_{j,k}}^n \sqrt{3(1 - \nu)/(1 + \nu)} \quad (5.100)$$

where $C_{b_{j,k}}^n$ is obtained from Eq. (5.43) with ρ, μ, and P evaluated at time t^n and position j,k.

139

Differencing the energy equation yields

$$E_{j,k}^{n+1} = E_{j,k}^{n} + (t^{n+1} - t^{n})\, V_{j,k}^{n+\frac{1}{2}}[(S_{xx}\dot{\epsilon}_{xx} + S_{yy}\dot{\epsilon}_{yy} + 2S_{xy}\dot{\epsilon}_{xy})_{j,k}^{n+\frac{1}{2}}$$

$$- (p_{j,k}^{n+\frac{1}{2}} + q_{j,k}^{n+\frac{1}{2}})\,(\dot{V}/V)_{j,k}^{n+\frac{1}{2}}] \qquad (5.101)$$

Assume

$$p^{n+\frac{1}{2}} = (P^{n+1} + P^{n})/2 \qquad (5.102)$$

$$q^{n+\frac{1}{2}} = (q^{n+1} + q^{n})/2 \qquad (5.103)$$

and calculate p^{n+1} from Eq. (5.41):

$$p_{j,k}^{n+1} = A_3 + \rho_0\Gamma_0 E_{j,k}^{n+1} \qquad (5.104)$$

where

$$A_3 = [\rho_0 C_0^2 n(1 - \Gamma_0 n/2)/(1 - s_n)^2]_{j,k}^{n+1} \qquad (5.105)$$

and

$$n_{j,k}^{n+1} = 1 - \rho_0/\rho_{j,k}^{n+1} \qquad (5.106)$$

Equations (5.101) through (5.105) can be combined to give

$$E_{j,k}^{n+1} = \frac{[E_{j,k}^{n} + b_1\Delta t - (\Delta t\dot{V}/2V)^{n+\frac{1}{2}}\,(A_3 + P_{j,k}^{n} + q_{j,k}^{n+1} + q_{j,k}^{n})V_{j,k}^{n+\frac{1}{2}}]}{(1 + V\rho_0\Gamma_0\Delta t\dot{V}/2V)_{j,k}^{n+\frac{1}{2}}} \qquad (5.107)$$

where $b_1 = [V(S_{xx}\dot{\epsilon}_{xx} + S_{yy}\dot{\epsilon}_{yy} + 2S_{xy}\dot{\epsilon}_{xy})]_{j,k}^{n+\frac{1}{2}}$ and $\Delta t = t^{n+1} - t^{n}$. Then

finally, once $E_{j,k}^{n+1}$ is known

$$p_{j,k}^{n+1} = A_3 + \rho_0\Gamma_0 E_{j,k}^{n+1} \qquad (5.108)$$

140

Thus, at each mesh point, variables are calculated for the new time in the same order as they are considered above.

5.4 Program Description

For each variable calculated, Table 5.2 shows the variables needed in the equation and the times at which they are needed. This table shows that the old values of the 12 variables $\dot{x}$, $\dot{y}$, x, y, v, M, S_{xx}, S_{xy}, S_{yy}, E, P, and q must be stored for each mesh point in order to advance the calculation to the new time step. Values do not need to be stored for every time step, since in each case, except for the variables x and y, the new value can replace the old value at the time it is calculated. Values of x and y are needed at the old time at mesh points surrounding the one being calculated. Referring again to Fig. 5.4, the calculation starts at the first j line and proceeds along all k values for each j value. When the calculation has reached point 1, which has the indices j,k in the figure, all points with a smaller j index have been moved to the new time, as have all points with the same j index and smaller k index. Due to the indexing system which gives mesh center ① the same index as mesh point 1 in Fig. 5.4, the quantities known at the mesh center ① are advanced to the new time at the same time as quantities known at the mesh point 1. At the time mesh point 1 is being advanced to the new time, points 2, 3, and 4 in Fig. 5.4 have already been advanced. However, the values of x and y at the old time are needed at these points in Eqs. (5.81), (5.82), and (5.83). Thus, the old values of x and y must be stored for the present and preceding k lines.

The only other storage required is for material properties. It would be possible to define different material properties for every point in the mesh, and this is the upper limit on the number of different materials allowed

141

TABLE 5.2. Quantities required to advance calculation
to new time step

Variable being advanced to new time	Variable required	
	Old time	New time
$\dot{x}$	$\dot{x},x,y,S_{xx},S_{xy},P,q$	
$\dot{y}$	$\dot{y},x,y,S_{yy},S_{xy},P,q$	
x	x	$\dot{x}$
y	y	$\dot{y}$
V		x,y
$\dot{\varepsilon}_{xx}$	y,V	$\dot{x},y,V$
$\dot{\varepsilon}_{yy}$	x,V	$\dot{y},x,V$
$\dot{\varepsilon}_{xy}$	x,y,V	$\dot{x},\dot{y},x,y,V$
W_{xy}	x,y,V	$\dot{x},\dot{y},x,y,V$
$\dot{V}/V$		$\dot{\varepsilon}_{xx},\dot{\varepsilon}_{yy}$
μ	V,P	V
S_{xy}	S_{xx},S_{yy},S_{xy}	$W_{xy},\dot{\varepsilon}_{xx},\dot{\varepsilon}_{yy},\dot{\varepsilon}_{xy},\mu$
S_{xx}	S_{xx},S_{xy}	$S_{xy},W_{xy},\mu,\dot{\varepsilon}_{xx},\dot{V}/V$
S_{yy}	S_{yy},S_{xy}	$S_{xy},W_{xy},\mu,\dot{\varepsilon}_{yy},\dot{V}/V$
q	V,P	$\dot{V}/V,V$
E	$E,S_{xx},S_{xy},S_{yy},$ P,q,V	$V,S_{xx},S_{xy},S_{yy},\dot{\varepsilon}_{xx},$ $\dot{\varepsilon}_{yy},\dot{\varepsilon}_{xy},\dot{V}/V,q$
P		V,E

142

in the problem. However it is assumed that all meshes with the same k value have the same material properties. Thus the k lines are the dividing lines between materials. The user specifies the number of different regions desired and the k values of the dividing lines between them. Thus material properties need to be stored only for each region.

At every mesh point the calculation requires values of variables at the surrounding mesh points. At the outer boundaries of the material, the surrounding points do not exist on one side. This problem is handled by creating one extra row of meshes outside the material boundary for which the quantities are not calculated but are set at the beginning of the program to values that will cause the material boundary to behave in the proper manner. Since all boundaries in the problem under consideration are free surfaces, values of the variables M, S_{xx}, S_{yy}, S_{xy}, E, P, and q are initially set to zero in the boundary meshes and not recalculated. This allows the material boundary to behave as a free surface. Thus, as can be seen in Fig. 5.5, if there are N j lines and M k lines, the calculation proceeds from j=2 to j=N-1 and from k=2 to k=M-1 for quantities known at mesh points, and from j=3 to j=N-1 and k=3 to k=M-1 for quantities known at mesh centers.

The boundary between projectile and wedge changes from two free surfaces before impact to a single material boundary after the point of contact between projectile and wedge has passed the mesh in question. The k line corresponding to the impact surface of the wedge is specified by the user and is designated as MIMP. The projectile is considered to extend from k=2 to k=MIMP-1, and the target from k=MIMP to k=M-1, as seen in Fig. 5.5. This leaves one row of intermediate meshes between the two, which has the index k=MIMP. This intermediate mesh is used to simulate the effect of a projectile striking a slanted surface. The line of contact between the projectile and

143
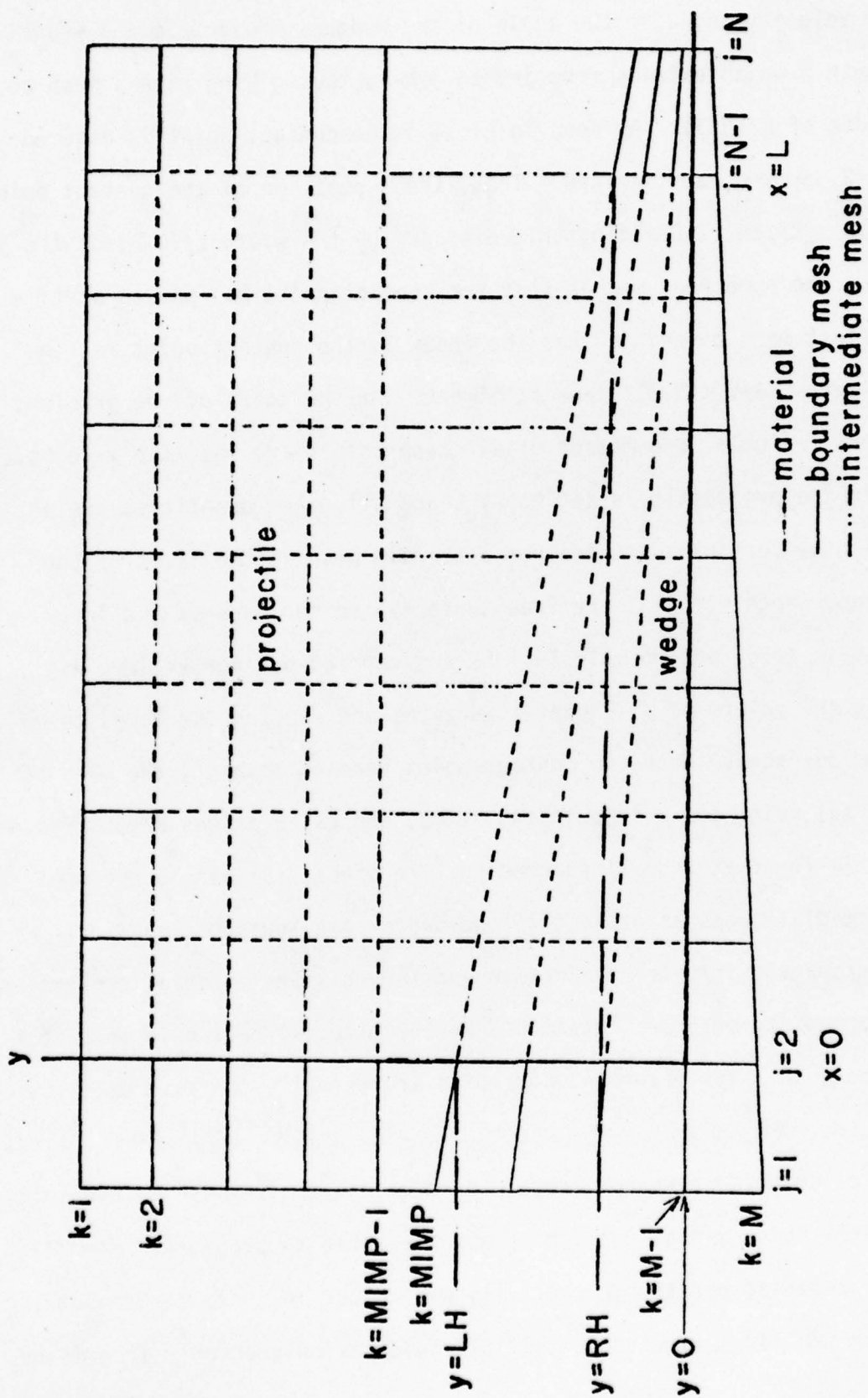
Fig. 5.5. Mesh setup for wedge impact problems

144

the wedge moves along the projectile face with velocity $V_p/\tan \alpha$, where V_p is projectile velocity and α is the angle of the wedge. Projectile and wedge have a length L which extends from j=2 to j=N-1, thus giving each j mesh an initial width of L/(N-3). As seen in Fig.5.5,the contact point is assumed to be at j=2, or x=0, at time t=0. Thus, the x position of the contact point at time t is $V_p t/\tan\alpha$. Dividing this distance by the width L/(N-3) of the j meshes gives the number of meshes that the contact point has passed at time t. Since the first mesh beyond j=2 has the index 3, the contact point is, in mesh coordinates, $3+V_p t(N-3)/L\tan\alpha$ at time t. At the start of the problem, the positions, volumes, and masses of all mesh points are set, the y velocity of points in the projectile is set to $-V_p$, and all other quantities are set to zero. Until the contact point reaches a certain mesh j' the faces of the projectile and wedge for j>j' are free surfaces, so the mass of the inter-mediate mesh is zero, and no calculations are carried out for k=MIMP, j>j', thus leaving the values of all quantities zero, and causing the faces to be-have as free surfaces. When the contact point reaches mesh j', the mass of the mesh is set using its volume at that time, and calculations are carried out in mesh j' for that and all succeeding time steps. Strain is produced in the intermediate mesh as projectile and wedge come together, causing signals to propagate into the projectile and target. The material properties for the intermediate mesh are determined by the material region in which that k line is included. Its material properties are normally the same as those of the impactor.

The calculation need not proceed through the entire mesh at every time, since for early times signals will have not been able to propagate into all parts of the material and thus no activity will occur in those meshes not yet reached. For the first time step, the full calculation goes only from meshes

145

j=2 to j=5 (unless the wedge angle is zero, in which case it goes through the entire j mesh), and from k=MIMP-3 to k=MIMP+3. However, the positions of all points of the moving projectile must be calculated at all time steps. Boundaries of the area of full calculation are expanded if the pressures at the present boundaries exceed a minimum value.

Stability of the finite difference method requires that Δt be such that $\Delta x / \Delta t > C$ where Δx is the characteristic size of the mesh, and C is sound speed in the material. Since signals can propagate only one mesh per time step, the above criterion guarantees that the numerical propagation of signals through the mesh will be able to keep pace with the physical signals. A strict stability analysis of the difference equations is much more complicated and has not been done for the equations in this program. The time step used is the same as that used in TOODY. The quantity

$$DTM = D_M / (B_2 C_L + B_1^2 D_M \left| \dot{V}/V \right| + \sqrt{B_2 C_L + B_1^2 D_M (\dot{V}/V)^2 + C_L^2}) \qquad (5.109)$$

is calculated for each mesh, where B_1 and B_2 are the same constants used in the artificial viscosity, and D_M is the smallest distance between mesh points defining the mesh. The minimum DTM over all meshes is found, and the new time is

$$t^{n+1} = t^n + \text{Min} \{DTM, 1.1 (t^n - t^{n-1})\} \qquad (5.110)$$

Input data required to define the problem include the number N of j lines, number M of k lines, value of the wedge impact surface line MIMP, length of the wedge, height of either side of the wedge, projectile velocity, artificial viscosity coefficients B_1 and B_2, and material properties for the regions defined. Material properties required are density, Poisson's ratio, yield strength in simple tension, coefficients C_0 and s in the U_s-U_p Hugoniot

146

relation

$$U_S = C_0 + sU_p,$$ (5.111)

and the Gruneisen parameter.

The program prints out the definition of the problem and values of the 12 variables stored in arrays for each mesh point at whatever cycle interval the user specifies. After the last time step, all arrays plus other information needed to define the problem are written on tape. This information can thus be recovered at a later time to restart the program at the last time step and run it farther, eliminating the need for running the first part of the problem again. This information is also accessible to other programs and can be analyzed or processed to gain further understanding of the problem. The program also writes the position and velocity of each mesh point on the wedge free surface on tape at each time step. This can be accessed by a program which uses this information to simulate the resistance wire records. Details of the auxiliary programs and results of the computer runs will be given in Chapter 8.

6. INCLUSION OF RATE EFFECTS

The computer code presented in Chapter 5 has an elastic-perfectly plastic equation of state. The yield stress in simple tension used in the Von Mises yield condition is assumed to be constant. This treatment produces a cusp in the Hugoniot of the material. If the material is shocked to a final pressure between points A and B in Fig. 6.1, the single wave breaks up into two waves.[62] The first is an elastic wave with amplitude P_A, and the second is a plastic wave. This elastic-perfectly plastic theory has been successful in describing much material behavior. However, experimental observations indicate that many materials can be better described if strain-rate effects are included.[63] The behavior described by the inclusion of strain-rate effects in the theory includes overshoot and decay of the elastic precursor,[64] and spreading of the plastic wave.[65] This chapter describes the inclusion of strain-rate effects in the present code.

As in Eq. (5.12), deviator stress rate is related to the elastic part of the deviator strain rate

$$\dot{S}_{ij} = 2\mu \dot{e}^e_{ij} \tag{6.1}$$

Plasticity theory assumes that the total strain rate is the sum of the elastic and plastic strain rates

$$\dot{e}^t_{ij} = \dot{e}^e_{ij} + \dot{e}^p_{ij} \tag{6.2}$$

where $\dot{e}^e_{ij}$ is the elastic strain rate and $\dot{e}^p_{ij}$ is the plastic strain rate.[66]

148
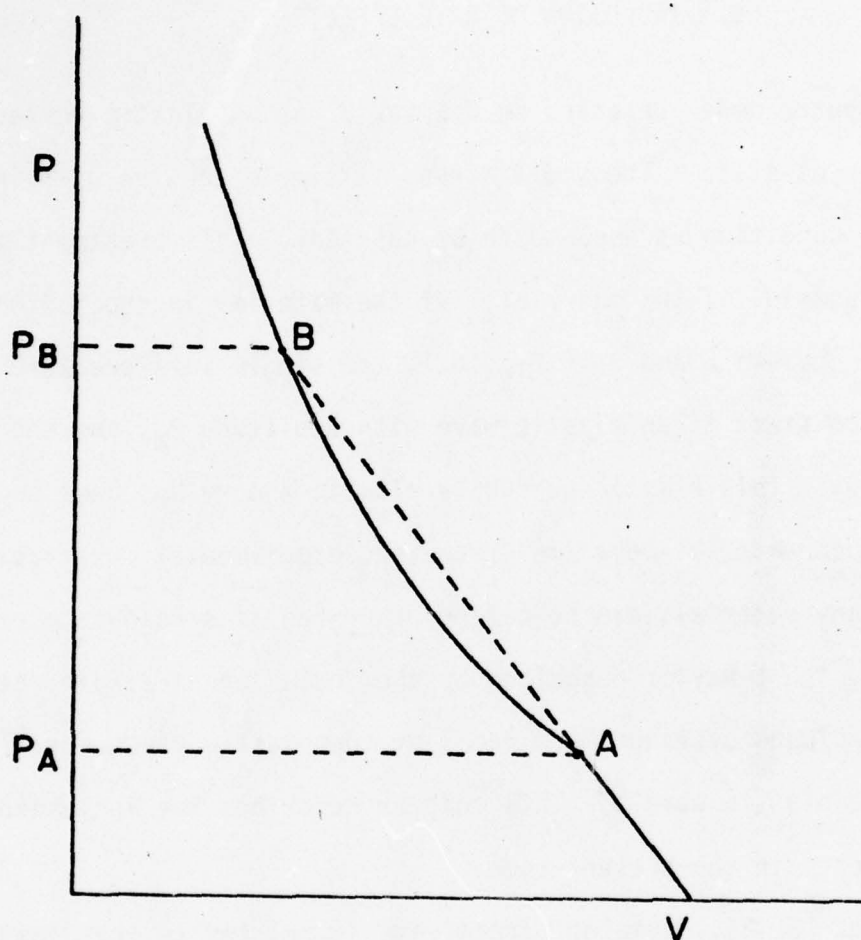
Fig. 6.1. Hugoniot curve for an elastic-plastic
material

Equation (6.1) becomes

$$\dot{S}_{ij} = 2\mu(\dot{e}_{ij}^{\,t} - \dot{e}_{ij}^{\,p}) \qquad\qquad (6.3)$$

where the total deviatoric strain-rate tensor is given by Eq. (5.13). Equation (6.3) should include the rigid body rotation terms given in Eqs. (5.25), (5.26), and (5.27). However, those terms are not affected by the results of this section and will be left out for simplicity of presentation. It will be understood that the rigid body rotation terms are to be added to the equations presented here in order to retain frame-indifference.

The strain rate-dependent behavior of the model is dictated by the form chosen for $\dot{e}_{ij}^{\,p}$. In fact, If $\dot{e}_{ij}^{\,p}$ is assumed to be some general function of stress and strain and their derivatives

$$\dot{e}_{ij}^{\,p} = F_{ij}(\sigma_{ij},\epsilon_{ij}) \qquad\qquad (6.4)$$

where F_{ij} is termed the relaxation function, then Eq. (6.3) becomes

$$\dot{S}_{ij} = 2\mu\dot{e}_{ij}^{\,t} - 2\mu F_{ij} \qquad\qquad (6.5)$$

This equation describes general stress-relaxing materials, including viscous effects[67] as well as elastic-plastic materials. This equation is the basis for the addition of rate effects to the code.

The crux of the problem is the relaxation function F_{ij}. The problem is simpler in one dimension since only the equation for the X component of S_{ij} is required and thus only F_X is needed. Several phenomenological forms have been used for F_X.[63,64,67,68,69] However, probably the most physical treatment of an elastic plastic model results when it is related to the results of dislocation theory.[70] This has been done for computer programs which calculate motion in one dimension.[71] In that case $\dot{e}_X^{\,p}$ is related to the

150

plastic shear strain rate $\dot{\gamma}$ in the plane of the maximum resolved shear stress, and $\dot{\gamma}$ is given from dislocation theory.

The general multidimensional case is shown in Fig. 6.2. As stated in Section 5.1, the state of the material is represented by a point in principal stress deviator space. The condition that the trace of the stress deviator be zero constrains the point to lie on a plane passing through the origin. This is the plane of Fig. 6.2. The circle is the intersection of the sphere described by the Von Mises yield condition, Eq. (5.28), with this plane. Points inside the circle represent elastic behavior, and those outside represent plastic. Suppose that during some time step the state of the material as given from Eq. (5.25), (5.26), and (5.27) using the total strain rate goes from point A to point B in Fig. 6.2. If the material were elastic-perfectly plastic, the stress state would be adjusted radially back to the yield surface at point C. This actually corresponds to a stress relaxing material which essentially relaxes immediately, so that the state always lies on the yield surface and no relaxation can be detected. The opposite case would be that of a perfectly elastic material which could sustain unlimited distortion. The material which is strain rate sensitive lies between these two extremes. In this case the material would relax, but not all the way back to the yield surface. The relaxed state of the material would be some intermediate point D between points B and C. Thus, the material would be seen to overshoot the yield point toward the elastic stress B and then relax back. This process can be thought of either as allowing the yield surface to be strain rate dependent, so that the material relaxes back to the instantaneous yield surface at D, or as allowing the material to relax only partially back to the static yield surface.
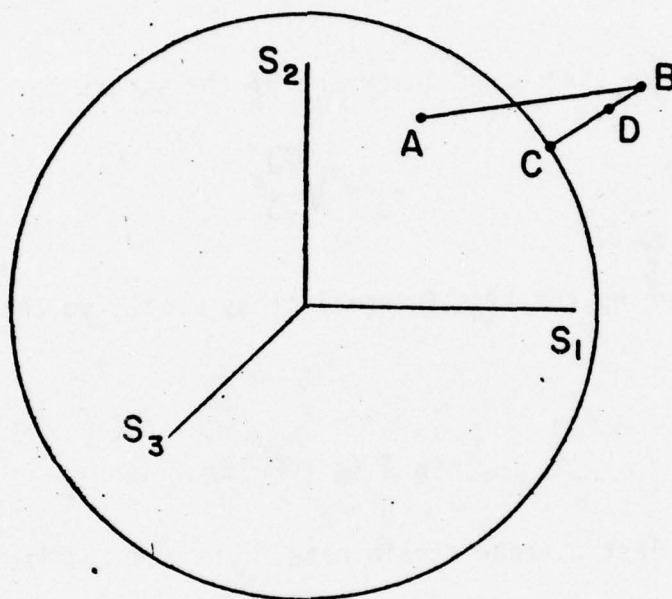
Fig. 6.2. Geometric representation of Von
Mises yield criterion in plane
$S_1 + S_2 + S_3 = 0$

Stress relaxation can be described phenomenologically by allowing the distance relaxed to be proportional to the distance between points B and C in Fig. 6.2 divided by some characteristic relaxation time. Wilkins[72,73] suggests that the amount of relaxation be related to dislocation theory. The amount of applied shear is given by the octahedral shear stress[73]

$$\tau_0 = \frac{1}{3}\sqrt{S_1^2 + S_2^2 + S_3^2} \qquad (6.6)$$

This is related to the second invariant of the stress deviator tensor

$$\tau_0 = \sqrt{\frac{2J_2}{3}} \qquad (6.7)$$

τ_0 is relaxed during the time interval Δt by $\mu \dot{\gamma} \Delta t$[73] so that the relaxed state is given by

$$\tau_R = \tau_0 - \mu \dot{\gamma} \Delta t \qquad (6.8)$$

where $\dot{\gamma}$ is the plastic shear strain rate. The assumed isotropy of the material allows this formulation. In terms of J_2,

$$\sqrt{\frac{2J_{2R}}{3}} = \sqrt{\frac{2J_2}{3}} - \mu \dot{\gamma} \Delta t \qquad (6.9)$$

where J_2 represents the state of the material as calculated elastically from Eqs. (5.25), (5.26), and (5.27), and J_{2R} represents the relaxed state. Thus

$$\sqrt{\frac{J_{2R}}{J_2}} = 1 - \frac{\mu \dot{\gamma} \Delta t}{\sqrt{\frac{2J_2}{3}}} \qquad (6.10)$$

Thus each component of the stress deviator tensor is multiplied by the constant C where

153

$$C = \sqrt{\frac{J_{2R}}{J_2}} \tag{6.11}$$

so that the resulting value of J_2 is

$$J_2' = \frac{1}{2} [(CS_1)^2 + (CS_2)^2 + (CS_3)^2] \tag{6.12}$$

or

$$J_2' = C^2 J_2$$

$$= J_{2R} \tag{6.13}$$

which is the desired result. The state must not be relaxed past the point C in Fig. 6.2, so the minimum value of C is

$$C_{min} = \sqrt{\frac{Y_0^2}{3J_2}} \tag{6.14}$$

From dislocation theory [66,70]

$$\dot{\gamma} = bNW \tag{6.15}$$

where b is the Burgers vector, N the mobile dislocation density, and W the dislocation velocity. The form for W is taken to be[73]

$$W = W_0 \exp(- D/\tau_{eff}) \tag{6.16}$$

where D is a characteristic drag stress and τ_{eff} is the effective component of shear stress above the yield value. In terms of J_2

$$\tau_{eff} = \sqrt{\frac{2J_2}{3}} - \sqrt{2} \, Y_0/3 \tag{6.17}$$

154

where the second term on the right hand side in Eq. (6.17) is τ_0 using the value of J_2 at yield as given by the Von Mises yield criterion. The form for N is[73]

$$N = \frac{1}{f} [1 + (fN^o - 1) \exp(-\alpha f \gamma / b)] \tag{6.18}$$

where α and f are constants, and N^o is the initial dislocation density. Thus

$$\dot{\gamma} = bW_o \exp\left(\frac{-D}{\sqrt{\frac{2J_2}{3}} - \sqrt{2}\, Y_0/3}\right) \frac{1}{f} [1 + (fN^o - 1) \exp(-\alpha f \gamma / b)] \tag{6.19}$$

This involves the plastic shear strain γ, which is found from

$$\gamma = \int \dot{\gamma}\, dt \tag{6.20}$$

This formalism must be finite-differenced to be included in the code. Equations (5.25), (5.26), and (5.27) are used to calculate J_2 as if the material were totally elastic. Each component of the stress deviator tensor is then multiplied by the constant C in Eq. (6.11) to obtain the relaxed state. Since S_{ij} is evaluated at integral times and mesh centers, the equation for the new deviators should be

$$S'_{ij}\Big|^{n+1}_{j,k} = C^{n+1}_{j,k}\, S_{ij}\Big|^{n+1}_{j,k} \tag{6.21}$$

However, not all quantities involved in C are known at time n+1. In keeping with the time centering of the rest of the program, time differentiated quantities are to be defined at half-integral times. Δt is also defined at half-integral times as is μ. Therefore μ, $\dot{\gamma}$, and Δt are not known at time n+1. Thus the form to be taken for C is

$$C_{j,k}^{n+1} = 1 - \frac{\mu_{j,k}^{n+\frac{1}{2}}\, \dot{\gamma}_{j,k}^{n+\frac{1}{2}}\, (t^{n+1} - t^n)}{\sqrt{\frac{2}{3}}\, J_{2_{j,k}}^{n+1}} \qquad (6.22)$$

This is not correctly centered. The centered time differencing method of Chapter 5 gives

$$\dot{\gamma}_{j,k}^{n+\frac{1}{2}} = \frac{\gamma_{j,k}^{n+1} - \gamma_{j,k}^{n}}{t^{n+1} - t^n} \qquad (6.23)$$

or

$$\gamma_{j,k}^{n+1} = \gamma_{j,k}^{n} + (t^{n+1} - t^n)\, \dot{\gamma}_{j,k}^{n+\frac{1}{2}} \qquad (6.24)$$

From the definition of $\dot{\gamma}$,

$$\dot{\gamma}_{j,k}^{n+\frac{1}{2}} = \left\{ bW_o \exp\left(\frac{-D}{\sqrt{\frac{2J_2}{3}} - \sqrt{2}\, Y_0/3}\right) \frac{1}{f}\left[1 + (fN^o - 1)\exp(-\alpha f\gamma/b)\right] \right\}_{j,k}^{n+\frac{1}{2}} \qquad (6.25)$$

Thus the equation for $\dot{\gamma}_{j,k}^{n+\frac{1}{2}}$ also requires $\gamma_{j,k}^{n+\frac{1}{2}}$ which is unknown. However,

$$\gamma_{j,k}^{n+\frac{1}{2}} = \frac{1}{2}\left(\gamma_{j,k}^{n+1} + \gamma_{j,k}^{n}\right) \qquad (6.26)$$

Combining Eqs. (6.24) and (6.26) yields

$$\gamma_{j,k}^{n+\frac{1}{2}} = \gamma_{j,k}^{n} + \frac{1}{2}(t^{n+1} - t^n)\, \dot{\gamma}_{j,k}^{n+\frac{1}{2}} \qquad (6.27)$$

Equation (6.27) is used for $\gamma_{j,k}^{n+\frac{1}{2}}$ in Eq. (6.25) to obtain an equation in which the only unknown is $\dot{\gamma}_{j,k}^{n+\frac{1}{2}}$. This may be solved by iteration. Then $\dot{\gamma}_{j,k}^{n+\frac{1}{2}}$ is known, and therefore $C_{j,k}^{n+1}$ from Eq. (6.22). Therefore the relaxed stress may be calculated. Equation (6.24) is used to find $\gamma_{j,k}^{n+1}$. This quantity must be stored for each mesh point in order to be used in the calculation at that mesh point during the next time step.

156

7.   INCLUSION OF PHASE TRANSITIONS

This chapter describes the alterations to the main program of Chapter 5 that are necessary in order to include the calculation of phase transitions. Although the basic program includes material strength, the relations presented here will be based upon hydrostatic thermodynamics, so that the thermodynamic state of the material depends only on the mean pressure and not upon the deviator components of the stress tensor. Although it is possible that shear stresses may affect transition points and rates,[74] the basic state of under-standing involving these phenomena is not advanced enough to warrant the added complications of non-hydrostatic thermodynamics. Thus, the procedures presented here will replace only Eqs. (5.54) and (5.41) which calculate the energy and mean pressure. The sound speed calculation will also be different, since Eq. (5.43) is based on the particular form of equation of state assumed in Chapter 5.

7.1 Calculation in a Mixed Phase

In order to advance the calculation to the next time step, the equation of state routine must provide the mean pressure for use in the equations of motion, given the total specific volume and the equation for conservation of energy. This is fairly straightforward for a single phase, and given the equation of state of Chapter 5 requires only Eqs. (5.54) and (5.41). The following describes the general procedure to be followed for a mixed phase.

The physical assumptions of the mixed phase theory for solid-solid transitions have been given previously.[75,76] Basically they are that pressure and temperature are common to both phases, and that no surface energy

157

is associated with the interface between the phases. Under these assumptions, the total specific volume may be written

$$V(P,T) = (1 - X) V_1(P,T) + XV_2(P,T) \tag{7.1}$$

where V_1 and V_2 are specific volumes of the first and second phases respectively. V is total specific volume of the mixture and X is mass fraction of the second phase. Although X has been previously used to denote position, in the remainder of this chapter it will denote the mass fraction of the second phase. Equation (7.1) follows directly from the assumption that the total volume of the mixture is equal to the sum of the total volumes of each phase, using the definition of specific volume as volume per unit mass and X as the mass of the second phase divided by the combined mass of both phases. Similarly, the absence of any surface energy implies that the total internal energy of the mixture is equal to the sum of the total internal energies of each phase. Therefore,

$$E(P,T) = (1 - X) E_1(P,T) + XE_2(P,T) \tag{7.2}$$

where E is the specific internal energy, or internal energy per unit mass, of the total mixture, and E_1 and E_2 are the specific internal energies of each phase. From Eqs. (7.1) and (7.2)

$$dV = (1 - X)dV_1 + XdV_2 + (V_2 - V_1)dX \tag{7.3}$$

$$dE = (1 - X)dE_1 + XdE_2 + (E_2 - E_1)dX \tag{7.4}$$

Expanding dV_i and dE_i in terms of P and T,

$$dV_i = \frac{\partial V_i}{\partial P}\Big|_T dP + \frac{\partial V_i}{\partial T}\Big|_P dT \tag{7.5}$$

$$dE_i = \frac{\partial E_i}{\partial P}\bigg|_T dP + \frac{\partial E_i}{\partial T}\bigg|_P dT \tag{7.6}$$

From the definitions of the coefficient of thermal expansion,

$$\alpha_i = \frac{1}{V_i} \frac{\partial V_i}{\partial T}\bigg|_P \tag{7.7}$$

the isothermal compressibility,

$$\beta_i = \frac{-1}{V_i} \frac{\partial V_i}{\partial P}\bigg|_T \tag{7.8}$$

and the specific heat per unit mass at constant pressure,

$$C_{Pi} = T \frac{\partial S_i}{\partial T}\bigg|_P \tag{7.9}$$

where S_i is the specific entropy of the ith phase, Eqs. (7.5) and (7.6) become[77]

$$dV_i = \alpha_i V_i dT - \beta_i V_i dP \tag{7.10}$$

$$dE_i = (C_{Pi} - \alpha_i V_i P)dT + (\beta_i V_i P - \alpha_i V_i T)dP \tag{7.11}$$

If Eqs. (7.10) and (7.11) are used in Eqs. (7.3) and (7.4), and conservation of energy is used to replace dE and there is no heat exchange between mass elements, the result after collecting terms in dT and dP is

$$a_1 dT + a_2 dP + a_3 = 0 \tag{7.12}$$

$$a_4 dT + a_5 dP + a_6 = 0 \tag{7.13}$$

where

$$a_1 = (1 - X)\alpha_1 V_1 + X\alpha_2 V_2 \qquad (7.14)$$

$$a_2 = -(1 - X)\beta_1 V_1 - X\beta_2 V_2 \qquad (7.15)$$

$$a_3 = (V_2 - V_1)dX - dV \qquad (7.16)$$

$$a_4 = (1 - X)(C_{P1} - \alpha_1 V_1 P) + X(C_{P2} - \alpha_2 V_2 P) \qquad (7.17)$$

$$a_5 = (1 - X)(\beta_1 V_1 P - \alpha_1 V_1 T) + X(\beta_2 V_2 P - \alpha_2 V_2 T) \qquad (7.18)$$

$$a_6 = PdV + (E_2 - E_1)dX \qquad (7.19)$$

Solving Eqs. (7.12) and (7.13) simultaneously for dT and dP,

$$dT = (a_6 a_2 - a_3 a_5)/D \qquad (7.20)$$

$$dP = (a_4 a_3 - a_1 a_6)/D \qquad (7.21)$$

where

$$D = a_1 a_5 - a_4 a_2 \qquad (7.22)$$

If α_i, β_i, V_i, C_{Pi}, and E_i are known as functions of P and T for i equal to 1 and 2, along with X, dX, and dV, Eqs. (7.20) and (7.21) become a set of coupled differential equations in P and T to which the differencing scheme of Chapter 5 may be applied.

If the changes occur in a time dT,

$$\dot{T} = (a_6 a_2 - a_3 a_5)/D \qquad (7.23)$$

$$\dot{P} = (a_4 a_3 - a_1 a_6)/D \qquad (7.24)$$

where a_3 and a_6 now become

$$a_3 = (V_2 - V_1)\dot{X} - \dot{V} \tag{7.25}$$

$$a_6 = P\dot{V} + (E_2 - E_1)\dot{X} \tag{7.26}$$

Using centered time differencing, Eqs. (7.23) and (7.24) become

$$T_{j,k}^{n+1} = T_{j,k}^{n} + (t^{n+1} - t^n) \, [(a_6 a_2 - a_3 a_5)/D]_{j,k}^{n+\frac{1}{2}} \tag{7.27}$$

$$P_{j,k}^{n+1} = P_{j,k}^{n} + (t^{n+1} - t^n) \, [(a_4 a_3 - a_1 a_6)/D]_{j,k}^{n+\frac{1}{2}} \tag{7.28}$$

The quantities in brackets on the right hand side of Eqs. (7.27) and (7.28) depend on the values of $P^{n+\frac{1}{2}}$ and $T^{n+\frac{1}{2}}$. Taking

$$P^{n+\frac{1}{2}} = \frac{1}{2} (P^{n+1} + P^n) \tag{7.29}$$

$$T^{n+\frac{1}{2}} = \frac{1}{2} (T^{n+1} + T^n) \tag{7.30}$$

Eqs. (7.27) and (7.28) become implicit equations for P^{n+1} and T^{n+1} which may be solved iteratively.

This procedure is completely general in that it involves no dependence on equations of state or transformation mechanisms. Since there are no approximations made about the materials involved, its implementation requires a large amount of thermodynamic information about both phases of the material being considered. The volume and its time derivative are calculated in a previous section of the program, and $\alpha_i(P,T)$ and $\beta_i(P,T)$ can be calculated if $V_i(P,T)$ are known, so that the information required is $V_i(P,T)$, $C_{pi}(P,T)$, $E_i(P,T)$, X, and $\dot{X}$. The curves of volume, internal energy, and specific heat for both phases must be extended into the metastable regions throughout the entire P-T plane so that rate-dependent transformations may be allowed. The functional

161

forms of X and Ẋ may be chosen to represent the transformation mechanism desired.

It is possible to construct the thermodynamic potential for a system by specifying less information than is required above,[78] so if all of the above quantities are specified independently it is possible that the description will be thermodynamically inconsistent. Moreover, sufficient experimental data usually do not exist for any given material to specify all of the information required. The best approach in most cases would therefore seem to be to adopt an approximate model and use it to construct a thermodynamic potential so that thermodynamic consistency is observed. This will be done for a specific example in the next section. This is done merely to illustrate the problem and not to recommend the equation of state derived there. The purpose of this work is to include the capability for calculation of phase transitions into the wavecode, and the choice of a specific equation of state depends upon the particular problem to be studied. It is for this reason that the procedure described in this section is kept as general as possible.

7.2 Equation of State

Since the quantities required are all assumed to be functions of P and T, it would seem that the Gibbs energy would be the most logical thermodynamic potential to construct. However, as will be seen, the assumptions which will be made make construction of the Helmholtz energy calculationally simpler.

The differential of the specific Helmholtz energy, which is the molar Helmholtz energy divided by the molecular weight, is

$$dF = -SdT - PdV \qquad (7.31)$$

162

where S is specific entropy, and V is specific volume. $F(T,V)$ can be obtained by integrating dF from a reference point $F(T_0,V_0)$. Figure 7.1 shows two possible paths of integration. Path 1 goes at constant temperature from (T_0,V_0) to (T_0,V) and at constant volume from (T_0,V) to (T,V). Along this path,

$$F(T,V) - F(T_0,V_0) = -\int_{V_0}^{V} P(T_0,V)dV - \int_{T_0}^{T} S(T,V)dT \qquad (7.32)$$

Path 2 goes at constant volume from (T_0,V_0) to (T,V_0) and at constant temperature from (T,V_0) to (T,V). Along path 2

$$F(T,V) - F(T_0,V_0) = -\int_{T_0}^{T} S(T,V_0)dT - \int_{V_0}^{V} P(T,V)dV \qquad (7.33)$$

Now

$$dS = \frac{\partial S}{\partial T}\bigg|_V dT + \frac{\partial S}{\partial V}\bigg|_T dV \qquad (7.34)$$

But

$$\frac{\partial S}{\partial T}\bigg|_V = \frac{C_V}{T} \qquad (7.35)$$

and

$$\frac{\partial S}{\partial V}\bigg|_T = \frac{\alpha}{\beta} \qquad (7.36)$$

However, using the definition of the Gruneisen parameter,

$$\Gamma \equiv V\frac{\partial P}{\partial E}\bigg|_V = \frac{\alpha V}{\beta C_V} \qquad (7.37)$$

Eq. (7.34) becomes

$$dS = \frac{C_V}{T} dT + \frac{\Gamma C_V}{V} dV \qquad (7.38)$$

Thus

$$S(\Gamma,V_0) - S(T_0,V_0) = \int_{T_0}^{T} \frac{C_V(T,V_0)}{T} dT \qquad (7.39)$$

163
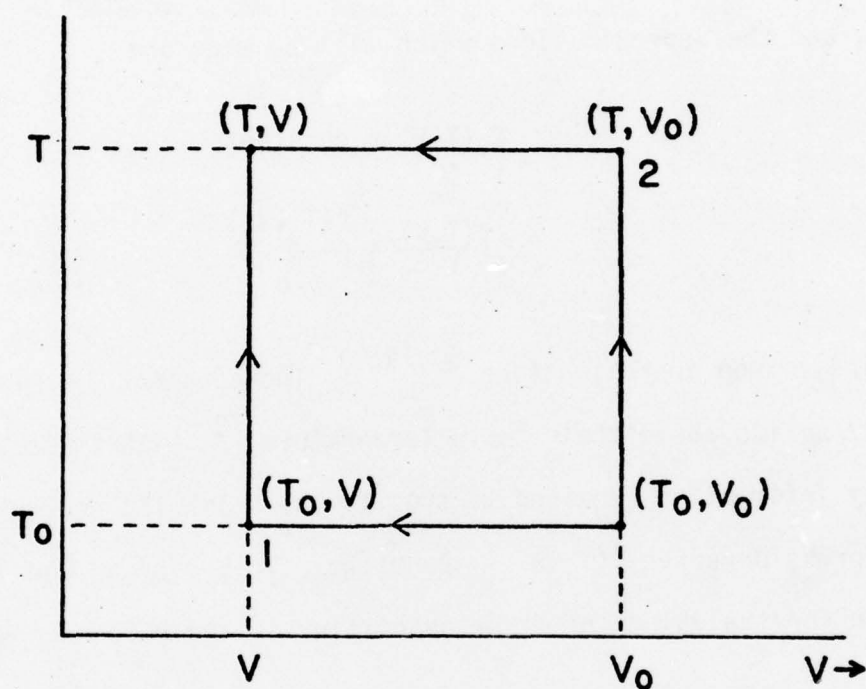
Fig. 7.1. Possible paths of integration in T,V plane

and along path 1

$$S(T,V) - S(T_0,V_0) = \int_{T_0}^{T} \frac{C_V(T,V_0)}{T}\, dT + \int_{V_0}^{V} \frac{\Gamma(T,V)C_V(T,V)}{V}\, dV \qquad (7.40)$$

Along path 1 the information required is $P(T_0,V)$, $C_V(T,V)$, and $\Gamma(T,V)$. Along path 2 the information required is $P(T,V)$ and $C_V(T,V_0)$. Path 1 will be chosen, and the approximations which will be made are

$$C_V(T,V) = \text{constant} \qquad (7.41)$$

$$\frac{\Gamma(T,V)}{V} = \frac{\Gamma(T_0,V_0)}{V_0} \qquad (7.42)$$

These are common approximations.[60,79,80] The constant C_V model is particularly good for solids above their Debye temperature.[78] With these approximations the only information required to specify the Helmholtz energy is the isothermal compression curve $P(T_0,V)$. Denoting $\Gamma(T_0,V_0)$ by Γ_0 and using similar notation for the values of other quantities in the reference state, Eq. (7.40) becomes

$$S = S_0 + C_V \ln \frac{T}{T_0} + \rho_0 \Gamma_0 C_V (V - V_0) \qquad (7.43)$$

and thus the Helmholtz potential is given by

$$F(T,V) = F_0 - \int_{V_0}^{V} P(T_0,V)dV - S_0(T - T_0) - \rho_0 \Gamma_0 C_V (V - V_0)(T - T_0)$$

$$- C_V T \ln \frac{T}{T_0} + C_V(T - T_0) \qquad (7.44)$$

A Murnaghan type of equation will be assumed for $P(T_0,V)$

$$P(T_0,V) = \frac{K_0}{n} \left[\left(\frac{V_0}{V}\right)^n - 1 \right] \qquad (7.45)$$

As long as n is not equal to 1

$$\int_{V_0}^{V} P(T_0, V) dV = \frac{K_0}{n} \left[\frac{V}{1-n} \left(\frac{V_0}{V}\right)^n - V - \frac{nV_0}{1-n} \right] \tag{7.46}$$

Then

$$F(T,V) = F_0 - \frac{K_0}{n} \left[\frac{V}{1-n} \left(\frac{V_0}{V}\right)^n - V - \frac{nV_0}{1-n} \right] - S_0(T - T_0)$$

$$- b_0 \Gamma_0 C_V (V - V_0)(T - T_0) - C_V T \ln\frac{T}{T_0} + C_V(T - T_0) \tag{7.47}$$

The pressure is given by

$$P(V,T) = \frac{-\partial F}{\partial V}\bigg|_T = \frac{K_0}{n} \left[\left(\frac{V_0}{V}\right)^n - 1 \right] + \rho_0 \Gamma_0 C_V(T - T_0) \tag{7.48}$$

Thus

$$V(P,T) = V_0 \left[\frac{P - \rho_0 \Gamma_0 C_V(T - T_0)}{K_0/n} + 1 \right]^{-1/n} \tag{7.49}$$

Differentiating Eq. (7.49)

$$\beta = \frac{1}{K_0} \left(\frac{V}{V_0}\right)^n \tag{7.50}$$

and from Eqs. (7.37) and (7.42),

$$\alpha = \rho_0 \Gamma_0 C_V \beta \tag{7.51}$$

The specific heats are related by

$$C_P = C_V + \frac{\alpha^2 V T}{\beta} \tag{7.52}$$

From Eqs. (7.51) and (7.52),

$$C_P = C_V(1 + \rho_0 \Gamma_0 \alpha VT) \tag{7.53}$$

166

Finally, the energy is given by

$$E = F + TS \qquad (7.54)$$

so, from Eqs. (7.43) and (7.47)

$$E = E_o - \frac{K_o}{n} \left[\frac{V}{1 - n} \left(\frac{V_o}{V}\right)^n - V - \frac{nV_o}{1 - n}\right] + \rho_o \Gamma_o C_V T_o (V - V_o) + C_V (T - T_o) \qquad (7.55)$$

where

$$E_o = F_o + T_o S_o \qquad (7.56)$$

Equations (7.49), (7.50), (7.51), (7.53), and (7.55) provide $V(P,T)$, $\beta(P,T)$, $\alpha(P,T)$, $C_p(P,T)$, and $E(P,T)$. This provides the equation of state information for each phase to be used in Eqs. (7.20) and (7.21). It is still necessary to determine the reference values of the variables in each phase and to specify X and $\dot{X}$.

Equation (7.55) gives the energy of a single phase in terms of P and T and the values of E_o and S_o in the reference state. The reference state (P_o, T_o) will be taken to be zero pressure and room temperature. Then for each phase V_{oi} is the value of V_i at (P_o, T_o). For the first phase the values of E_{o1} and S_{o1} may be taken to be zero. The values of E_{o2} and S_{o2} are then determined and must be calculated.

S_{o2} may be calculated by use of the Clapeyron equation,[78]

$$\frac{dP}{dT} = \frac{S_2 - S_1}{V_2 - V_1} \qquad (7.57)$$

The procedure is to use Eq. (7.34) for the first phase to find the value of S_1 at the transition pressure at room temperature. Given the slope of the phase line at T_o, Eq. (7.49) and (7.57) give the value of S_2 at the transition

167

pressure at room temperature. Equation (7.43) may then be used for the second phase to find the value of S_{o2} at (P_o, T_o). Thus the transition pressure and slope of the phase line must be known to find the reference values of entropy in the second phase.

Once S_{o2} is known, E_{o2} may be found by equating the values of the Gibbs energy at the transition pressure and room temperature. The Gibbs energy is given by

$$G = F + PV \qquad (7.58)$$

From Eqs. (7.47) and (7.49)

$$G = E_o - T_o S_o + \frac{K_o V_o}{1 - n} - S_o(T - T_o) + \rho_o \Gamma_o C_V V_o (T - T_o)$$

$$- C_V T \ln \frac{T}{T_o} + C_V(T - T_o)$$

$$+ \frac{n V_o}{n - 1} \left(\frac{K_o}{n}\right)^{1/n} [P - \rho_o \Gamma_o C_V(T - T_o) + \frac{K_o}{n}]^{1 - 1/n} \qquad (7.59)$$

Then setting

$$G_1(P_T, T_o) = G_2(P_T, T_o) \qquad (7.60)$$

where P_T is the transition pressure at T_o provides an equation in which the only unknown is E_{o2}.

Once the values of all quantities in the reference state have been determined, the only variables left undetermined are X and $\dot{X}$. These may be determined by physical considerations of the nucleation and growth of the second phase,[79] but the procedure here will be to determine $\dot{X}$ by a relaxation law of the form[81]

$$\dot{X} = \frac{X_{eq} - X}{\tau} \qquad (7.61)$$

168

where X_{eq} is the equilibrium value of the mass fraction of the second phase, and τ is a characteristic relaxation time. X is then given by

$$X = \int \dot{X} dT \qquad (7.62)$$

The equilibrium mass fraction is determined as follows. The phase line giving the values of pressure and temperature at which the two phases may coexist in equilibrium may be found by equating the Gibbs energies for the two phases. This gives

$$G_1(P,T) = G_2(P,T) \qquad (7.63)$$

Since all the constants in this equation have been determined, it may be solved for P as a function of T. This is the phase line $P_T(T)$. This implies that when the system is in the mixed phase in equilibrium the pressure is a function of temperature alone. Thus, the three-dimensional equilibrium PVT surface consists of the two surfaces given by Eq. (7.49) for each phase, connected by the surface described by the equation $P=P_T(T)$ in PVT space. If the system is in equilibrium, the state point must always be on this surface. Figure 7.2 shows a constant T section of the equilibrium PVT surface. At temperature T' the transition pressure is $P_T(T')$. The volumes of the two phases at this temperature and pressure are $V_1(P_T(T'),T')$ and $V_2(P_T(T'),T')$. If the temperature is T' and the total volume is greater than $V_1(P_T(T'),T')$, the equilibrium state point must be on curve OA, so the equilibrium mass fraction of the second phase is zero. Similarly, if T is equal to T' and V is less than $V_2(P_T(T'),T')$, then X_{eq} is equal to 1. If T is equal to T' and V is between $V_1(P_T(T'),T')$ and $V_2(P_T(T'),T')$, the state point is on curve AB, the system is in the mixed phase, and the mass fraction is given by Eq. (7.1). Therefore, given the phase line $P_T(T)$, the total specific volume V, and the

169
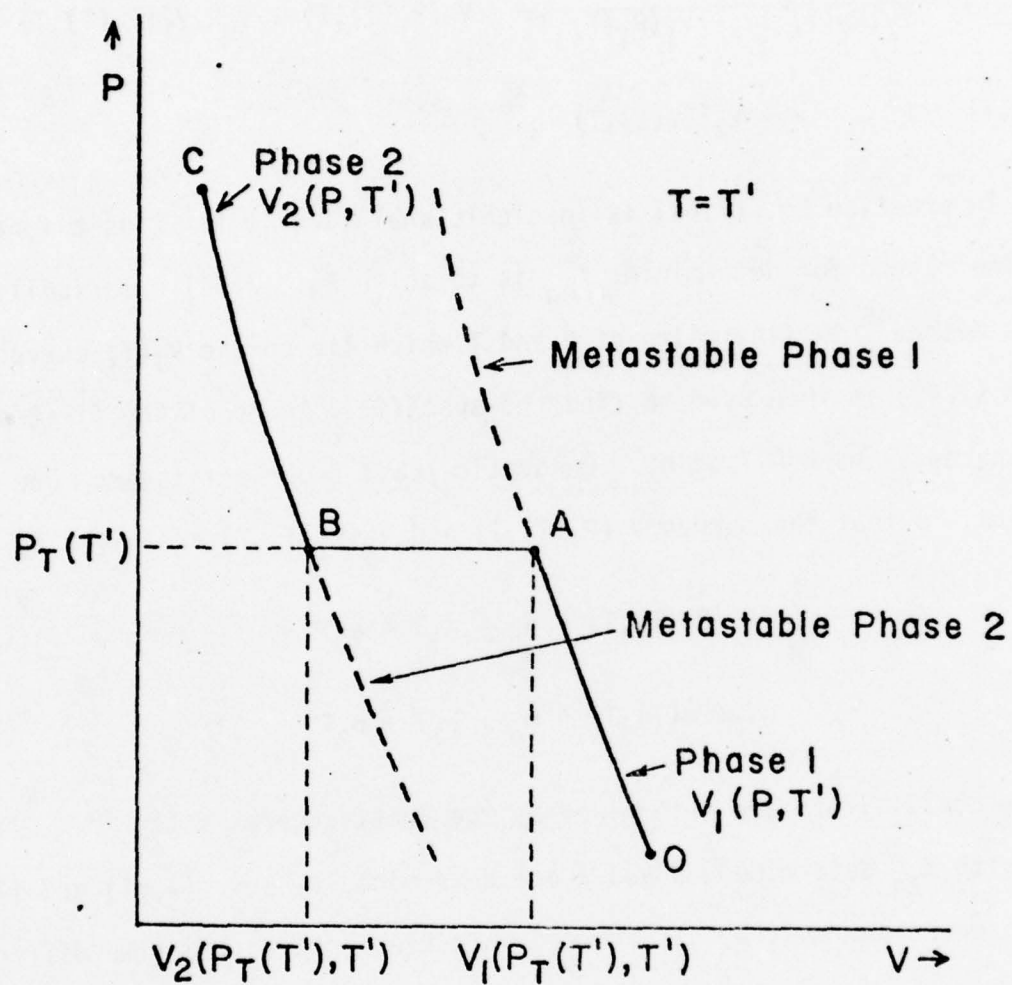
Fig. 7.2. Constant T section of equilibrium PVT surface for a material undergoing a phase transition

temperature T,

$$X_{eq}(V,T) = 0 \qquad V > V_1(P_T(T),T)$$

$$X_{eq}(V,T) = \frac{V - V_1(P_T(T),T)}{V_2(P_T(T),T) - V_1(P_T(T),T)} \qquad V_2(P_T(T),T) < V < V_1(P_T(T),T) \quad (7.64)$$

$$X_{eq}(V,T) = 1 \qquad V < V_2(P_T(T),T)$$

In practice Eq. (7.64) is insoluble analytically for P as a function of T. The method for determining X_{eq} is to solve Eq. (7.64) numerically by Halley's method[46] to find pairs of P and T which lie on the $P_T(T)$ curve. Equation (7.49) is then used to find the specific volumes of the first and second phases at each P-T point. Quadratic least squares fits are made to these data, so that the curves $V_1(P_T(T),T)$ and $V_2(P_T(T),T)$ are given by

$$V_1(P_T(T),T) = a_o + a_1T + a_2T^2 \qquad (7.65)$$

$$V_2(P_T(T),T) = b_o + b_1T + b_2T^2 \qquad (7.66)$$

where the coefficients are determined by the least-squares fits.

With X_{eq} determined, X and $\dot{X}$ are determined by Eqs. (7.61) and (7.62). These two equations must be differenced. In keeping with the time differencing of the rest of the code, $\dot{X}$ is defined at half-integral times, and X is defined at integral times. From Eq. (7.61),

$$\dot{X}_{j,k}^{n+\frac{1}{2}} = \frac{X_{eq_{j,k}}^{n+\frac{1}{2}} - X_{j,k}^{n+\frac{1}{2}}}{\tau} \qquad (7.67)$$

X and $\dot{X}$ are related by

$$X_{j,k}^{n+1} = X_{j,k}^{n} + (t^{n+1} - t^n)\,\dot{X}_{j,k}^{n+\frac{1}{2}} \qquad (7.68)$$

171

Defining

$$X_{j,k}^{n+\frac{1}{2}} = \frac{1}{2} (X_{j,k}^{n+1} + X_{j,k}^{n}) \tag{7.69}$$

and using Eq. (7.68)

$$X_{j,k}^{n+\frac{1}{2}} = X_{j,k}^{n} + \frac{1}{2} (t^{n+1} - t^{n}) \dot{X}_{j,k}^{n+\frac{1}{2}} \tag{7.70}$$

Using this in Eq. (7.67) and solving for $\dot{X}_{j,k}^{n+\frac{1}{2}}$,

$$\dot{X}_{j,k}^{n+\frac{1}{2}} = \frac{X_{eq_{j,k}}^{n+\frac{1}{2}} - X_{j,k}^{n}}{\tau + \frac{1}{2}(t^{n+1}-t^{n})} \tag{7.71}$$

$X_{j,k}^{n+1}$ is then found from Eq. (7.68) and is stored for each mesh point. The values of X and $\dot{X}$ are required at half-integral times in Eqs. (7.27) and (7.28) so Eq. (7.69) is used for $X_{j,k}^{n+\frac{1}{2}}$. This completes the determination of all quantities required in Eqs. (7.27) and (7.28) to calculate the pressure at time t^{n+1}.

7.3 Sound Speed

The sound speed given by Eq. (5.43) depends on the specific form of the equation of state assumed in Eq. (5.36). In general, the bulk sound speed is given by

$$c_b^2 = -V^2 \left. \frac{\partial P}{\partial V} \right|_S \tag{7.72}$$

In terms of quantities defined in Section 7.2, this becomes

$$c_b^2 = [\frac{\beta}{V} - \frac{\alpha^2 T}{C_p}]^{-1} \tag{7.73}$$

This is easily evaluated if the material is not in the mixed phase, since in that case all quantities on the right hand side of Eq. (7.73) refer only to

172

a single phase. Thus, α, β, V, and C_p are equal to α_i, β_i, V_i, and C_{pi}, respectively for i equal to either 1 or 2. However, if the material is in the mixed phase, α, β, and C_p are not so clearly defined. For instance, defining

$$\alpha = \frac{1}{V} \left(\frac{\partial V}{\partial T}\right)_P \tag{7.74}$$

and using Eq. (7.1) for V results in a partial derivative of X in the expression. This poses problems, since X would have to be determined from Eqs. (7.61) and (7.62). The procedure to be followed here will be to evaluate the sound speed for the frozen mixture.[82] This is clearly not correct, but should not be too bad an approximation for long relaxation times. In any event, the sound speed is required only in the expression for the artificial viscosity, Eq. (5.49), and in the time step criterion, Eq. (5.109). Therefore, it should not affect the form of the solution.

If X is taken as constant, Eqs. (7.1) and (7.73) yield

$$\alpha = \frac{1}{V} \left[(1 - X) \frac{\partial V_1}{\partial T}\Big|_P + X \frac{\partial V_2}{\partial T}\Big|_P \right] \tag{7.75}$$

From Eq. (7.7)

$$\alpha = \frac{1}{V} \left[(1 - X)\alpha_1 V_1 + X\alpha_2 V_2 \right] \tag{7.76}$$

Similarly

$$\beta = \frac{1}{V} \left[(1 - X)\beta_1 V_1 + X\beta_2 V_2 \right] \tag{7.77}$$

and

$$C_p = (1 - X)C_{p1} + XC_{p2} \tag{7.78}$$

173

Equations (7.76), (7.77), and (7.78) allow the sound speed to be determined from Eq. (7.73). These equations also hold for the case in which the material is in a pure phase.

7.4 Applications

The calculational procedure for the mixed phase described in this chapter has been used for iron and KCl to compare to the experiments described in Chapter 4. The values of the equation of state constants described in Section 7.2 are given in Table 7.1. Results are given in Chapter 8.

The wavecode described in this work is capable of handling elastic-plastic stress relaxing materials which undergo phase transitions. Of course, it is not necessary to include all these forms of behavior in any given calculation. Appropriate choice of the equation of state constants allows whatever material description is desired. For instance, the hydrodynamic case may be chosen by setting the yield strength to zero. The phase boundary is controlled by the choice of the constants in Eqs. (7.65) and (7.66), and if desired these may be chosen so that the material does not undergo a phase transition. The stress relaxation constants in Eq. (6.19) may be chosen to give elastic-perfectly plastic or totally elastic behavior. Thus, it is possible to choose whatever combination of material properties is desired.

One interesting problem is a phase transition occurring in a material with strength. The thermodynamics describing the phase transitions are purely hydrodynamic, so it is not possible to consider directly the effects of stress deviators on the phase transition. However, it is possible to use the code to study the effects of a phase transition on the elastic properties of the material. The elastic properties such as the yield strength and Poisson's ratio are included in subroutines so that any functional form may be chosen for them without alteration of the main code. This allows the effects of a given

174

TABLE 7.1. Material properties for Fe and KCl

Material	Specific volume V_o (g/cm^3)	Bulk modulus K_o (Mb)	Bulk modulus derivative n	Gruneisen parameter Γ_o	Specific heat C_v (Mb cm^3/gm°K)	Internal energy E_o (Mb cm^3/gm)
Fe, phase 1	.1270	1.627	5.917	1.628	4.169×10^{-6}	0
Fe, phase 2	.1203	1.658	5.102	2.000	4.169×10^{-6}	9.925×10^{-4}
KCl, phase 1	.5030	.3460	2.460	1.660	6.600×10^{-6}	0
KCl, phase 2	.4340	.7950	4.590	2.860	6.600×10^{-6}	2.624×10^{-3}

theory governing the elastic properties of the material during a phase transition to be determined. For instance, it is possible to allow material strength up to the transition pressure, and assume that the phase transition annihilates the stress deviators. The material could then either remain hydrostatic, or the deviatoric components could again be allowed to build. Examination of code runs based on such theories would help determine the validity of the assumptions made.

In the study of phase transitions the interesting parameter to vary is the relaxation time τ used in Eq. (7.61). It must be noted that although Eq. (7.71) seems to be valid as τ goes to zero, it appears that the procedure described in Section 7.2 does not work for the equilibrium transition. The problem is that when X is equal to X_{eq} and P is equal to $P_T(T)$, Eqs. (7.64) and (7.1) become identical. Thus, if Eq. (7.64) is used for X in Eq. (7.1) and the resulting equation is solved for V, it becomes indeterminant. Analytically Eqs. (7.20) and (7.21) are two equations in the three unknowns P, T, and X, and Eq. (7.64) is redundant. In the numerical calculation the solution becomes oscillatory as τ becomes small compared to the time step. This oscillation could also be produced by the fact that the sound speed calculation in Section 7.3 is incorrect in the mixed phase, producing an artificial viscosity and time step that allow oscillations. However, it is expected that the correct calculation would give a smaller value of the sound speed than that given by Section 7.3. This would just decrease the artificial viscosity and increase the time step, which is the opposite effect required to stop oscillations. Andrews[83] also notes the possibility of difficulties if the relaxation time is less than the time step.

A correct calculation of the equilibrium transition can be made by an alternate procedure. In this case Eq. (7.20) is divided by Eq. (7.21) to

176

END
FILMED
3 -86
DTIC
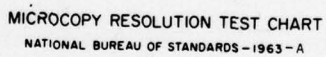
MICROCOPY RESOLUTION TEST CHART

NATIONAL BUREAU OF STANDARDS-1963-A

obtain dP/dT. This value is given along the phase line, since the phase line $P_T(T)$ is known. The resulting equation is then solved for dX, which is used in Eq. (7.21) to solve for dP. This procedure has been used to calculate the equilibrium transition without difficulty.[84]

8. CALCULATIONAL RESULTS

This chapter will present the results of some calculations done with
the wavecode described in Chapters 5, 6, and 7. A listing of this program is
given in Appendix B. Two types of calculations will be presented. The first
type is one-dimensional. These were done to compare to analytical solutions
so that it could be determined that the code was working correctly. The sec-
ond type of calculation utilizes the full two-dimensional capabilities of the
wavecode. These results can be compared to the experimental results described
in Chapter 4, thus checking the accuracy of both the code and the experimental
technique. The plots presented in this chapter as well as those in Chapter 4
were done on the CalComp 663 pen plotter[35] system auxiliary to the IBM 360/67
at Washington State University.

8.1 One-Dimensional Calculations

The one-dimensional calculations are done using the general wavecode
of Appendix B without Eqs. (5.75) and (5.79) which compute the X positions
and velocities of the mesh points. Thus there is no motion in the X direction
and the problem becomes one of one-dimensional strain in the Y direction. For
the one-dimensional strain problem and the equations of state given in Chap-
ters 5 and 7, it is possible to do an analytical calculation of the Hugoniots
of the materials. The method of calculating the Hugoniot is given in Appendix
C. The one-dimensional wavecode calculations are done for the problem of a
symmetric impact, so that the particle velocity behind the shock is one-half
the projectile velocity. This allows the values of pressure, density, temp-

erature, and so forth behind the first shock as given by the wavecode to be compared to the analytical values on the Hugoniot to see if the wavecode is functioning properly.

Figure 8.1 shows a plot of pressure versus position for the symmetric impact of an iron flyer on an iron target. Both flyer and target are .45 centimeters thick, and there are 90 meshes in each. The projectile velocity is .025 centimeters/microsecond in the negative Y direction, and the Y coordinate of the rear surface of the target is zero, so that the original impact occurred at .45 centimeters. Waves propagate into both the flyer and target. In this run the yield strength of the iron is zero so the problem is hydrodynamic. Figure 8.1 shows the pressure profile as a function of Eulerian position coordinate .759 microseconds after impact. The equation of state constants for the iron are those shown in Table 7.1. The Hugoniot calculation for this problem yields a particle velocity of .0125 centimeters/microsecond, a pressure of 47.4 kilobars, a specific volume of .124 cubic centimeters/gram, and a temperature of 314 degrees Kelvin behind the shock. The wavecode calculation agrees excellently with these figures, with a deviation of less than .5% in any quantity.

Figure 8.2 shows the pressure profile for the same problem except that the iron is now considered to have a yield strength in simple tension of 10 kilobars. This figure was chosen in order to produce a large amplitude elastic wave and not because it represents the actual yield strength of iron. Poisson's ratio is taken to be .29. The pressure plotted in Fig. 8.2 is the Y component of stress and not the mean pressure. The two-wave structure generated by the inclusion of material strength is clearly visible. The Hugoniot calculation for this problem yields a particle velocity of .0125 centimeters/microsecond, a Y stress component of 50.9 kilobars, a specific

179

T=0.75938 μsec

Flyer   Interface   Target
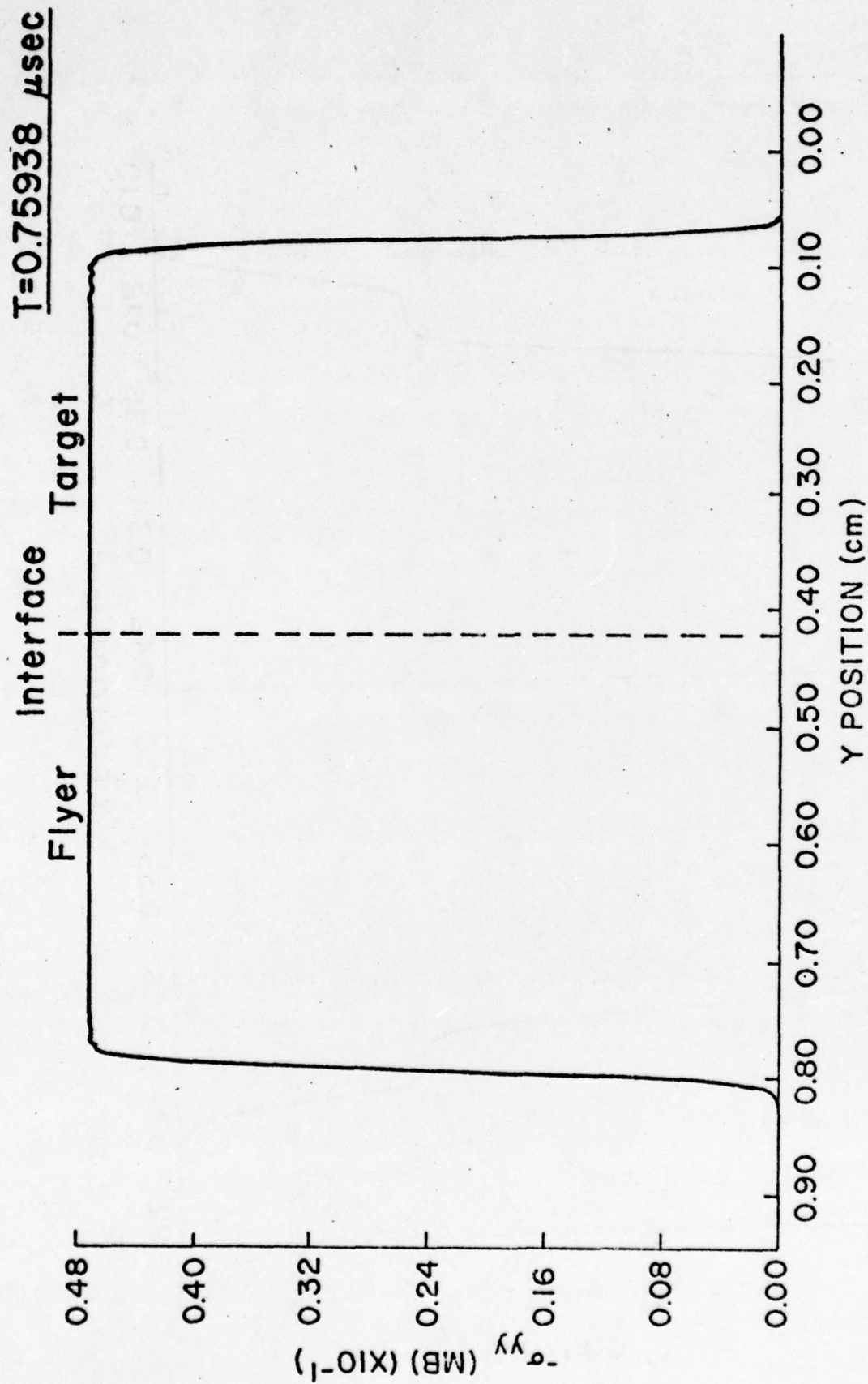
Fig. 8.1.   Pressure profile for the impact of an iron flyer on an iron target with no material strength included

180
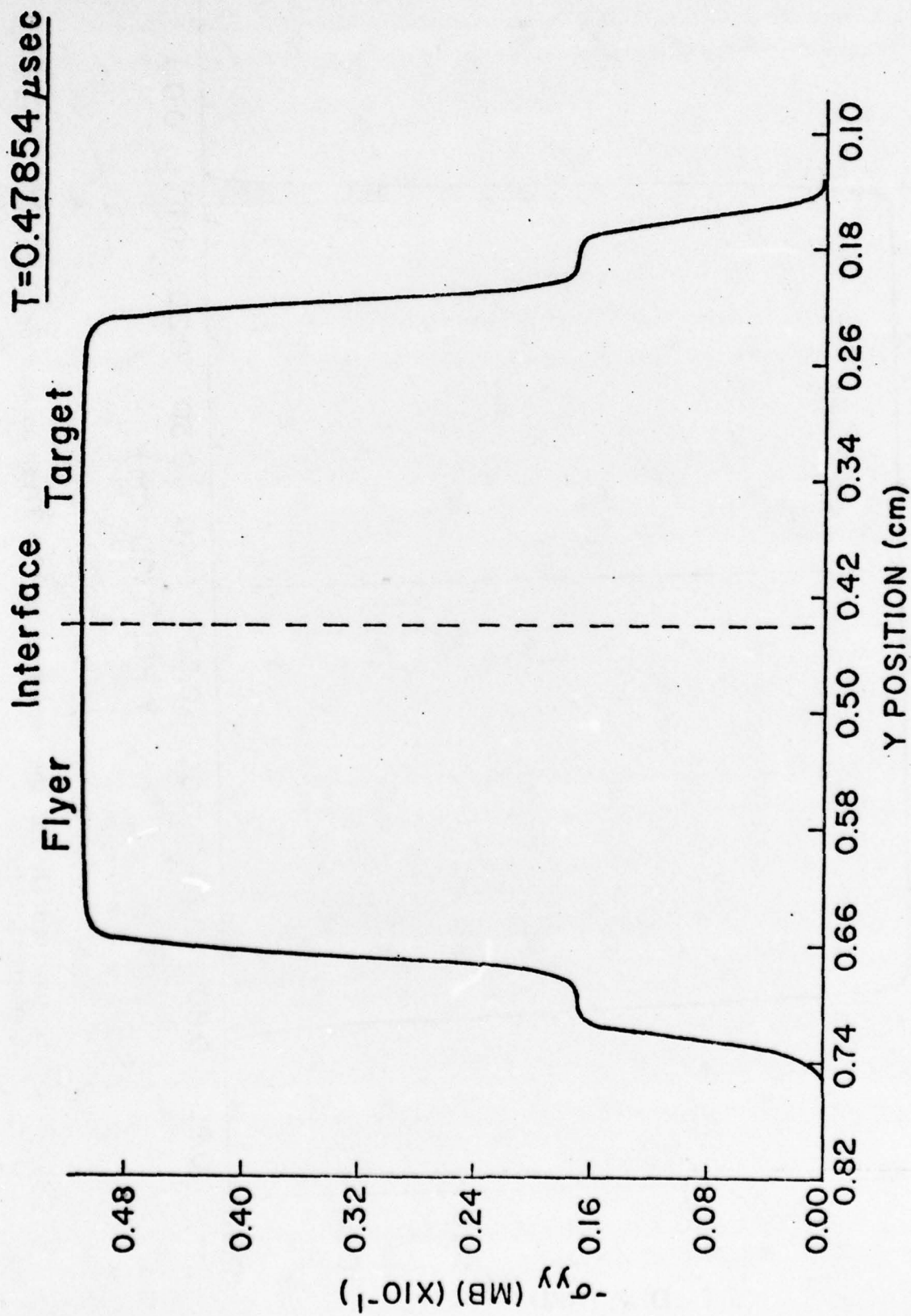
Fig. 8.2. σ_{yy} profile for the impact of an iron flyer on an iron target with material strength included

181

volume of .124 cubic centimeters/gram, and a temperature of 316 degrees Kelvin behind the second wave. The Y stress component in the elastic precursor is 16.9 kilobars. The wavecode again shows excellent agreement with these values.

Figure 8.3 shows the evolution of the wavefront with time when stress relaxation is included in the problem. The problem is again the impact of an iron flyer on an iron target. The mesh length in the Y direction is now .0005 centimeters. The yield strength is 10 kilobars, and the projectile velocity is .025 centimeters/microsecond. The figure shows the Y component of stress at the wavefront in the target versus distance from the original impact line at different times. The parameters behind the second wave are essentially the same as those for the elastic-perfectly plastic case of Fig. 8.2, and the overshoot and decay of the elastic precursor is immediately evident. The values for the constants required in Eq. (6.25) are those given by Wilkins.[73]

Figure 8.4 shows the time evolution of the wavefront in a material undergoing a phase transition. The situation is again the impact of an iron flyer on an iron target, but the projectile velocity is .12 centimeters/microsecond, so that the material undergoes the 130 kilobar α-ε phase transition. The mesh length in the Y direction is .005 centimeters. The yield strength is set to zero, so that the material is hydrodynamic. The equation of state constants for the first and second phases are those given in Table 7.1. The constant τ in Eq. (7.61) is .05 microseconds. The Hugoniot calculation for this problem gives a value of .06 centimeters/microsecond for particle velocity, .109 cubic centimeters/gram for specific volume, 210 kilobars for the Y component of stress, and 392 degrees Kelvin for the temperature behind the second wave. The wavecode gives excellent agreement with these values, and the decay of the first wave is evident.
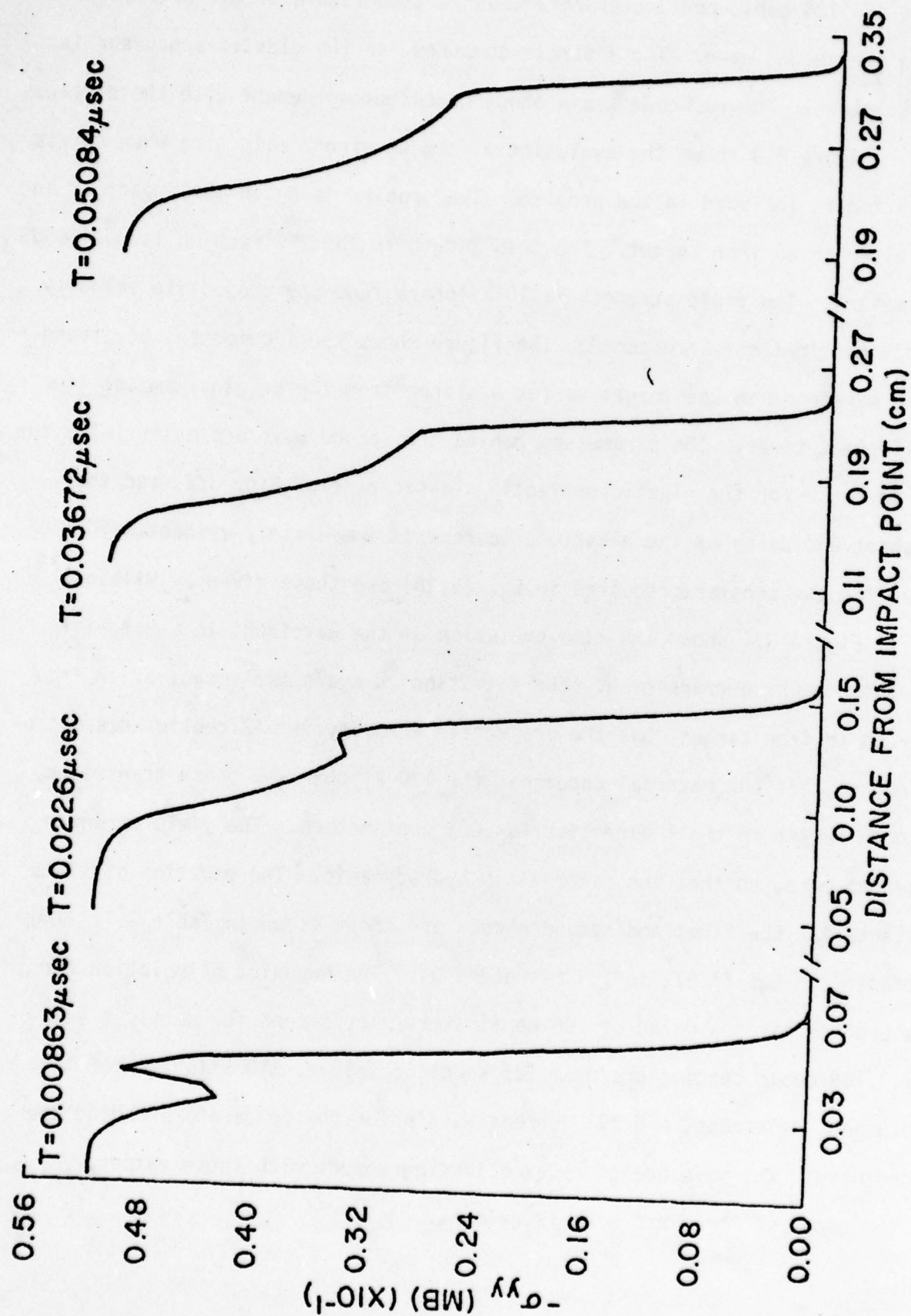
Fig. 8.3. Evolution of the wavefront in an elastic-plastic stress relaxing material
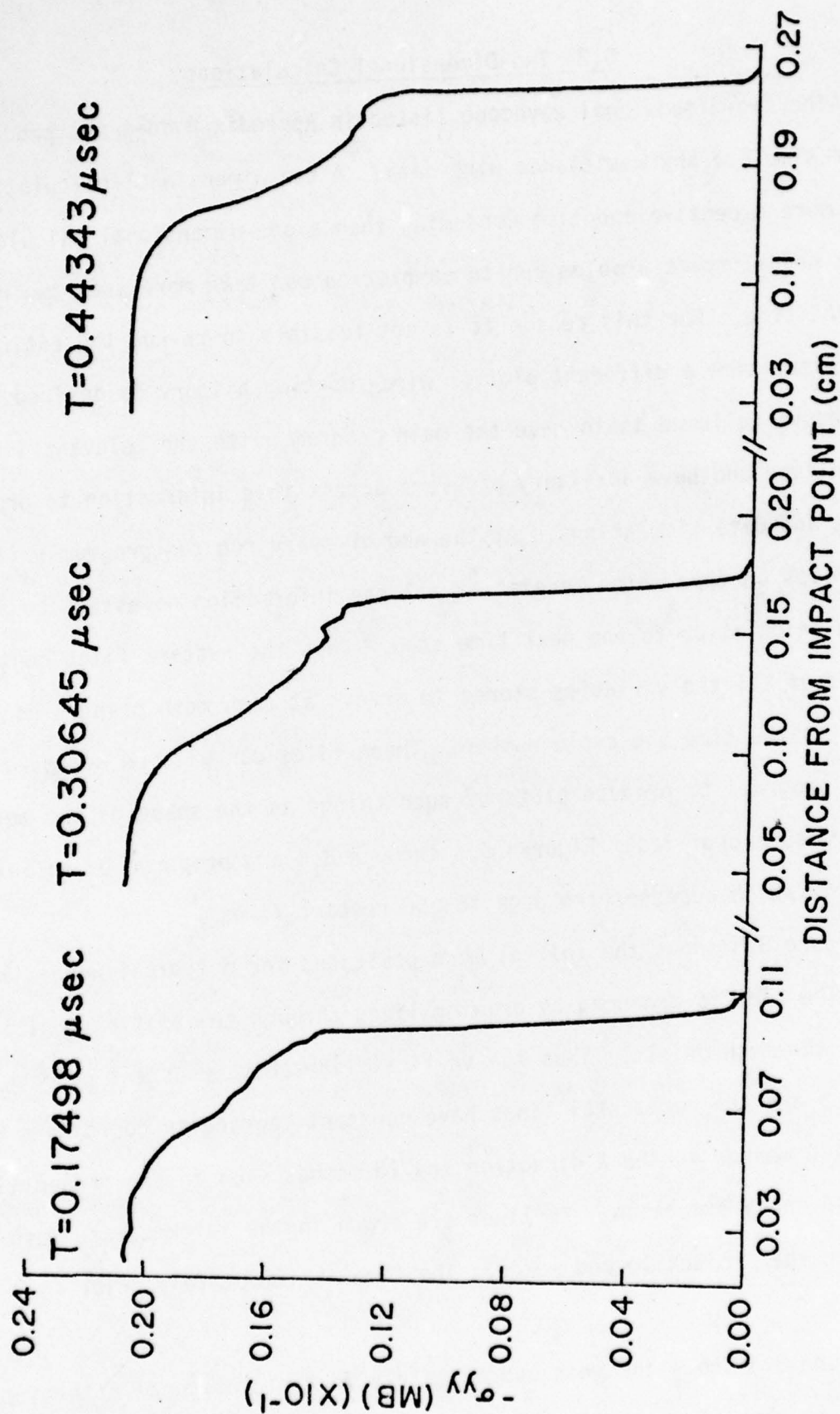
Fig. 8.4. Evolution of the wavefront in iron undergoing the 130 kilobar α-ε phase transition

184

8.2 Two-Dimensional Calculations

The two-dimensional wavecode listed in Appendix B does not produce plots or simulate any resistance wire data. A two-dimensional calculation is much more expensive and time-consuming than a one-dimensional calculation. A single wedge impact problem run to completion can take more than two hours of machine time. For this reason it is not feasible to re-run the entire problem every time a different plot or wire-shorting history is desired. The procedure followed is to have the main program write the relevant information on tape and have auxiliary programs access this information to produce the plots and data simulations. At the end of every run the program writes restart files on tape which consist of all the information necessary to advance the calculation to the next time step. Thus the restart files contain the values of all the variables stored in arrays at each mesh point plus other data such as the time and cycle number. These files can also be accessed by auxiliary programs to produce plots of such things as the shape of the mesh and the pressure profiles. Figures 8.5 through 8.8 are produced by an auxiliary program which accesses the data in the restart files.

Figure 8.5 shows the initial mesh positions for a typical wedge impact problem. The plot is produced by drawing lines through the spatial positions of each of the mesh points. Thus the vertical lines have constant Lagrangian coordinate j and the horizontal lines have constant Lagrangian coordinate k. There are 110 meshes in the X direction and 10 meshes each in the projectile and wedge in the Y direction. No lines are drawn in the intermediate mesh zone between the projectile and wedge. The time is immediately prior to impact.

Figure 8.6 shows the mesh approximately four microseconds after impact. The problem is that of an aluminum projectile striking an aluminum wedge. The

185

Fig. 8.5. Original mesh position for a wedge impact problem

186
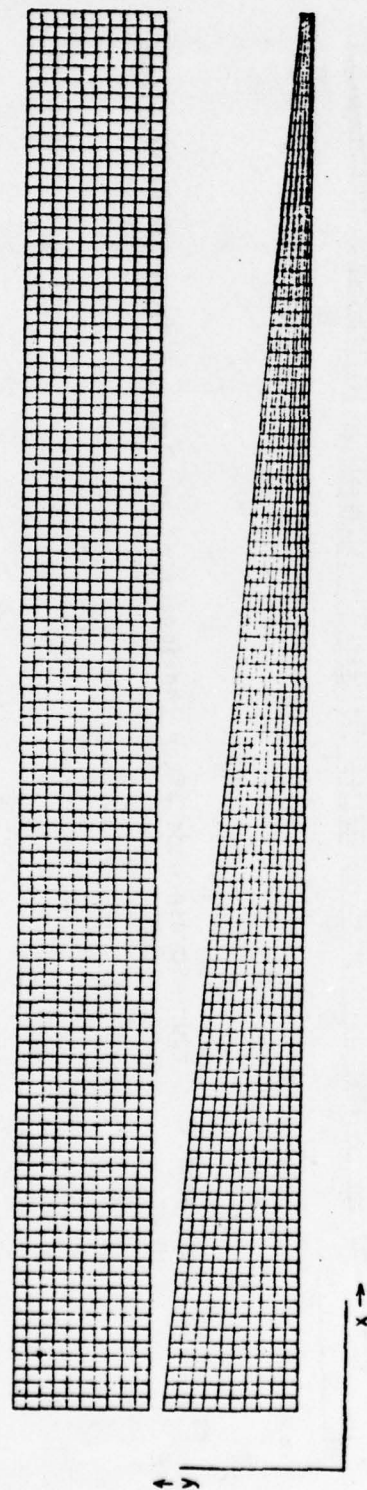
Fig. 8.5. Original mesh position for a wedge impact problem
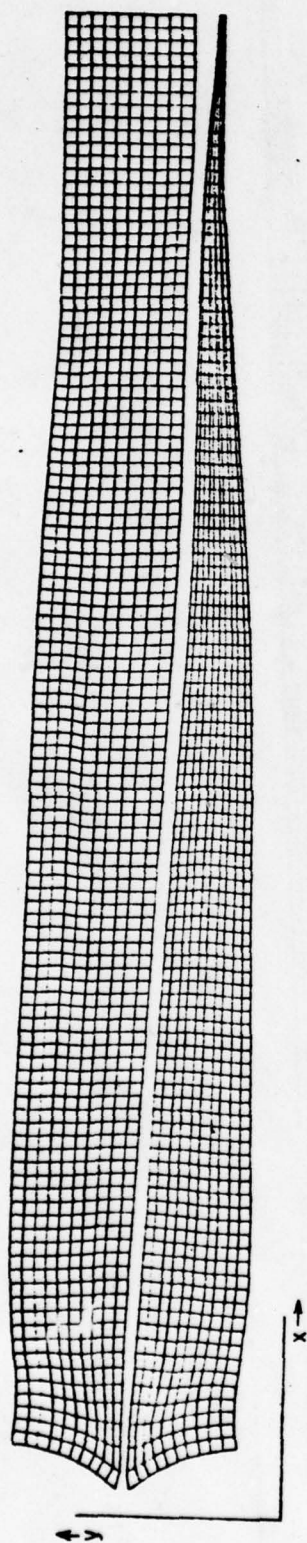
Fig. 8.6. Mesh positions four microseconds after the impact of an aluminum flyer on an aluminum target
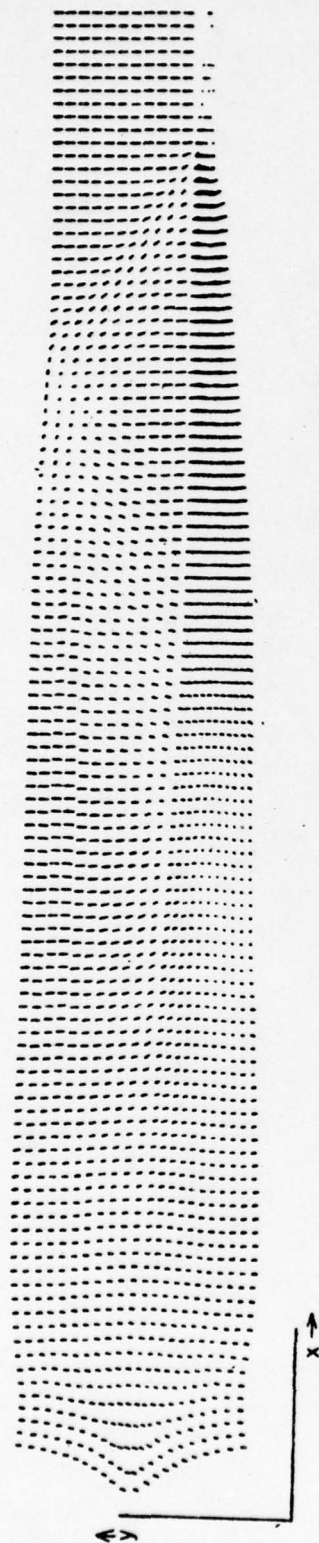
Fig. 8.7. Velocity plot four microseconds after the impact of an aluminum flyer on an aluminum target
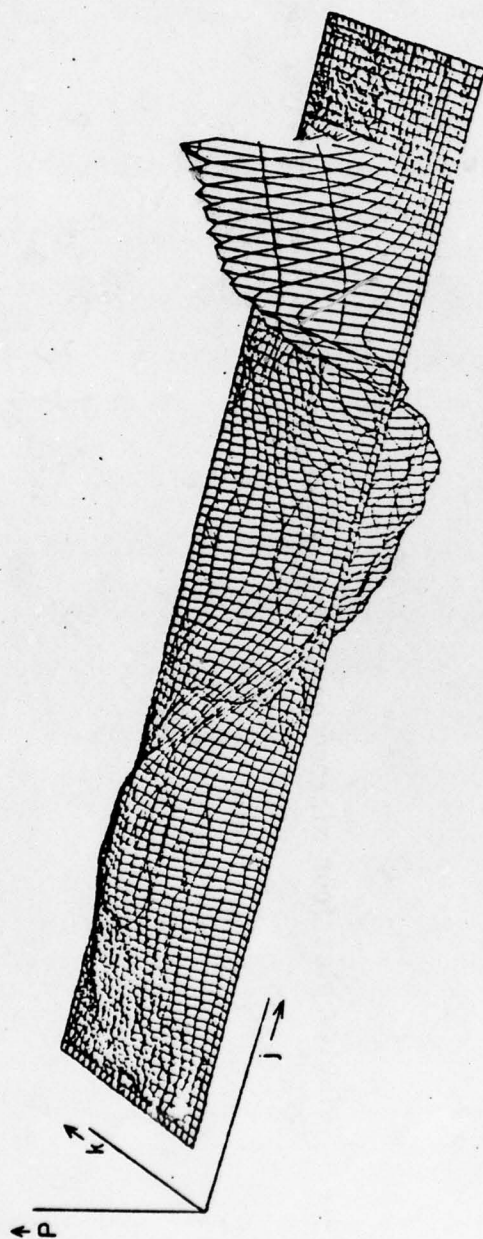
Fig. 8.8. Lagrangian pressure profile in wedge and projectile

189

projectile velocity is .088 centimeters/microsecond in the negative Y direction. The projectile and wedge are both 4.44 centimeters long. The high end of the wedge was originally .405 centimeters high, and the tip was .017 centimeters high. The wedge angle is approximately five degrees. There are 110 meshes in the X direction and 10 each in the projectile and wedge in the Y direction. There is no stress relaxation or phase transition in the problem so the equation of state used is that of Chapter 5. The material is assumed to have a yield strength of 10 kilobars. This value is chosen not from physical considerations but to demonstrate the effects of material strength. The contact point between projectile and wedge has moved most of the way down the wedge impact surface. The intermediate meshes are not drawn in order to clearly distinguish between the projectile and wedge. The effects of rarefaction from the initial impact point can be clearly seen in Fig. 8.6. The material is moving to the left and the rarefactions result in curvature of the two free surfaces near the initial impact side. This curvature of the free surface results in the discontinuous jump seen in the shorting records, since the first point on the wedge free surface to contact the wire is not at the left end of the wedge.

Figure 8.7 shows a velocity plot for the same problem and time shown in Fig. 8.6. This is produced by drawing a line at each mesh point in the direction of the velocity vector of that point whose length is proportional to the magnitude of the velocity. The wave structure in the material can be clearly seen in a figure of this type. At the right end of the projectile the mesh points all have the projectile velocity in the negative Y direction. The shock turning the flow can be clearly seen emanating from the contact point. The region of uniform flow behind the shocks gets very small near the tip of the wedge since the rarefaction from the wedge free surface is separated from

190

the shock in the projectile by only the wedge thickness at this point. The intersection of the shock in the projectile with the projectile free surface results in a rarefaction which travels back to the wedge free surface and disturbs the uniform region in the wedge behind the rarefaction from the wedge free surface. The wires must be placed close enough to the wedge free surface that they are contacted by the wedge free surface before the rarefaction from the projectile free surface reaches it.

Figure 8.8 shows a two-dimensional projection of the three-dimensional surface formed by plotting the mean pressure as a function of the Lagrangian coordinates j and k. The problem is the same as that of Figs. 8.6 and 8.7. The plot is produced using a three-dimensional perspective plotting routine with a hidden line feature which is available on the IBM 360/67 system at Washington State University. The pressure is a function of the Lagrangian coordinates so that the wedge is rectangular rather than wedge shaped. The figure includes both the projectile and wedge with the interface running lengthwise through the center of the figure. The projectile is in the foreground and the wedge is behind. The high pressure region following the shocks extends from the wedge free surface to the projectile free surface. The high pressure region is thin in the opposite direction because of the rarefaction from the wedge free surface. The intersection of the rarefactions from the two free surfaces produces a negative pressure region in the center of the material. Although the material is elastic-plastic, there is no two wave structure evident. This is because in-core storage limitations of the computer restrict the number of meshes allowed, and the mesh spacing is larger than the separation of the two waves.

In order to simulate the experimental records, the main program writes the positions and velocities of the mesh points on the wedge free surface on

191

tape at every time step. This information is then accessed by an auxiliary program which produces the simulated wire shorting histories. The wedge free surface is originally at Y coordinate zero, and moves in the negative Y direction. Given a wire offset D, the program searches through the positions of the free surface mesh points at each time step to find the mesh point with the largest j coordinate which has crossed the offset distance D during that time step. The velocity of that point during the time step and its position at the old time step are used to find the exact time and position at which the point crossed the wire offset distance. This time and position are then used as a point in the wire shorting history. To obtain the measured free surface velocity interpolation is used between two shorting histories for different wire offsets to find the difference between the times that the two contact points were at the same wedge coordinate. Thus the simulated free surface velocity records are produced in the same way that the experimental records are produced.

Figure 8.9 compares the calculated free surface velocity profile for aluminum to that produced by shot 75-081. The two records agree exceptionally well even in the curvature toward the thick end of the wedge. The calculation is that of an aluminum projectile striking an aluminum wedge. The given projectile velocity was .088 centimeters/microsecond, and the calculation ran to 4.34 microseconds after impact. The yield strength of the aluminum was taken as zero so that material was hydrodynamic. The equation of state used was that in Chapter 5. The U_s-U_p relation was $U_s = .538 + 1.337 \, U_p$ and the Gruneisen parameter was 2.

Figure 8.10 shows the code calculation for the measured free surface velocity in iron compared to the results of shot 75-082. The agreement is again exceptional. The calculation included the 130 kilobar phase transition
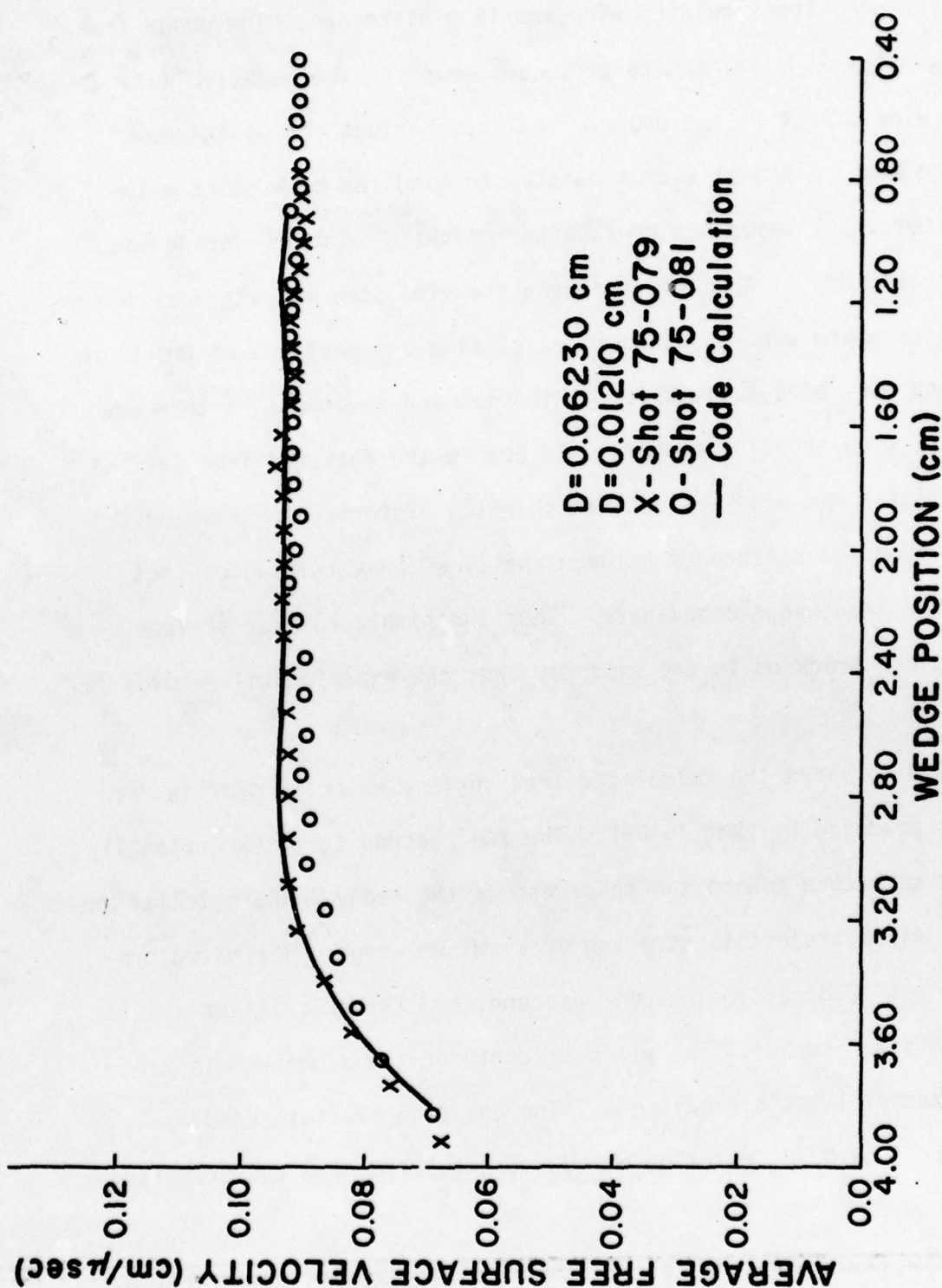
Fig. 8.9. Free surface speed versus aluminum wedge position for shots 75-079 and 75-081 compared to code calculation
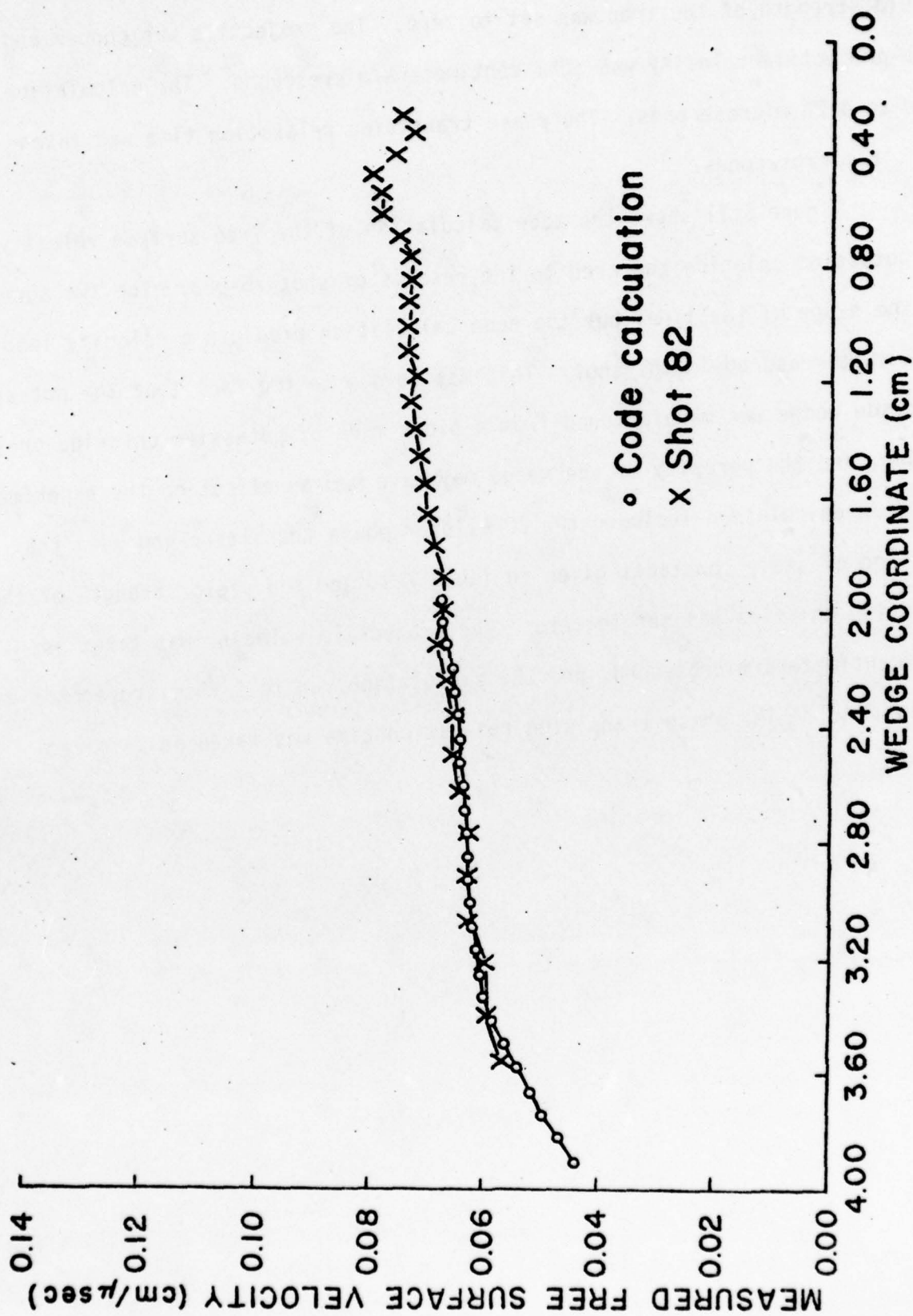
Fig. 8.10. Comparison of code calculation to shot 75-082

MEASURED FREE SURFACE VELOCITY (cm/µsec)

WEDGE COORDINATE (cm)

○ Code calculation
× Shot 82

in iron using the equation of state constants given in Table 7.1, and the yield strength of the iron was set to zero. The projectile was copper and the projectile velocity was .068 centimeters/microsecond. The calculation ran to 4.22 microseconds. The phase transition relaxation time was taken as .18 microseconds.

Figure 8.11 shows the code calculation of the free surface velocity in potassium chloride compared to the results of shot 75-083. The two agree in the slope of the line, but the code calculation predicts a velocity less than that measured in the shot. This may be due to the fact that the potassium chloride wedge was manufactured from a block made of potassium chloride pressed powder, and the porosity of the wedge may have had an effect on the experiment. The code calculation included the 20 kilobar phase transition and used the equation of state constants given in Table 7.1, and the yield strength of the potassium chloride was set to zero. The projectile velocity was taken as .056 centimeters/microsecond, and the calculation ran to 4.75 microseconds after impact. The phase transition relaxation time was taken as .1 microseconds.
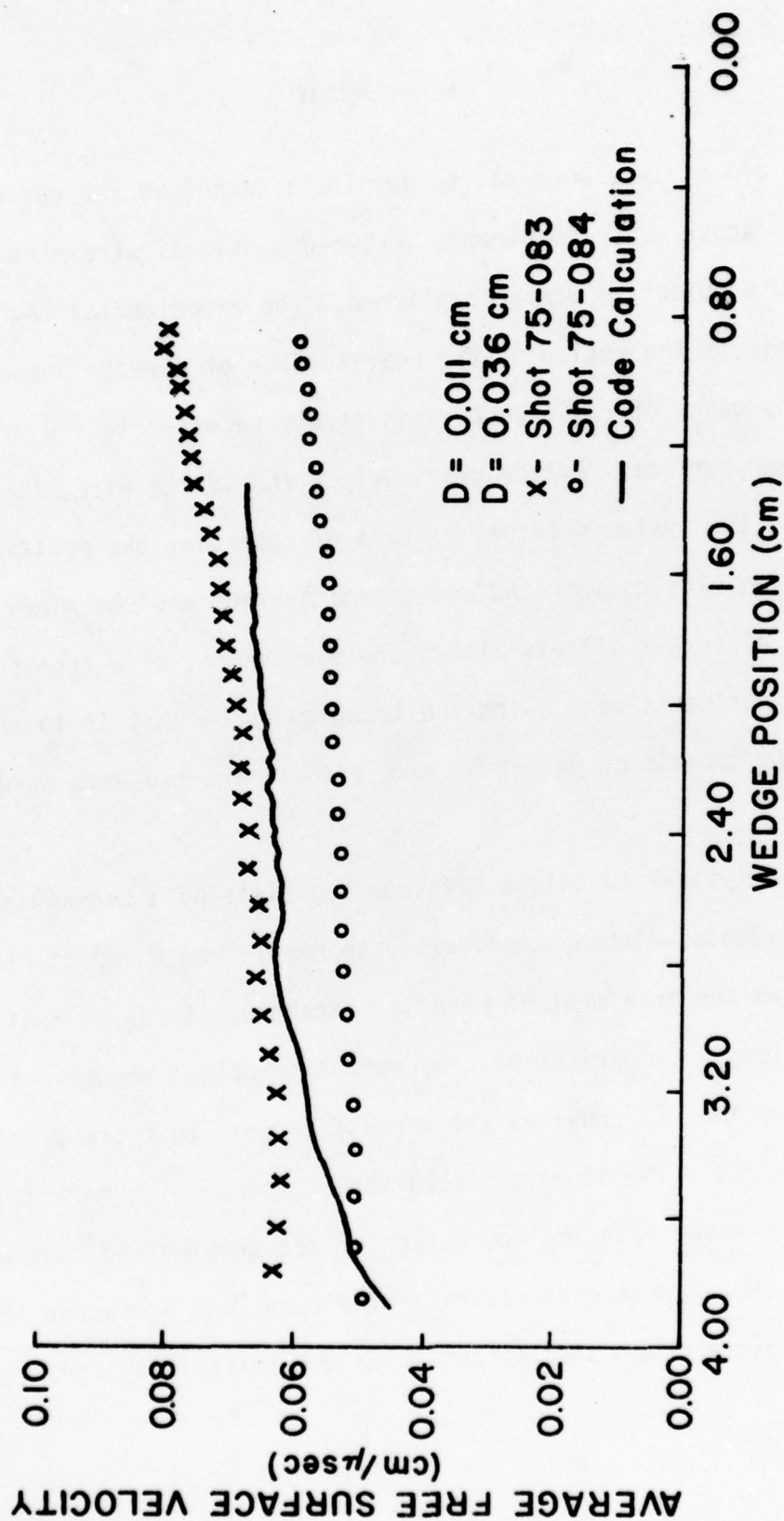
Fig. 8.11. Free surface speed versus potassium chloride wedge position for shots 75-083 and 75-084 compared to code calculation

9. SUMMARY

The aim of this work was to develop a technique for performing and
interpreting shock wave experiments in two-dimensional strain using a light
gas gun. This objective was accomplished. The experimental technique
developed detects the motion of the rear surface of a wedge impacted by a
projectile by means of resistance wires strung parallel to and offset from
the wedge rear surface. As the rear surface shorts the wire, the changing
resistance of the system provides a means of recording the position history
of the contact point between the wedge free surface and the wire. Using
two wires at different offsets allows the measurement of a free surface
velocity. Experiments done using the technique show that it is reproducible
and that it is capable of detecting rate effects and two-wave structure in
the wire.

The analytical technique developed consists of a Lagrangian finite-
difference wavecode written specifically to handle wedge impact problems.
The code allows the treatment of material strength, stress relaxation, and
phase transitions. Comparison of code runs to problems amenable to analytic
solutions shows that it provides the correct answers to those problems. The
code gives the full time dependent solution of the problem including all
interactions of waves with the boundaries of the problem and thus allows
simulation of the experimental records. The excellent agreement between the
experiments and the code calculations shows the reliability and utility of
both.

197

The initial motivation for doing experiments in two-dimensional strain using a gas gun was the study of phase transitions. It was felt that the two-dimensional experiment with its capability for making measurements over a continuous range of propagation distances in a single experiment would provide a quick survey technique for locating phase transitions in many different materials. Such a technique would obviously provide a tremendous labor-saving over the experimental program required to accomplish the same objective using one-dimensional experiments.

It is felt that the measurement technique and analytical method developed can be useful in a program of experiments designed to locate phase transitions. The experimental method is not the final solution to the problems of accuracy and resolution. However, it has been shown to be capable of detecting effects related to phase transitions. A quick survey technique for locating phase transitions must be relatively fast and easy and does not require tremendous resolution. Thus the measurement technique developed can be useful in such a program and is a first step toward more sophisticated two-dimensional instrumentation.

The finite-difference wavecode developed is a useful means of analyzing and interpreting the experiments. It has the disadvantages that details of the wave structure which are smaller than the mesh spacing are lost, and several runs using different relaxation times must be made in order to estimate the relaxation rates of the transitions. Complete analytic solutions would be preferable, but the finite-difference method is far better than the analytic solutions which can be found for these types of problems.

Although the techniques developed in this work will show immediate applicability in the study of phase transitions, the capability for performing

and analyzing two-dimensional strain experiments using a light gas gun should prove useful in other areas. The two-dimensional geometry may provide more and different kinds of information than one-dimensional geometries and therefore is worthy of further study and development.

APPENDIX A

ANALYTIC SOLUTION OF THE PROBLEM OF INTERSECTING FLOWS

The eight equations in the eight variables shown in Fig. 2.9 are

1. $q_0 \cos \theta = q_1 \cos(\theta - \delta)$ (A.1)

2. $P_1 = \rho_0 q_0 \sin \theta [q_0 \sin \theta - q_1 \sin(\theta - \delta)]$ (A.2)

3. $q_0 \sin \theta = A + B[q_0 \sin \theta - q_1 \sin(\theta - \delta)]$ (A.3)

4. $q_0' \cos \theta' = q_1' \cos(\theta' - \delta')$ (A.4)

5. $P_1' = \rho_0' q_0' \sin \theta' [q_0' \sin \theta' - q_1' \sin(\theta' - \delta')]$ (A.5)

6. $q_0' \sin \theta' = A' + B'[q_0' \sin \theta' - q_1' \sin(\theta' - \delta')]$ (A.6)

7. $\delta + \delta' = \alpha$ (A.7)

8. $P_1 = P_1'$ (A.8)

From Eqs. (A.3) and (A.6)

$$q_0 \sin \theta - q_1 \sin(\theta - \delta) = \frac{q_0 \sin \theta - A}{B} \tag{A.9}$$

$$q_0' \sin \theta' - q_1' \sin(\theta' - \delta') = \frac{q_0' \sin \theta' - A'}{B'} \tag{A.10}$$

Using Eqs. (A.9) and (A.10) in Eqs. (A.2) and (A.6) and equating P_1 and P_1' yields the following function definition.

$$F(\theta,\theta') = \rho_o q_o \sin \theta \left(\frac{q_o \sin \theta - A}{B}\right)$$

$$- \rho_o' q_o' \sin \theta' \left(\frac{q_o' \sin \theta' - A'}{B'}\right) \qquad (A.11)$$

$$= 0$$

Solving Eqs. (A.3) and (A.6) for δ and δ', replacing q_1 and q_1' using Eqs. (A.1) and (A.4), and inserting the result in Eq. (A.7) yields a second function definition

$$G(\theta, \theta') = \theta - \arctan\left[\frac{\tan \theta}{B} \left(B + \frac{A}{q_o \sin \theta} - 1\right)\right]$$

$$- \alpha + \theta' - \arctan\left[\frac{\tan \theta'}{B'} \left(B' + \frac{A'}{q_o' \sin \theta'} - 1\right)\right] \quad (A.12)$$

$$= 0$$

Thus Eqs. (A.1) through (A.8) have been reduced to $F(\theta, \theta')=0$ and $G(\theta, \theta')=0$. The following program solves these two equations by Newton-Raphson iteration[46] and yields the values of θ, δ, q_1, P_1, θ', δ', q_1', P_1' in Fig. 2.9.

APPENDIX B

PROGRAM LISTING

This appendix gives a listing of the two-dimensional wavecode des-
cribed in Chapters 5, 6, and 7. The entire program is written as a subroutine
to a calling routine which does nothing more than create storage for the
variably dimensioned arrays in the rest of the program. This allows the
storage allocation to be the minimum amount required for each run, but does
not require the entire program to be recompiled each time the number of
meshes is changed.

The subroutine called by the main program is WDGPT. This subroutine
initializes the values of the arrays and writes all required information on
tape. It also calls subroutine RITE which prints all arrays at a cycle
increment specified by the user. Subroutine WDGPT also calls subroutine
READIN which reads in the equation of state constants required for whatever
form of equation of state is to be used. Calculation of the variables
specified in Table 5.2 is done in subroutine CALC. Values of α_i, β_i, C_{p_i},
V_i, E_i, X, and $\dot{X}$ are passed to CALC from subroutine EQSTAT. This contains
the only equation of state dependent calculations done in the program.
Communication between READIN and EQSTAT is by means of common blocks, so
that the main part of the program does not have to be modified to change the
equation of state. Subroutine RELF calculates the constant C in Eq. (6.21)
and this subroutine also communicates with READIN by means of common blocks
so that the form of the stress relaxation is independent of the main program.
SPEED is an alternate entry to EQSTATE which provides α_i, C_{p_i}, β_i, and V_i

202

for use in the sound speed calculation of Eq. (7.72). GNUF is an alternate entry to RELF which calculates the value of Poisson's ratio.

```
  1.            IMPLICIT REAL*8 (A-H,C-Z)
  2.            DIMENSION X(113,24),Y(113,24),XD(113,24),YD(113,24),
  3.           1SX(113,24),SY(113,24),SXY(113,24),TM(113,24),V(113,24),
  4.           2T(113,24),P(113,24),C(113,24),PX(24),PY(24),OY(24),
  5.           3OX(24),XMF(113,24),G(113,24)
  6.            CALL WDGPT(X,Y,XD,YD,SX,SY,SXY,TM,V,T,P,Q,PX,PY,
  7.           1OX,OY,XMF,G,113,24)
  8.            STOP
  9.            END
 10.            SUBROUTINE WDGPT(X,Y,XD,YD,SX,SY,SXY,TM,V,T,P,Q,PX,PY,OX,OY,
 11.           1XMF,G,NJ,MK)
 12.            IMPLICIT REAL*8 (A-H,C-Z)
 13.            DIMENSION X(NJ,MK),Y(NJ,MK),XD(NJ,MK),YD(NJ,MK),KL(5),
 14.           1SX(NJ,MK),SY(NJ,MK),SXY(NJ,MK),TM(NJ,MK),V(NJ,MK),RO(5),
 15.           2T(NJ,MK),P(NJ,MK),C(NJ,MK),PX(MK),PY(MK),OY(MK),CO(5),
 16.           3OX(MK),FMT3(8),G(NJ,MK),T13(5),T15(5),
 17.           4OX(4),OY(4),TI1(5),TI2(5),TI3(5),TI4(5),TI5(5),TI6(5),XMF(NJ,MK),
 18.           5TI7(5),TI8(5),TI9(5),T10(5),T11(5),T12(5),FMT1(8),FMT2(8),S(5)
 19.            COMMON FMT1,FMT2,NCOL
 20.            COMMON /MONST/ AL,B1,B2,DT,EX,EY,HL,HR,PJ,OO,TL,VD,VO,VP,XEQ,TRMU,
 21.           1EXY,SYO,SXO,TIV,VNP,WXY,RHON,RHGO,SXYO,CB2,DTANAL,OPN,OPM,B12,
 22.           2PTEST,DTM,MAGNO,MAGNL,JF,KF,KS,KSP,MIMP,NM1,MM1
 23.            COMMON /PROBV/ TEMPO,TC,TAM,J,K,M,N,NTRL
 24.            COMMON /MPSMAL/RO,CO,S,KL,NR
 25.            COMMON /TINY/ TN,MC
 26.         10 FORMAT(2I3,5D11.4,2I3)
 27.         15 FORMAT(3I3,2D11.4)
 28.         20 FORMAT(1X,'A NUMERICAL SOLUTION OF THE FLOW ECUATIONS',
 29.           1' IN TWO DIMENSIONS FOR THE'/' PROBLEM CF A WEDGE',F7.3,
 30.           2' CENTIMETERS LONG WITH A LEFT HEIGHT OF',F6.3,/
 31.           3' CENTIMETERS AND RIGHT HEIGHT',F6.3,' CENTIMETERS',
 32.           4' IMPACTED BY A PROJECTILE')
 33.         21 FORMAT(' WITH A VELOCITY CF',F6.3,' CM/MICROSEC.',
 34.           1' THE MESH SIZE IS',I4,' BY',I3,'. THE'/' TIME LIMIT IS',
 35.           2F6.2,' MICROSECONDS, AND THE CYCLE LIMIT IS',I4,' CYCLES.')
 36.         25 FORMAT(' THE FIRST TIME STEP IS',F6.3,' MICROSECONDS.',
 37.           1' THE ARTIFICIAL VISCCSITY'/' COEFFICIENTS ARE',F6.3,
 38.           2' AND',F6.3,'. PRINTCUT IS EVERY',I4,' CYCLES. TEST'/
 39.           3' PRESSURE FCR ADVANCING CALC IS',D9.2,' M6. IMPACT IS AT K=',I3,
 40.           4'. FLYER'/' THICKNESS IS',F6.3,' CM. INITIAL TEMPERATURE',
 41.           1' IS',F5.0,' DEGREES')
 42.         35 FORMAT(8A8)
 43.         36 FORMAT(3A8,4A4)
 44.         70 FORMAT(/' THIS PROGRAM IS A RESTART. THE LAST',
 45.           1' CYCLE WAS',I4,'. THE STARTING TIME IS',F6.3,
 46.           2' MICROSECONDS'/)
 47.            DATA TI1/'      ',' X P','CSIT','ION ','    '/
 48.            DATA TI2/'      ',' Y P','OSIT','ION ','    '/
 49.            DATA TI3/'      ','CELL',' VOL','UME ','    '/
 50.            DATA TI4/'      ',' X V','ELOC','ITY ','    '/
 51.            DATA TI5/'      ',' Y V','ELOC','ITY ','    '/
 52.            DATA TI6/'      ','CELL',' MAS','S   ','    '/
 53.            DATA TI7/' X S','TRES','S DE','VIAT','OR  '/
 54.            DATA TI8/' Y S','TRES','S DE','VIAT','OR  '/
 55.            DATA TI9/' XY ','STRE','SS C','EVIA','TOR '/
 56.            DATA T10/'      ','TEMF','ERAT','URE ','    '/
 57.            DATA T11/'      ',' PR','ESSU','RE  ','    '/
 58.            DATA T12/'      ',' VI','SCOS','ITY ','    '/
 59.            DATA T13/'   M','ASS ','FRAC','TION','    '/
```

```
60.              DATA T15/'   P','LAST','IC S','TRAI','N    '/
61.              READ(5,10)N,M,TL,VP,TMAX,FTS,TEMPO
62.              READ(5,10)NCM,NCP,HL,HR,PTEST,FT
63.              READ(5,15)IRSTRT,NCCL,MIMF,B1,B2
64.              READ(5,35)(FMT1(I),I=1,8)
65.              READ(5,35)(FMT2(I),I=1,8)
66.              READ(5,35)(FMT3(I),I=1,8)
67.              WRITE(6,20)TL,HL,HR
68.              WRITE(6,21)VP,N,M,TMAX,NCM
69.              WRITE(6,25)FTS,B1,B2,NCP,PTEST,MIMP,FT,TEMPO
70.              CALL READIN
71.              B12=B1**2
72.              DPN=N
73.              DPM=M
74.              NM1=N-1
75.              MM1=M-1
76.              DTANAL=(HL-HR)/TL
77.              AL=DATAN(DTANAL)
78.              MARK=1
79.              IF(DTANAL .GT. 1.D-5)GC TC 1100
80.              MARK=0
81.              DTANAL=VP*FTS*(DPN-3.C0)/(3.C0*TL*DPN)
82.        1100  IF(IRSTRT .EQ. 1) GG TC 1600
83.              DO 1110 I=1,NR
84.              IF(KL(I) .GT. MIMP) GC TO 1120
85.        1110  CONTINUE
86.        1120  NRP=I
87.              DO 1130 I=1,NR
88.              IF(KL(I) .GT. MIMP+1) GO TO 1135
89.        1130  CONTINUE
90.        1135  NRT=I
91.              A=RO(NRT)*S(NRT)-RC(NRP)*S(NRP)
92.              B=RO(NRT)*CO(NRT)+RC(NRP)*(CC(NRP)+2.DO*S(NRP)*VP)
93.              C=VP*RC(NRP)*(CC(NRP)+VP*S(NRP))
94.              IF(A .EQ. 0.CO)GO TO 1140
95.              TIV=(-B+DSQRT(B**2-4.CO*A*C))/2.DO*A
96.              GO TO 1150
97.        1140  TIV=C/B
98.        1150  DO 1500 J=1,N
99.              NTRL=1
100.             DPJ=J
101.             DO 1200 K=1,M
102.             DPK=K
103.             X(J,K)=FX(DPN,DPM,DPJ,DPK,TL,AL,HL,HR,TIV,VP,J,K,N,M,MIMP,FT,MARK)
104.             Y(J,K)=FY(DPN,DPM,DPJ,DPK,TL,AL,HL,HR,TIV,VP,J,K,N,M,MIMP,FT,MARK)
105.             XD(J,K)=FXD(DPN,DPM,DPJ,DPK,TL,AL,HL,HR,TIV,VP,J,K,N,
106.            1M,MIMP,FT,MARK)
107.             YD(J,K)=FYD(DPN,DPM,DPJ,DPK,TL,AL,HL,HR,TIV,VP,J,K,N,
108.            1M,MIMP,FT,MARK)
109.        1200 CONTINUE
110.             V(J,1)=0.DO
111.             DO 1400 K=1,M
112.             IF(K-1 .EQ. KL(NTRL))NTRL=NTRL+1
113.             T(J,K)=TEMPO
114.             XMF(J,K)=0.DO
115.             G(J,K)=0.DO
116.             SX(J,K)=0.DO
117.             SY(J,K)=0.DO
118.             SXY(J,K)=0.DO
119.             P(J,K)=0.DO
```

```
120.            Q(J,K)=0.D0
121.            IF(J .EQ. 1 .OR. K .EQ. 1) GO TO 1360
122.            V(J,K)=(((X(J-1,K)-X(J,K-1))*(Y(J,K)-Y(J-1,K-1))+(X(J,K)
123.           1-X(J-1,K-1))*(Y(J,K-1)-Y(J-1,K)))/2.D0
124.            IF(J .EQ. 2 .OR. K .EQ. 2 .CR. J .EQ. N .OR.
125.           1K .EQ. M .OR. K .EQ. MIMP) GO TO 1350
126.      1300 TM(J,K)=V(J,K)*RC(NTRL)
127.            GO TO 1400
128.      1350 IF(K .EQ. MIMP .AND. J .NE. 2 .AND. J .NE. N
129.           1.AND. MARK .EQ. 0) GO TO 1300
130.      1360 TM(J,K)=0.D0
131.      1400 CONTINUE
132.      1500 CONTINUE
133.            MC=0
134.            KS=MAX0(2,MIMP-3)
135.            KF=MIN0(M-1,MIMP+3)
136.            JF=MIN0(N-1,5)
137.            IF(MARK .EQ. 0)JF=N-1
138.            T0=0.D0
139.            TNM=0.D0
140.            TN=FTS
141.            MAGNU=2
142.            IF(MARK .EQ. 0)MAGNU=N+1
143.            GO TO 2000
144.      1600 READ(10,FMT3)((X(J,K),J=1,N),K=1,M)
145.            READ(10,FMT3)((Y(J,K),J=1,N),K=1,M)
146.            READ(10,FMT3)((XD(J,K),J=1,N),K=1,M)
147.            READ(10,FMT3)((YD(J,K),J=1,N),K=1,M)
148.            READ(10,FMT3)((SX(J,K),J=1,N),K=1,M)
149.            READ(10,FMT3)((SY(J,K),J=1,N),K=1,M)
150.            READ(10,FMT3)((SXY(J,K),J=1,N),K=1,M)
151.            READ(10,FMT3)((TM(J,K),J=1,N),K=1,M)
152.            READ(10,FMT3)((V(J,K),J=1,N),K=1,M)
153.            READ(10,FMT3)((T(J,K),J=1,N),K=1,M)
154.            READ(10,FMT3)((P(J,K),J=1,N),K=1,M)
155.            READ(10,FMT3)((Q(J,K),J=1,N),K=1,M)
156.            READ(10,FMT3)((XMF(J,K),J=1,N),K=1,M)
157.            READ(10,FMT3)((G(J,K),J=1,N),K=1,M)
158.            READ(10,FMT3)(PX(K),PY(K),K=1,M)
159.            READ(10,36)TN,TC,TNM,MC,KS,KF,JF
160.            WRITE(6,70)MC,TN
161.            REWIND 10
162.            MAGNU=MIN0(IDINT(VP*TC*(DPN-3.D0)/(TL*DTANAL))+3,N-1)
163.      2000 CALL CALC(X,Y,XD,YD,SX,SY,SXY,TM,V,T,P,Q,PX,PY,OX,OY,
164.           1XMF,G,NJ,MK)
165.            WRITE(12,FMT3)(X(J,MM1),J=1,N)
166.            WRITE(12,FMT3)(Y(J,MM1),J=1,N)
167.            WRITE(12,FMT3)(XD(J,MM1),J=1,N)
168.            WRITE(12,FMT3)(YD(J,MM1),J=1,N)
169.            WRITE(12,36)TN
170.            IF(MOD(MC,NCP) .NE. 0 .AND. MC .GT. 10) GO TO 2870
171.            CALL RITE(X,TI1,2,JF,KS,KF,N,M)
172.            CALL RITE(Y,TI2,2,JF,KS,KF,N,M)
173.            CALL RITE(XD,TI4,2,JF,KS,KF,N,M)
174.            CALL RITE(YD,TI5,2,JF,KS,KF,N,M)
175.            CALL RITE(V,TI3,3,JF,KSP,KF,N,M)
176.            CALL RITE(TM,TI6,3,JF,KSP,KF,N,M)
177.            CALL RITE(SX,TI7,3,JF,KSP,KF,N,M)
178.            CALL RITE(SY,TI8,3,JF,KSP,KF,N,M)
179.            CALL RITE(SXY,TI9,3,JF,KSP,KF,N,M)
```

```
180.             CALL RITE(T,T10,3,JF,KSP,KF,N,M)
181.             CALL RITE(P,T11,3,JF,KSP,KF,N,M)
182.             CALL RITE(O,T12,3,JF,KSP,KF,N,M)
183.             CALL RITE(XMF,T13,3,JF,KSP,KF,N,M)
184.             CALL RITE(G,T15,3,JF,KSP,KF,N,M)
185.      2870 IF(TN .GT. TMAX .OR. MC .GE. NCM) GO TO 2900
186.             TNM=TO
187.             TO=TN
188.             TN=TN+DMIN1(DTM,1.1D0*(TC-TAM))
189.             GO TO 2000
190.      2900 REWIND 12
191.             IF(MCD(MC,NCP) .EQ. 0) GO TC 3000
192.             CALL RITE(X,TI1,2,JF,KS,KF,N,M)
193.             CALL RITE(Y,TI2,2,JF,KS,KF,N,M)
194.             CALL RITE(XD,TI4,2,JF,KS,KF,N,M)
195.             CALL RITE(YD,TI5,2,JF,KS,KF,N,M)
196.             CALL RITE(V,TI3,3,JF,KSP,KF,N,M)
197.             CALL RITE(TM,TI6,3,JF,KSP,KF,N,M)
198.             CALL RITE(SX,TI7,3,JF,KSP,KF,N,M)
199.             CALL RITE(SY,TI8,3,JF,KSP,KF,N,M)
200.             CALL RITE(SXY,TI9,3,JF,KSP,KF,N,M)
201.             CALL RITE(T,T10,3,JF,KSP,KF,N,M)
202.             CALL RITE(P,T11,3,JF,KSP,KF,N,M)
203.             CALL RITE(O,T12,3,JF,KSP,KF,N,M)
204.             CALL RITE(XMF,T13,3,JF,KSP,KF,N,M)
205.             CALL RITE(G,T15,3,JF,KSP,KF,N,M)
206.      3000 WRITE(11,FMT3)((X(J,K),J=1,N),K=1,M)
207.             WRITE(11,FMT3)((Y(J,K),J=1,N),K=1,M)
208.             WRITE(11,FMT3)((XD(J,K),J=1,NJ,K=1,M)
209.             WRITE(11,FMT3)((YD(J,K),J=1,N),K=1,M)
210.             WRITE(11,FMT3)((SX(J,K),J=1,N),K=1,M)
211.             WRITE(11,FMT3)((SY(J,K),J=1,N),K=1,M)
212.             WRITE(11,FMT3)((SXY(J,K),J=1,N),K=1,M)
213.             WRITE(11,FMT3)((TM(J,K),J=1,N),K=1,M)
214.             WRITE(11,FMT3)((V(J,K),J=1,N),K=1,M)
215.             WRITE(11,FMT3)((T(J,K),J=1,N),K=1,M)
216.             WRITE(11,FMT3)((P(J,K),J=1,N),K=1,M)
217.             WRITE(11,FMT3)((C(J,K),J=1,N),K=1,M)
218.             WRITE(11,FMT3)((XMF(J,K),J=1,N),K=1,M)
219.             WRITE(11,FMT3)((G(J,K),J=1,N),K=1,M)
220.             WRITE(11,FMT3)(PX(K),PY(K),K=1,M)
221.             WRITE(11,36)TN,TC,TNM,MC,KS,KF,JF
222.             REWIND 11
223.             RETURN
224.             END
225.             SUBROUTINE RITE(Q,A,JS,JF,KS,KF,N,M)
226.             IMPLICIT REAL*8 (A-H,C-Z)
227.             DIMENSIONQ(N,M),A(5),KK(15),FMT1(8),FMT2(8)
228.             COMMON FMT1,FMT2,NCCL
229.             COMMON /TINY/ TN,MC
230.        10 FORMAT(/1X,'TIME=',F6.3,' MICRCSEC.',3X,5A4,' CYCLE=',I3)
231.             NI=((KF-KS+1)/NCCL)+1
232.             NUM=MOD(KF-KS+1,NCCL)
233.             WRITE(6,'0)TN,A,MC
234.             DO 2000 .=1,NI
235.             LIM=NCCL
236.             IF(I .EQ. NI)LIM=NUM
237.             IF(LIM .EQ. 0) GO TC 2000
238.             DO 1000 L=1,LIM
239.             KK(L)=L+(I-1)*NCCL+KS-1
```

207

```
240.       1000 CONTINUE
241.            WRITE(6,FMT1)(KK(L),L=1,LIM)
242.            DO 1500 J=JS,JF
243.            WRITE(6,FMT2)J,(Q(J,L+(I-1)*NCOL+KS-1),L=1,LIM)
244.       1500 CONTINUE
245.       2000 CONTINUE
246.            RETURN
247.            END
248.            SUBROUTINE CALC(X,Y,XD,YD,SX,SY,SXY,TM,V,T,P,G,PX,PY,QX,QY,
249.           1XMF,G,NJ,MK)
250.            IMPLICIT REAL*8 (A-H,C-Z)
251.            DIMENSION X(NJ,MK),Y(NJ,MK),XD(NJ,MK),YD(NJ,MK),KL(5),
252.           1SX(NJ,MK),SY(NJ,MK),SXY(NJ,MK),TM(NJ,MK),V(NJ,MK),PO(5),
253.           2T(NJ,MK),P(NJ,MK),G(NJ,MK),PX(MK),PY(MK),QY(MK),CO(5),
254.           3QX(MK),FMT3(8),G(NJ,MK),TI3(5),TI5(5),
255.           4QX(4),QY(4),TI1(5),TI2(5),TI3(5),TI4(5),TI5(5),TI6(5),XMF(NJ,MK),
256.           5TI7(5),TI8(5),TI9(5),TI0(5),TI1(5),TI2(5),FMT1(8),FMT2(8),S(5)
257.            COMMON FMT1,FMT2,NCOL
258.            COMMON /MONST/ AL,B1,B2,DT,EX,EY,HL,HR,PJ,QQ,TL,VD,VO,VP,XEQ,TRMU,
259.           1EXY,SYO,SXO,TIV,VNP,WXY,RHOA,RHOG,SXYO,CBZ,DTANAL,DPN,DPM,B12,
260.           2PTEST,DTM,MAGNO,MAGNU,JF,KF,KS,KSP,MIMP,NM1,MM1
261.            COMMON /PROBV/ TEMPO,TC,TNM,J,K,M,N,NTRL
262.            COMMON /MPSMAL/RC,CC,S,KL,NR
263.            COMMON /TINY/ TN,MC
264.         50 FORMAT(/' CYCLE',I4,5X,'TIME',D16.9,5X,'DELTA T',D16.9,
265.           15X,'TIME CONTROLLING MESH',2I4,/' MINIMUM MESH POINT ',
266.           2'SEPARATION',D16.9,' AT MESH',2I4,' BETWEEN POINTS',
267.           3I2,' AND',I2/' CONTACT PT',I4,'  JF',I4),
268.         60 FORMAT(/2I3,5(4X,D16.9))
269.       2000 DTM=100000.D0
270.            TSD=DTM
271.            KSP=KS+1
272.            KFLL=0
273.            KFLU=0
274.            JFL=0
275.            MC=MC+1
276.            DT=TN-TO
277.            MAGNO=MAGNU
278.            MAGNU=MINO(IDINT(VF*TN*(DPN-3.D0)/(TL*DTANAL))+3,N-1)
279.            JF=MINO(N-1,MAXO(JF,MAGNU+2))
280.            DO 2800 J=2,NM1
281.            NTRL=1
282.            DPJ=J
283.            DO 2150 K=1,M
284.            IF(J .EQ. 2) GO TO 2050
285.            QY(K)=PY(K)
286.            QX(K)=PX(K)
287.            GO TO 2100
288.       2050 QY(K)=Y(1,K)
289.            QX(K)=X(1,K)
290.       2100 PX(K)=X(J,K)
291.            PY(K)=Y(J,K)
292.       2150 CONTINUE
293.            DO 2700 K=2,KF
294.            IF(K-1 .EQ. KL(NTRL))NTRL=NTRL+1
295.            IF(K .GT. MIMP-1 .AND. J .GT. JF) GO TO 2800
296.            CC=(SY(J+1,K+1)-P(J+1,K+1)-G(J+1,K+1))*(X(J+1,K)-X(J,K+1))
297.            RA=TM(J+1,K)+TM(J,K)+TM(J,K+1)+TM(J+1,K+1)
298.            YD(J,K)=YD(J,K)+(TN-TNM)*(SXY(J+1,K)*(PY(K-1)-
299.           1Y(J+1,K))+SXY(J,K)*(QY(K)-PY(K-1))+SXY(J,K+1)*(Y(J,
```

```
300.          2K+1)-OY(K))+SXY(J+1,K+1)*(Y(J+1,K)-Y(J,K+1))-
301.          3(SY(J+1,K)-P(J+1,K)-C(J+1,K))*(PX(K-1)-X(J+1,K))-
302.          4(SY(J,K)-P(J,K)-Q(J,K))*(CX(K)-PX(K-1))-(SY(J,K+1)-
303.          5P(J,K+1)-C(J,K+1))*(X(J,K+1)-OX(K))-CC)/RA
304.          Y(J,K)=Y(J,K)+YD(J,K)*CT
305.          IF(K .LT. KS) GC TC 2700
306.          IF(J .GT. JF) GO TO 2700
307.          CC=SXY(J+1,K+1)*(X(J+1,K)-X(J,K+1))
308.          XD(J,K)=XD(J,K)+(TN-TNP)*((SX(J+1,K)-P(J+1,K)-Q(J+1,
309.          1K))*(PY(K-1)-Y(J+1,K))+(SX(J,K)-P(J,K)-Q(J,K))*(OY(K)
310.          2-PY(K-1))+(SX(J,K+1)-P(J,K+1)-C(J,K+1))*(Y(J,K+1)-
311.          30Y(K))+(SX(J+1,K+1)-P(J+1,K+1)-Q(J+1,K+1))*(Y(J+1,K)
312.          4-Y(J,K+1))-SXY(J+1,K)*(PX(K-1)-X(J+1,K))-SXY(J,K)*
313.          5(OX(K)-PX(K-1))-SXY(J,K+1)*(X(J,K+1)-OX(K))-CC)/RA
314.          IF(DABS(XD(J,K)) .LT. 1.0-20)XD(J,K)=0.D0
315.          X(J,K)=X(J,K)+XD(J,K)*CT
316.     2155 IF(J .EQ. 2 .OR. K .LE. KS)GO TO 2700
317.          VO=V(J,K)
318.          V(J,K)=((X(J-1,K)-X(J,K-1))*(Y(J,K)-Y(J-1,K-1))+(X(J,K)
319.          1-X(J-1,K-1))*(Y(J,K-1)-Y(J-1,K)))/2.D0
320.          IF(K .NE. MIMP) GO TC 2165
321.          IF(J .GT. MAGNU) GO TO 2700
322.          IF(J .GT. MAGNO) GO TC 2160
323.          GO TO 2165
324.     2160 TM(J,K)=V(J,K)*RO(NTRL)
325.          RHCO=PC(NTRL)
326.          GO TO 2170
327.     2165 RHCO=TM(J,K)/VO
328.     2170 RHON=TM(J,K)/V(J,K)
329.          VNP=(VC+V(J,K))/2.D0
330.          VNP4=4.D0*VNP
331.          EX=((XC(J-1,K)-XD(J,K-1))*(Y(J,K)+PY(K)-Y(J-1,K-1)-
332.          1OY(K-1))+(XC(J,K)-XC(J-1,K-1))*(Y(J,K-1)+PY(K-1)-
333.          2Y(J-1,K)-OY(K)))/VNP4
334.          IF(DABS(EX) .LT. 1.0-20)EX=C.D0
335.          EY=-((YD(J-1,K)-YD(J,K-1))*(X(J,K)+PX(K)-X(J-1,K-1)-
336.          1OX(K-1))+(YC(J,K)-YO(J-1,K-1))*(X(J,K-1)+PX(K-1)-X(J-1,
337.          2K)-OX(K)))/VNP4
338.          IF(DABS(EY) .LT. 1.0-20)EY=0.D0
339.          A=-((XC(J-1,K)-XO(J,K-1))*(X(J,K)+PX(K)-X(J-1,K-1)-
340.          1OX(K-1))+(XC(J,K)-XC(J-1,K-1))*(X(J,K-1)+PX(K-1)-X(J-1,
341.          2K)-OX(K)))/VNP4
342.          IF(DABS(A) .LT. 1.D-20)A=0.C0
343.          B=((YD(J-1,K)-YD(J,K-1))*(Y(J,K)+PY(K)-Y(J-1,K-1)-
344.          1OY(K-1))+(YC(J,K)-YC(J-1,K-1))*(Y(J,K-1)+PY(K-1)-Y(J-1,
345.          2K)-OY(K)))/VNP4
346.          IF(DABS(B) .LT. 1.D-20)B=0.C0
347.          EXY=(A+B)/2.D0
348.          WXY=A-B
349.          VD=EX+EY
350.          SXO=SX(J,K)
351.          SXYO=SXY(J,K)
352.          SYO=SY(J,K)
353.          XM=XMF(J,K)
354.          CALL SPEED(XM,V1,V2,BT1,BT2,AL1,AL2,CP1,CP2,P(J,K),T(J,K))
355.          RHCN=RC(NTRL)
356.          BETA=RHON*((1.D0-XM)*BT1*V1+XM*BT2*V2)
357.          ALPHA=RHON*((1.D0-XM)*AL1*V1+XM*AL2*V2)
358.          CP=(1.D0-XM)*CP1+XM*CF2
359.          CB2=1.C0/(BETA*RHCN-(T(J,K)/CP)*ALPHA**2)
```

```
360.                GNU=GNUF(X,Y,XO,YO,SX,SY,SXY,TM,V,T,
361.               1P,Q,PX,PY,CX,OY,XMF,G,AJ,MK)
362.                TRMU=3.DO*(1.DO-2.CO*GAU)*(FHOC+RHON)
363.               1*CB2/(2.CO*(1.DO+GNU))
364.                SXY(J,K)=(SXYO*(1.DO-(CT*WXY/2.DO)**2)+DT*(TRMU*EXY+
365.               1WXY*(2.DO*(SYO-SXC)+TRMU*CT*(EY-EX))/4.DO))/(1.DO+
366.               2(DT*WXY/2.DO)**2)
367.                IF(DABS(SXY(J,K)) .LT. 1.D-20)SXY(J,K)=0.DO
368.                SX(J,K)=SXO+DT*((SXY(J,K)+SXYO)*WXY/2.DO+TRMU*(EX-VD/3.DO))
369.                IF(DABS(SX(J,K)) .LT. 1.D-20)SX(J,K)=0.DO
370.                SY(J,K)=SYO+DT*(-(SXY(J,K)+SXYC)*WXY/2.DO+TRMU*(EY-VD/3.DO))
371.                IF(DABS(SY(J,K)) .LT. 1.D-20)SY(J,K)=0.DO
372.                PJ=SX(J,K)**2+SY(J,K)**2+SXY(J,K)**2+SX(J,K)*SY(J,K)
373.                C=RELF(X,Y,XO,YO,SX,SY,SXY,TM,V,T,
374.               1P,Q,PX,PY,CX,OY,XMF,G,AJ,MK)
375.                SX(J,K)=SX(J,K)*C
376.                SY(J,K)=SY(J,K)*C
377.                SXY(J,K)=SXY(J,K)*C
378.         2175   QO=Q(J,K)
379.                IF(V(J,K) .LT. 0.DO .OR. CB2 .LT. 0.DO) GO TO 2850
380.                Q(J,K)=-VD*(TM(J,K)+B12*DABS(VD)+RHON*B2*DSQRT(3.DO*
381.               1(1.DO-GNU)*CB2*V(J,K)/(1.DO+GNU)))
382.                IF(DABS(Q(J,K)) .LT. 1.D-20)Q(J,K)=0.DO
383.                IF(VD .GT. 0.DO)Q(J,K)=0.DO
384.                SPVNP=VNP/TM(J,K)
385.                SPV=1.DO/RHON
386.                TOLD=T(J,K)
387.                POLD=P(J,K)
388.                XMO=XMF(J,K)
389.                DO 2180 I=1,9
390.         .      PMAV=P(J,K)
391.                PNP=(P(J,K)+PGLO)/2.CO
392.                TNP=(T(J,K)+TOLD)/2.DO
393.                CALL EQSTAT(XM,XMNP,XDM,V1NP,V2NP,BT1NP,BT2NP,A1NP,A2NP,CP1,
394.               1CP2,E1,E2,TNP,PNP,SPVNP,XMO,T(J,K),SPV)
395.                A1NP=A1NP*V1NP
396.                A2NP=A2NP*V2NP
397.                BT1NP=BT1NP*V1NP
398.                BT2NP=BT2NP*V2NP
399.                A1=(1.CO-XMNP)*A1NP+XMNP*A2NP
400.                A2=-(1.DO-XMNP)*BT1NP-XMNP*BT2NP
401.                A3=(V2NP-V1NP)*XDM-VNP*VD/TM(J,K)
402.                A4=(1.DO-XMNP)*(CP1-A1NP*PNP)+XMNP*(CP2-A2NP*PNP)
403.                A5=(1.DO-XMNP)*(BT1NP*PNP-A1NP*TNP)+XMNP*(BT2NP*PNP-A2NP*TNP)
404.                A6=(E2-E1)*XDM-VNP*((SX(J,K)+SXC)*EX+(SY(J,K)+SYO)*EY+
405.               12.DO*(SXY(J,K)+SXYO)*EXY-(PNP*2.DO+Q(J,K)+QO)*VD)/(2.DO*TM(J,K))
406.                D=A1*A5-A4*A2
407.                T(J,K)=TOLD-DT*(A3*A5-A6*A2)/D
408.                P(J,K)=POLD-DT*(A1*A6-A4*A3)/D
409.                IF(P(J,K) .EC. 0.DO)GC TO 2180
410.                IF(DABS((P(J,K)-PMAV)/P(J,K)) .LT. 1.D-3) GO TO 2190
411.         2180   CONTINUE
412.         2190   XMF(J,K)=XM
413.         2195   CALL SPEED(XM,V1,V2,BT1,BT2,AL1,AL2,CP1,CP2,P(J,K),T(J,K))
414.                BETA=RHON*((1.DO-XM)*BT1*V1+XM*BT2*V2)
415.                ALPHA=RHON*((1.DO-XM)*AL1*V1+XM*AL2*V2)
416.                CP=(1.DO-XM)*CP1+XM*CP2
417.                CB2=1.DO/(BETA*RHON-(T(J,K)/CP)*ALPHA**2)
418.                CX(1)=X(J,K)
419.                DX(2)=X(J,K-1)
```

210

```
420.                DX(3)=X(J-1,K-1)
421.                DX(4)=X(J-1,K)
422.                DY(1)=Y(J,K)
423.                DY(2)=Y(J,K-1)
424.                DY(3)=Y(J-1,K-1)
425.                DY(4)=Y(J-1,K)
426.                DM=100000.00
427.                DO 2300 I=2,4
428.                DO 2200 L=I,4
429.                D=DSQRT((DX(I-1)-DX(L))**2+(DY(I-1)-DY(L))**2)
430.                IF(D .GE. DM) GO TO 2200
431.                DM=D
432.                NP1=I-1
433.                NP2=L
434.           2200 CONTINUE
435.           2300 CONTINUE
436.                IF(DM .GE. TSD) GO TO 2350
437.                TSD=DM
438.                NP1S=NP1
439.                NP2S=NP2
440.                JSD=J
441.                KSD=K
442.                GNU=GNUF(X,Y,XD,YD,SX,SY,SXY,TM,V,T,
443.           1P,Q,PX,PY,QX,QY,XMF,G,NJ,NK)
444.           2350 IF(V(J,K) .LT. 0.D0 .OR. CB2 .LT. 0.D0) GO TO 2850
445.                C=DSQRT(3.D0*(1.D0-GNU)*CB2/(1.D0+GNU))
446.                DDT=DM/(B2*C+B12*DM*DABS(VD)+DSQRT(B2*C+B12*DM*(VD
447.           1**2)+C**2))
448.                IF(DDT .GE. DTM) GO TO 2360
449.                DTM=DDT
450.                JSTS=J
451.                KSTS=K
452.           2360 IF(K .EQ. KS+2) GO TO 2400
453.                IF(K .EQ. KF-1) GO TO 2500
454.                IF(J .EQ. JF-2) GO TO 2600
455.                GO TO 2700
456.           2400 IF(P(J,K) .GT. PTEST)KFLU=1
457.                GO TO 2700
458.           2500 IF(P(J,K) .GT. PTEST)KFLL=1
459.                GO TO 2700
460.           2600 IF(P(J,K) .GT. PTEST) JFL=1
461.           2700 CONTINUE
462.           2800 CONTINUE
463.                GO TO 2860
464.           2850 MC=NCM+NCP
465.                WRITE(6,60)J,K,EX,EY,A,B,TRMU,PJ,CB2
466.           2860 WRITE(6,50)MC,TN,DTM,JSTS,KSTS,TSD,JSD,KSD,NP1S,NP2S,MAGNU,JF
467.           2870 IF(KFLU .EQ. 1)KS=MAXC(2,KS-1)
468.                IF(KFLL .EQ. 1) KF=MINC(M-1,KF+1)
469.                IF(JFL .EQ. 1) JF=MINO(N-1,JF+1)
470.                RETURN
471.                END
472.                SUBROUTINE EOSTAT(XM,XPNP,XCM,V1,V2,BT1,BT2,AL1,AL2,CP1,
473.           1CP2,E1,E2,T,P,V,XMC,TEMPN,VN)
474.                IMPLICIT REAL*8 (A-H,C-Z)
475.                DIMENSION VO(5,2),CKC(5,2),DN(5,2),GO(5,2),CV(5,2),EO(5,2),
476.           1AO(5,2),A1(5,2),A2(5,2),CO(5,2),S(5,2),BS(5,2),WOS(5,2),DS(5,2),
477.           2FS(5,2),DNOS(5,2),ALFS(5,2),GNU(5,2),YOS(5,2),TAU(5)
478.                COMMON /MPLRGE/ VO,CKO,DN,GO,CV,EO,AO,A1,A2,CO,S,BS,WOS,
479.           1DS,FS,DNOS,ALFS,GNU,YOS,TAU
```

211

```
480.          COMMON /TINY/ TN,MC
481.          COMMON /PROBV/ TO,TC,TAM,J,K,M,N,NR
482.          DT=TN-TO
483.          IF(TAU(NR) .EQ. 0.D0) GO TO 3000
484.          VA=AO(NR,1)+A1(NR,1)*T+A2(NR,1)*T**2
485.          VB=AO(NR,2)+A1(NR,2)*T+A2(NR,2)*T**2
486.          XEQ=1.D0
487.          IF(V .GE. VA) GO TO 1000
488.          IF(V .LE. VB) GO TO 2000
489.          XEQ=(V-VA)/(VB-VA)
490.          GO TO 2000
491.     1000 XEQ=0.D0
492.     2000 XDM=(XEQ-XMO)/(TAU(NR)+DT/2.D0)
493.          XM=XMO+DT*XDM
494.          IF(XM .LT. 0.D0)XM=0.D0
495.          IF(XM .GT. 1.D0)XM=1.D0
496.          GO TO 3500
497.     3000 VA=AO(NR,1)+A1(NR,1)*TEMPN+A2(NR,1)*TEMPN**2
498.          VB=AO(NR,2)+A1(NR,2)*TEMPN+A2(NR,2)*TEMPN**2
499.          XM=1.D0
500.          IF(VN .GE. VA) GO TO 3100
501.          IF(VN .LE. VB) GO TO 3200
502.          XM=(VN-VA)/(VB-VA)
503.          GO TO 3200
504.     3100 XM=0.D0
505.     3200 XDM=(XM-XMO)/DT
506.     3500 XMNP=(XM+XMO)/2.D0
507.     4000 DO 5000 I=1,2
508.          IF(XMNP .EQ. 1.D0 .AND. I .EQ. 1) GO TO 5000
509.          RO=1.D0/VO(NR,I)
510.          A=(P-RO*GO(NR,I)*CV(NR,I)*(T-TO))*DN(NR,I)/DKO(NR,I)
511.          V=((A+1.D0)**(-1.D0/CN(NR,I)))/RO
512.          BT=((RO*V)**DN(NR,I))/CKO(NR,I)
513.          AL=RO*GO(NR,I)*CV(NR,I)*BT
514.          A=T*CV(NR,I)*BT*V*(RO*GO(NR,I))**2
515.          CP=CV(NR,I)*(1.D0+A)
516.          A=V*(1.D0/(BT*DKO(NR,I))-1.D0)+CN(NR,I)*(V-VO(NR,I))
517.          B=-DKO(NR,I)*A/((1.D0-CN(NR,I))*DN(NR,I))+CV(NR,I)*(T-TO)
518.          E=EO(NR,I)+B+RO*GO(NR,I)*CV(NR,I)*TO*(V-VO(NR,I))
519.          IF(I .EQ. 2 .AND. XMNP .NE. 1.D0) GO TO 6000
520.          V1=V
521.          BT1=BT
522.          AL1=AL
523.          CP1=CP
524.          E1=E
525.          IF(XMNP .EQ. 0.D0) GO TO 6000
526.     5000 CONTINUE
527.     6000 V2=V
528.          BT2=BT
529.          AL2=AL
530.          CP2=CP
531.          E2=E
532.          RETURN
533.          ENTRY SPEED(XM,V1,V2,BT1,BT2,AL1,AL2,CP1,CP2,P,T)
534.          DO 7000 I=1,2
535.          IF(XM .EQ. 1.D0 .AND. I .EQ. 1) GO TO 7000
536.          RO=1.D0/VO(NR,I)
537.          A=(P-RO*GO(NR,I)*CV(NR,I)*(T-TO))*DN(NR,I)/DKO(NR,I)
538.          V=((A+1.D0)**(-1.D0/CN(NR,I)))/RO
539.          BT=((RO*V)**DN(NR,I))/CKO(NR,I)
```

212

```
540.            AL=RO*GO(NR,I)*CV(NR,I)*BT
541.            A=T*CV(NR,I)*BT*V*(RO*GO(NR,I))**2
542.            CP=CV(NR,I)*(1.D0+A)
543.            IF(I .EQ. 2 .AND. XM .NE. 1.D0) GO TO 8000
544.            V1=V
545.            BT1=BT
546.            AL1=AL
547.            CP1=CP
548.            IF(XM .EQ. 0.D0) GO TO 8000
549.       7000 CONTINUE
550.       8000 V2=V
551.            BT2=BT
552.            AL2=AL
553.            CP2=CP
554.            RETURN
555.            END
556.            SUBROUTINE READIN
557.            IMPLICIT REAL*8 (A-H,C-Z)
558.            DIMENSION VO(5,2),DKO(5,2),DN(5,2),GO(5,2),CV(5,2),EO(5,2),KL(5),
559.           1AO(5,2),A1(5,2),A2(5,2),CO(5,2),S(5,2),BS(5,2),WOS(5,2),DS(5,2),
560.           2FS(5,2),DNOS(5,2),ALFS(5,2),GNU(5,2),YOS(5,2),ROP(5),COP(5),SP(5)
561.           3,TAU(5)
562.            COMMON /MPLRGE/ VO,DKO,DN,GO,CV,EO,AO,A1,A2,CO,S,BS,WOS,
563.           1DS,FS,DNOS,ALFS,GNU,YOS,TAU
564.            COMMON /MPSMAL/ROP,COP,SP,KL,NR
565.         10 FORMAT(20I3)
566.         20 FORMAT(' THERE ARE', I3,' REGIONS. DIVIDING LINES ARE AT K =',9I4)
567.         30 FORMAT(6D12.5)
568.         40 FORMAT(39X,'REGION',I4/33X,'PHASE 1',8X,'PHASE 2')
569.         50 FORMAT(' SPECIFIC VOLUME',T31,2(D12.5,3X)/' BULK MODULUS'
570.           1,T31,2(D12.5,3X)/' BULK MODULUS DERIVATIVE'
571.           2,T31,2(D12.5,3X)/' GRUNEISEN PARAMETER'
572.           3,T31,2(D12.5,3X)/' CV SPECIFIC HEAT',T31,2(D12.5,3X)
573.           4/' STP ENERGY',T31,2(D12.5,3X))
574.         60 FORMAT(' ZEROTH T COEFF OF TRANS V'
575.           1,T31,2(D12.5,3X)/' FIRST T COEFF OF TRANS V'
576.           2,T31,2(D12.5,3X)/' SECOND T COEFF OF TRANS V'
577.           3,T31,2(D12.5,3X)/' SOUND SPEED',T31,2(D12.5,3X)/' US-UP CONST'
578.           4,T31,2(D12.5,3X)/' BURGERS VECTOR',T31,2(D12.5,3X))
579.         70 FORMAT(' MAX DISLOCATION VELOCITY'
580.           1,T31,2(D12.5,3X)/' CHARACTERISTIC DRAG STRESS'
581.           2,T31,2(D12.5,3X)/' DISLOCATION CONST #1'
582.           3,T31,2(D12.5,3X)/' INITIAL DISLOCATION DENSITY'
583.           4,T31,2(D12.5,3X)/' DISLOCATION CONST #2'
584.           5,T31,2(D12.5,3X)/' POISSION',1H','S RATIO'
585.           6,T31,2(D12.5,3X)/' YEILD STRENGTH',T31,2(D12.5,3X))
586.         80 FORMAT(' PHASE TRANSITION RELAXATION TIME',T46,D12.5)
587.            READ(5,10)NR,(KL(I),I=1,NR)
588.            WRITE(6,20)NR,(KL(I),I=1,NR)
589.            DO 1000 L=1,NR
590.            DO 500 I=1,2
591.            READ(5,30)VO(L,I),DKO(L,I),DN(L,I),GO(L,I),CV(L,I),EO(L,I),
592.           1AO(L,I),A1(L,I),A2(L,I),CO(L,I),S(L,I),BS(L,I),WOS(L,I),DS(L,I),
593.           2FS(L,I),DNOS(L,I),ALFS(L,I),GNU(L,I),YOS(L,I)
594.        500 CONTINUE
595.            READ(5,30)TAU(L)
596.            WRITE(6,40)L
597.            WRITE(6,50)(VO(L,I),I=1,2),(DKO(L,I),I=1,2),(DN(L,I),I=1,2),
598.           1(GO(L,I),I=1,2),(CV(L,I),I=1,2),(EO(L,I),I=1,2)
599.            WRITE(6,60)(AO(L,I),I=1,2),(A1(L,I),I=1,2),(A2(L,I),I=1,2),
```

213

```
600.              1(CO(L,I),I=1,2),(S(L,I),I=1,2),(BS(L,I),I=1,2)
601.               WRITE(6,70)(WOS(L,I),I=1,2),(DS(L,I),I=1,2),(FS(L,I),I=1,2),
602.              1(DNOS(L,I),I=1,2),(ALFS(L,I),I=1,2),(GNU(L,I),I=1,2),
603.              2(YOS(L,I),I=1,2)
604.               WRITE(6,80)TAU(L)
605.               ROP(L)=1.D0/VO(L,1)
606.               COP(L)=CO(L,1)
607.               SP(L)=S(L,1)
608.          1000 CONTINUE
609.               RETURN
610.               END
611.               DOUBLE PRECISION FUNCTION RELF(X,Y,XD,YD,SX,SY,SXY,TM,V,T,
612.              1P,Q,PX,PY,CX,OY,XMF,G,NJ,MK)
613.               IMPLICIT REAL*8 (A-H,O-Z)
614.               DIMENSION X(NJ,MK),Y(NJ,MK),XD(NJ,MK),YD(NJ,MK),
615.              1SX(NJ,MK),SY(NJ,MK),SXY(NJ,MK),TM(NJ,MK),V(NJ,MK),
616.              2T(NJ,MK),P(NJ,MK),Q(NJ,MK),PX(MK),PY(MK),OY(MK),
617.              3OX(MK),XMF(NJ,MK),G(NJ,MK)
618.               DIMENSION VO(5,2),DKO(5,2),DN(5,2),GO(5,2),CV(5,2),EO(5,2),
619.              1AO(5,2),A1(5,2),A2(5,2),CO(5,2),S(5,2),BS(5,2),WOS(5,2),DS(5,2),
620.              2FS(5,2),DNOS(5,2),ALFS(5,2),GNU(5,2),YOS(5,2),TAU(5)
621.               COMMON /MPLRGE/ VO,DKO,DN,GO,CV,EO,AO,A1,A2,CO,S,BS,WOS,
622.              1DS,FS,DNOS,ALFS,GNU,YOS,TAU
623.               COMMON /MONST/ AL,B1,B2,DT,EX,EY,HL,HR,PJ,QO,TL,VD,VO,VP,XEQ,TRMU,
624.              1EXY,SYD,SXO,TIV,VNP,WXY,RHON,RHOO,SXYO,CB2,DTANAL,DPN,DPM,B12,
625.              2PTEST,DTM,MAGNO,MAGNU,JF,KF,KS,KSP,MIMP,NM1,MM1
626.               COMMON /TINY/ TN,MC
627.               COMMON /PROBV/ TO,TO,TAM,J,K,M,N,NR
628.               YO=(1.D0-XMF(J,K))*YOS(NR,1)+XMF(J,K)*YOS(NR,2)
629.               IF(YO .EQ. 0.D0) GO TO 2000
630.               B=(1.D0-XMF(J,K))*BS(NR,1)+XMF(J,K)*BS(NR,2)
631.               WO=(1.D0-XMF(J,K))*WOS(NR,1)+XMF(J,K)*WOS(NR,2)
632.               D=(1.D0-XMF(J,K))*DS(NR,1)+XMF(J,K)*DS(NR,2)
633.               F=(1.D0-XMF(J,K))*FS(NR,1)+XMF(J,K)*FS(NR,2)
634.               DNO=(1.D0-XMF(J,K))*DNOS(NR,1)+XMF(J,K)*DNOS(NR,2)
635.               ALF=(1.D0-XMF(J,K))*ALFS(NR,1)+XMF(J,K)*ALFS(NR,2)
636.               YO23=YO**2/3.D0
637.           900 IF(PJ .LE. YO23) GO TO 1000
638.               IF(DNO .EQ. 0.D0) GO TO 1000
639.               IF(F .EQ. 0.D0) GO TO 3000
640.               GOLD=G(J,K)
641.               CC=B*WO*DEXP(-D/(DSQRT(PJ)-YO/DSQRT(3.D0)))/F
642.               DO  950 L=1,3
643.               GD=CC*(1.D0+(F*NO-1.D0)*DEXP(-ALF*F*(GOLD+.5D0*DT*GD)/B))
644.           950 CONTINUE
645.               G(J,K)=GOLD+DT*GD
646.               RELF=DMAX1(1.D0-TRMU*GD*DT/(2.D0*DSQRT(PJ)),DSQRT(YO23/PJ))
647.               RETURN
648.          1000 RELF=1.D0
649.               RETURN
650.          2000 RELF=0.D0
651.               RETURN
652.          3000 RELF=DSQRT(YO23/PJ)
653.               RETURN
654.               ENTRY GNUF(X,Y,XD,YD,SX,SY,SXY,TM,V,T,
655.              1P,Q,PX,PY,CX,OY,XMF,G,NJ,MK)
656.               GNUF=(1.D0-XMF(J,K))*GNU(NR,1)+XMF(J,K)*GNU(NR,2)
657.               RETURN
658.               END
659.               DOUBLE PRECISION FUNCTION FX(DPN,DPM,DPJ,DPK,TL,AL,HL,
```

```
660.              1HR,TIV,VP,J,K,N,M,MIMF,FT,MARK)
661.              IMPLICIT REAL*8 (A-H,C-Z)
662.              FX=((DPJ-2.DO)/(DPN-3.CO))*TL
663.              RETURN
664.              ENTRY FY(CPN,DPM,DPJ,CPK,TL,AL,HL,
665.              1HP,TIV,VP,J,K,N,M,MIMP,FT,MARK)
666.              DI=MIMP
667.              IF(K-MIMP)1000,2000,20C0
668.      1000 FY=HL*(1.DO/(DPM-DI-1.CO)+1.CO)+FT*(DI-1.DO-DPK)/(DI-3.DO)
669.              RETURN
670.      2000 FY=(DPM-1.CO-DPK)*((HR-HL)*(DPJ-2.CO)/(DPN-3.DO)+HL)/
671.              1(DPM-CI-1.DO)
672.              RETURN
673.              ENTRY FXD(DPN,DPM,CPJ,CPK,TL,AL,HL,
674.              1HR,TIV,VP,J,K,N,M,MIMF,FT,MARK)
675.              FXD=0.DO
676.              RETURN
677.              ENTRY FYD(DPN,DPM,CPJ,CPK,TL,AL,HL,
678.              1HR,TIV,VP,J,K,N,M,MIMF,FT,MARK)
679.              IF(K-MIMP)3000,4000,5CC0
680.      3000 FYD=-VP
681.              RETURN
682.      4000 FYD=-TIV
683.              IF(MAPK .NE. 0)FYD=0.DO
684.              RETURN
685.      5000 FYD=0.DO
686.              RETURN
687.              END
```

215

APPENDIX C

ANALYTIC CALCULATION OF HUGONIOT

The jump conditions for a shock moving into a state denoted by A are

1) Mass

$$\rho(D - U) = \rho_A(D - U_A) \tag{C.1}$$

2) Momentum

$$P_X - P_{XA} = \rho_A(D - U_A)(U - U_A) \tag{C.2}$$

3) Energy or Rankine Hugoniot Relation

$$E - E_A = \frac{1}{2}(P_X + P_{XA})(V_A - V) \tag{C.3}$$

where P_X is the component of stress in the direction of motion. Combining (C.1) and (C.2) yields

$$P_X - P_{XA} = \frac{(U - U_A)^2}{V_A - V} \tag{C.4}$$

and using this in Eq. (C.3) yields

$$E - E_A = P_{XA}(V_A - V) + \frac{1}{2}(U - U_A)^2 \tag{C.5}$$

The equations of state used in this work are of the general form

$$E = f(V) + \frac{P}{\rho_0 \Gamma_0} \tag{C.6}$$

216

where P is the mean pressure, which is related to P_X in one-dimensional strain by

$$P = AP_X + B \qquad (C.7)$$

where[86]

1) $A = 1, B = 0$

if the material is hydrodynamic $\qquad (C.8)$

2) $A = \dfrac{1 + \nu}{3(1 - \nu)}, \; B = 0$

if the material is elastic $\qquad (C.9)$

3) $A = 1, \; B = \dfrac{-2Y_0}{3}$

if the material is plastic $\qquad (C.10)$

Using Eqs. (C.4) and (C.6), Eq. (C.5) can be solved for $(U - U_A)^2$

$$(U - U_A)^2 = \frac{E_A + P_{XA}(V_A - V) - f(V) - \dfrac{B}{\rho_0 \Gamma_0} - \dfrac{AP_{XA}}{\rho_0 \Gamma_0}}{\dfrac{A}{\rho_0 \Gamma_0}(V_A - V) - \dfrac{1}{2}} \qquad (C.11)$$

Thus given V and the state ahead of the shock, U and then P_X and E can be found. This can be used to find the Hugoniot if there is a two-wave structure involved.

The computational method of Section 7.1 can be used to calculate the Hugoniot incrementally for an arbitrary equation of state. This was done for the equation of state in Eq. (C.6) and matched the analytic solution exactly.

217

REFERENCES

1. G. R. Fowles, G. E. Duvall, J. Asay, P. Bellamy, F. Feistmann, D. Grady, T. Michaels, and R. Mitchell, Rev. Sci. Instrum. 41, 984 (1970).

2. G. E. Duvall, "Kinetics of Shock-Induced Phase Transitions," Army Materials and Mechanics Research Center Semi-Annual Report (July, 1973).

3. G. E. Duvall, "Kinetics of Shock-Induced Phase Transitions," Army Materials and Mechanics Research Center Annual Report (September, 1974).

4. D. B. Hayes, "Experimental Determination of Phase Transformation Rates in Shocked Potassium Chloride," Ph.D. Thesis, Washington State University, Pullman, 1973.

5. Y. Horie, "The Kinetics of Phase Change in Solids by Shock Wave Compression," Ph.D. Thesis, Washington State University, Pullman, 1966.

6. G. E. Duvall, "Shock Waves in Condensed Media," in Physics of High Energy Density (Academic Press, Inc., New York, 1971).

7. R. Courant and K. O. Friedrichs, Supersonic Flow and Shock Waves (Interscience Publishers, Inc., New York, 1948).

8. G. R. Fowles, "Experimental Technique and Instrumentation," in Dynamic Response of Materials to Intense Impulsive Loading, edited by P. C. Chou and A. K. Hopkins (Air Force Materials Laboratory, 1972), p. 405.

9. A series of papers was published by G. E. Duvall and J. O. Erkman between 1955 and 1960 as technical reports from Poulter Laboratories, Stanford Research Institute, Menlo Park, California.

10. L. M. Barker and R. E. Hollenbach, J. Appl. Phys. 43, 4669 (1972).

11. G. E. Ingram and R. A. Graham, "Quartz Gauge Technique for Impact Experiments," presented at the Fifth Symposium on Detonation, 1970.

12. D. J. Edwards, J. O. Erkman, and S. J. Jacobs, "The Electromagnetic Velocity Gage and Applications to the Measurement of Particle Velocity in PMMA," Naval Ordnance Laboratory Report NOLTR 70-79 (July, 1970).

13. G. E. Duvall, J. Appl. Phys. 45, 3439 (1974).

14. D. R. Curran, J. Appl. Phys. 32, 1811 (1961).

15. S. Katz, D. G. Doran, and D. R. Curran, J. Appl. Phys. 30, 568 (1959).

16. B. R. Breed and D. Venable, J. Appl. Phys. 39, 3222 (1968).

17. R. H. Warnes, J. Appl. Phys. 38, 4629 (1967).

18. J. M. Walsh, R. G. Shreffler, and F. J. Willig, J. Appl. Phys. 24, 349 (1953).

19. L. M. Barker and R. E. Hollenbach, Rev. Sci. Instrum. 35, 742 (1964).

20. J. O. Erkman, "Shock Waves Obliquely Incident on a Free Surface," Poulter Laboratories Technical Report 004-55 (1955).

21. J. Pearson and J. S. Rinehart, J. Acoust. Soc. Am. 25, 217 (1953).

22. W. Herrman, "Basic Response Phenomenology and Analytical Techniques," Sandia Laboratories Report SC-R-68-1784 (August, 1968).

23. J. H. Giese, "A Bibliography for the Numerical Solution of Partial Differential Equations," Ballistic Research Laboratories Report BRL MR 1991 (July, 1969).

24. W. Herrman and D. L. Hicks, "Numerical Analysis Methods," in Metallurgical Effects at High Strain Rates, edited by R. W. Rohde, B. M. Butcher, J. R. Holland, and C. H. Karnes (Plenum Publishing Corp., New York, 1973), p. 57.

25. O. C. Zienkiewicz, The Finite Element Method in Engineering Sciences (McGraw-Hill, New York, 1971).

26. R. Karpp, "The Method of Characteristics," in Dynamic Response of Materials to Intense Impulsive Loading, edited by P. C. Chou and A. K. Hopkins (Air Force Materials Laboratory, 1972), p. 283.

27. N. E. Hoskin, "Solution by Characteristics of the Equations of One-Dimensional Unsteady Flow," in Methods in Computational Physics, edited by B. Alder, S. Fernbach, and M. Rotenburg (Academic Press, New York, 1964), Vol. 3, p. 265.

28. R. T. Walsh, "Finite Difference Methods," in Dynamic Response of Materials to Intense Impulsive Loading, edited by P. C. Chou and A. K. Hopkins (Air Force Materials Laboratory, 1972), p. 363.

29. R. Karpp, p. 339.

30. W. D. Schulz, "Two Dimensional Lagrangian Hydrodynamic Difference Equations," in Methods in Computational Physics, edited by B. Alder, S. Fernbach, and M. Rotenburg (Academic Press, New York, 1964, Vol. 3, p. 1.

31. L. D. Bertholf, L. D. Buxton, B. J. Thorne, R. K. Byers, A. L. Stevens, and S. L. Thompson, J. Appl. Phys. 46, 3776 (1975).

32. W. F. Noh, "Cel: A Time-Dependent, Two-Space-Dimensional, Coupled Eulerian-Lagrange Code," in Methods in Computational Physics, edited by B. Alder, S. Fernbach, and M. Rotenburg (Academic Press, New York, 1964), Vol. 3, p. 117.

33. R. M. Frank and R. B. Lazarus, "Mixed Eulerian Lagrangian Method," in Methods in Computational Physics, edited by B. Alder, S. Fernbach, and M. Rotenburg (Academic Press, New York, 1964), Vol. 3, p. 47.

34. F. H. Harlow, "The Particle-in-Cell Computing Method for Fluid Dynamics," in Methods in Computational Physics, edited by B. Alder, S. Fernbach, and M. Rotenburg (Academic Press, New York, 1964), Vol. 3, p. 319.

35. J. L. Baylor, M. P. Bieniek, and J. P. Wright, "Tranal: A 3-D Finite Element Code for Transient Nonlinear Analysis," Weidlinger Associates Final Report DNA 3501F (June, 1974).

36. S. L. Thompson, "CSQ - A Two Dimensional Hydrodynamic Program with Energy Flow and Material Strength," Sandia Laboratories Report SAND74-0122 (August, 1974).

37. L. D. Bertholf and S. E. Benzley, "Toody II. A Computer Program for Two-Dimensional Wave Propagation," Sandia Laboratories Report SC-RR-68-41 (November, 1968).

38. M. L. Wilkins, "Calculation of Elastic-Plastic Flow," Lawrence Radiation Laboratory Report UCRL-7322 (January, 1969).

39. L. M. Barker, "SWAP-9: An Improved Stress-Wave Analyzing Program," Sandia Laboratories Report SC-RR-69-233 (August, 1969).

40. B. M. Butcher, "A Computer Program, STRATE, for the Study of Strain-Rate Sensitive Stress Wave Propagation, Part 1," Sandia Laboratories Report SC-RR-65-298 (September, 1966).

41. G. E. Duvall and J. O. Erkman, "Limiting Conditions for Stable Flow in Plane Impact," Poulter Laboratories Report (unpublished).

42. J. Von Neumann, "Theory of Shock Waves," Office of Scientific Research and Development Report No. 1140 (January, 1943).

43. G. E. Duvall and G. R. Fowles, "Shock Waves," in High Pressure Physics and Chemistry, edited by R. S. Bradley (Academic Press, New York, 1963).

44. G. E. Duvall, "Shock Waves in Solids," in Shock Metamorphism of Natural Materials, edited by B. M. French and N. M. Short (Mono Book Corporation, Baltimore, Maryland, 1968).

45. J. O. Erkman, "Oblique Shock Variables for Flow at the Extreme Angle in Metals," Poulter Laboratories Report 030-56 (August, 1956).

46. A. Ralston, A First Course in Numerical Analysis (McGraw-Hill, New York, 1965), p. 348.

47. L. M. Barker, "Determination of Shock Wave and Particle Velocities from Slanted Resistor Data," Sandia Laboratories Report SC-4611(RR) (May, 1961).

48. L. M. Barker, "Measurement of Free Surface Motion by the Slanted Resistor Technique," Sandia Laboratories Report SCDR 78-61 (May, 1961).

49. Y. Beers, Introduction to the Theory of Errors (Addison-Wesley Publishing Co., Reading, Massachusetts, 1953), p. 34.

50. F. W. Sears and M. W. Zemansky, University Physics (Addison-Wesley Publishing Co., Reading, Massachusetts, 1964), p. 662.

51. H. K. Mao, W. A. Bassett, and T. Takahashi, J. Appl. Phys. 38, 272 (1962).

52. S. N. Vaidya and G. C. Kennedy, J. Phys. Chem. Solids 32, 951 (1971).

53. W. Band, Introduction to Mathematical Physics (D. Von Nostrand Co., Inc., Princeton, New Jersey, 1959), p. 70.

54. Ibid., p. 29.

55. G. E. Mase, Schaum's Outline of Theory and Problems of Continuum Mechanics (McGraw-Hill, New York, 1970), p. 112.

56. W. Herrmann and J. W. Nunziato, "Nonlinear Constitutive Equations," in Dynamic Response of Materials to Intense Impulsive Loading, edited by P. C. Chou and H. K. Hopkins (Air Force Materials Laboratory, 1972), p. 130.

57. W. Band, p. 27.

58. P. C. Chou, "Discontinuous Stress Waves," in Dynamic Response of Materials to Intense Impulsive Loading, edited by P. C. Chou and A. K. Hopkins (Air Force Materials Laboratory, 1972), p. 66.

59. M. L. Wilkins, "Calculation of Elastic-Plastic Flow," in Methods in Computational Physics, edited by B. Alder, S. Fernbach, and M. Rotenburg (Academic Press, New York, 1964), Vol. 3, p. 216.

60. R. G. McQueen, S. P. Marsh, J. W. Taylor, J. N. Fritz, and J. W. Carter, "The Equation of State of Solids from Shock Wave Studies," in High Velocity Impact Phenomena, edited by R. Kinslow (Academic Press, New York, 1970), p. 294.

61. J. Von Neumann and R. D. Richtmyer, J. Appl. Phys. 21, 232 (1950).

62. W. Band and G. E. Duvall, Am. J. Phys. 29, 780 (1961).

63. W. Herrmann, R. J. Lawrence, and D. S. Mason, "Effect of Strain Hardening and Strain Rate in Elastic-Plastic Wave Propagation," Sandia Laboratories Report SC-DC-69-1964 (May, 1971).

64. G. E. Duvall, "Propagation of Plane Shock Waves in a Stress-Relaxing Medium," in Stress Waves in Anelastic Solids, edited by H. Kolsky and W. Prager (Springer-Verlag, Berlin, 1964), p. 20.

65. J. N. Johnson and L. M. Barker, "Dislocation Dynamics and Steady Plastic Wave Profiles in 6061-T6 Aluminum," Sandia Laboratories Report (unpublished).

66. J. N. Johnson, "Shock Waves in Stress-Relaxing Solids," Ph.D. Thesis, Washington State University, Pullman (1966).

67. R. J. Lawrence, "A General Viscoelastic Constitutive Relation for Use in Wave Propagation Calculations," Sandia Laboratories Report SC-RR-72 0114 February, 1972).

68. W. Herrmann, "Development of a High Strain Rate Constitutive Equation for 6061-T6 Aluminum," Sandia Laboratories Report SLA-73 0897 (January, 1974).

69. R. E. Swanson and C. L. Mader, "One-Dimensional Elastic-Plastic Calculations Involving Strain-Hardening and Strain-Rate Effects for Aluminum," Los Alamos Laboratories Report LA-5831 (May, 1975).

70. J. W. Taylor, J. Appl. Phys. 36, 3146 (1965).

71. J. N. Johnson and W. Band, J. Appl. Phys. 38, 1578 (1967).

72. M. L. Wilkins, "The Calculation of Elastic-Viscous-Plastic Effects in Materials," Lawrence Radiation Laboratory Report UCRL-72639 (August, 1970).

73. M. L. Wilkins, "Calculations of the Dynamic Strength of a Material," in Behaviour of Dense Media under High Dynamic Pressures (Dunad, Paris and Gordon and Breach, New York, 1968), p. 269.

74. M. S. Paterson, Rev. Geophys. Space Phys. 11, 355 (1973).

75. Y. Horie and G. E. Duvall, "Shock Waves and the Kinetics of Solid-Solid Transitions," WSU-SDL 68-06 (November, 1968).

76. D. J. Andrews, J. Comput. Phys. 7, 310 (1971).

77. H. B. Callen, Thermodynamics (John Wiley & Sons, Inc., New York, 1960).

78. E. A. Desloge, Thermal Physics (Holt, Rinehart & Winston, Inc., New York, 1968).

79. J. N. Johnson, "Considerations for the Calculations of Shock-Induced Phase Transformations in Solids," Sandia Laboratories Report SC-RR-72 0626 (September, 1972).

80. M. Cowperthwaite, Am. J. Phys. 34, 1025 (1966).

81. G. E. Duvall, G. R. Fowles, and Y. Horie, "Equations of State in Solids,"
     WSU-SDL 67-01 (February, 1967).

82. G. E. Duvall and S. M. Taylor, Jr., J. Comp. Mater. 5, 130 (1971).

83. D. J. Andrews, "Equation of State of the Alpha and Epsilon Phases of Iron,"
     Ph.D. Thesis, Washington State University, Pullman (1970).

84. C. T. Tung, G. E. Duvall, S. M. Taylor, Jr., and D. P. Dandekar, "Equation
     of State in Solids," WSU-SDL 70-02 (March, 1970).

85. Users Guide, Washington State University Computing Center, Second Edition,
     March 1, 1971.

86. G. E. Duvall, "Shock Waves and Equations of State," in Dynamic Response of
     Materials to Intense Impulsive Loading, edited by P. C. Chou and A. K.
     Hopkins (Air Force Materials Laboratory, 1972), p. 95.

DISTRIBUTION LIST

Office of Secretary of Defense
Office of the Director of Defense Research and Engineering
ATTN: Mr. J. Persh, Staff Specialist for Materials   1
       and Structures
The Pentagon
Washington, D. C. 20301

Commander
U. S. Army Material Command
ATTN: AMCRD-TT, Dr. R. Zentner   1

5001 Eisenhower Avenue
Alexandria, VA 22333

Ballistic Missile Defense Program Office
ABMDA/W (Provisional)
ATTN: DACS-BMT, Mr. C. McLain   1
       DACS-BMT, Mr. V. Kupelian   1
Commonwealth Bldg., Room 1100
1300 Wilson Blvd.
Arlington, VA 22209

Director
Ballistic Missile Defense Advanced Technology Center
ATTN: ATC-M, Mr. M. Whitfield   1
       ATC-M, Dr. D. Harmon   1
       ATC-X, Mr. W. Davis   1
P. O. Box 1500
Huntsville, AL 35807

Commander
Ballistic Missile Defense Systems Command
ATTN: BMDSC-TEN, Mr. N. J. Hurst   1
P. O. Box 1500
Huntsville, AL 35807

Director
Defense Nuclear Agency
ATTN: SPAS, Mr. J. F. Moulton, Jr.   1
       SPAS, Mr. M. Rubenstein   1

Washington, D. C. 20305

Office of Chief of Research Development and Acquisition
Department of the Army
ATTN: DAMA-CSS, Dr. J. Bryant   1
Washington, D. C. 20310

Director
Army Ballistic Research Laboratory
ATTN: Mr. J. Meszaros   1
       Dr. E. Bloore   1
       Dr. G. L. Moss   1
Aberdeen Proving Ground, MD   21005

Commander
U. S. Army Missile Command
ATTN: Dr. R. Rhodes   1
       Dr. S. Smith   1
Huntsville, AL 35809

Commander
Harry Diamond Laboratories
ATTN: AMXDO-RBF, Dr. R. Oswald   1
       AMXDO-NP, Dr. F. Wimenitz   1
2800 Powder Mill Road
Adelphi, MD 20783

Commander
Picatinny Arsenal
ATTN: Mr. M. Allen   1
       Mr. M. Weinstein   1
       Mr. B. Frank   1
Dover, NJ 07801

Commander
U. S. Army Combat Development Command
ATTN: Technical Library   1
Institute of Nuclear Studies
Fort Bliss, TX 79916

Commander
Air Force Materials Laboratory
Air Force Systems Command
ATTN: LNE/Major H. Keck   1
       LNC/Dr. D. Schmidt   1
Wright-Patterson Air Force Base, OH   45433

Department of the Navy
Naval Ordnance Systems Command
ATTN: ORD-03331, Mr. M. Kinna   1
Washington, D. C. 20360

Commander
Naval Surface Weapons Center
ATTN: Mr. L. Gowen   1
       Mr. F. Koubek   1
Silver Springs, MD 20910

Los Alamos Scientific Laboratory
ATTN: GMX-6, Dr. J. W. Taylor   1
P. O. Box 1663
Los Alamos, NM 87544

Space and Missile Systems Organization
ATTN: RSSE/Major L. Hudak   1
           Major J. McCormack   1
P. O. Box 92960
World Way Postal Center
Los Angeles, CA 90009

Sandia Laboratories
ATTN: Dr. D. Munson   1
       Dr. W. Herrmann   1
       Dr. L. D. Bertholf   1
       Dr. B. Butcher   1
       Dr. J. Lipkin   1
P. O. Box 5800
Albuquerque, NM 87115

Aerospace Corporation
ATTN: Dr. R. Cooper   1
       Dr. W. Barry   1
P. O. Box 92957
Los Angeles, CA 90009

AVCO Corporation
Government Products Group
ATTN: Dr. W. Reinecke   1
       Mr. P. Rolincik   1
201 Lowell Street
Wilmington, MA 01997

Bell Telephone Laboratories, Inc.
ATTN: Mr. E. G. Denigris   1
       Mr. M. F. Stevens   1
Murray Hill, NJ   07871

Effects Technology, Inc.
ATTN: Dr. R. Wengler   1
       Mr. E. Steele   1
P. O. Box 30400
Santa Barbara, CA   93105

Fiber Materials, Inc.
ATTN: Mr. Maurice Subilia, Jr.   1
       Mr. L. Landers   1
Biddeford Indistrial Park
Biddeford, ME   04005

General Electric Company
Valley Forge Space Technology
ATTN: Mr. K. Hall   1
       Mr. R. Sullivan   1
       Mr. J. Brazel   1
P. O. Box 8555
Philadelphia, PA   19101

Kaman Sciences Corporation
ATTN: Mr. F. Shelton   1
P. O. Box 4763
Colorado Springs, CO   80933

Ktech
ATTN: Dr. D. Keller   1
       Mr. N. H. Froula   1
911 Pennsylvania Avenue, N.E.
Albuquerque, NM   87110

Lockheed Missiles and Space Company
ATTN: Mr. D. Aspinwall   1
P. O. Box 504
Sunnyvale, CA   94088

Martin Marietta Aerospace
ATTN: Mr. J. Potts   1
       Mr. L. Kinnaird   1
       Mr. A. Ossin   1
P. O. Box 5837
Orlando, FL   32805

McDonnell Douglas Corporation
ATTN: Dr. H. Hurwicz   1

5301 Bolsa Avenue
Huntington Beach, CA   92647

Prototype Development Associates, Inc.
ATTN: Dr. J. I. Slaughter   1
       Mr. J. Schutzler   1
1740 Garry Avenue, Suite 201
Santa Ana, CA   92705

R & D Associates
ATTN: Dr. A. Field   1
525 Wilshire Blvd.
Santa Monica, CA   90025

Southwest Research Institute
ATTN: Mr. A. Wenzel   1
8500 Culebra Road
San Antonio, TX   78206

Stanford Research Institute
ATTN: Dr. D. Curran   1
       Dr. L. Seaman   1
333 Ravenswood Avenue
Menlo Park, CA   90250

TRW Systems Group
ATTN: Mr. D. Gamble   1
One Space Park
Redondo Beach, CA   90278

Defense Documentation Center   2
Cameron Station, Bldg. 5
5010 Duke Station
Alexandria, VA   22314

Director
Army Materials and Mechanics Research Center
ATTN: AMXMR-H, Mr. J. Dignam   1
       AMXMR-H, Mr. L. Aronin   1
       AMXMR-H, Dr. S. C. Chou   1
       AMXMR-H, Dr. D. Dandekar   1
       AMXMR-H, Major L. Abramson   1
       AMXMR-AP   1
       AMXMR-PL   2
       AMXMR-PR   1
Watertown, MA 02172

Stanford University
Department of Applied Mechanics
ATTN: Prof. E. H. Lee   1
Stanford, CA 94305

Terra Tek, Inc.
ATTN: Dr. A. H. Jones   1
420 Wakara Way
University Research Park
Salt Lake City, UT 84108

Commander
Watervliet Arsenal
SARWV-RR-ME, Dr. T. E. Davidson   1
Watervliet, NY 12189

ABSTRACT CARD

AD
UNCLASSIFIED
UNLIMITED DISTRIBUTION

Army Materials and Mechanics Research Center
Watertown, Massachusetts 02172
KINETICS OF SHOCK-INDUCED PHASE
TRANSITIONS - J. W. Swegle, G. E. Duvall,
and J. J. Dick, Washington State Univer-
sity, Pullman, WA 99163
Final Report AMMRC CTR 76-18, June, 1976,
241 pp - illus - tables, Contract DAAG46-
75-C-0035, D/A Project 1W062105A661, AMCMS
Code 612105.11.07000

Key Words

Finite difference code
Phase transitions
Shock waves
Stress relaxation
Two-dimensional flow
Measuring instruments

A method is developed for performing and interpreting shock wave experiments in two-dimensional strain using a light gas gun. The experimental configuration consists of the impact of a projectile on a wedge whose impact face makes an angle α with the projectile impact face. The instrumentation consists of resistance wires stretched parallel to and offset from the wedge rear surface in order to detect free surface motion. The system has the capability of making measurements over a continuous range of shock propagation distances in a single experiment. The repeatability of the technique is good to within three to four percent. The analytical technique consists of a Lagrangian finite-difference code written specifically to handle wedge impact problems. It includes material strength, stress relaxation, and phase transitions. Experiments were done on aluminum wedges and on iron and KCl wedges shocked past their transition points. Comparisons with computer calculations of the problems show excellent agreement.

ABSTRACT CARD

AD
UNCLASSIFIED
UNLIMITED DISTRIBUTION

Army Materials and Mechanics Research Center
Watertown, Massachusetts 02172
KINETICS OF SHOCK-INDUCED PHASE
TRANSITIONS - J. W. Swegle, G. E. Duvall,
and J. J. Dick, Washington State Univer-
sity, Pullman, WA 99163
Final Report AMMRC CTR 76-18, June, 1976,
241 pp - illus - tables, Contract DAAG46-
75-C-0035, D/A Project 1W062105A661, AMCMS
Code 612105.11.07000

Key Words

Finite difference code
Phase transitions
Shock waves
Stress relaxation
Two-dimensional flow
Measuring instruments

ABSTRACT CARD

AD
UNCLASSIFIED
UNLIMITED DISTRIBUTION

Army Materials and Mechanics Research Center
Watertown, Massachusetts 02172
KINETICS OF SHOCK-INDUCED PHASE
TRANSITIONS - J. W. Swegle, G. E. Duvall,
and J. J. Dick, Washington State Univer-
sity, Pullman, WA 99163
Final Report AMMRC CTR 76-18, June, 1976,
241 pp - illus - tables, Contract DAAG46-
75-C-0035, D/A Project 1W062105A661, AMCMS
Code 612105.11.07000

Key Words

Finite difference code
Phase transitions
Shock waves
Stress relaxation
Two-dimensional flow
Measuring instruments

ABSTRACT CARD

AD
UNCLASSIFIED
UNLIMITED DISTRIBUTION

Army Materials and Mechanics Research Center
Watertown, Massachusetts 02172
KINETICS OF SHOCK-INDUCED PHASE
TRANSITIONS - J. W. Swegle, G. E. Duvall,
and J. J. Dick, Washington State Univer-
sity, Pullman, WA 99163
Final Report AMMRC CTR 76-18, June, 1976,
241 pp - illus - tables, Contract DAAG46-
75-C-0035, D/A Project 1W062105A661, AMCMS
Code 612105.11.07000

Key Words

Finite difference code
Phase transitions
Shock waves
Stress relaxation
Two-dimensional flow
Measuring instruments

END

FILMED

3-86

DTIC